US Army Corps of Engineers

TECHNICAL REPORT GL-91-20

(2)

SITE-SPECIFIC SEISMIC EVALUATION OF THE GROUND BASED FREE ELECTRON - TECHNOLOGY INTEGRATION EXPERIMENT (GBFEL-TIE) PROJECT WHITE SANDS MISSILE RANGE, NEW MEXICO

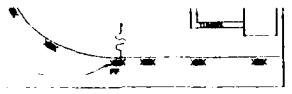

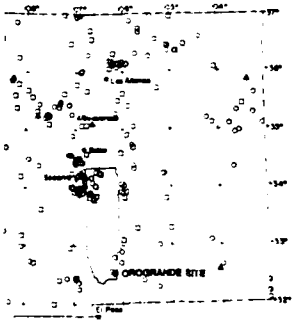

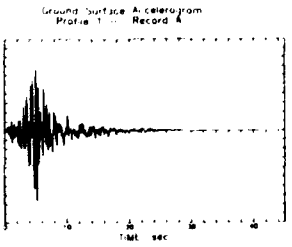

by

Ronald E. Wahl, Mary E. Hynes
Michael K. Sharp, Joseph P. Koester

Geotechnical Laboratory

DEPARTMENT OF THE ARMY
Waterways Experiment Station, Corps of Engineers
3909 Halls Ferry Road, Vicksburg, Mississippi 39180-6199

and

Al Branch

DEPARTMENT OF THE ARMY
US Army Engineer District, Fort Worth
PO Box 17300
Fort Worth, Texas 76102-0300

September 1991
Final Report

Approved For Public Release; Distribution Unlimited

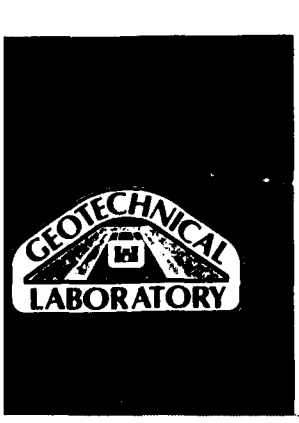

Prepared for US Army Engineer District, Fort Worth
Fort Worth, Texas 76102-0300

and US Army Engineer Division, Huntsville
Huntsville, Alabama 35807-4301

Destroy this report when no longer needed. Do not return it to the originator.

The findings in this report are not to be construed as an official Department of the Army position unless so designated by other authorized documents.

The contents of this report are not to be used for advertising, publication, or promotional purposes. Citation of trade names does not constitute an official endorsement or approval of the use of such commercial products.

REPORT DOCUMENTATION PAGE

Form Approved
OMB No. 0704-0188

1. AGENCY USE ONLY *(Leave blank)*	2. REPORT DATE	3. REPORT TYPE AND DATES COVERED
	September 1991	Final report

4. TITLE AND SUBTITLE Site Specific Seismic Evaluation of the Ground Based Free Electron - Technology Integration Experiment (GBFEL-TIE) Project, White Sands Missile Range, New Mexico

5. FUNDING NUMBERS

Intra-Army Order
Reimbursable Services
No. E87890351

6. AUTHOR(S)

Ronald E. Wahl, Mary E. Hynes
Michael K. Sharp, Joseph P. Koester

7. PERFORMING ORGANIZATION NAME(S) AND ADDRESS(ES)

See reverse

8. PERFORMING ORGANIZATION REPORT NUMBER

Technical Report
GL-91-20

9. SPONSORING / MONITORING AGENCY NAME(S) AND ADDRESS(ES)

See reverse

10. SPONSORING / MONITORING AGENCY REPORT NUMBER

11. SUPPLEMENTARY NOTES

Available from National Technical Information Service, 5285 Port Royal Road, Springfield, VA 22161.

12a. DISTRIBUTION / AVAILABILITY STATEMENT

Approved for public release; distribution unlimited

12b. DISTRIBUTION CODE

13. ABSTRACT *(Maximum 200 words)*

A site-specific seismic evaluation was performed in support of the seismic design of the Ground Based Free Electron - Technology Integration Experiment (GBFEL-TIE) facilities at the White Sands Missile Range, NM. GBFEL-TIE Project specifications called for the facilities to be designed to withstand the motions of the operating basis earthquake (OBE) which had a peak ground acceleration of 0.15 g. The principal objectives of this study included the (a) evaluation of the probability of exceeding the design peak acceleration of 0.15 g, (b) development of a set of site-specific accelerograms considered representative of the OBE which could be used subsequently in design, and (c) development of a representative set of response spectra for design. Seismic hazard and one-dimensional dynamic response analyses were performed to provide the guidance necessary for proper design.

14. SUBJECT TERMS			15. NUMBER OF PAGES
Dynamic response analysis	Seismic hazard analyses		238
Earthquakes	White Sands Missile Range		16. PRICE CODE
New Mexico			

17. SECURITY CLASSIFICATION OF REPORT	18. SECURITY CLASSIFICATION OF THIS PAGE	19. SECURITY CLASSIFICATION OF ABSTRACT	20. LIMITATION OF ABSTRACT
UNCLASSIFIED	UNCLASSIFIED		

7. PERFORMING ORGANIZATION NAME(S) AND ADDRESS(ES)

USAE Waterways Experiment Station
Geotechnical Laboratory
3909 Halls Ferry Road, Vicksburg, MS 39180-6199

US Army Engineer District, Fort Worth
PO Box 17300
Fort Worth, TX 76102-0300

9. SPONSORING/MONITORING AGENCY NAME(S) AND ADDRESS(ES)

US Army Engineer District, Fort Worth
PO Box 17300
Fort Worth, TX 76102-0300

US Army Engineer Division, Huntsville
PO Box 1600
Huntsville, AL 35807-4301

PREFACE

The US Army Engineer Waterways Experiment Station (WES) was authorized to conduct this study by the US Army Engineer Division, Huntsville (CEHND), through the US Army Engineer District, Fort Worth (CESWF), by Intra-Army Order for Reimbursable Services No. E87890351. This report summarizes studies performed to evaluate the seismicity of the proposed Ground Based Free Electron-Technology Integration Experiment Project at the Orogrande Site, White Sands Missle Range (WSMR), New Mexico.

The work performed in this report is a joint endeavor between CESWF and CEWES. Mr. Richard Suever, CEHND, was Project Manager, and Mr. Al Branch, CESWF, was the Projects Technical Coordinator. Mr. Ronald E. Wahl, Earthquake Engineering and Seismology Branch (EESB), Earthquake Engineering and Geosciences Division (EEGD), and Dr. Mary E. Hynes, Chief, EESB and EEGD, Geotechnical Laboratory, (GL), were Co-Principal Investigators for this project. Primary Engineers on the WES team for this study were Mr. Wahl (Seismic Hazard Analysis and 1-D Dynamic Response Analysis), Dr. Hynes, (Idealization of Soil Profiles), Messrs. Michael K. Sharp (Response Spectra Analysis) and Joseph Koester (Accelerogram Selection). Mr. Donald E. Yule modified the computer program "RISK" to run on personal computers. Key contributions were also made by Messrs. Frank Chang, Gregory Comes, David W. Sykora, and Ezell Allen, EESB. Mr. Branch provided input to the site idealization and characterization process for the 1-D dynamic response. General supervision at WES was provided by Dr. A. G. Franklin, Chief, EEGD, and Dr. W. F. Marcuson III, Chief, GL.

COL Larry B. Fulton, EN, is Commander and Director of WES. Dr. Robert W. Whalin is Technical Director.

CONTENTS

Conversion Factors, Non-SI to SI (Metric) Units of Measurment

Non-SI units of measurement used in this report can be converted to SI (metric) units as follows:

Multiply	By	To Obtain
degrees (angle)	0.01745329	radians
feet	0.03048	metres
g's, standard free fall	9.806650	metres per second squared
square feet	0.09290304	square metres

SITE SPECIFIC SEISMIC EVALUATION OF THE GROUND BASED FREE ELECTRON-TECHNOLOGY INTEGRATION EXPERIMENT (GBFEL-TIE) PROJECT WHITE SANDS MISSILE RANGE, NEW MEXICO

PART I: INTRODUCTION

Background

1. The White Sands Missile Range (WSMR), New Mexico, has been selected as the site for the facilities of the proposed Ground Based Free Electron - Technology Integration Experiment (GBFEL-TIE). The facilities will be constructed at the Orogrande Site of the WSMR. A plan view of the Orogrande site is shown on Figure 1. This report documents work performed by the Earthquake Engineering and Geosciences Division (CEWES-GG) of the Geotechnical Laboratory (GL) at the US Army Engineer Waterways Experiment Station (WES) to evaluate the seismicity at the Orogrande site and provide recommendations for accelerograms and reponse spectra to be used in the design of the facilities.

2. The GBFEL-TIE facilities will be used for laser research and testing and are part of a national research program under the Strategic Defense Initiative (SDI). The laser generating equipment will be housed in conventional surface structures, large buried structures, and in tunnels. Additionally, a beam control structure (geometry unknown) will extend to a height at least 60 ft* above the ground surface. The beam generating and projecting apparatuses will be complex and delicate and will require precision alignment to guarantee that the beam is accurately projected to the distant targets. The seismic evaluation is necessary to ensure that this vibration sensitive equipment is designed to tolerate the earthquake induced ground motions which might be expected to occur during the 25 year life of the GBFEL-TIE Project.

* A table of factors for converting non-SI units of measurement to SI (metric) units is presented on page 4.

Purpose and Scope

3. The CEWES-GG was tasked by the US Army Engineer Division, Huntsville (CEHND), through the US Army Engineer District, Fort Worth (CESWF), to evaluate the seismic hazard and provide information for the seismic design of critical facilities at the Orogrande site. The specific project objectives which CEWES-GG set out to address included:

a. Evaluation of the probability of exceeding a peak acceleration of 0.15 g at the free field ground surface over the 25-year life of the project.

b. Development of site specific accelerograms applicable to the free field ground surface of the Orogrande site which can be used in subsequent earthquake design analysis of the complex GBFEL-TIE facilities.

c. Development of response spectra which can be used in the design of the project. These spectra were developed from the site specific accelerograms discussed in the previous component. Response spectra of equal hazard, estimated from seismic hazard analysis techniques, were used as an aid in developing the design response spectra for the project.

This report documents the analysis that was pursued to fulfill the outlined scope of work.

PART II: SUMMARY OF PREVIOUS WORK

4. Detailed geological, seismological, and site investigations were completed under the direction of CEHND and CESWF in support of the seismological evaluation of the GBFEL-TIE Project. The data and the results of these studies were used as input into the analyses performed as part of this study. The main ideas from these previous geologic and seismological investigations which are relevant to this study are briefly summarized in the following paragraphs.

Geology

5. The WSMR is located at the southern end of the Basin and Range physiographic province and is situated in the Rio Grande Rift. The Rio Grande Rift is a major tectonic structure of the earth's crust. It began forming approximately 30 million years ago and is still evolving. Rifting has produced regional normal faulting and volcanic deposits throughout much of the rift area.

6. Figure 1 shows that the WSMR is contained within two shallow northeast trending valleys. These valleys, formed by rifting, are filled with fluvial, colluvial, aeolian, and volcanic deposits. The Tularosa Basin, the eastern valley, makes up the the southern portion of the WSMR while the Jornado del Muerto Basin comprises the northern section of WSMR. The valleys are separated by the Organ and the San Andres Mountains. The Rio Grande River flows through the Jornado del Muerto Basin.

7. The Orogrande site is located near the southeastern corner of WSMR within the Tularosa Basin as shown in Figure 1. The Tularosa Basin is bounded on the west by the San Andres, Organ, and Franklin Mountains and on the east by the Sacramento Mountains.

8. Geophysical and boring data show that the Tularosa Basin is an asymetric, west tilted graben. Geologic cross sections of the southern section of the WSMR through the Orogrande site show the general geology and subsurface structure of the valley in the vicinity of the Orogrande site (Seager, Hawley, Kottlowski, and Kelly 1987). The asymmetry of the basin is due to higher rates of movement along faults on the western side more than to

movements along faults on the eastern side. The fault movements have influenced valley filling with the valley deposits on the western side being deeper than those on the eastern side. The thickness of the deposits ranges from depths of a few feet near the mountain base to at least 5,500 ft near the WSMR headquarters area. Based on limited borehole information, the basin fill deposits are approximately 1,000 ft thick in the vicinity of the Orogrande site. The valley fill deposits are Quarternary and consist of fluvial deposits from ancient drainage of the Rio Grande, lacustrine, and beach facies formed by large ancient basin lakes, alluvial fans and colluvial aprons at the mountain front, and extensive wind blown sand dune deposits.

Seismology and Peak Ground Motion Parameters for Design

9. A thorough investigation of the seismicity of the region surrounding the WSMR was made by Krinitzsky and Dunbar (1988). Based on their findings, they assigned peak ground motion parameters to the Orogrande site for the Maximum Credible Earthquake (MCE), the Operating Basis Earthquake(OBE), and an earthquake with a 25-year return period.

10. Based on their analysis of the seismological and geological data available, Krinitzsky and Dunbar (1988) used a deterministic approach to select peak ground motion parameters for the MCE, OBE, and the 25 year earthquakes. They identified the faults in the area of WSMR as the primary sources for major earthquake activity which would affect the Orogrande site. The locations of the faults relative to the Orogrande site are shown in Figure 2. The faults in the figure are keyed by number to Table 1 where data pertaining to each fault are listed: name, dimensions, age since last movement, and closest distance to the site. The estimated maximum magnitudes, M (Richter Magnitude), and epicentral Modified Mercalli intensities, I_O, are listed in Table 2. The table also lists the Modified Mercalli intensity, I_S, predicted for the site after attenuation over the shortest distance from the source to the site. The subsurface interbasin fault (designated as 9 in Table 1 and Figure 2) gave the strongest site motions since it lies directly beneath the site, even though the Organ Mountain, Southern Andres, and intrabasin surface faults gave the same site intensity (I_S = XI) for their estimated maximum magnitude earthquakes.

11. The peak ground motion parameters determined for the MCE, OBE, and 25-year earthquakes are listed in Table 3. The listed values are based on the largest of Krinitzsky and Chang's (1987) "mean" level interpretations for the I_s values given in Table 2 for each event. The MCE is defined as the largest earthquake that can be reasonably expected to occur. The OBE is the earthquake for which a structure is designed to remain operational. If properly designed the structure will survive the OBE without structural damage and sustain some nonstructural damage that is easily repairable. Based on Krinitzsky and Dunbar's (1988) methodology, the return period for the OBE is 100 years. Ground motions were selected for the 25-year event because this is the expected life of the GBFEL-TIE facilities. All motions for the MCE, OBE, and 25-year events were specified for a soft site according to the site classification criteria of Krinitzsky and Chang (1987). The site motions from each fault were determined using Krinitzsky and Chang's attenuation curves for near field or far field events as appropriate.

12. CESWF and CEHND decided that all technical facilities were to be designed to withstand the motions of the OBE with the exceptions of facilities which store hazardous wastes or are of extremely critical technical importance. This study focuses on the motions associated with the OBE.

PART III: SEISMIC HAZARD ANALYSIS

Description and Objective of SHA

13. A Seismic Hazard Analysis (SHA) provides a means for quantifying the effects of uncertainty on the seismicity influencing a site. The objective of the SHA is to evaluate the probability of exceeding a specified level of some ground motion parameter over a period of time. The evaluation is carried out by application of the laws of probability which account for the uncertain and random nature inherently associated with geologic and seismological variables which effect seismicity.

14. Four basic steps are involved in the performance of an SHA:

a. Identify potential sources of earthquakes which may have an effect on the site.

b. Determine the recurrence relation for each seismic source identified. The recurrence relationship quantifies the rate at which different magnitude earthquakes occur within the zone.

c. Select an appropriate relationship that accounts for the attenuation of the ground motion parameter over the distance between the source and the site.

d. Use a probabilistic model to compute the probability of exceeding a certain level of the ground motion parameter over a specified time interval.

15. The probalistic model used in this study was the computer program RISK which was developed by McGuire (1976) for the United States Geological Survey (USGS). RISK models the SHA as a homogenous Poisson process which implies that the following assumptions are made: (a) Earthquakes are spatially independent; (b) Earthquakes are temporally independent; (c) the probability of two events occurring at the same time approaches zero.

16. Two primary objectives were sought from the SHA for the Orogrande site. First, the probability of exceeding a peak acceleration of 0.15 g at the Orogrande site over a 25-year period was evaluated. The results of the SHA were used to estimate which range of magnitudes made the greatest contribution to the overall probability of exceedance. The accelerograms for the dynamic response analysis were selected from earthquakes whose magnitudes were in the range most likely to affect the site (See Part IV). The

contribution of each seismic source was also evalutated to determine which had the greatest effect on the site.

17. The second objective of the SHA was to determine uniform hazard spectra for the site which was used as an aid to the development of response spectra for design. Uniform hazard spectra are spectral values which carry the same probability of exceedance for all natural periods. In this study, uniform hazard spectra for pseudovelocity were computed for the purpose of evaluating the probabilities that the design spectra would be exceeded at the 5 percent damping level.

18. The ensuing sections of Part III include discussions of the data associated with each of the major components of the SHA. First, the seismicity of the region surrounding the WSMR is discussed, and seismic source zones are identified. Two sets of source zones were used in the analysis. The first set included those determined from historical and geologic data. The second set were source zones published by Algermissen et al.(1982). Recurrence relations for each seismic source zone were then determined from seismological and geological data or from the Algermissen et al. publication depending on the case. The attenuation functions of Joyner and Boore (1981 and 1987) were used for estimating the probabilities of exceeding the peak ground acceleration and spectral velocities (for uniform hazard spectra). Finally, the results of the SHA are presented and discussed.

Determination of Seismic Source Zones From Analysis of Historical Seismicity and Faulting

Source zones for SHA analysis

19. Two separate sets of seismic source zones were used in the SHA. These source zones were:

a. Case 1 zones - Determined by analysis of the historical and instrumental seismicity of New Mexico and the geologic data pertaining to faulting near WSMR.

b. Case 2 zones - Determined by use of Algermissen et al.(1982) published seismic source zones.

20. The probability of exceeding 0.15 g over a 25 year period was evaluated using both Case 1 and Case 2 seismic sources zones and the results were compared. The uniform hazard spectra were computed using only the Case 1 sources.

21. In the analyses the seismic source zones determined from Case 1 will give a more detailed picture of the regional seismicity effecting the Orogrande site than will the Algermissen et al. zones. However, it was felt that the the application of these zones (Case 2) to the SHA would serve as a convenient and useful check of the detailed seismicity.

Historical seismicity

22. The historic record for New Mexico is short, dating back only to 1849. During the period 1849-1980, a total of 155 earthquakes of Modified Mercalli Intensity (MMI) of IV or greater were observed. The locations of the historic earthquakes having MMI of IV or greater are shown on Figure 3. Of these, the vast majority were less than MMI VI. Only four earthquakes of MMI VII or VIII were observed in New Mexico during this period. These events occurred near Socorro during 1906. Sporadic earthquake swarms were noted during the years 1906-07 in the Socorro area. The majority of the historic earthquakes are primarily concentrated along the Rio Grande Valley, the axis of the Rio Grande Rift. The section of the river between Albuquerque and Socorro contains the highest concentration of events. The seismicity near Socorro has been attributed to a deep magma body which has been identified from interpretations of geophysical data. The data base in Figure 3 clearly shows that most felt earthquakes reported during the period of interest occurred along the stretch of the Rio Grande just south of Socorro to Albuquerque.

23. Most of the earthquakes shown on the Figure 3 were discovered from old newspaper accounts (Northrop 1961 and 1976). Many areas of New Mexico are sparsely populated; therefore, the historical data base of felt earthquakes is probably incomplete and biased toward areas having population concentrations such as the cities of Socorro and Abuquerque. However, the bias is reduced by restricting the earthquakes plotted on Figure 3 only to those having MM IV or greater (Sanford, Olsen, and Haksha 1981 and Coffman and von Hake 1973). Thus, this information does indicate that the most significant region of seismic activity in New Mexico is in the Socorro-Albuquerque region. It is probably significant that the data in Figure 3 shows no historic earthquakes of MMI IV or greater near the WSMR.

Instrumentally recorded seismicity

24. Sufficient seismographic recording stations were located in New Mexico beginning in 1962 to accurately identify and locate all significant seismic events, including microearthquakes. Microearthquakes are useful in delineating, identifying, and establishing recurrence relationships for seismic source zones. The distribution of microearthquakes for the period 1962 to 1977 was reported by Sanford, Olsen, and Jaksha (1981) and is shown in Figure 4. The vast majority of parameters for these earthquakes were determined by the New Mexico Institute of Technology in Socorro.

25. The recording stations that were in place beginning in 1962 were located in Albuquerque, Socorro, and Las Cruces, New Mexico, Payson and Tucson, Arizona, and Lubbock, Texas. In 1973 seismic arrays were added to the network at Los Alamos and in the Albuquerque-Behlen Basin. Sanford, Olsen, and Jaksha (1981) studied the data acquired from these stations and concluded that the data in the state for very small earthquakes were biased due to the location of the recording stations. Sanford, Olsen, and Jaksha concluded that the minimum magnitude earthquake that could be reliably detected and located within the state of New Mexico was a Magnitude 2.2. Sanford also concluded from error analysis that about 95 percent of the earthquake locations in Figure 4 are within 20 km of their true location.

26. The data base of earthquakes used for this study is included in Appendix A and was compiled and reported by Sanford, Olsen, and Jaksha (1981). The data base includes the dates, epicentral coordinates, magnitudes, number of detecting stations, and the name of the locating organization for all earthquakes of magnitude 1.5 or greater during the 16-year period between 1962 and 1977. All earthquakes in the data base are reported in terms of local magnitude. The largest earthquake detected by the network during this period was a magnitude 4.29 event on January 23, 1966 at Dulce, NM, located near the New Mexico-Colorado border.

27. The data from the historic and instrumental record were analyzed and interpreted to identify the seismic source zones in New Mexico which might affect the Orogrande site. Two source zones were interpreted from the statewide data as shown on Figure 5. The area near Socorro was identified as the first seismic source zone since both the historic and instrumental data sets show pronounced activity there. The remainder of earthquakes appear to be more or less randomly distributed throughout the state and do not identify

any major source of seismic activity in the state. Thus, this second group of earthquakes was attributed to the background seismicity of New Mexico which represent the second seismic source zone for this study. The recurrence established for the Socorro area and the background seismicity is discussed later in this part.

Faults near WSMR

28. The major faults which are of significance to this study are near the Tularosa Basin and the Orogrande site are shown on Figure 2 (Seager et al. 1987; Callender, Seager, and Swanberg 1983). As discussed previously, these faults were determined to have the highest potential for generating earthquakes at the WSMR (Krinitzsky and Dunbar 1988). The faults can be divided into three basic groups. The first group includes fault systems on the western edge of the Tularosa Basin at the fronts of the San Andres faults (3, 4, and 5), Organ fault (2), and Franklin Mountains fault (1). The second group includes the Alamagordo faults (6 and 7) at the fronts of the Sacramentc Mountains at the eastern edge of the Basin. The third group of faults identified are within the basin (8 and 9). All faults except for one of the interbasin faults (9) were identified by surface expressions. The subsurface interbasin fault, the Jarilla Fault Zone (9) was identified by geophysical methods (gravity) and was interpreted to be located directly beneath the Orogrande site. This fault zone (of unknown throw and age, Table 1) appears in the cross-sectional view of Figures 6 and 7. In their analysis, Krinitzsky and Dunbar (1988) judged this fault to have the potential of generating the strongest ground motions affecting the site.

29. Matchette (1987) performed a geologic assessment of the area and dated the movements on the surface faults around WSMR. Matchette indicated that Holocene fault movements may have occurred on the Franklin Mountain (1), Organ Mountain (2), San Andres Southern (3), and Alamagordo (6) fault systems. Table 1 lists the most recent movement which occurred on each fault. Due to the recent Holocene movements, Krinitzsky and Dunbar (1988) in their seismological study judged that the faults were still active and capable of producing earthquakes. Therefore, due to the geologic and seismological reasoning, the nine faults shown on Figure 5 and listed in Table 1 were each considered as a source of earthquakes for the seismic hazard analysis. The

recurrence relationships used in the SHA for each of the faults is discussed later in this part.

Algermissen's Published Seismic Source Zones

30. In 1982, Algermissen et al. (1982), published probabilistic maps of the United States which could be used to estimate the peak accelerations and velocities anywhere in the United States which have 10 percent probabilties of being exceeded for periods of 10, 50, and 250 years. Algermissen et al. used a probabilistic model of the United States to develop his estimates. In his model, Algermissen et al. essentially divided the continental United States into 178 seismic source zones as shown in Figure 8. Algermissen et al. identified source zones for the model by holding workshops in which experts were conferred with seismicity from that region. The rectangle in the figure shows the source zones that were used in the SHA for this study. The 13 seismic source zones used for this study are shown in expanded scale in Figure 9. These zones were developed from data of the Southern Rocky Mountain Region. Algermissen et al. (through Sanford, Olsen, and Jaksha 1981) identified the Rio Grande Rift as the most seismically active feature in New Mexico based on the historic record. The Rio Grande Rift is identified by zones 2, 4, and 9 in Figure 9. The Algermissen et al. recurrence relationships for each source zone are discussed in the following paragraphs.

Recurrence Relationships

31. A recurrence relationship must be determined for each seismic source zone identified in the probabilistic model. The recurrence relationship describes and quantifies the expected degree of earthquake activity likely to occur in each source zone over a certain period of time (usually annual). The recurrence relationships used in this study assume that the magnitudes have an exponential distribution which are represented by following form:

$$\log_{10}(N) = a - b_M \times M \qquad (1)$$

where: M = magnitude

N = number of earthquakes exceeding Magnitude M during some period of time

a = constant determined from data

b_M = magnitude related constant determined from data

The recurrence relationship is valid only for earthquakes below M_{max} for that zone. The recurrence parameters and how they were determined for each of the two sets of source zones are discussed in following paragraphs.

Recurrence for Case 1 seismic zones

32. The Case 1 source zones included the nine faults near the WSMR, the Socorro area, and the background seismicity of New Mexico. The objective of the analysis for recurrence was to determine the a and b constants in Equation (1) and the M_{max}.

33. The recurrence for the Socorro area and the background seismicity were estimated from a statistical analysis of the data base compiled by Sanford, Olsen, and Jaksha (1981) of instrumentally recorded earthquakes in Appendix A. Only events having magnitudes greater than 2.2 were used in the analysis for the estimation of the parameters a and b.

34. The statewide data base was queried to sort the earthquake data in each seismic zone. The data for each seismic zone was sorted into magnitude intervals having widths of 0.1 magnitude unit (e.g. $2.2 \leq M < 2.3$). The number of earthquakes in each interval was counted. The cumulative number of earthquakes exceeding the upper bound values (for the 16-year period) for each interval were counted and plotted against magnitude for the middle of the interval. The cumulative data were determined by considering the whole state, the Socorro area, and the background (residual) as separate source zones for the 16-year period of the data base. The cumulative data is plotted in Figure 10 for each of these source zones. The plot shows that the data for each source zone can be approximated closely by a straight line which is almost parallel to the others. Analysis of the trends indicates that the seismicity of the Socorro area accounted for about 20 percent of the state's seismicity during this period. A statistical regression was performed to determine the best fit line for the data for each of the three source zones. The results of this analysis are presented in Table 4. A comparison between the state wide recurrence parameters determined for this study with those reported by Sanford, Olsen, and Jaksha (1981) show very close agreement. The comparison

Sanford, Olsen, and Jaksha (1981) show very close agreement. The comparison served as a control to verify that the statistical computational procedures were being carried out correctly. The annual recurrence parameters assigned to each zone for input into the SHA are presented in Table 5. The annual values for "a" were reached by subtracting $\log_{10}(16)$ from the "a" parameter determined for the 16-year period and listed in Table 4. The annual "b" value is the same as that for the 16-year "b" value. Also listed in Table 5 is the maximum magnitude parameter, M_{max}, that was used as input to the SHA. In Table 5 the background recurrence parameters were adjusted to reflect the seismicity per 10,000 km^2. This area adjusted value was used to describe the background seismicity.

35. The recurrence parameters for the nine faults near the WSMR were determined from the Matchette (1987) dating of fault movements which was discussed earlier. Matchette was able to identify five large magnitude surface ruputuring earthquake events on four of the faults shown on Figure 2. The four faults were the East Franklin (Fault 1, 1 movement), Organ Mountain (Fault 2, 2 movements), South San Andres (Fault 3, 1 movement) and Almagordo (Fault 6, 1 movement). Though Matchette did not interpret movements on all nine faults, Krinitzsky and Dunbar (1988) recommended that each of the faults should be considered active. Thus, based on these facts and for lack of more detailed information, it was estimated that on the average there would be one fault movement every 2,000 years (0.0005 movements/year) for the entire group of faults. Since the historical and instrumental data presented earlier showed virtually no earthquake activity near the WSMR and since Matchette only made note of movements associated with large earthquakes, each fault was considered capable of generating only one magnitude earthquake which was a characteristic earthquake of magnitude 7.5. If the overall probability of exceeding a magnitude 7.5 event in any one year for the group is shared equally among all the faults, then the annual number of magnitude 7.5 events on any one of the faults is 0.0000555 (0.0005 events per year for the entire group of nine faults).

36. A summary of the the Case 1 recurrence parameters for the three seismic source zones used in the SHA is listed in Table 6. A plot showing the recurrence relationships for each Case 1 source zone is shown in Figure 11.

Recurrence for Case 2 source zones

37. Algermissen et al. (1982) published recurrence parameters for each of the seismic source zones listed in Figure 8. The parameters for each of the 13 Case 2 source zones of this study are presented in Table 7. The recurrence relationships for each Case 2 source zone is shown in Figure 12. Table 7 lists the zone number for this study, the zone number referenced in Algermissen's report, the annual number of events having epicentral Modified Mercalli Intensities of V or higher, the a and b parameters, and the maximum magnitude event expected for that zone. All parameters except the "a" parameter were taken directly from Algermissen's report. The "a" parameter was computed from the number of MMI events exceeding V per year, Algermissen's estimate of the "b" parameter, b_I (determined from intensities), and by using Equation 1. The magnitude associated with an MMI = V event was computed using the following correlation between epicentral intensity and magnitude (Gutenburg and Richter 1942):

$$M = 1.3 + 0.6 \times I_o \qquad (2)$$

Thus, a magnitude of 4.3 is associated with an MMI V event. In the study by Algermissen et al. (1982), the b_I parameter was converted to the b_M of Equation 1 by multiplying by 1.67. This factor was determined using the relationships of Equations 1 and 2. Equation 1 was solved for the "a" parameter after the magnitude was set to 4.3 for each source zone.

Attenuation Functions

38. The attenuation function is the third major element of the SHA. The attenuation functions are used to establish the relationship between the ground motion parameter and distance from the source. The attenuation function of Joyner and Boore (1981) for peak horizontal ground acceleration was used in this study. The equation is empirical and was selected because it is based on a data base of strong motion accelerograms for the Western United States including those recorded on deep alluvial sites from the Imperial Valley Earthquake of 1979. The equation has following form:

$$\log_{10}(A) = -1.02 + 0.249 \times M - \log(r) - 0.00255 \times r + 0.26 \times P \qquad (3)$$

where

A = peak horizontal ground acceleration in g's

M = moment magnitude

r = distance to point of rupture, km.

$= (d^2 + 7.32)^{0.5}$

d = distance to epicenter, km

P = 0 for 50th percentile

P = 1 for 84th percentile

Equation 3 was used in the 50th percentile form. The standard deviation about the 50th percentile was taken to be 0.26 A plot of the attenuation of peak acceleration versus distance for selected earthquake magnitudes is shown in Figure 13.

Probabilistic Model and Results

39. The fourth component of the SHA is the computation of the probabilities of exceeding the peak ground motion parameter being investigated over the specified time period. The model used in this study was the computer program RISK which was developed by McGuire (1976) for the United States Geological Survery (USGS). The program was written in FORTRAN and adapted to run on a personal computer by CEWES-GG. The assumptions for the homogeneous Poisson process modeled by RISK were stated earlier in Part III. RISK treats all seismic sources as areas. Faults, which are best approximated as line sources, can be input to RISK as areas having narrow widths.

40. As stated earlier, the SHA computations were conducted using two sets of source zones. The Case 1 source zones are based on analysis of data of the historical and geological information which were part of this study. The Case 2 source zones are based on those published by Algermissen et al. (1982).

Case 1 results

41. The Case 1 results of the RISK analysis are shown on the plot of Figure 14. The curve on this figure shows the annual probability of exceeding a specified value of peak acceleration, a_{max}. The return period for a_{max} can be determined from the ordinate axis on the right-hand side of the figure.

The return period is simply the reciprocal of the annual probability of exceedance. As might be expected, the curve shows that the probabilities of exceedance decrease as the level of acceleration increases. The plot shows that the annual probability of exceeding a peak acceleration of 0.15 g is 0.149×10^{-3} (i.e. return period of about 6,700 years). The probability of exceeding a certain peak acceleration for an "n" year period was calculated from the annual probability using Equation 4 is shown:

$$R_n = 1 - (1 - R_a)^n \qquad (4)$$

where: R_a = annual probability
R_n = probability over an "n" year period
n = time period in years

Thus, the probability of exceeding 0.15 g in a 25-year period is about 0.37 percent.

42. The plot on Figure 15 shows the contribution of each of the seismic source zones to the overall annual probability of exceedance. Figure 15 shows probability of exceedance curves from the RISK analysis for all sources combined (same as curve on Figure 14), the faults near WSMR, the Socorro area, and the background seismicity. The plot shows that the faults near WSMR and the background seismicity contribute almost equally to the probability of exceeding 0.15 g at the site. Each source contributes approximately 50 percent to the overall total probability of exceedance. The plot also indicates that the contribution of the Socorro seismic source to the overall probability is negligible at the 0.15 g acceleration level.

43. The probability of exceedance breakdown for various magnitude ranges is shown in Figure 16. The plot shows probability of exceedance curves for the following magnitude ranges:

$M \leq 7.5$	Overall probability
$6.5 < M \leq 7.5$	
$5.5 < M \leq 6.5$	
$4.5 < M \leq 5.5$	
$M \leq 4.5$	

The plot shows that the 0.15 g peak acceleration level will most likely generated by an earthquake having a magnitude between 6.5 and 7.5. This magnitude interval contributes about a 49-percent share to the overall probability of exceedance for 0.15 g annually. This is consistent with the finding that the faults near WSMR are a major contributor to the overall probability of exceedance since these faults were interpreted to be capable of generating only a characteristic earthquake with a magnitude of 7.5. The contributions to the overall probability of exceedance at the 0.15 g peak acceleration level for the other magnitude ranges are listed in Table 8. It is important to note that the relationships between the contributions of the various magnitude intervals to the overall probability changes with the level of peak acceleration.

Case 2 results

44. The probability of exceedance curve from the SHA for the Case 2 seismic source zones is shown in Figure 17. The annual probability of exceeding 0.15 g is 0.774×10^{-4} (return period is 12,900 years). The probability of exceeding amax over a 25-year period was determined to be about 0.19 percent using Equation 4. At this peak acceleration the computer output showed only that zones 2 and 12 contributed to the annual probability of exceeding 0.15 g at the site. Figure 8 shows that the Orogrande site is located within zone 2 and is very near to zone 12. Interestingly, Figure 9 also shows that zone 11 at its closest point is about as the same distance from the site as zone 12, yet the RISK results showed that its contribution to the overall probability was negligible. This is attributed to the the recurrence parameters shown in Table 7 which show that Algermissen et al.(1982) evaluated zone 11 as a zone of low seismicity which spanned a very large area. The Case 2 analysis indicates that the probability of an earthquake from a distant source causing a peak acceleration of 0.15 g at the site is remote. This finding is consistent with that of Case 1 where the contribution of the Socorro source to the overall risk was negligble due to its distance to the Socorro site.

Comparison of Case 1 and Case 2 Results

45. The overall probabilties of exceedance for different levels of peak accelerations at the Orogrande Site for the Case 1 and Case 2 source zones are compared on Figure 18. This plot show that the Case 2 (Algermissen et al. (1982)) source zone will have a higher probability of being exceeded for all peak accelerations up to 0.12 g. Above a peak acceleration of 0.12 g, the Case 1 source zones will have a higher probability of exceedance. The results of the comparison between Cases 1 and 2 for a peak acceleration of 0.15 g are listed in Table 9. As discussed earlier, the annual probabilities of exceeding 0.15 g were 0.149×10^{-3} and 0.774×10^{-4} for Cases 1 and 2, respectively. These are equivalent to the 25-year probabilities of exceedance of 0.37 percent for Case 1 and 0.19 percent for Case 2, respectively. The overall results are in good agreement for Cases 1 and 2.

Uniform hazard spectra

46. The second primary objective of the SHA was to estimate uniform hazard spectra for the Orogrande site. Uniform hazard spectra (UHS) are response spectra values at different periods each of which has an equal probability of being exceeded. In this study, UHS were evaluated in terms of the pseudospectral velocity (Sv). The UHS were computed with RISK using the same basic techniques as were employed for the probabilistic analysis of the peak acceleration. The seismic source zones and recurrence relationships which used the UHS analysis were the Case 1 zones. The attenuation function, in terms of Sv, was developed by Joyner and Boore (1987) and is shown as Equation 5,

$$\log_{10}(Sv) = a + b(M-6) + c(M-6)2 + d(\log10(r)) + kr + s \qquad (5)$$

where

Sv = spectral velocity for the period defined by the empirical constants

M = moment magnitude $(5.0 < M \leq 7.7)$

$r = (r_0^2 + h^2)^{1/2}$

a, b, c, h, d, k, s = empirical constants which depend upon the period of the spectral value

The Joyner and Boore equation is empirical and was developed based on data from the larger of the two horizontal components of pseudovelocity response at a recording station. The predictive equation is applicable for 5-percent damping only. Table 10 lists the period dependent empirical constants used in the predictive equation for Sv attenuation. Graphical representations of the attenuation function for Sv for periods of 0.5 and 1.0 second are shown in Figures 19 and 20, respectively.

47. The uniform hazard spectra for the Orogrande site for 5-percent damping are shown on Figure 21. Uniform hazard pseudovelocity spectra having probabilities of exceedance of 0.01, 0.03, 0.10, 0.3, 1, 5, 10, and 50 percent for a 25-year period were estimated. As expected, for a given period, the higher the spectral velocity the lower the probability that spectral velocity will be exceeded over 25 years. The hazard spectra shown in Figure 21 were useful in Part V of this report in developing the response spectra used for design.

Comments on the Seismic Hazard Analysis

48. Evaluating the probabilities of exceeding certain ground motion parameters for the area near WSMR is a very difficult problem. Perhaps the most difficult aspect of the SHA lay in estimating the recurrence relationships for each zone. This estimation is made difficult by the short time frame over which earthquake activity was observed in New Mexico. The vast majority of events collected over the 16-year period, during which accurate seismic measuments were made, had very small magnitudes (less than 3.5). The return period for larger magnitude events must be extrapolated from the straight line trends indicated in Figure 10. This straight line extrapolation can not be validated due to the lack of large magnitude events over the historic record. The 2,000-year return period for magnitude 7.5 events on the faults surrounding the WSMR also reflects a great uncertainty due to the inaccuracies associated with geologic dating of fault movements. Matchette dated fault movements by correlation with the degree of weathering on the fault (slope angle). The probabilities of exceedance associated with the peak acceleration of 0.15 g and those associated with the uniform hazard spectra

should be taken as estimates and not as absolute values. However, the probabilisitic estimates do serve to give some indication that though the Rio Grande Rift in New Mexico is seismically active, it is an area of relatively low seimic activity when compared to other regions such as southern California. It is also encouraging to note that the probabilities computed from Case 1 sources were similar to those of Case 2. Surely, Algermissen et al. (1982) experienced the same difficulty with the recurrence relationships in making their estimates.

PART IV: SELECTION AND DEVELOPMENT OF ACCELEROGRAMS FOR USE IN DESIGN OF THE GBFEL-TIE FACILITIES

49. The selection and development of site specific design accelerograms are discussed in this part of the report. These accelerograms were developed for the ground surface of the free field and were to be used as input to subsequent design analysis of the GBFEL-TIE facilities. Each design accelerogram has a peak acceleration of 0.15 g which is the peak acceleration level selected for design by CESWF and CEHND. The site investigation revealed that the free field soil profile at the site could be characterized as 1,000 ft of firm alluvium.

50. The ground surface accelerograms used in this study were developed from two primary sources:

a. The ground surface response of a one-dimensional dynamic response analysis in which hard site (rock outcrop) accelerograms were used to excite characteristic profiles at the Orogrande site.

b. Firm soil site accelerograms recorded at the ground surface of deep alluvial sites somewhat similar to the Orogrande site.

51. In this study, 15 ground surface accelerograms were developed. To the greatest extent possible, these accelerograms were selected from large magnitude earthquakes ($6.5 < M \leq 7.5$), since, in the SHA discussed in Part III, events in this range were most likely to bring ground motions with a peak acceleration of 0.15 g to the Orogrande site. Of these, nine were investigated using the 1-D techniques and six were developed from the selection of soft soil records. In the end, five accelerograms were recommended for use in design. The response spectra from all records in the study were used to aid in the development of the design response spectra which will be discussed in Part V.

Development of Accelerograms from 1-D Dynamic Response Analysis Techniques

52. The basic strategy for using the 1-D dynamic response analysis to develop ground surface accelerograms from the rock outcrop input records is shown in Figure 22. At the outcrop location, the accelerogram is scaled to

some value of peak acceleration and deconvolved to baserock beneath the soil profile. In the analysis, the baserock motions are assumed to be vertically propagated as shear waves through the soil column. The dynamic response of the soil system to these input motions determines the acceleration at the ground surface. The rock outcrop accelerogram was scaled so that the peak acceleration at the ground surface was 0.15 g, as shown on the Figure 22. This procedure was modified for some of the dynamic responses as truncated soil profiles 200 ft deep were used rather than the full 1,000 ft column. This modification will be discussed later in the report. The 1-D methods were also used to estimate the fundamental period of the site and determine the variation of peak acceleration with depth. Response spectra from the ground surface accelerograms were also used to develop the design response spectra which will be discussed in Part V.

53. The essential features in performing the 1-D dynamic response analysis included:

a. Characterization of the site using field data

b. Determination of representive soil profiles and properties for use as input to the dynamic response analysis.

c. Selection of representative hard site accelerograms recording during earthquakes of magnitudes similar to those expected at the Orogrande site.

d. Estimation of the fundamental period of the soil profile after performing the 1-D response analysis of the soil profile to selected accelerograms.

All 1-D dynamic response analyses were performed using the computer program SHAKE.

54. In the following sections of Part IV, the background pertaining to each of the major components will be discussed. The data relevant to each element will be presented and analyzed, and the results will be discussed.

Description of SHAKE

55. The 1-D computer program SHAKE was used to evaluate the dynamic responses of the characteristic soil profiles to the rock outcrop accelerograms. SHAKE was developed by Schnabel, Lysmer, and Seed (1972).

SHAKE solves the wave equation in the frequency domain through the use of the Fast Fourier Transform (FFT). SHAKE handles the nonlinear strain dependent soil properties of shear modulus and damping with the equivalent linear procedure, an iterative process which converges upon strain compatible values for modulus and damping. The 1-D analysis performed by SHAKE is a total stress analysis. The strain dependent damping and modulus degradation curves used for the materials of this study are shown in Figure 23. This chart was developed by Zen and Higuchi (1984) and recommended for use by Sun, Goleshorki, and Seed, (1988).

56. SHAKE was constructed based upon the following assumptions:

a. All layers in the soil profile are horizontal and of infinite lateral extent. Level ground conditions are assumed to exist, thus prior to the earthquake there are no static shear stresses existing on horizontal planes.

b. Each soil layer in the profile is defined and described by its shear modulus, damping, and total density and thickness.

c. The response of the soil profile is caused by shear waves propagating upward through the soil layers in the system.

d. The acceleration history which excites the soil profile is due to shear waves.

e. The equivalent linear procedure satisfactorily models the nonlinear strain dependent modulus and damping of the soils in the profile.

Site Characterization Studies

57. Engineering studies coordinated by CESWF were performed at the site for the purpose of characterizing the site and obtaining the engineering properties of the subsurface materials. These studies are described in detail in "Seismic Assessment and Design Recommendations: Ground Based Free Electron Laser-Technology Integration Experiment Project (GBFEL-TIE) , White Sands Missile Range, New Mexico," (US Army Engineer District, Fort Worth, 1988). Only results of these investigation pertinent to the earthquake response calculations are described in this section.

58. The layout of the field investigation is shown in Figure 24. These engineering investigations were limited to a depth of about 200 ft. The site investigation included a conventional drilling and sampling program designed

to retrieve samples, both disturbed and undisturbed, for the purpose of identifying and classifying subsurface soils and performing tests in the laboratory. The drilling and sampling program was supplemented with Cone Penetration Tests (CPT) which were useful in stratigraphic evaluation.

59. The generalized subsurface stratigraphic profile as interpreted by the CESWF is presented in Figure 25a, and more detailed profiles are presented in Figures 25b through 25e. These figures show interpreted profiles for sections B-B', C-C', D-D', and E-E', respectively, and are all perpendicular to section A-A'. The profiles generally reflect the stratgraphy of only the upper 100 ft of the site. These soil profiles are typical for the geologic environment and depositional processes that lead to the formation of this site. The site generally consists of alternating layers which are primarily sandy or clayey. Layer thicknesses vary from a few feet to a few tens of feet. The upper 60 ft of the deposit is primarily sandy material, with occasional clay layers. Below this depth to about 100 ft, the materials are predominately clayey, with occasional layers of sand.

60. One deep well log (not presented) was available for inspection. The well log extends to a depth of 1,175 ft, and indicates that approximately 1,000 ft of valley fill exists on top of basement rock. The basement rock was estimated to be of Permian age. The well log indicates that the valley fill consists of alternating layers of materials which are predominately sandy or clayey throughout the 1,000-ft depth. Data obtained from the log indicate that the water table was encountered at a depth of about 270 ft.

61. A series of geophysical tests were performed to obtain information which could be used in the dynamic response analysis discussed later in this report. Seismic refraction tests were performed to measure the compression wave velocities of the soils at the site and to locate and determine the depths of layers with increasing velocities. A profile of compression wave velocities as determined by the refraction lines is shown on Figure 26. Crosshole tests (locations shown on Figure 24) were performed for the purpose of obtaining the low strain amplitude shear wave velocities of subsurface materials. Low strain amplitude shear moduli which are required for the dynamic analysis can be determined from the shear wave velocity measurments. The compression and shear wave velocities measured in the crosshole tests are presented in Figure 27.

62. Shear wave velocities and site stratigraphy are the two most important input parameters for obtaining meaningful site dynamic response results. The crosshole geophysical tests provide the best measure of the shear wave velocities of the materials at the site and were used to develop input velocities for the analysis response profiles. The shear wave velocities shown in Figure 27 were used to estimate average and upper bound K_{2max} values for 10-ft intervals by means of the following formula:

$$K_{2max} = \frac{(V_s^2 \times \gamma)}{(1{,}000 \times g \times (\sigma_m')^{1/2})} \qquad (6)$$

where

V_s = shear wave velocity, fps

g = 32.2 ft/sec2

σ = mean normal stress, psf

γ = unit weight, pcf

The shear wave velocities are translated to corresponding K_{2max} values for input to the dynamic analyses. The K_{2max} values are proportionality constants which relate soil stiffness (in terms of shear modulus or S-wave velocity) to the square root of the mean normal effective pressure. Knowledge of the K_{2max} values for the various strata assists with the site interpretation and assignment of input geometry and material stiffnesses for the dynamic response analyses.

63. The average and upper-bound K_{2max} values for 10-ft intervals are plotted in Figure 28. This plot indicates that the soil profile is relatively homogeneous with respect to low strain stiffness, even though the geology indicates a much more complex stratigraphy. The average K_{2max} layers and seven columns of upper-bound K_{2max} layers were investigated to identify the potential variability of dynamic response with depth at the site and to identify the appropriate elevation for the base rock in SHAKE computations. These columns are shown in Figures 29 and 30.

Input Accelerograms

64. Nine hard site accelerograms were used in this study to develop ground surface accelerograms from the 1-D dynamic response analyses. A list of these accelerograms is shown on Table 11. The list gives an identification letter which is used for this study, the name, magnitude, and date of the earthquake event during which the accelerogram was recorded. Also shown in the table are the location of the recording station and the horizontal directional component. These accelerograms were mainly selected from large magnitude earthquakes, M > 6, to stay in keeping with the findings of the SHA. Plots of each of the acceleration histories (shown scaled to 0.15 g) and the 5-percent damped acceleration response spectra are shown in Figures 31 through 48.

1-D Dynamic Response Analysis

65. As mentioned previously, the 1-D dynamic analyses were performed with SHAKE to develop ground surface accelerograms which could be used in development of design response spectra and in design analysis of the GBFEL-TIE structures. The soil profiles, developed from the data obtained during the site investigations (Figures 29 and 30), were designed to study the sensitivity of the dyanamic response results to:

a. Boundary effects, in which the effect of the dynamic response to a varying the soil height was studied.

b. Stratigraphic changes, in which the sensitivity of the dynamic responses to variations in material types and stiffnesses present in the subsurface at the site were studied.

66. The essential output sought from SHAKE included the variation of peak acceleration with depth, the fundamental site period, and the ground surface accelerograms and response spectra.

Sensitivity of the Dynamic Response to Changing Soil Height

67. The basic strategy employed for performing the SHAKE analysis was discussed earlier and illustrated in Figure 22. However, a variation to this procedure was ultimately adopted in developing the ground surface accelerograms. Truncated soil profiles, 200-ft deep, were ultimately adopted for evaluating the dynamic responses of the soil columns to the various rock outcrop accelerograms selected for input. The truncated soil profiles offer the advantage of studying the responses in the upper 200 ft, the zone of engineering interest, in greater detail since the computer program limited in the number of layers for which it can provide output.

68. The truncated profiles were applicable for use in the analysis after finding that under the conditions of this study the dynamic response was relatively insensitive to the height of the soil profile if all other variables were held unchanged. In the sensitivity study, the dynamic responses of soil columns having heights of 1,000, 500, and 200 ft were compared for both the upper bound and average stiffness profiles. The profiles are presented on Figures 29 and 30 under the headings of boundary effects for the upper bound and average stiffnesses. For each case, the profiles were excited using the accelerogram for Record A, shown in Figure 31. Record A was selected as the input accelerogram for studying the sensitivity of the results to the height of the soil column because its 5-percent damped acceleration spectrum in Figure 32 indicates that it is relatively rich in frequencies having periods between 0.0 and 1.0 sec.

69. The dynamic responses for the Upper Bound Profiles are discussed in this paragraph. The upper bound profiles used in the sensitivity analysis were designated as PA-1000, PA-500, and PA-200 for heights of 1,000, 500, and 200 ft, respectively. For the upper bound profiles all materials were treated as clays having a plasiticity index of 30 percent. Thus, the modulus reduction curve for materials having a PI of 30 percent from Figure 23 was assigned to the clay layers in each profile. The strain dependent damping curve assigned to each layer is also shown in Figure 23. The 200- and 500-ft profiles were derived by truncating the 1,000-ft profile (P1-1000). Thus, the properties of all profiles are identical over comparable depth ranges with the only difference being the height of the profile. The base layer of each

profile was treated as an elastic material having the velocities indicated in Figure 29. The velocities at the bases of the 200-and 500-ft profiles were determined by estimating the effective mean normal pressure at the base, and substituting a K_{2max} value of 115 into Equation 5. The profiles were excited by applying Record A as an outcrop of the base layer. SHAKE was used to compute the dynamic response of each profile to Record A. Record A was scaled so that the resulting peak acceleration obtained at ground surface was 0.15 g. The results of each dynamic response calculation are compared in the form of peak acceleration versus depth profiles and the pseudovelocity response spectra obtained for the ground surface. Figure 49 shows that the peak acceleration profiles for each of the profiles are very similar and that the differences are small especially in the upper 150 ft. The response of each profile shows that the peak acceleration decreases as a function of depth. Figure 50 is a plot which compares the response spectra (5-percent) damping) for the three profiles. As with the case of the peak acceleration, the plot shows that the response spectra obtained from each of the three profiles are very similar. The greatest differences occur at periods which are greater than 1.0 sec where the 500-ft profile gives the lowest spectral velocities and the 200-ft profile gives the highest velocities. However, the differences are of no significance for this study, and the results show that the response in the upper sections of the profile are fairly insensitive to varying the soil profile height.

70. The dynamic responses for the average stiffness profiles were determined in like manner to those for the upper bound. The average stiffness profiles used in the sensitivity analysis were designated as P1-1000, P1-500, and P1-200 representing profiles with of 1000-, 500-, and 200-ft depths, respectively. For the average stiffness profiles Figure 30 shows that the upper 200 ft of material includes layers of clays and sands. The clays were assigned the modulus reduction curve corresponding to a PI of 30-percent in Figure 23 and the sands were assigned a modulus reduction curve corresponding to a material having a PI of 0-percent. As before, the peak accelerations and ground surface response spectra are compared to determine the sensitivity of the dynamic responses to the varying soil height. Plots of peak accelerations versus depths for each profile are compared on Figure 51. As for the upper bound profiles, the results of each are in very close agreement in the upper 200 ft. Even though the results for each profile are somewhat divergent at

depths between 75 and 200 ft, the peak accelerations for each of the three profiles are still within 0.03 g of each other at a depth of 200 ft. Figure 52 shows that the ground surface response spectra for each of the three profiles are in close agreement with no differences of major significance.

71. This analysis indicates that the dynamic responses for both the upper bound and average stiffness profiles are relatively insensitive to variations in the depth if the depth is between 200 and 1,000 ft if the processing scheme described (in the preceding paragraph) was employed. Due to the insensitivity of the response in the area of engineering interest to varying soil height, the ground surface accelerograms and response spectra were developed using soil profiles which were 200-ft deep. However, since the fundamental period of the site depends on the dimensions of the soil profile, it was estimated as using 1,000-ft soil profiles PA-1000 for the upper bound case and P1-1000 for the average case. The estimate of the fundamental period is discussed in the following paragraphs of this part.

72. It is also worth mentioning that the dynamic shear strains for the upper bound and average responses remained below 0.015 percent for each layer. This indicates that the soil response for both upper and lower bound stiffness profiles remains essentially in the elastic region for this level of excitation (Figure 23).

Estimation of Fundamental Period

73. The estimated range of site periods were determined from the 1,000-ft upper bound and average stiffness level soil profiles, PA-1000 and P1-1000. The preearthquake and effective periods for each profile were determined by using SHAKE and the excitations of Record A. The results are listed in Table 12. The low strain (preearthquake) period was estimated by scaling the outcrop accelerogram to 0.0001 g to ensure that there was virtually no degradation of modulus and the response remained totally elastic. The effective period is that computed for the moduli effective during the level of shaking induced in the profile by the design earthquake. Thus, the difference between the preearthquake and effective periods of a soil profile are a measure of the level of strain softening (nonlinear effect) which the soil layers in the profile might be expected to experience during the design earthquake. The preearthquake and effective periods for profile P1-1000

(upper bound stiffness profile) are 1.69 and 1.76 sec, respectively. The preearthquake and effective periods for profile PA-1000 (average stiffness profile) are 1.53 and 1.60 sec, respectively. Each profile shows that the site period lengthens slightly due to the levels of shaking caused by the design earthquake. This indicates that modulus reductions in each of the soil profiles is relatively minor and that for the shaking levels of the design earthquake (a_{max} at the ground surface) the response of the soil profiles is in the essentially elastic range. Thus, if the average and upper bound stiffnesses profiles are representative of the site conditions, the effective site period can be expected to be between 1.60 and 1.76 sec.

Sensitivity of the Dynamic Response to Variations in Site Stratigraphy

74. The effects of variations in the site stratigraphy on the dynamic responses of profiles with upper bound and average stiffnesses were evaluated. The stratigraphic variations were modeled with SHAKE with several profiles which characterize realistic variations in material type (sand or clay) and stiffness (slight variations from the upper bound and average stiffnesses) which were revealed from data gathered in the field investigations. All profiles studied in the analysis of stratigraphic effects had heights of 200 ft.

75. The upper bound stiffness profiles used for evaluating the sensitivity of the dynamic response at the site to the stratigraphic variations were Profile PA through PF shown on Figure 29. In each profile the material assigned to any layer was a sand (designated as S) or a clay (designated as C). Materials designated as sands were assigned the modulus reduction curve for PI = 0 in Figure 23 and clays were assigned the reduction curve for PI = 30. The strain dependent damping curve on Figure 23 was used for both sands and clays. In each case, the base layer was assumed to be elastic and was assigned a shear wave velocity of 1,900 fps. The dynamic response of each system was evaluated by inputting Record A (Figure 31) at the outcrop of the base layer.

76. The sensitivity of the dynamic responses to stratigraphy was evaluated comparing the relationships between peak acceleration and depth and the ground surface response spectra for Profiles PA through PE. Plots of peak

acceleration versus depth for the six upper bound stiffness profiles, Profiles PA through PE, are presented in Figure 53 through 57, respectively. Each of these plots shows that the peak acceleration decreases with increasing depth. Figure 58 is a compilation plot of the peak accelerations for Profiles PA through PE. The peak accelerations for all profiles plot within a very narrow range which indicates that the response of each system is insensitive to variations in the stratigraphy. Further evidence of this insensitivity is given by the comparison of the response spectra (pseudovelocity) of the ground surface motions from each of the profiles shown on Figure 59. This figure shows that the spectral velocities of each profile fall within a very narrow range for all periods.

77. Similar analyses were performed on the average stiffness profiles to evaluate the sensitivity of the dynamic response to variations in stratigraphy. Profiles P1 through P5 in Figure 30 were used to make this evaluation. Each of these profiles was 200 ft high and was excited by Record A as discussed previously. Plots of peak acceleration versus depth for Profiles P1 through P6 are presented in Figures 60 through 64, respectively. Each plot shows that the peak acceleration decreases with increasing depth. Figure 65 is a compilation of the peak accelerations for the six average stiffness profiles. This plot shows that the peak accelerations from each profile are similar and fall within a narrow range which serves as an indication that the responses are insensitive to stratigraphy variations. The ground surface response spectra for the six profiles are shown on Figure 66. The spectral velocities for all profiles are very similar and fall within a narrow band for nearly all periods. The only exception is that the spectral velocities of Profile P1 for periods greater than 1.5 sec are greater than those for Profiles P2 through P5. However, for practical purposes, the response spectra also indicate that the dynamic responses are relatively insensitive to variations in material types.

78. Since the preceding analysis indicates that the dynamic responses for both the upper and average stiffness profiles are insensitive to stratigraphic variations, it is necessary to only select a single representative profile from each set. Hence, for remaining dynamic analysis Profile A (200 ft) was considered as representative of the upper bound stiffness profiles and Profile P1 was considered as representative of the average stiffness profiles. In the sensitivity analysis, it was noticed that

the strain levels in all profiles (for both upper and average stiffnesses) the dynamic shear strains were less than 0.015 percent. Figure 23 shows there is only a slight reduction in shear modulus at these low strain levels. This figure also shows that at these strain levels there is only a slight difference in the reduction factors between materials with plasiticity indices of 0 and 30 percent, which is how sands and clays were characterized in the dynamic analysis.

Responses of Upper and Lower Bound Stiffness Profiles to Selected Hard Site Accelerograms

79. The responses of Profiles PA-200 and P1-200, the representative upper bound and average stiffness profiles, to Records A through I were performed using SHAKE to develop the site specific ground surface accelerograms and response spectra to be used in design. The responses of each profile to these accelerograms were evaluated on the basis of peak acceleration versus depth and the characteristics of the spectral velocities of the ground surface motions. Profiles PA-200 and P1-200 were modified slightly to include more layers to provide a more detailed solution in the upper 200 ft of the valley fills which is the area of engineering signficance for this study. The modified profiles are presented on Figure 67. Each of the hard site accelerograms was input at the base outcrop location. As before, the base was treated as an elastic material which had the shear wave velocities indicated on Figure 67.

80. Plots of peak acceleration versus depth obtained from the responses of the upperbound stiffness profile, P1, to Records A through I are shown in Figure 68 through 76. Each of these plots shows a general trend for the peak accelerations to decrease with depth over the 200-ft depth range studied. Figures 77 through 85 show plots of the target ground surface accelerograms resulting from the SHAKE analysis. Response spectra were computed for each at damping levels of 1, 2, 5, 7, 10 and 20 percent. These results will be discussed in the following paragraphs.

81. Similarily, peak accelerations, ground surface acceleration histories, and response spectra were obtained from the average stiffness profile, PA, to Record A through I. Figures 86 through 94 show plots of peak acceleration versus depth resulting from the response of Profile A for Record

A through I. As for the upperbound stiffness results discussed previously, the peak accelerations decrease with depth. Computed ground surface accelerograms resulting from the responses of Profile PA to Records A through I are presented in Figures 95 through 103. Response spectra which were computed from these ground surface motions will be discussed in the following paragraphs.

82. Response spectra from the ground surface motions of Profiles PA and P1 for Records A through I are compared in Figures 104 through 112, respectively. The response spectra shown in these figures are in terms of pseudospectral velocities for the 5-percent damping level. For each input accelerogram, the response spectra of the ground surface motions for P1 and PA are in very close agreement. This indicates that for a given input accelerogram the resulting ground surface motions for PA and P1 are very similar in frequency content. Thus, for practical purposes the set of ground surface accelerograms for Profiles PA and P1 are equivalent and do not significantly differ from one another. Thus, for the duration of this study the set of ground surface motions from Profile PA will be considered representative for the Orogrande site and the recommendations of the developed site specific accelerograms will be made from this set. Also, the design response spectra which will be discussed in Part V of this report will be developed from the set of accelerograms from Profile PA.

Accelerograms Recorded During Earthquakes at Firm Soil Sites

83. Existing accelerograms recorded on firm soil sites were the second source of ground surface acceleration histories for this study. Six accelerograms were selected as potential candidates for use in design and in the development of design response spectra. These records will be referred to as Records 1 through 6 in this report. The accelerograms were selected from earthquakes in the Western United States having magnitudes of 5.8 or greater. Table 13 is a list containing information as to the reference record number used in this study, the earthquake event name, date, and magnitude, the recording station location and component, and the peak acceleration recorded at the site. Figures 113 through 124 show the acceleration histories and

5-percent damped response spectra for each of Records 1 through 6, respectively. Each of these accelerograms was scaled to the peak acceleration value of 0.15 g specified for design of the GBFEL-TIE facilities.

Recommendations for Design Accelerograms

84. A list summarizing some of the characteristics of the 15 design accelerograms studied for the GBFEL-TIE Project is presented in Table 14. For each ground surface accelerogram the table includes information on the source of the accelerogram (1-D or soft site record), the report figure where it is displayed, the peak acceleration, and the peak velocity (centimetres/second). From this list, two accelerograms were selected for use as input into a design finite element soil-structure interaction analysis of the project facilities. The two recommended accelerograms are the ground surface accelerogram derived from Record A (Figure 77) as part of the 1-D analysis and Record 1 (Figure 119) from the set of firm soil site accelerograms. These records were selected based upon there frequency content and the degree to which their peak ground motion parameters matched those specified by Krinitzsky and Dunbar (1988). Specifically, the frequency contents of each record was evaluated by examination of its response spectrum to ensure that a wide band of frequencies was present without holes or gaps. The peak velocity of each record was checked to ensure that it was within reasonable range of the 10 cm/sec value specified for this study. Though only 2 accelerograms were recommended for the design analysis, the entire set fifteen accelerograms was used to develop the design response spectra discussed in Part V.

PART V: DEVELOPMENT OF DESIGN RESPONSE SPECTRA

85. Design response spectra were developed from a statistical analysis of the response spectra of the ground motions of the 15 ground surface accelerograms used in this study and discussed in Part IV. The response spectra (in terms of pseudovelocity) were computed at damping levels of 1, 2, 5, 7, 10, and 20 percent for each accelerogram. The periods of interest ranged from 0.05 to 5.0 sec. The objective of the analysis was to the mean and upper and lower bound envelopes for each period based on the spectra for each of the 15 accelerograms for each of the 6 damping levels. Conservatively, smoothed upper bound envelopes were recommended for use in design.

86. Figures 125 through 133 are plots showing the spectral velocities for the 1-, 2-, 5-, 7-, 10- and 20-percent damping levels of the ground surface accelerograms of Records A through I. These spectra were developed from the 1-D dynamic response analysis discussed in Part IV. Figures 134 through 139 are response spectra for the same damping levels which were computed from the six firm soil site accelerograms from Records 1 through 6.

Statistical Analysis of Spectral Velocities

87. A statistical analysis was performed to estimate the range in spectral velocities which might be expected at the Orogrande site in the event of the design earthquake. This range estimate was performed for damping levels of 1, 2, 5, 7, 10 and 20 percent. The range level was determined by sorting the spectral velocities presented on Figures 125 through 139 according to damping level. This sorting of the spectral data resulted in the plots of Figures 140 through 145 which shows the spectral velocities of each of the 15 accelerograms for damping levels of 1, 2, 5, 7, 10, and 20 percent, respectively. Examination of these plots shows that the range of spectral velocities widens as the period increases which reflects the variation in frequency content present in the fifteen accelerograms studied.

88. The data on Figures 140 through 145 were analyzed further to develop average and upper- and lower-bound estimates of the design response spectra for the design earthquake at the Orogrande site. The resulting

average and upper- and lower-bound spectal velocities for damping levels of 1, 2, 5, 7, 10, and 20-percent are shown on Figures 146 through 151, respectively.

Recommended Design Response Spectra

89. Smoothed response spectra were developed from the upper bound spectral envelopes in Figures 146 through 151. These site specific smoothed response spectra, recommended for design, are presented in Figures 152 through 157 for damping levels of 1, 2, 5, 7, 10 and 20 percent, respectively. The recommended 5-percent damped spectra are compared with response spectra predicted by procedures developed by: (a) Newmark and Hall, and (b) Seed on Figure 158. These procedures are described in Army TM 5-890-10-1 (Headquarters, Departments of the Army, Navy, and Air Force 1986). The plot shows that the recommended site specific spectra agree with the Newmark-Hall and Seed spectra.

90. Additionally, the 5-percent damped spectrum recommended for design (Figure 154) was compared with the UHS (Figure 21) in the plot on Figure 159. The comparison shows that the probability of the design response spectrum being exceeded in a 25-year period are between 0.10 and 0.30 percent for all periods of interest. This result was considered to be consistent with the SHA estimate that the probability of exceeding the design peak acceleration of 0.15 g is on the order of less than 1 percent based on the analysis of Part II. The comparison was only made for the 5-percent damping level since the Joyner and Boore (1981, 1987) correlations are for the spectral velocities were only developed for this level.

PART VI: SUMMARY AND CONCLUSIONS

91. A site specific seismic evaluation has been performed in support of the seismic design for the GBFEL-TIE Project at the White Sands Missile Range, New Mexico. The GBFEL-TIE facilities will be constructed at the Orogrande site in the southeastern section of WSMR. The project is to be designed for the motions expected during the OBE. A peak acceleration of 0.15 g which was specified for the OBE by Krinitzsky and Dunbar (1988) in their seismological investigation of WSMR. The motions were specified for a soil site. The expected economic life of the GBFEL-TIE Project is 25 years. The principal objectives undertaken in the seismic evaluation of this study included:

a. Evaluation the probability of exceeding the design peak acceleration of 0.15 g during the 25 year life of the project.

b. Development of a set of site specific acclerograms which could be considered representative of those which might be expected in the event of the OBE. These accelerograms were developed for subsequent use in the seismic analysis of the facilities.

c. Development of response spectra which could also be used in the design of the project facilities.

92. An SHA was performed to evaluate the probability of exceeding a peak acceleration of 0.15 g at the Orogrande site. Seismic sources and their recurrence intervals were determined from a study of historical, instrument recorded, and geologic data. The analysis showed that the probabilties of exceeding the design peak acceleration was less than 1 percent over the 25-year project life. The SHA also indicated that faults near WSMR (in the Tularosa Basin) had a significant potential for generating an earthquake which could cause the design peak acceleration to be exceeded. The SHA also indicated that probability of exceeding the design peak acceleration of 0.15 g comes mainly from a large magnitude earthquake in the magnitude range between 6.5 and 7.5. The results of the SHA are dependent upon the seismological data available for New Mexico which has several shortcomings. Some of these shortcomings include the short period of historical seismicity in New Mexico (1849-1977 for this study), the problems associated with the uncertainty of dating fault movements from geologic investigations. Nonetheless, the data at

hand suggests that though New Mexico is seismically active, it's seismicity is relatively low compared to other parts of the United States.

93. The information from the SHA was used as an aid to the development of a set of accelerograms which would ultimately be recommended for design. The accelerograms were developed from two sources:

a. From a 1-D dynamic response analysis in which motions recorded at hard sites were propagated through the valley fills of the WSMR to determine the acceleration history at the ground surface (peak acceleration of 0.15 g).

b. Accelerograms recorded on deep alluvial (firm) soil sites similar to the valley fills at WSMR.

Two accelerograms were recommended for use in subsequent design and soil structure interaction analysis are indicated in Table 14.

94. Fifteen accelerograms were used in the development of the design response spectra for the Orogrande site. Design response spectra (in terms of pseudospectral velocities) were developed for levels of 1-, 2-, 5-, 7-, 10-, and 20-percent damping. Conservatively, the response spectra recommended for design for each damping level envelope the response spectra of the 15 accelerograms at each damping level. These recommended spectra for each damping level are presented in Figures 152 through 157.

REFERENCES

Algermissen, S. T., Perkins, D. M., Thenhaus, P. C., Hanson, S. L., and Bender, B. L. 1982. "Probabilistic Estimates of Maximum Acceleration and Velocity in Rock in the Contiguous United States," Open File Report 82-1033, US Department of the Interior, Geological Survey, Denver, CO.

Callender, J. F., Seager, W. R., Swanberg, C. A. 1983. "Late Tertiary and Quarternary Tectonics and Volcanism," Geothermal Resources of New Mexico Map Series, National Geophysical Data Center, National Oceanic and Atmospheric Administration, Denver, CO.

Coffman, J. L., and von Hake, C. A. 1973. "Earthquake History of the United States," US Department of Commerce, National Oceanic and Atmospheric Administration, Publication 41-1, revised edition (through 1970), pp 59-58, Denver, CO.

Gutenberg, B. and Richter, C. F. 1942. "Earthquake Magnitude, Intensity, Energy, and Acceleration," Bulletin of the Seismological Society of America, Vol 32, pp 163-191.

Headquaters, Departments of the Army, Navy, and Air Force. 1986. "Technical Manual - Seismic Design Guidelines for Essential Buildings," Army TM 5-890-10-1, Navy NAVFAC P-355.1, Air Force AFM 88-3, Chapter 13, SEC A, Washington, DC.

Joyner, W. B., and Boore, D. M 1981. "Peak Horizontal Acceleration and Velocity from Strong-Motion Records Including Records from 1979 Imperial Valley, California, Earthquake," Bulletin of the Seismological Society of America. Vol 71, No. 6, pp 2011-2038.

Joyner, W. B., and Boore, D. M. 1987. "Measurement, Characterization, and Prediction of Strong Ground Motion," Proceedings, Earthquake Engineering and Soil Dynamics II - Recent Advances in Ground Motion Evaluation, American Society of Civil Engineers, New York, NY.

Krinitzky, E. L. and Chang, F. K. 1987. "State-of-the-Art for Assessing Earthquake Hazards in the United States: Parameters for Specifiying Intensity-Related Earthquake Ground Motions," Miscellaneous Paper S-73-1, US Army Engineer Waterways Experiment Station, Vicksburg, MS.

Krinitzky, E. L., and Dunbar, J. B. 1988. "Geological and Seismological Evaluation of Earthquake Hazards at White Sands Missile Range, New Mexico", Project Report, US Army Engineer, Waterways Experiment Station, Vicksburg, MS.

Matchette, M. N. 1987. "Preliminary Assessment of Paleoseismicity at White Sands Missle Range, Southern New Mexico: Evidence for Recency of Faultin, Fault Segmentation, and Repeat Intervals for Major Earthquakes in the Region," US Geological Survey, Open File Report 87-444, Denver, CO.

McGuire, R. K. 1976. "Fortran Program for Seismic Risk Analysis," US Geological Survey, Open File Report 76-67, Denver, CO.

Northrop, S. A. 1976. "New Mexico's Earthquake History, 1849-1975", Tectonics and Mineral Resources of Southwestern North America, Woodward and Northrop, Ed., New Mexico Geological Society, Socorro, NM.

Northrop, S. A. 1961. "Earthquakes of Central New Mexico", Guidebook 12th Field Conference, New Mexico Geological Society, pp 151-152, Socorro, NM.

Sanford, A. R., Olsen, K. H., and Jaksha, L. H. 1981. "Earthquakes in New Mexico, 1849-1977," New Mexico Bureau of Mines and Mineral Resources, Circular 171, Socorro, NM.

Schnabel, P. B., Lysmer, J., and Seed, H. B. 1972. "SHAKE, A Computer Program for Earthquake Response Analysis of Horizontally Layered Sites," Report EERC 72-12, Earthquake Engineering Research Center, College of Engineering, University of California Berkley, CA.

Seager, W. R. 1980. "Quartenary Fault System in the Tularosa and Hueco Basins, Southern New Mexico and West Texas," New Mexico Geological Society Guidebook, 31st Field Conference, Trans-Pecos Region, pp 131-135.

Seager, W. R., Hawley, J. W., Kottlowski, F. E., and Kelley, S. A. 1987. "Geology of East Half of Las Cruces and Northeast El Paso 1° x 2° Sheet, New Mexico, "New Mexico Bureau of Mines and Mineral Resources, Geologic Map 57, Socorro, NM.

Sun, J. I., Goleshorki, R., and Seed, H. B. 1988. "Dynamic Moduli and Damping Ratios for Cohesive Soils," Report UCB/EERC-88/15, Earthquake Engineering Research Center, University of California, Berkley, CA.

US Army Engineer District, Fort Worth. 1988. "Seismic Assessment and Design Recommendations: Ground Based Free Electron Laser Project (GBFEL-TIE), White Sands Missile Range, New Mexico," Fort Worth, TX.

Zen, K., and Higuchi, Y. 1984. "Prediction of Vibratory Shear Modulus and Damping Ratio for Cohesive Soils," Proceedings, Eighth International Conference on Earthquake Engineering, San Francisco, CA, July, Vol 3, pp 23-30.

Table 1
Fault Zones In and Adjacent to the Tularosa Basin*

No.	Fault Zone	Total Scarp Height, m	Single Event Height, m	Fault Length, km	Fault Age**	Distance From Site, km
1	Franklin Mtn	30-50	3-5	45	vlp-h	55
2	Organ Mt. (Cox Ranch)	>30	1.9-4.6	42	h	27
3	San Andres (Southern)	15-22	2.8-4.8	36	vlp-h?	24
4	San Andres (Central)	26-28	2.7-5.4	48	vlp	42
5	San Andres			22	lp	82
6	Alamagordo	9-10	2.0-2.9	57	vlp-h	33
	Alamagordo + (East splay)			32		75
7	Alamagordo (NW Splay)			22		75
8	Intrabasin (surface)	7-28	3	5-20	≤mp	15
9	Tularosa# Basin (sub-surface)			++		

Note: from Krinitzsky and Dunbar (1988)

* Data on faults primarily from Matchette (1987) with supplemental data from Gile (1987); Seager (1980); and Seager et al. (1987)

** Age of most recent movement: h = holocene (≤10 ka); vlp = latest Pleistocene (10-35 ka); lp = late Pleistocene (10-130 ka); mp = middle Pleistocene (130-750 ka)

\+ Not shown, buried by alluvium

++ Total length is >100 km; individual segments estimated at 35 to 50 km.

\# Jarilla Fault Zone

Table 2

Source-Site (I_o - I_s) MM Intensity*

No.	Fault Zone	Distance From Site km	M	MM I_o	MM I_s
1	Franklin Mt.	55	7.5	XI	X
2	Organ Mt. (Cox Ranch)	25	7.5	XI	XI
3	San Andres (Southern)	20	7.5	XI	XI
4	San Andres (Central)	42	7.5	XI	X
5	San Andres (Northern)	82	7.5	XI	IX
6	Alamorgordo	33	7.5	XI	X
8	Intrabasin (surface)	15	7.5	XI	XI
9	Tularosa Basin** (subsurface)	0	7.5	XI	XI

* Krinitzsky and Dunbar (1988)

** Jarilla Fault Zone

TABLE 3

Mean Peak Ground Motion Parameters for the Orogrande Site at WSMR, NM*

	MCE	OBE	25-yr Event
Acceleration (cm/sec^2)	1000.0	150.0	100.0
Velocity (cm/sec)	125.0	9.0	10.0
Duration (sec)	52.0	6.0	4.0
Magnitude	7.5	5.0	4.5

* Krinitzsky and Dunbar (1988)

Table 4

Statistical Analysis to Determine the Recurrence of Source From the Microseismicity Data Base of Sanford (1962-1977)

Zone	a	b	Standard Deviation of b	r
Whole state	4.144	0.988	0.046	-0.996
Whole state (Sanford, Olsen and Jaksha(1981))	4.150	0.970	0.020	-0.996
Socorro area	3.945	1.212	0.024	-0.998
Background	3.900	0.923	0.0434	-0.996

Table 5

Annual Recurrence of Source Zones
Determined from the Microseismicity of
New Mexico and Used as Input to Seismic Hazard Analysis

Zone	a	b	Standard Deviation of b	M_{max}
Whole state	2.940	0.988	0.046	7.5
Socorro area	2.741	1.212	0.024	7.5
Background	2.696	0.923	0.043	7.5
Background per 10,000 km^2	1.2313	0.923	0.043	7.5

Table 6

Annual Recurrences for Seismic Hazard Analysis

Zone	a	b	M_{max}
Each of the nine faults near WSMR	5.5×10^{-5}	0.001	7.5
Socorro	2.741	-1.212	7.5
Background	2.696	-0.923	7.5

Table 7

Recurrence Parameters

Used for Case 2 Seismic Source Zones based on

Published Source Zones (Algermissen et al. (1982))

Zone	Algermissen Zone	Number Exceeding MMI V per year*	a**	b_I	b_M	M_{max}
1	001	0.227	4.602	0.73	1.22	7.3
2	003	0.088	4.190	0.73	1.22	6.1
3	004	0.227	3.226	0.54	0.90	7.3
4	007	0.419	4.868	0.73	1.22	7.3
5	008	0.211	4.570	0.73	1.22	6.1
6	006	0.135	4.376	0.73	1.22	7.3
7	016	0.146	4.410	0.73	1.22	6.1
8	041	0.244	4.633	0.73	1.22	7.3
9	042	0.018	3.501	0.73	1.22	6.1
10	043	0.046	3.909	0.73	1.22	7.3
11	077	0.0347	1.851	0.46	0.77	7.3
12	002	0.036	3.802	0.73	1.22	7.3
13	005	0.0910	4.205	0.73	1.22	7.3

* For this study MMI V was taken to be M = 4.3

** Computed assuming M = 4.3 using: $\log(N) = a - b_M \times M$

Table 8

Contribution Of Selected Magnitude Intervals
To The Overall Probability Of Exceeding a_{max} = 0.15g

Magnitude Interval	$p(a_{max} > 0.15g)$ n = 1 year	$p(a_{max} > 0.15g)$ n = 25 years	% of Total
$6.5 < M \leq 7.5$	7.34×10^{-5}	1.83×10^{-3}	49
$5.5 < M \leq 6.5$	8.30×10^{-6}	2.08×10^{-4}	6
$4.5 < M \leq 5.5$	3.89×10^{-5}	9.72×10^{-4}	26
$M \leq 4.5$	2.84×10^{-5}	7.10×10^{-4}	19
Total ($M \leq 7.5$)	1.49×10^{-4}	3.71×10^{-3}	100

Table 9
Probabilities of Exceeding 0.15 g
in 25 Years for Cases 1 and 2

Case	$p(a > 0.15\ g \mid n\ years)$ n = 25 years	$p(a > 0.15\ g \mid n\ years)$ n = 1 year
Case 1	0.37×10^{-4}	0.149×10^{-3}
Case 2	0.19×10^{-4}	0.774×10^{-4}

Table 10

Parameters in the Predictive Equations of Joyner and Boore(1987)
for the Larger of Two Horizontal Components
of Pseudovelocity Response (cm/sec) at 5 Percent Damping
and of Peak Acceleration (g) and Velocity (cm/sec)

Period (sec)	a	b	c	h	d	k	s	Vso	e	Standard Deviation of log y
0.10	2.24	0.30	-0.09	10.6	-1.00	-0.0067	-0.06			0.27
0.15	2.46	0.34	-0.10	10.3	-1.00	-0.0063	-0.05			0.27
0.20	2.54	0.37	-0.11	9.3	-1.00	-0.0061	-0.03			0.27
0.30	2.56	0.43	-0.12	7.0	-1.00	-0.0057	-0.04	650	-0.20	0.27
0.40	2.54	0.49	-0.13	5.7	-1.00	-0.0055	0.09	870	-0.26	0.30
0.50	2.53	0.53	-0.14	5.2	-1.00	-0.0053	0.12	1050	-0.30	0.32
0.75	2.46	0.61	-0.15	4.7	-1.00	-0.0049	0.19	1410	-0.39	0.35
1.00	2.41	0.66	-0.16	4.6	-1.00	-0.0044	0.24	1580	-0.45	0.35
1.50	2.32	0.71	-0.17	4.6	-1.00	-0.0034	0.30	1780	-0.53	0.35
2.00	2.26	0.75	-0.18	4.6	-1.00	-0.0025	0.32	1820	-0.59	0.35
3.00	2.17	0.78	-0.19	4.6	-1.00	0.0	0.29	1620	-0.67	0.35
4.00	2.10	0.80	-0.20	4.6	-0.98	0.0	0.24	1320	-0.73	0.35

Table 11

Hard Site Records Used in this Study

Record	Earthquake	Recording Station	Component	Date	Magnitude	A_{max} g.
A	Mt. Hamilton	Anderson Dam	340°	4/24/84	6.1	0.28
B	Whittier	Mt. Wilson	90°	10/1/87	6.1	0.118
C	San Fernando	Lake Hughes	S21°W	2/9/71	6.5	0.144
D	San Fernando	Castaic Ridge	N21°E	2/9/71	6.5	0.183
E	Helena, Mont	Carroll Coll.	S00°W	1/23/85	6.0	0.146
F	Parkfield, CA	Temblor	S65°	6/27/66	5.5	0.225
G	San Franciso	Golden Gate	S80°	3/22/57	5.5	0.09
H	Nahanni, NWT*	Site 1	10°	1/23/85	6.9	0.23
I	Nahanni, NWT*	Site 2	330°	1/23/85	6.9	0.39

* Northwest Territories

Table 12

Fundamental Site Periods

Profile	Fundamental Period, sec	
	Low Strain Amplitude	Effective Strain Amplitude
P1 (Average)	1.69	1.76
PA (Upper bound)	1.53	1.60

Table 13

Firm Soil Site Records Used in this Study

No.	Event, EQ	Date	Magnitude	Station	Comp.	A_{max} g
1	Whittier	Oct 1, 1987	6.1	Los Angeles-Baldwin Hills	90°	0.153
2	Morgan Hill	Apr 24, 1984	6.2	Gilroy #2	90°	0.214
3	Superstition Hills	Nov 24, 1987	5.8	Wild Life Liq. Array	90°	0.129
4	Whittier	Oct 1, 1987	6.1	Los Angeles-Baldwin Hills	0°	0.142
5	Morgan Hill	Apr 24, 1984	6.2	Gilroy #2	0°	0.157
6	El Centro	Oct 15, 1979	6.6	Array 12 Brockman Rd.	140°	0.142

Table 14

Summary of Ground Surface Acceleration Histories Used in this Study

Record	Source of Record	Figure	Amax g	Peak Vel cm/sec
A*	1-D Analysis	95	0.15	13.6
B	1-D Analysis	96	0.15	4.8
C	1-D Analysis	97	0.15	9.4
D	1-D Analysis	98	0.15	10.4
E	1-D Analysis	99	0.15	8.1
F	1-D Analysis	100	0.15	8.2
G	1-D Analysis	101	0.15	5.2
H	1-D Analysis	102	0.15	5.6
I	1-D Analysis	103	0.15	15.6
1	Firm Soil Site	113	0.15	6.6
2	Firm Soil Site	115	0.15	18.2
3	Firm Soil Site	117	0.15	9.7
4*	Firm Soil Site	119	0.15	8.1
5	Firm Soil Site	121	0.15	5.0
6	Firm Soil Site	123	0.15	19.1

* Accelerograms recommended for use in design

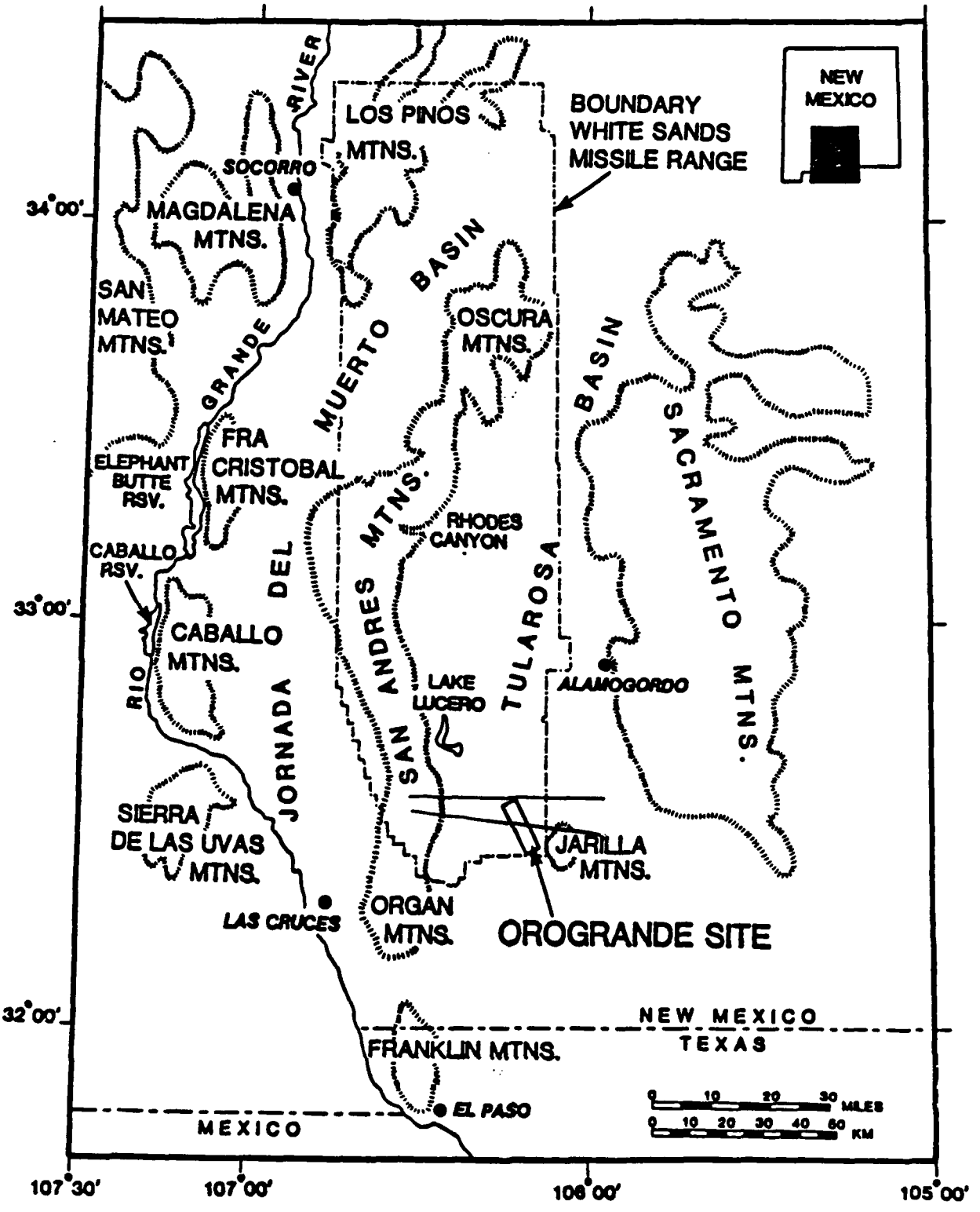

Figure 1. Location of WSMR, Orogrande site, and principal mountain ranges

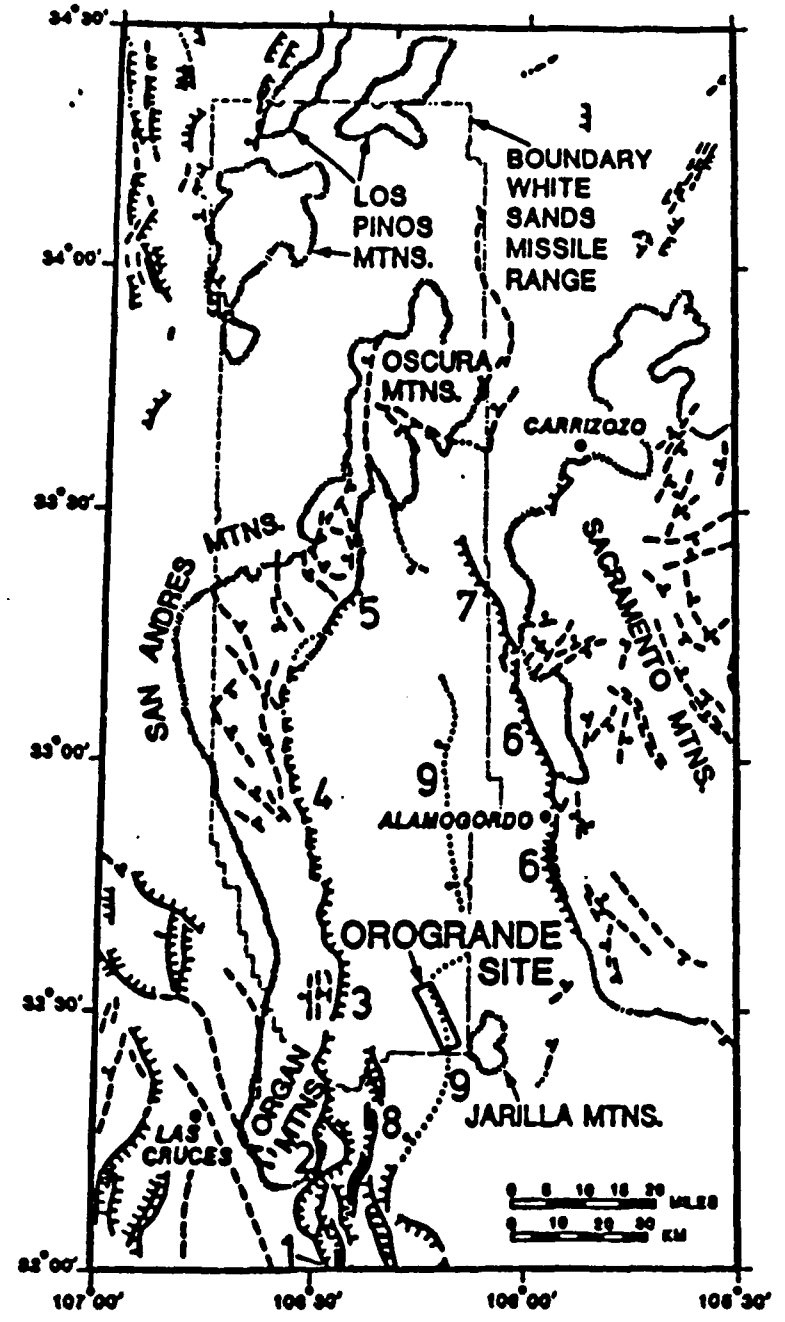

LEGEND

FAULT (LESS THAN 1,000,000 YEARS); HACHURE DOWNTHROWN INCLUDES HOLOCENE MOVEMENT

FAULT, CONCEALED, AGE UNKNOWN; BALL DOWNTHROWN

FAULT CUTS LATE PLIOCENE OR EARLY PLEISTOCENE (1-4 MILLION YEARS); BALL DOWNTHROWN

Figure 2. Faults near WSMR

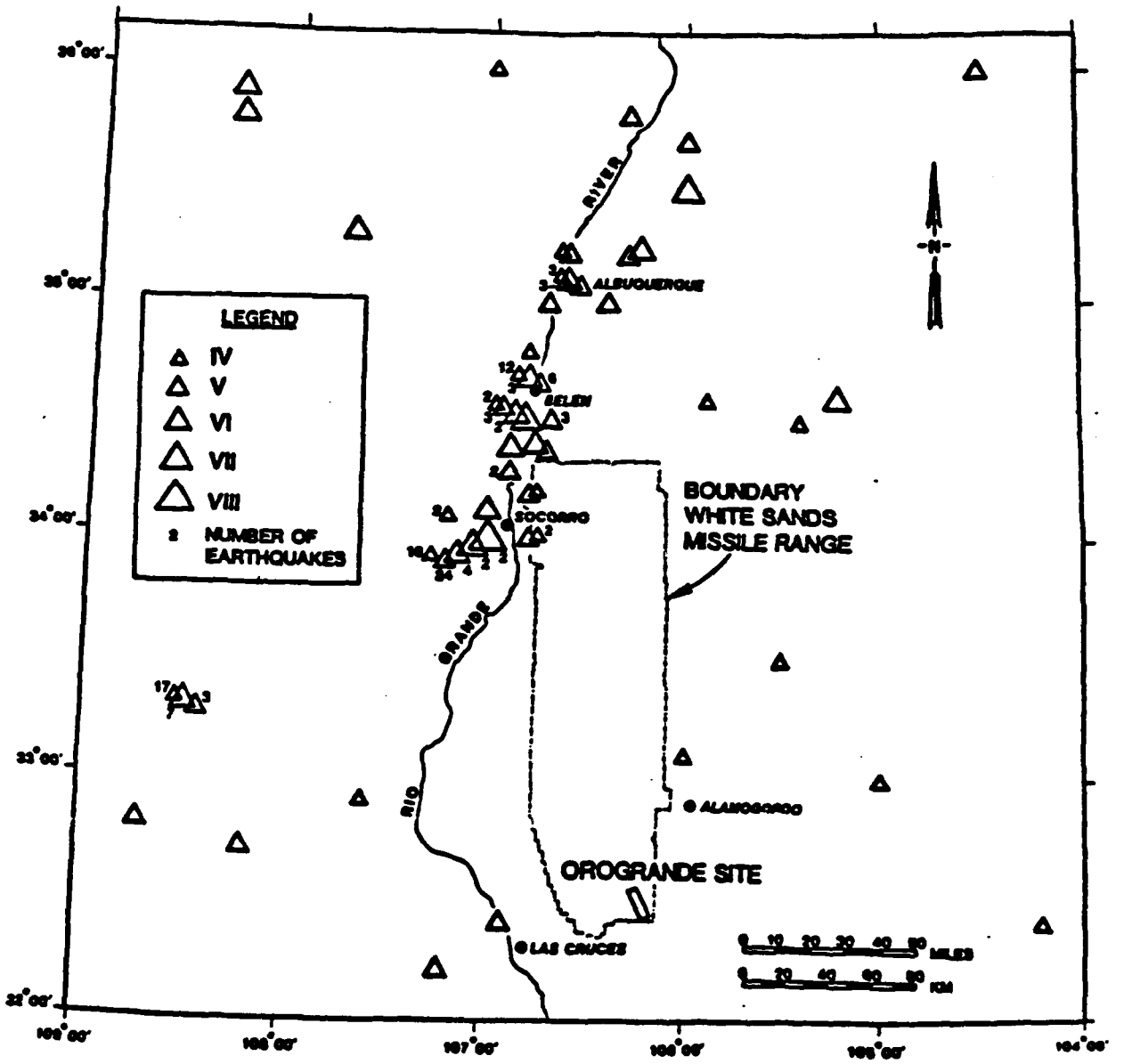

Figure 3. Distribution of earthquakes of intensity MM IV and greater between 1849 and 1980

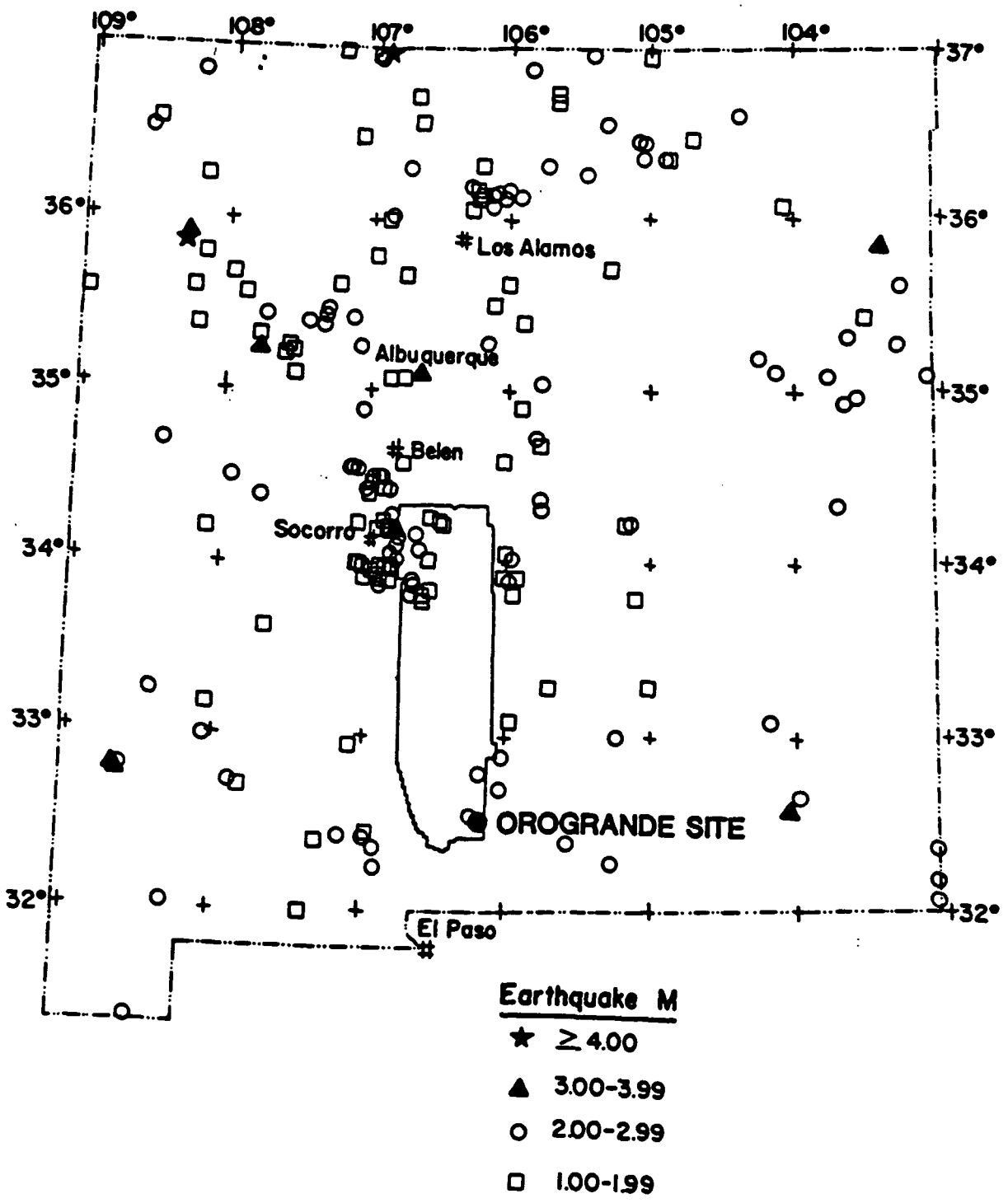

Figure 4. Instrumentally recorded earthquakes occurring within New Mexico between 1962 and 1977

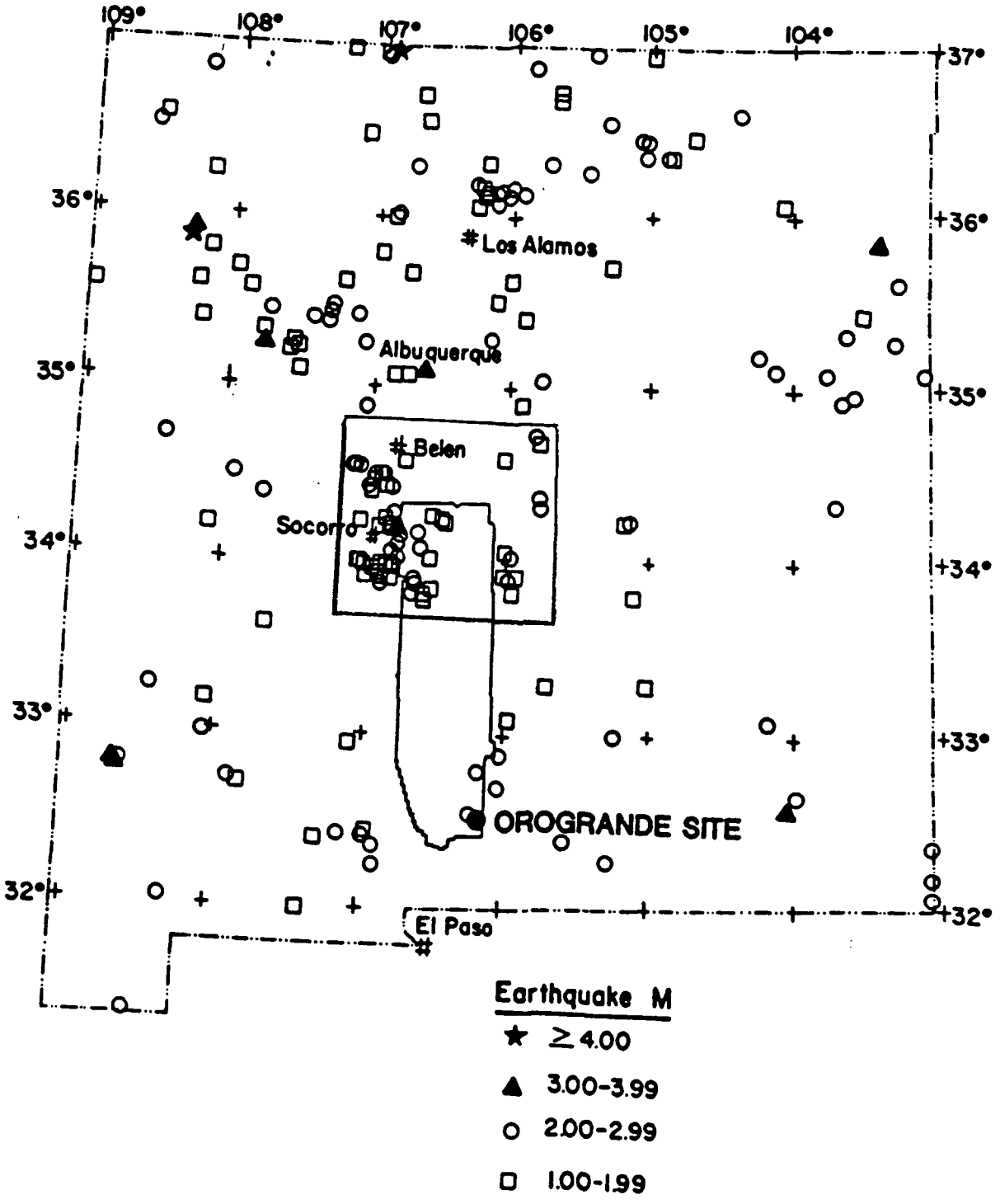

Figure 5. Case 1 source zones determined from data from the historic and instrumentally recorded data

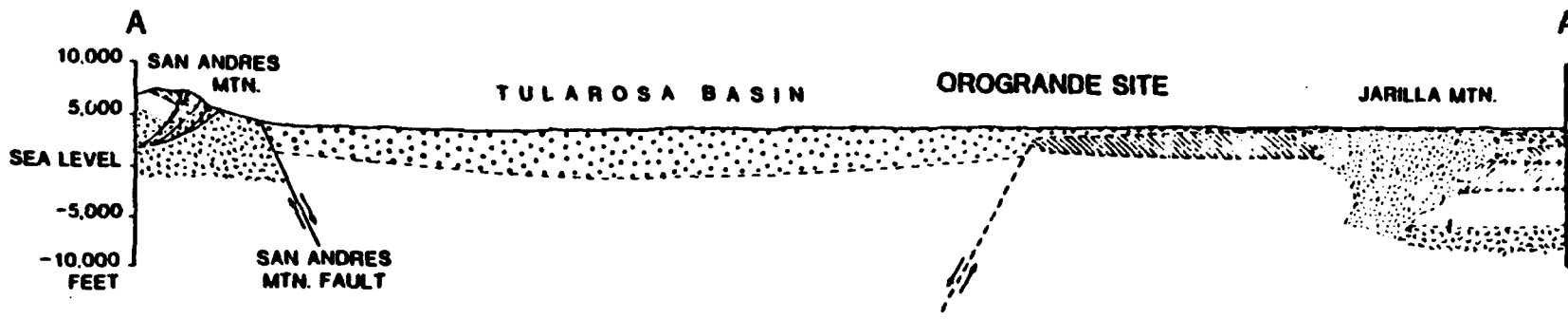

Symbol	Description
	Tertiary - Quaternary Sediments; primarily Quaternary alluvium
	Tertiary Volcanics
	Permian Sedimentary Rocks; mostly marine
	Pennsylvanian Sedimentary Rocks; mostly limestone and shale
	Mississippian - Cambrian Sedimentary Rocks; sandstone, shale, limestone and dolomite
	Metamorphic and Granitic Rocks

Figure 6. Cross section A-A' showing subsurface fault

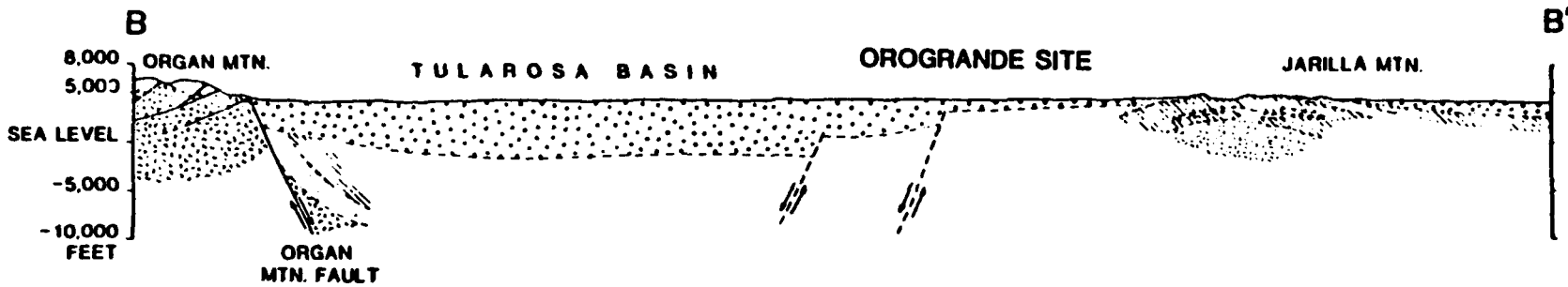

Symbol	Description
	Tertiary - Quaternary Sediments; primarily Quaternary alluvium
	Tertiary Volcanics
	Permian Sedimentary Rocks; mostly marine
	Pennsylvanian Sedimentary Rocks; mostly limestone and shale
	Mississippian - Cambrian Sedimentary Rocks; sandstone, shale, limestone and dolomite
	Metamorphic and Granitic Rocks

Figure 7. Cross section B-B' showing subsurface fault beneath Orogrande site

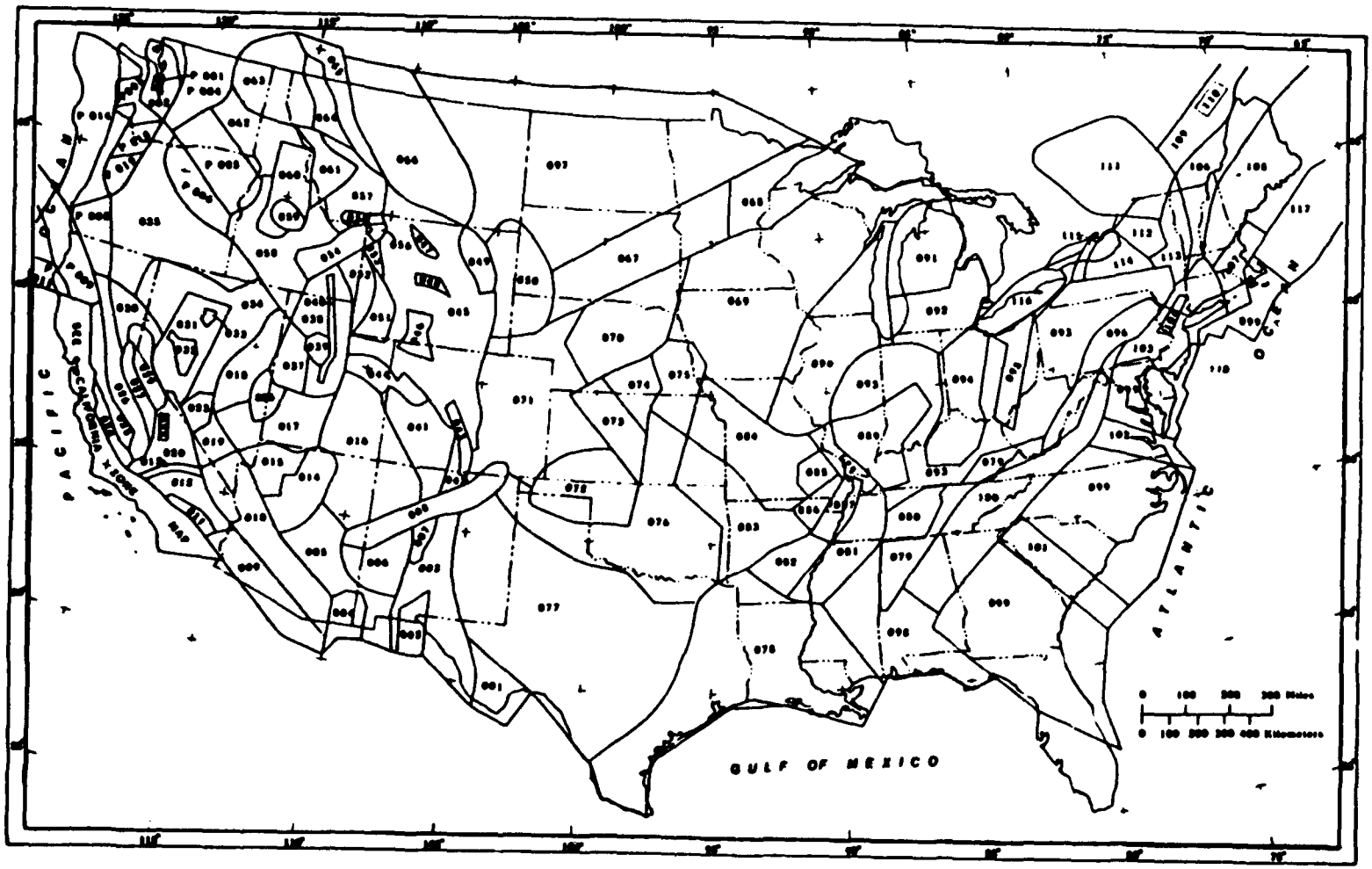

Figure 8. National map of source zones (Algermissen et al. (1982))

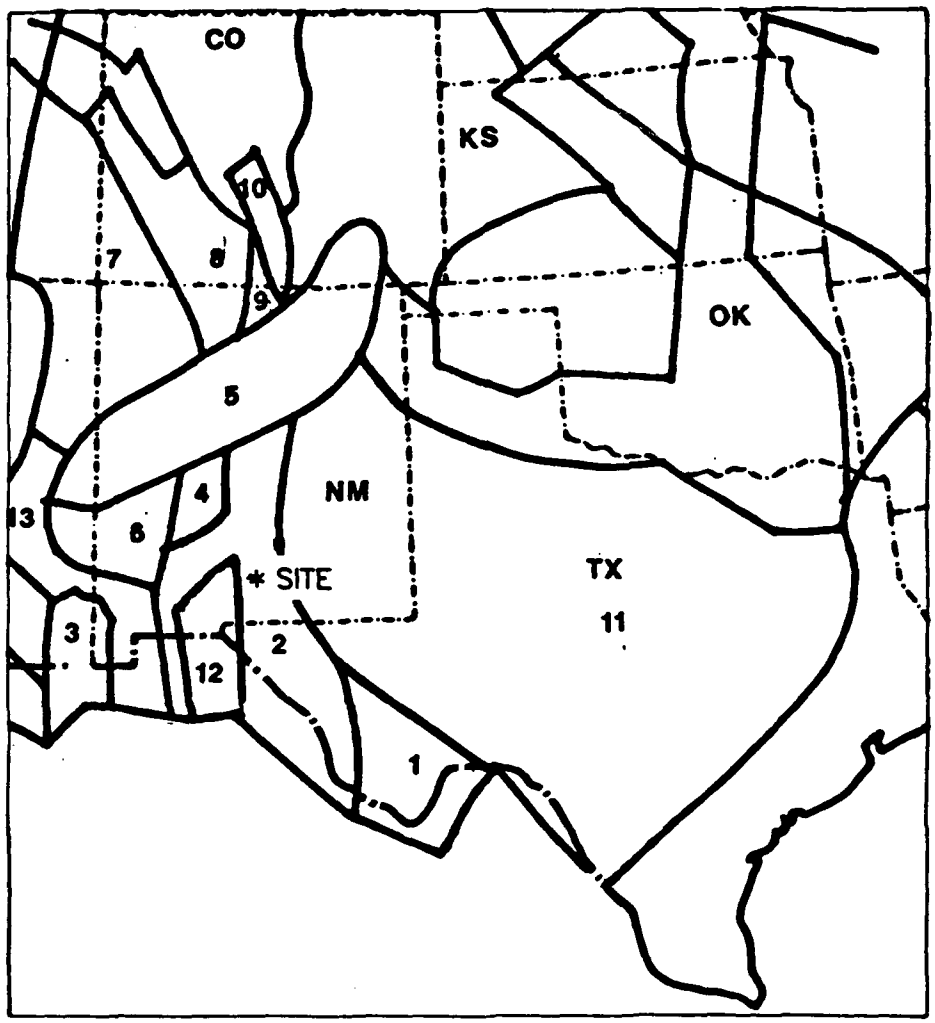

ALGERMISSEN'S SOURCE ZONES
USED FOR THIS STUDY

Figure 9. Case 2 source zones (Algermissen et al. (1982))

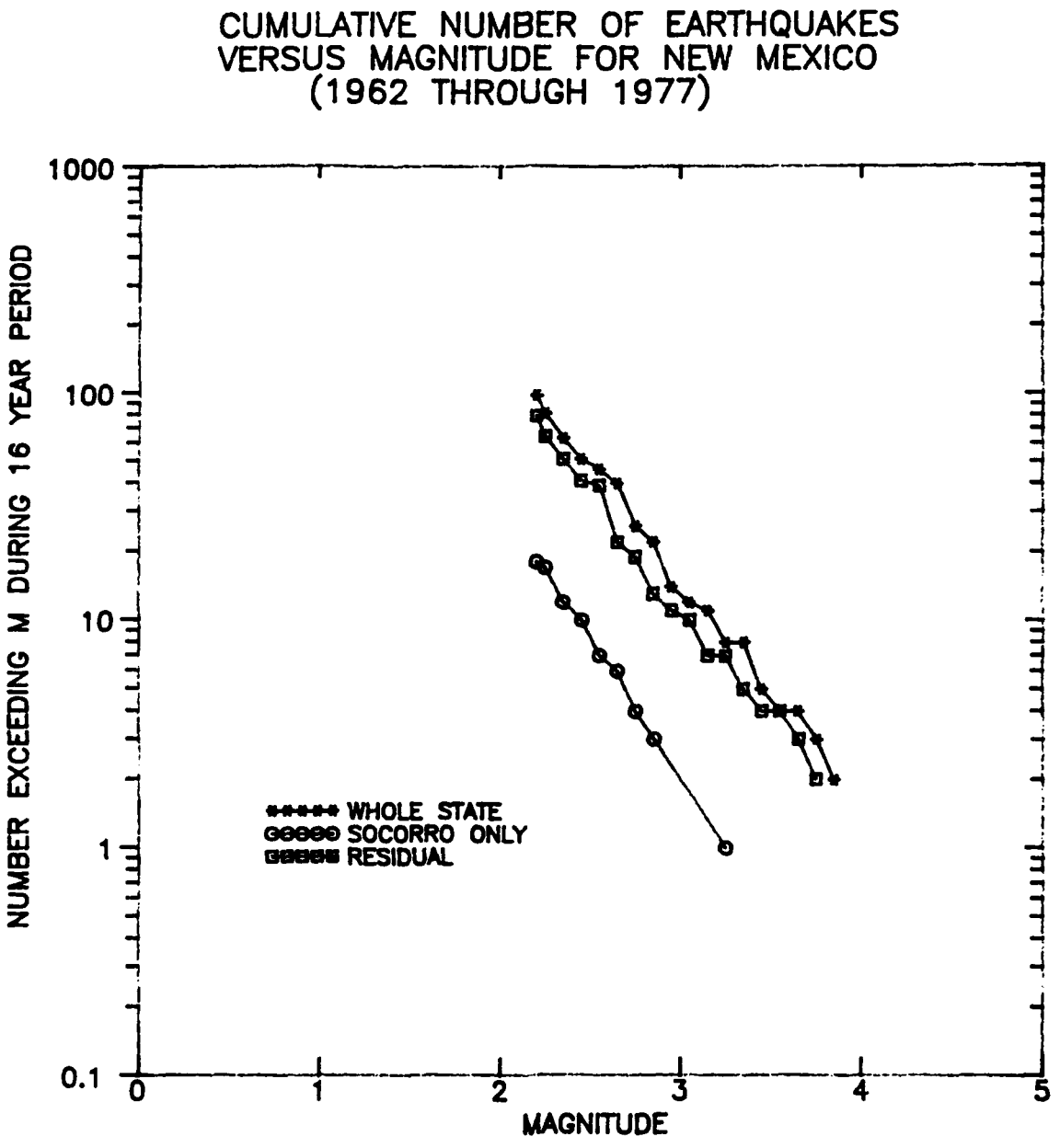

Figure 10. Cumulative number of earthquakes from instrumentally recorded strong motion records (1962-1977)

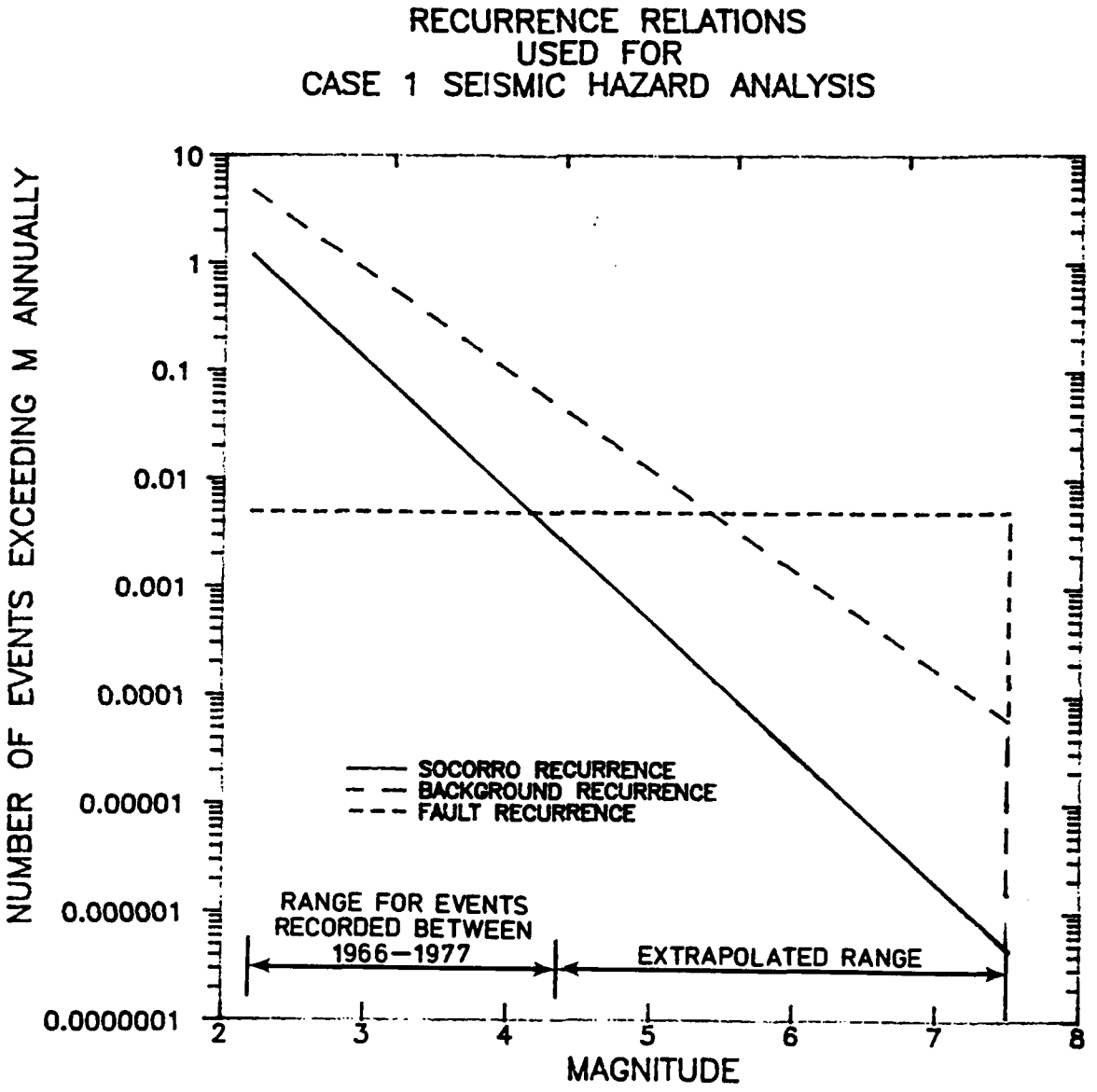

Figure 11. Recurrence relationships for Case 1 sources

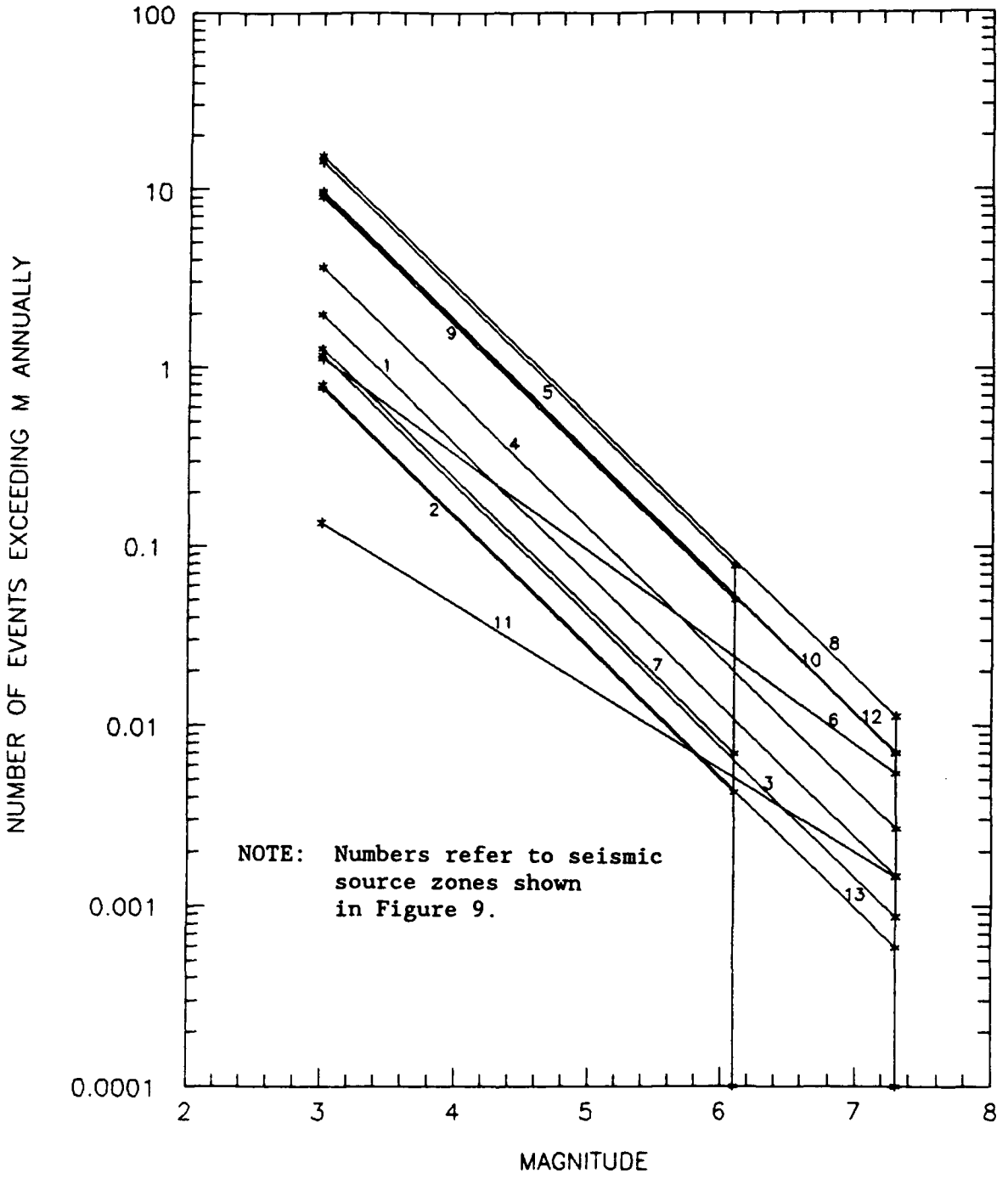

Figure 12. Recurrence relationships for Case 2 sources

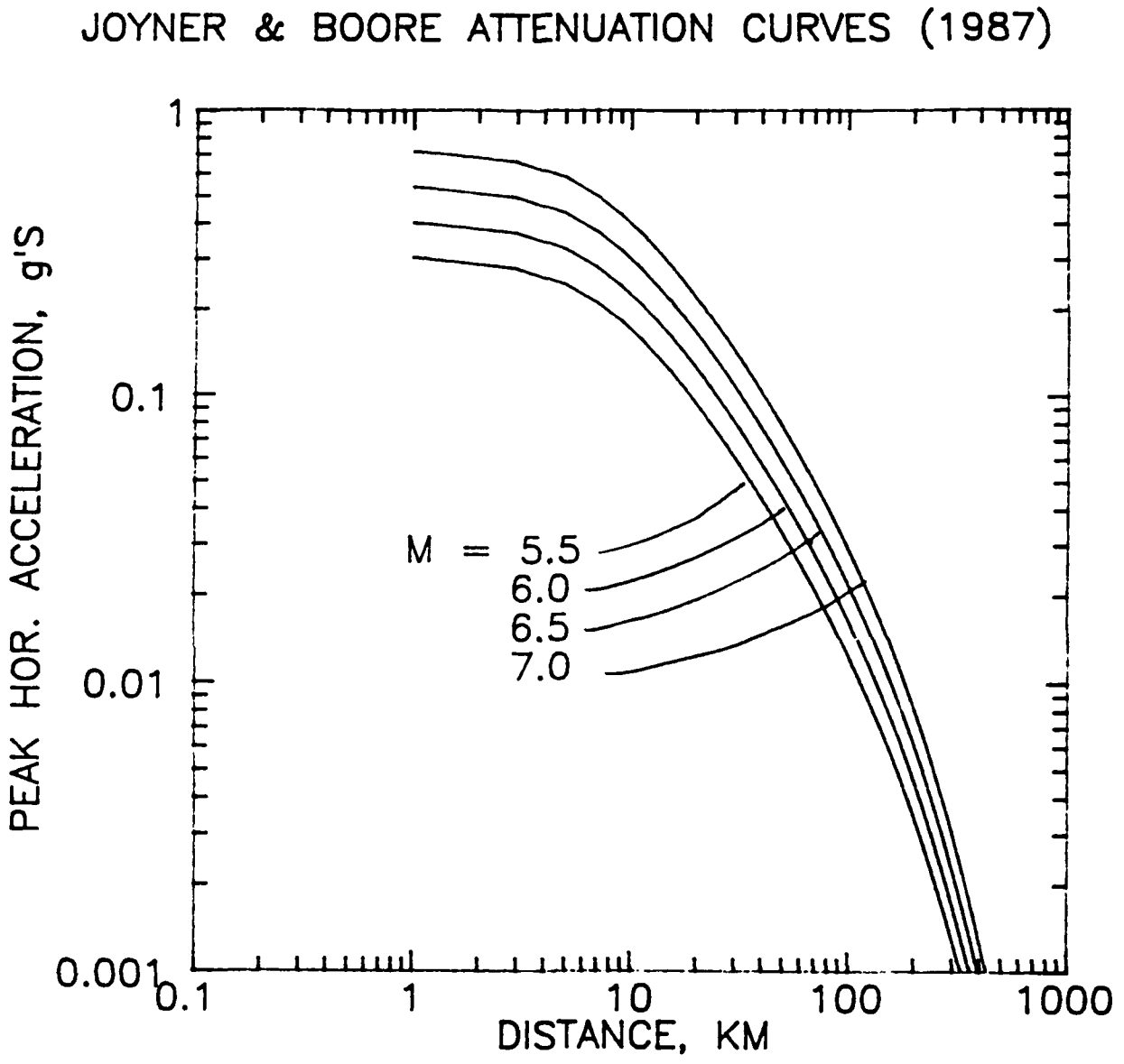

Figure 13. Attenuation functions for peak acceleration used in this study (After Joyner and Boore (1987))

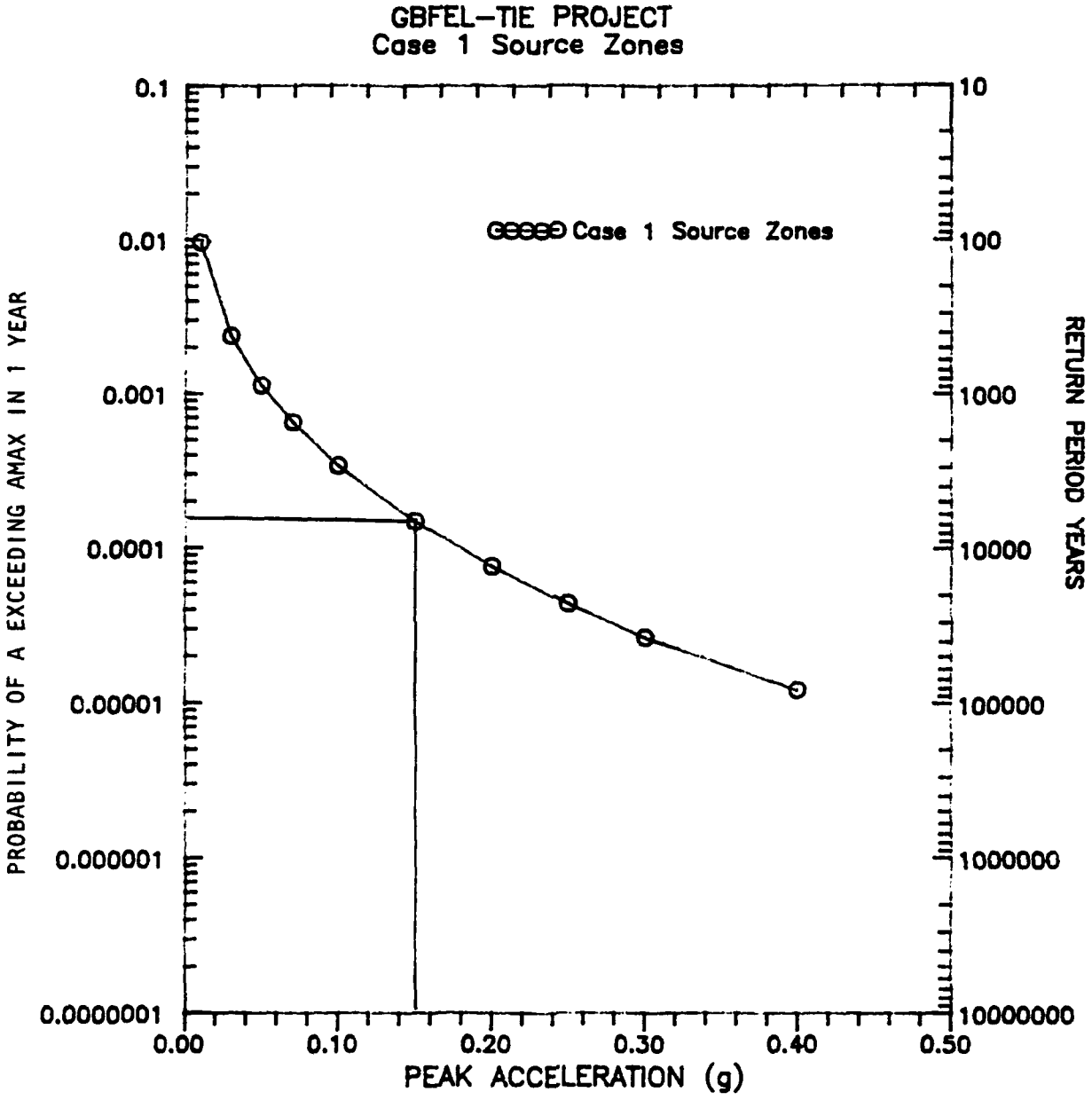

Figure 14. CASE 1 - Seismic hazard analysis results

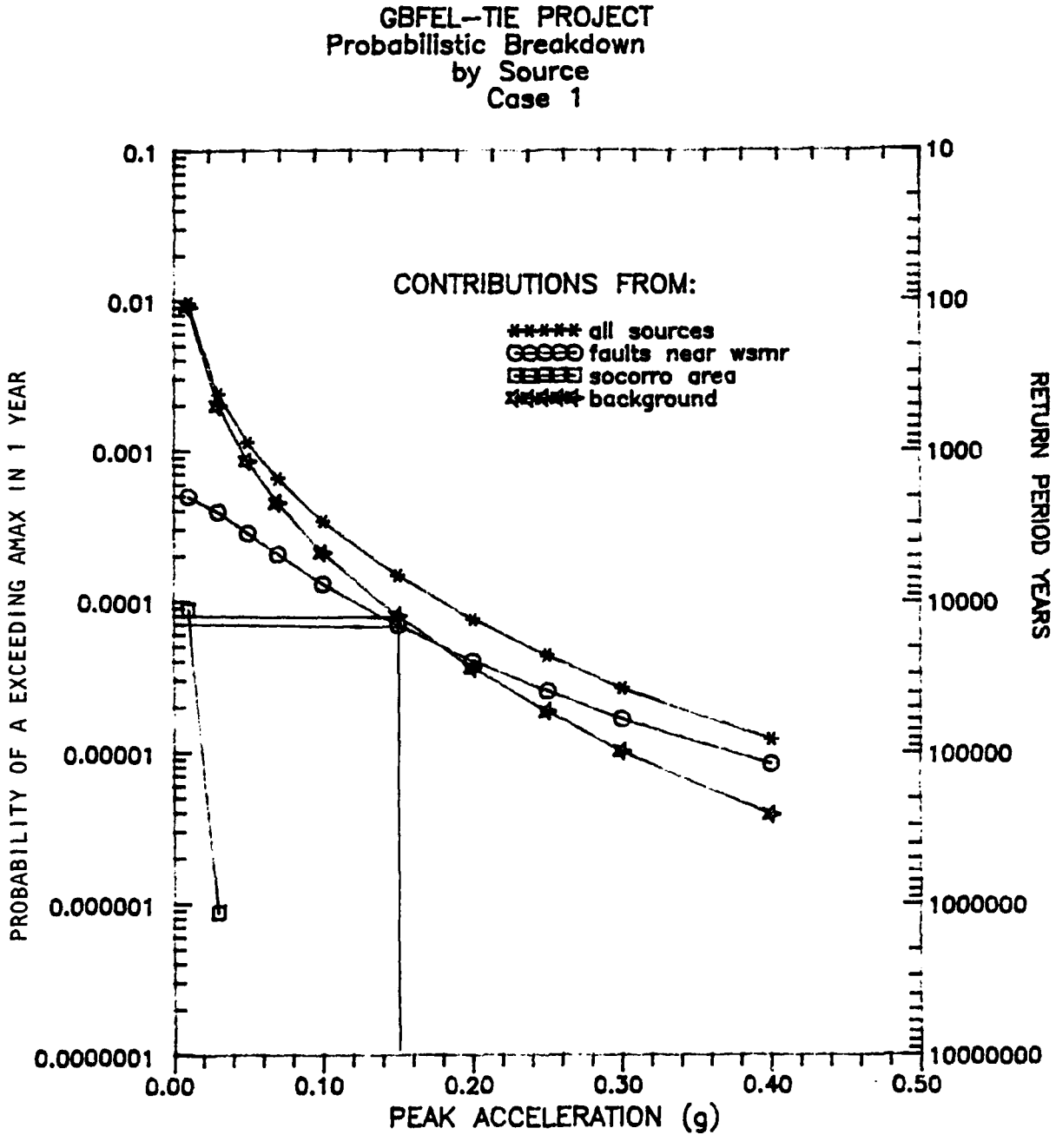

Figure 15. CASE 1 - Probability breakdown by source

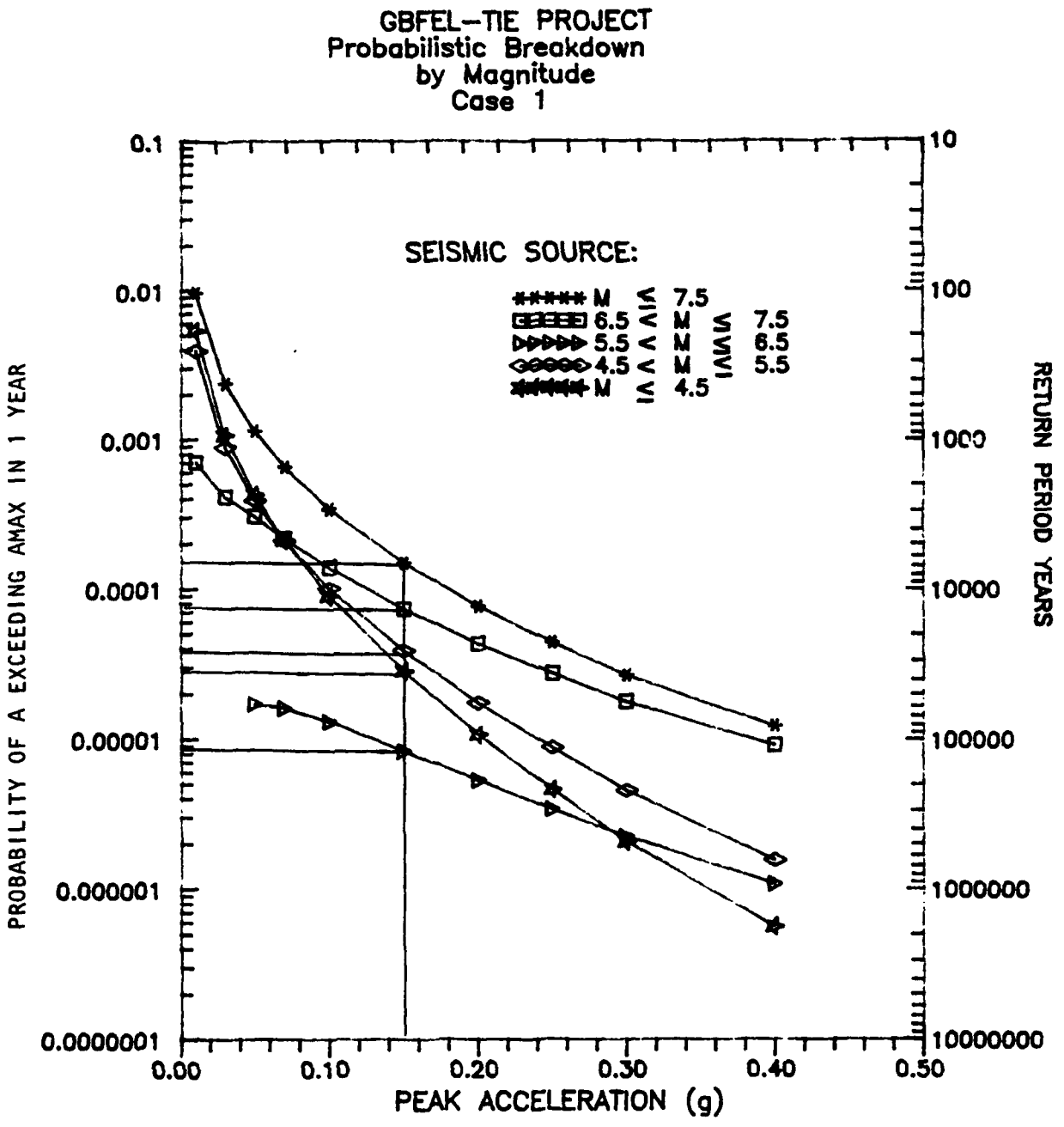

Figure 16. CASE 1 - Magnitude-source breakdown

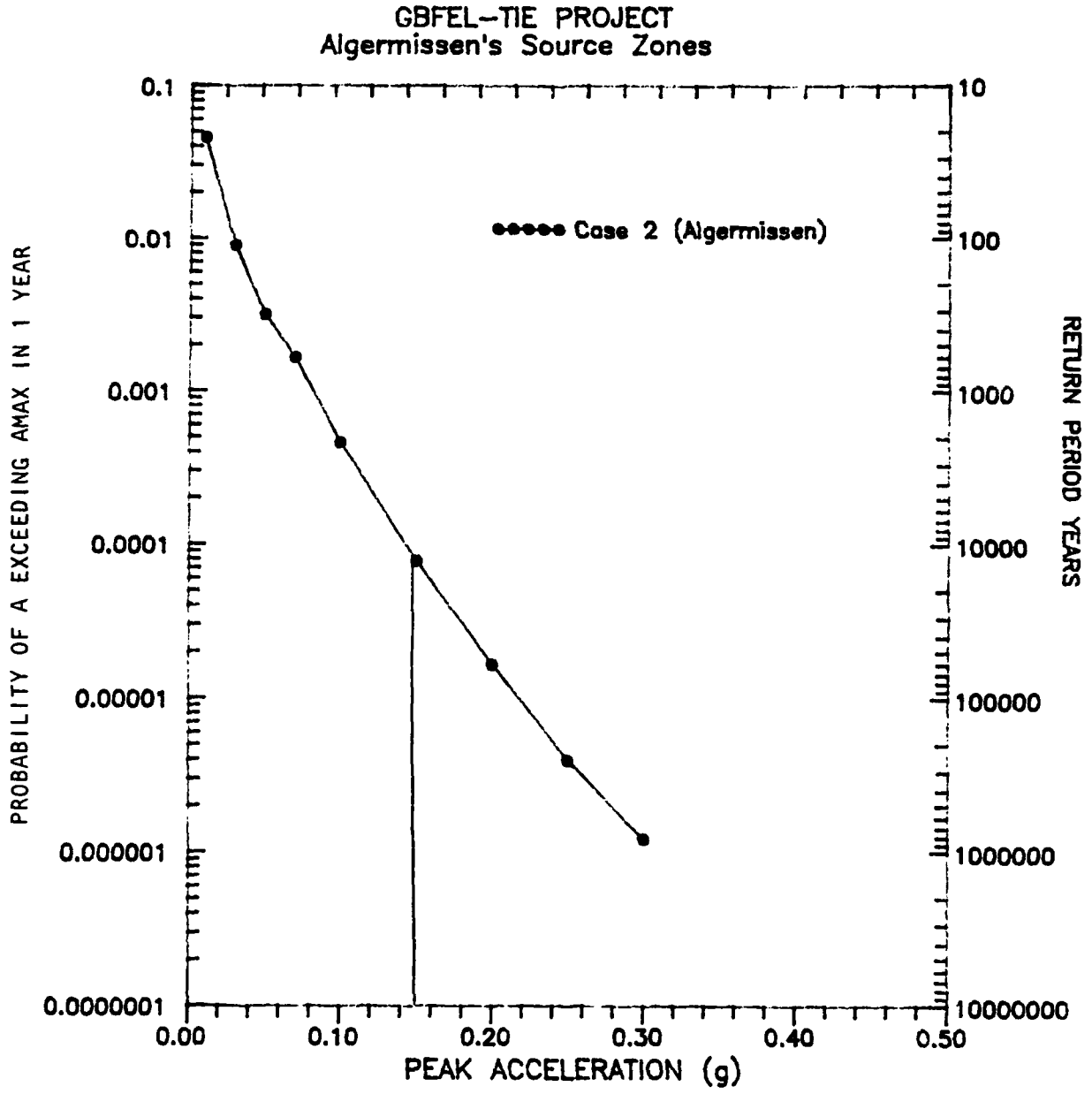

Figure 17. CASE 2 - Seismic hazard analysis results (Algermissen et al. (1982))

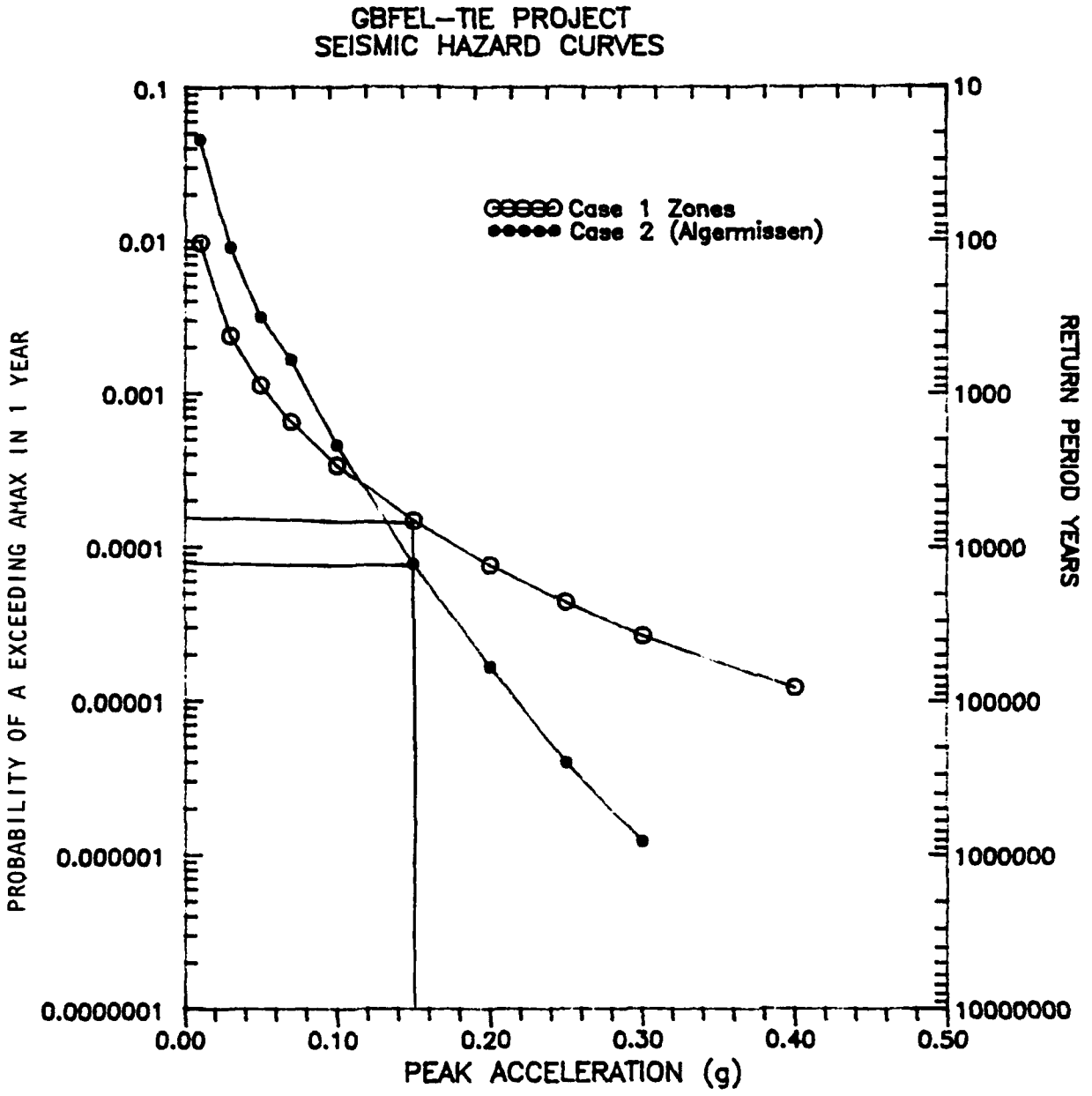

Figure 18. Comparison of CASE 1 and CASE 2 results

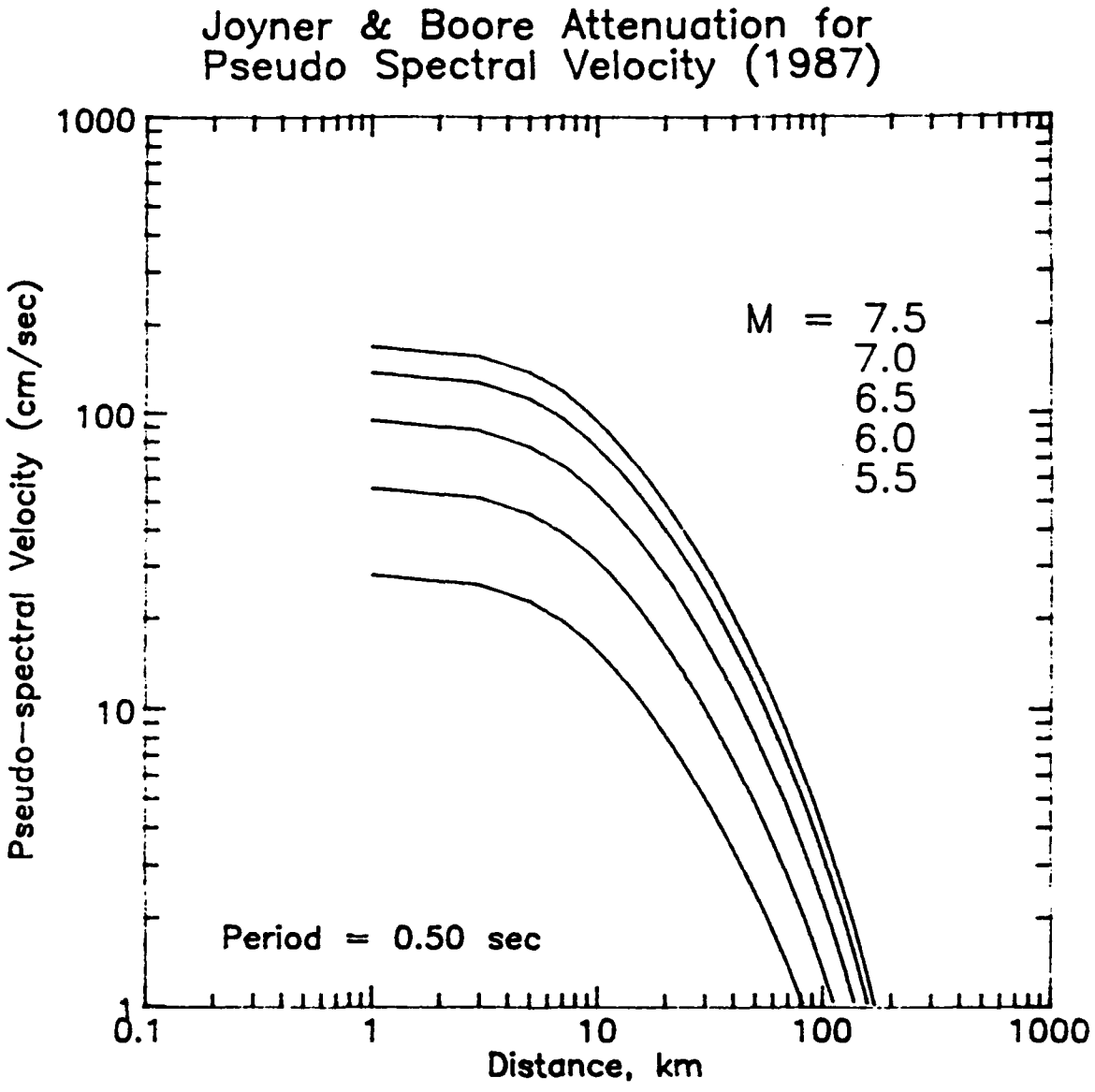

Figure 19. Attenuation of spectral velocity for T = 0.5 sec (After Joyner and Boore (1987))

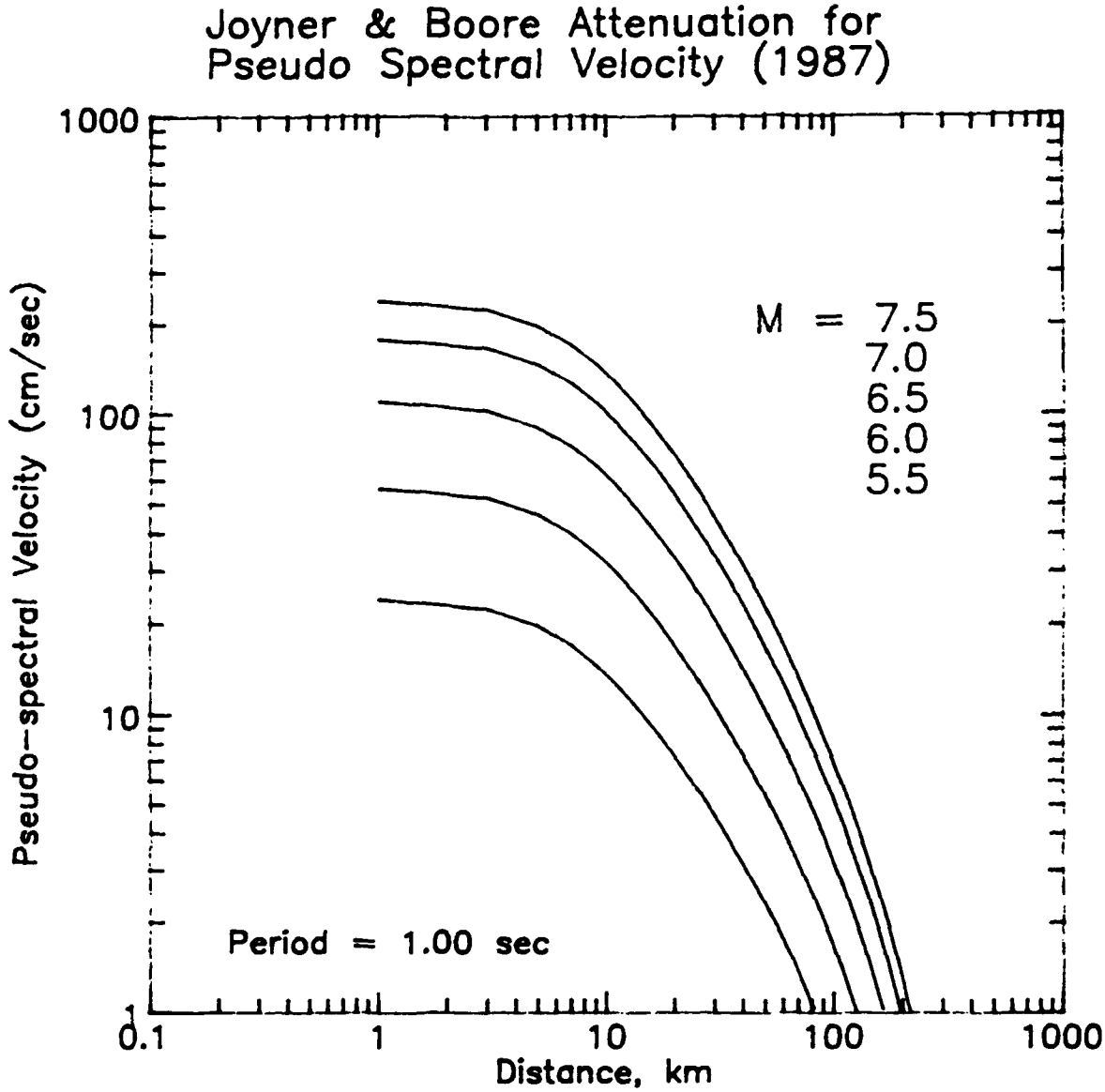

Figure 20. Attenuation of spectral velocity for T = 0.5 sec (Joyner and Boore (1987))

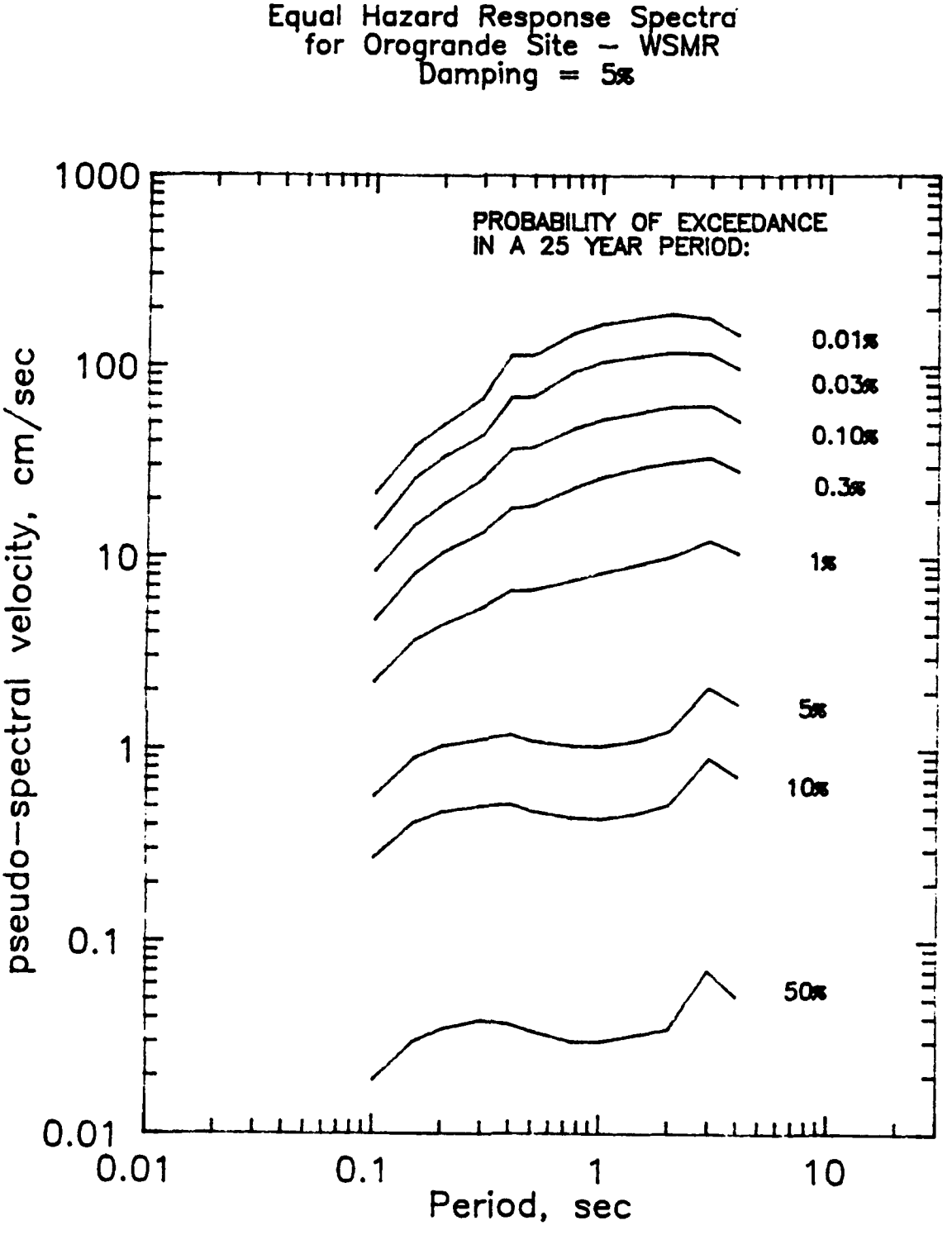

Figure 21. Equal hazard spectra from CASE 1 source zones

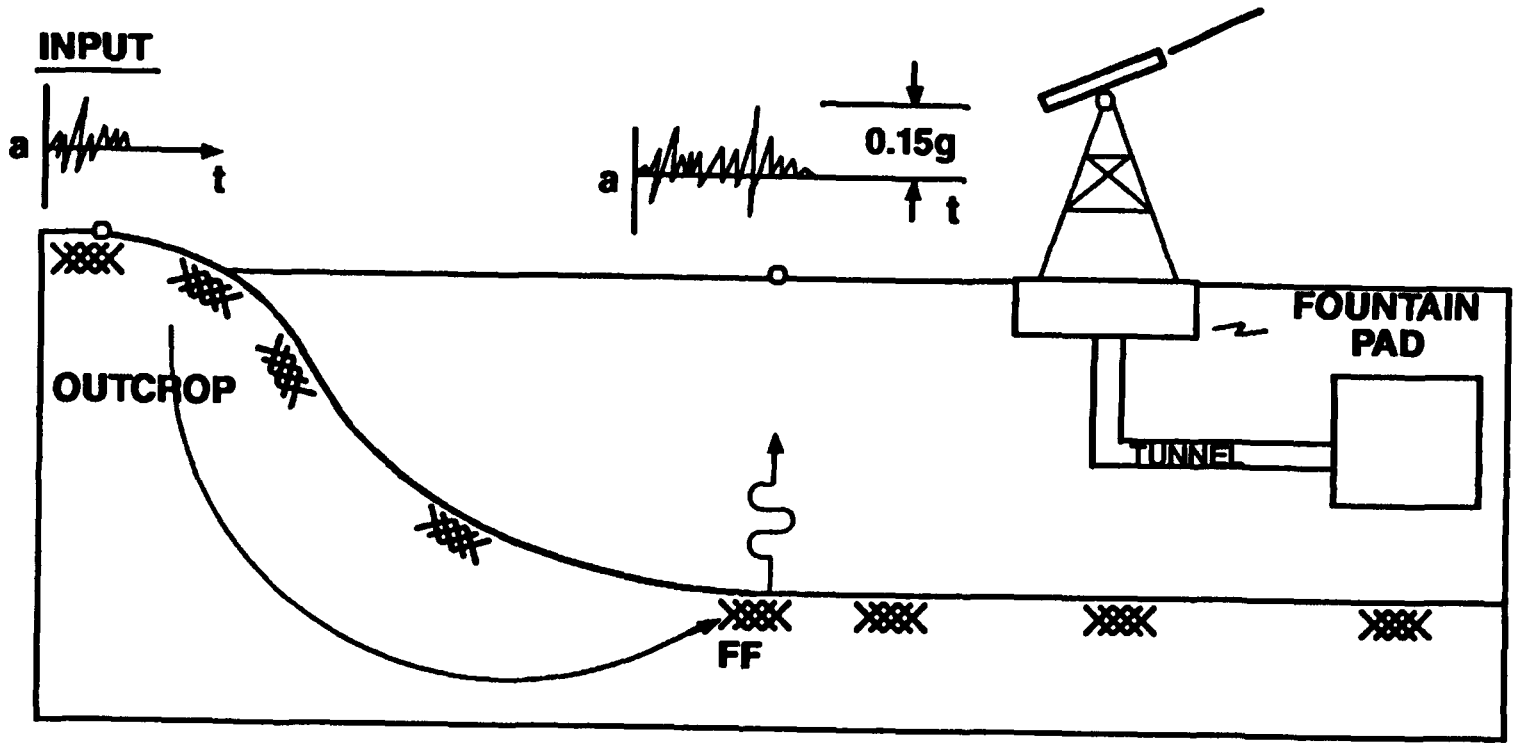

Figure 22. Strategy for development of accelerograms

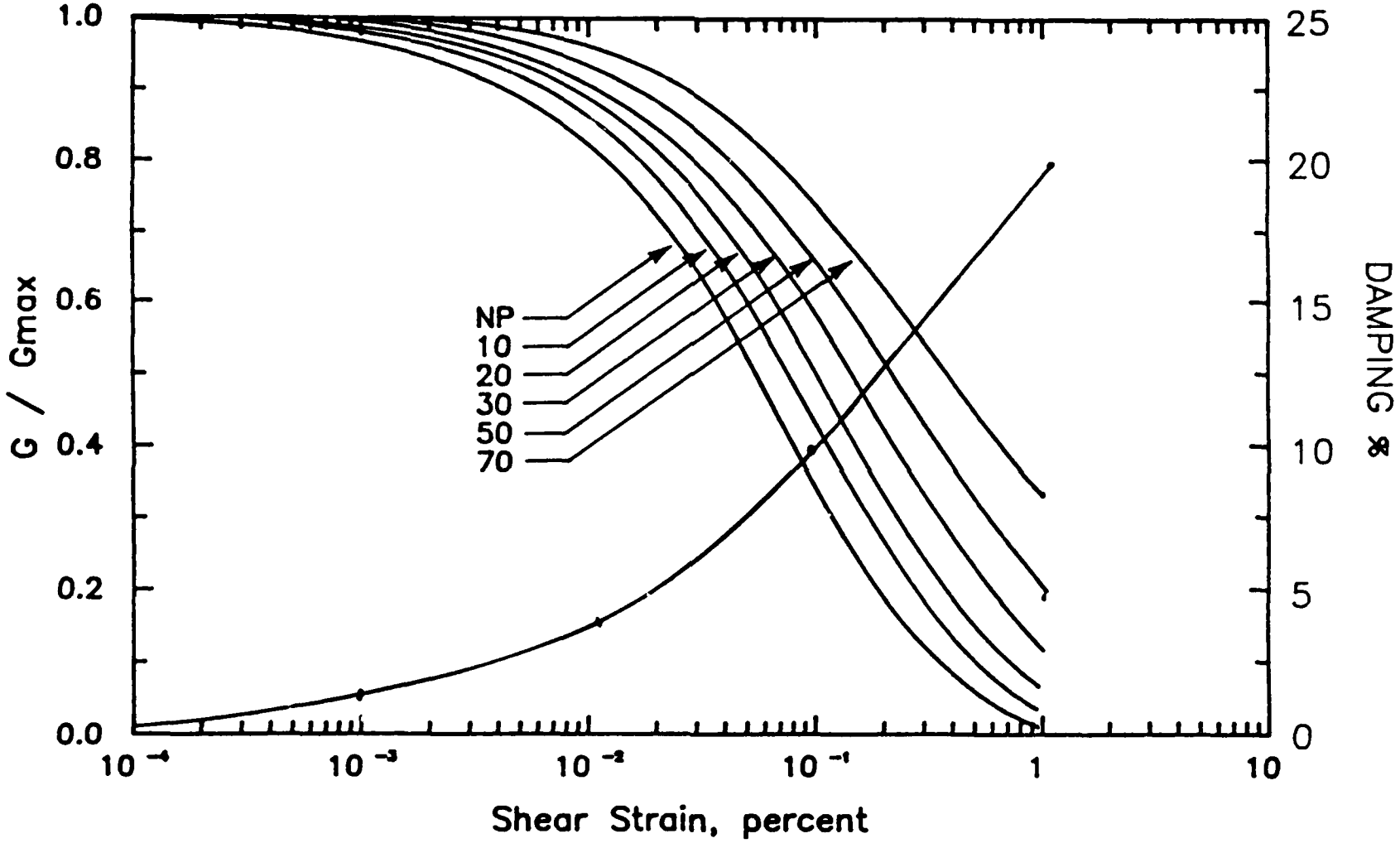

Figure 23. Normalized modulus reduction versus shear strain relationships for laboratory clay samples with different plasticity indices (After Zen et al. (1984))

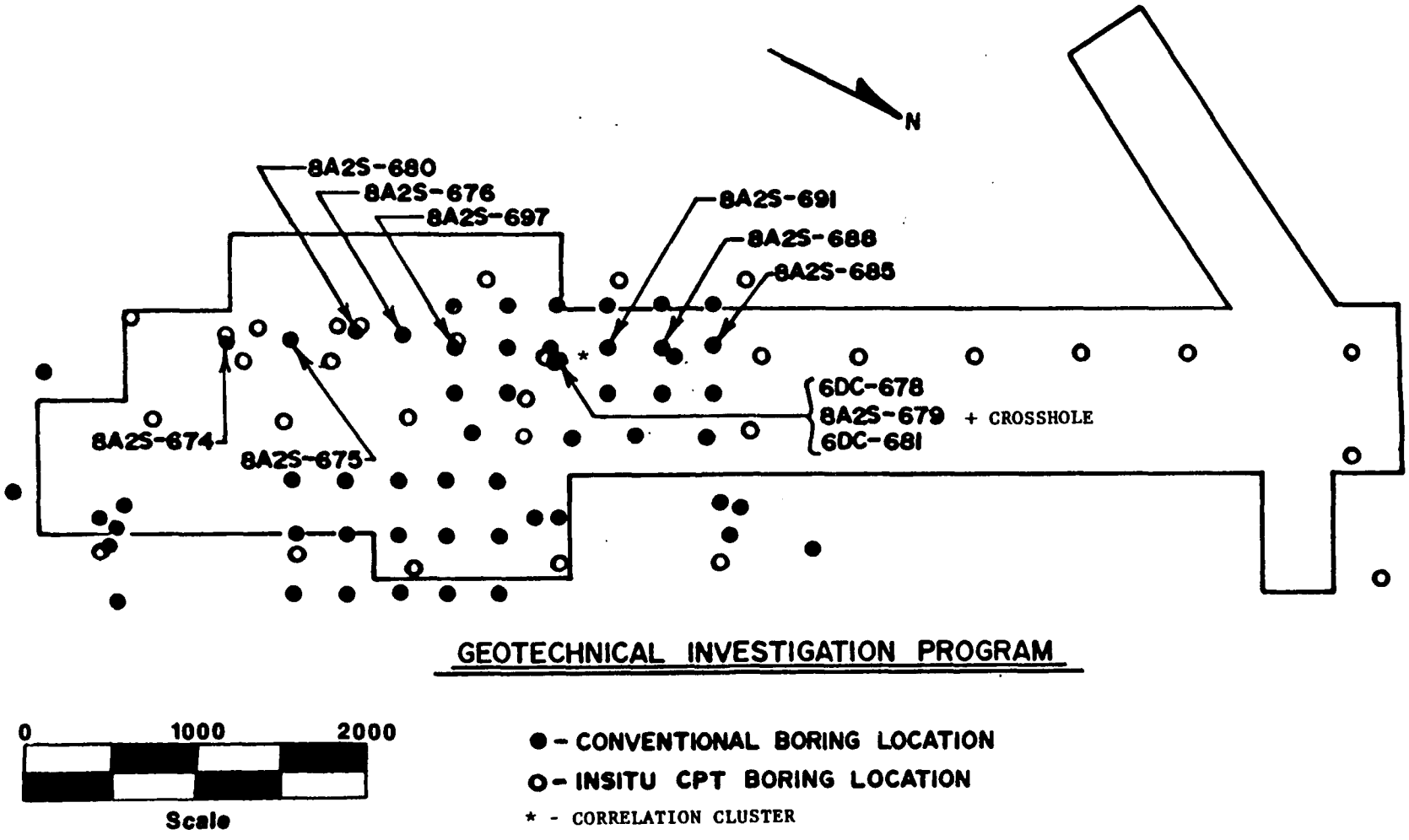

Figure 24. Layout of field investigations

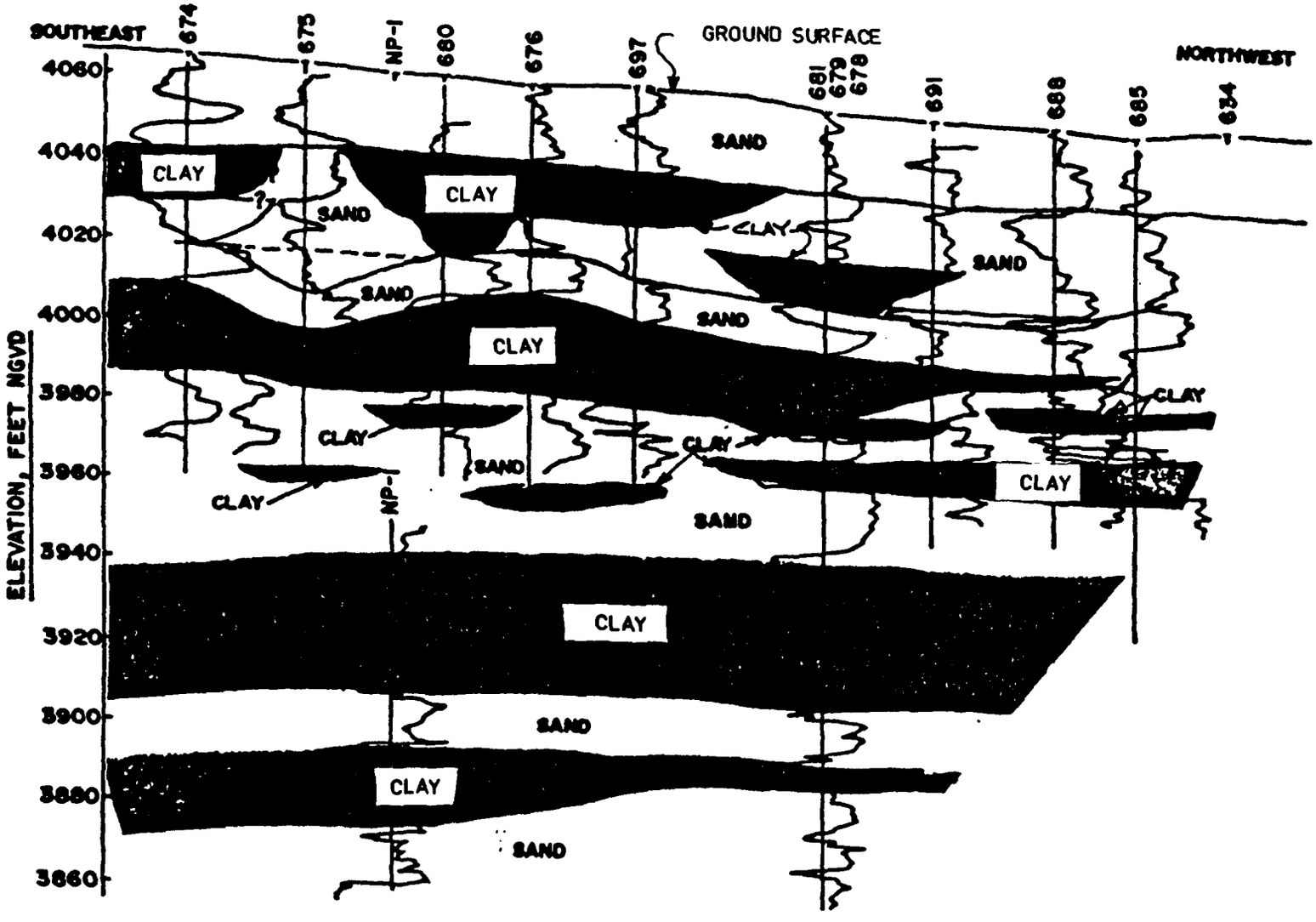

a. Stratigraphic profile of section A-A' (Sheet 1 of 5)

Figure 25. Generalized stratigraphic profiles of five sections

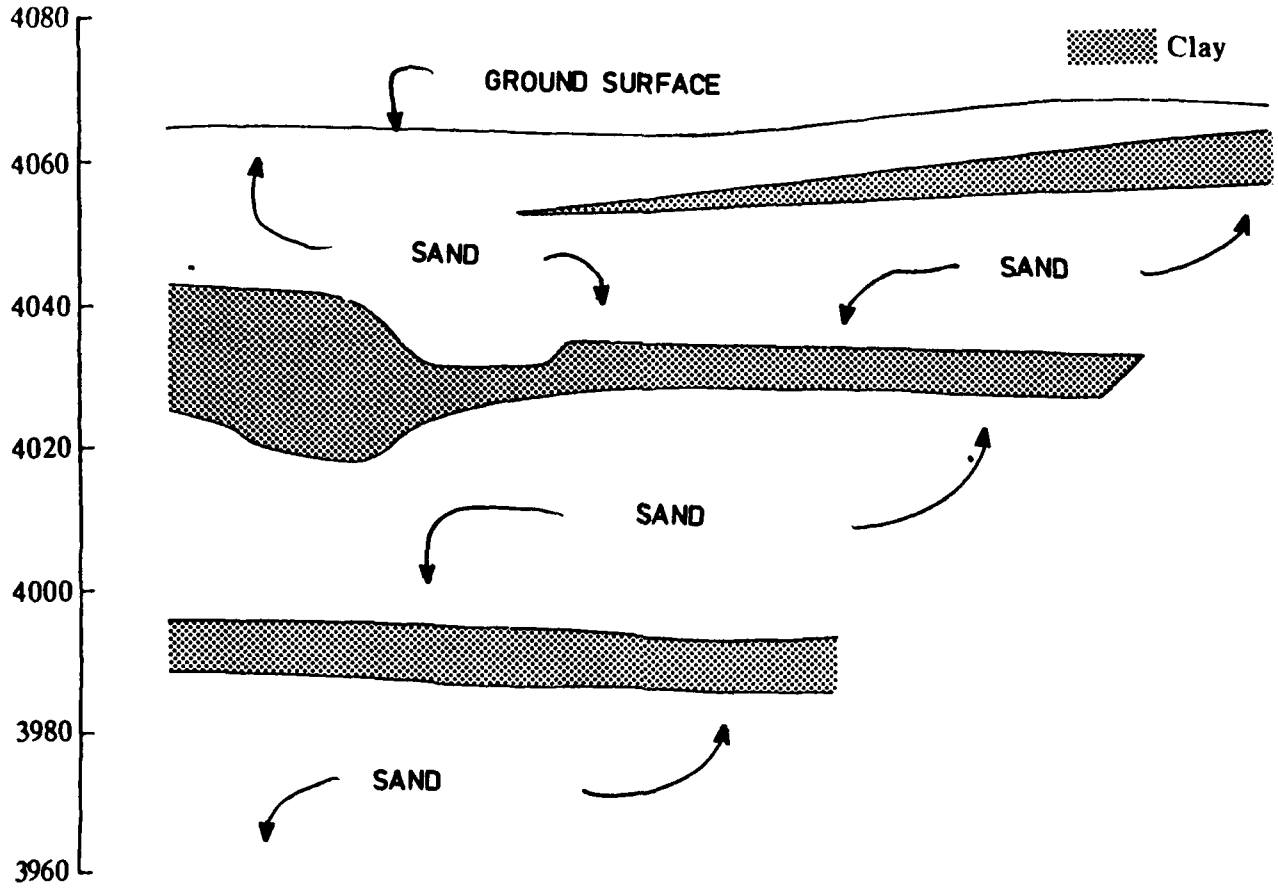

b. Stratigraphic profile of section B-B' (Sheet 2 of 5)

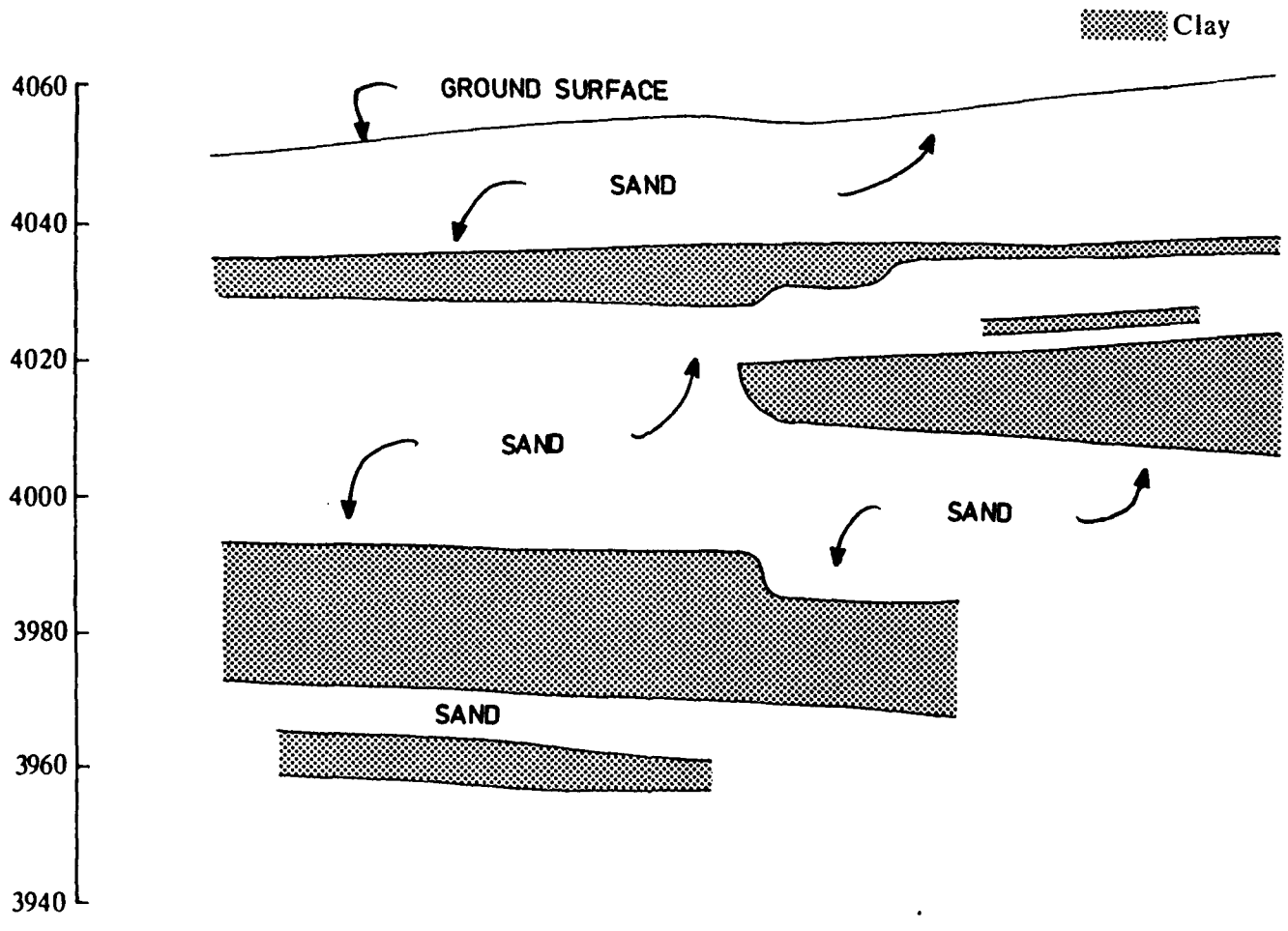

c. Stratigraphic profile of section C-C' (Sheet 3 of 5)

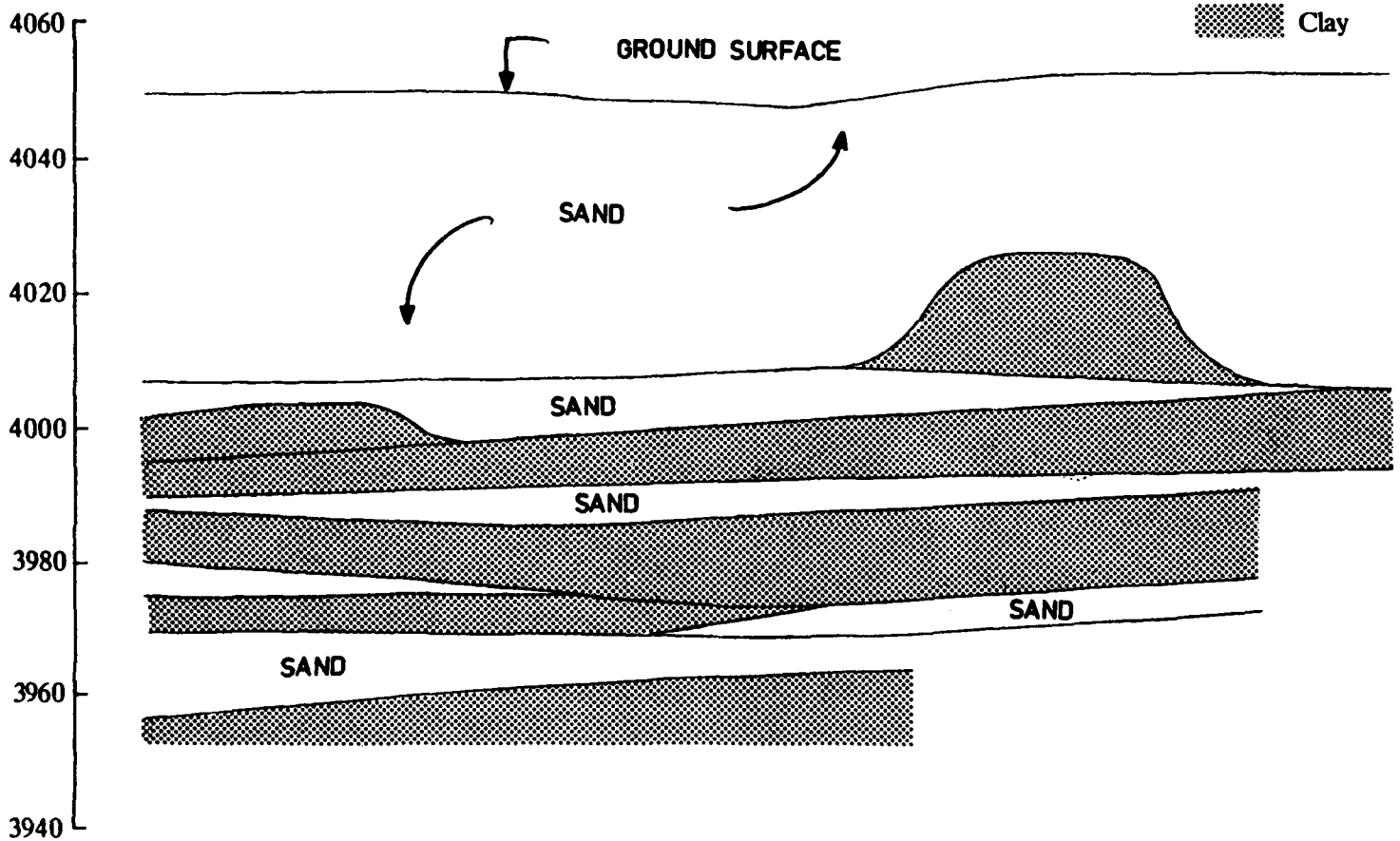

d. Stratigraphic profile of section D-D' (Sheet 4 of 5)

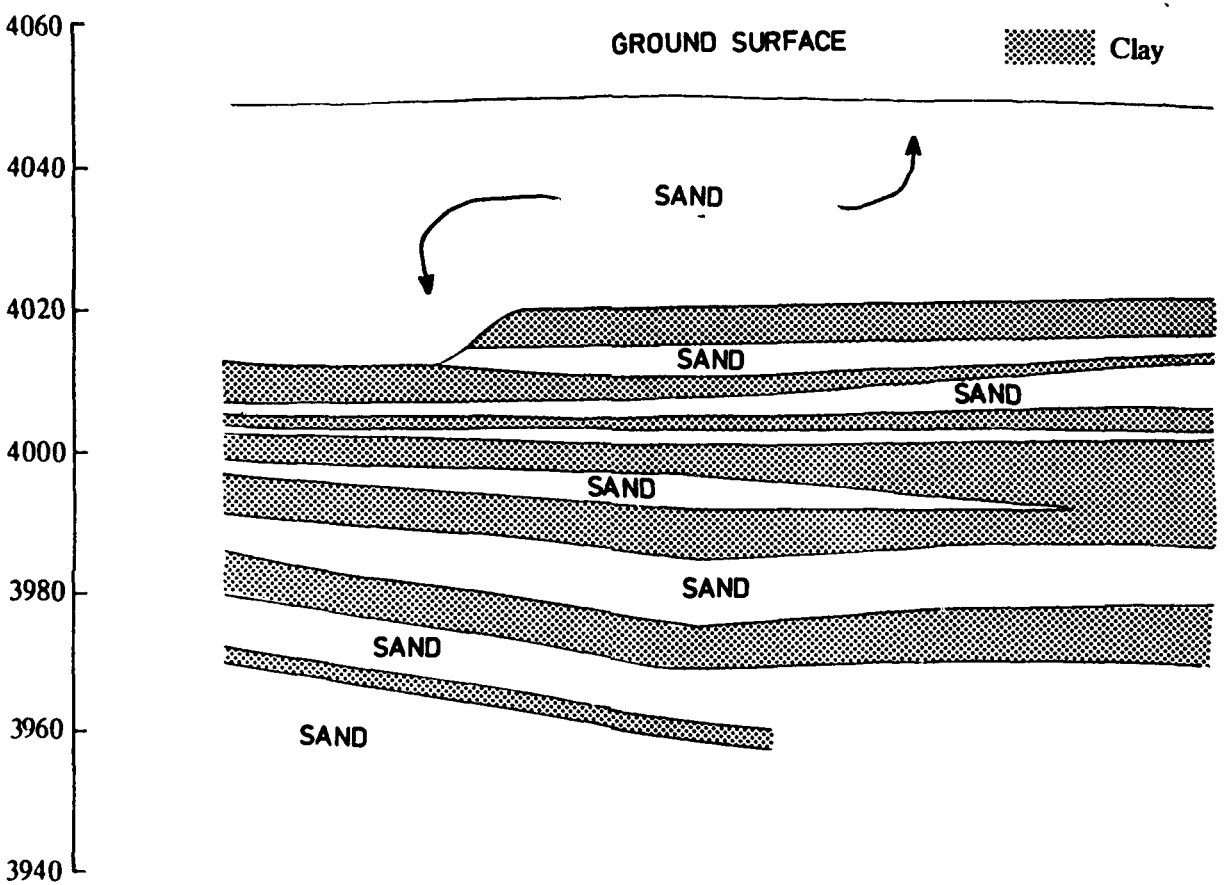

e. Stratigraphic profile of section E-E' (Sheet 5 of 5)

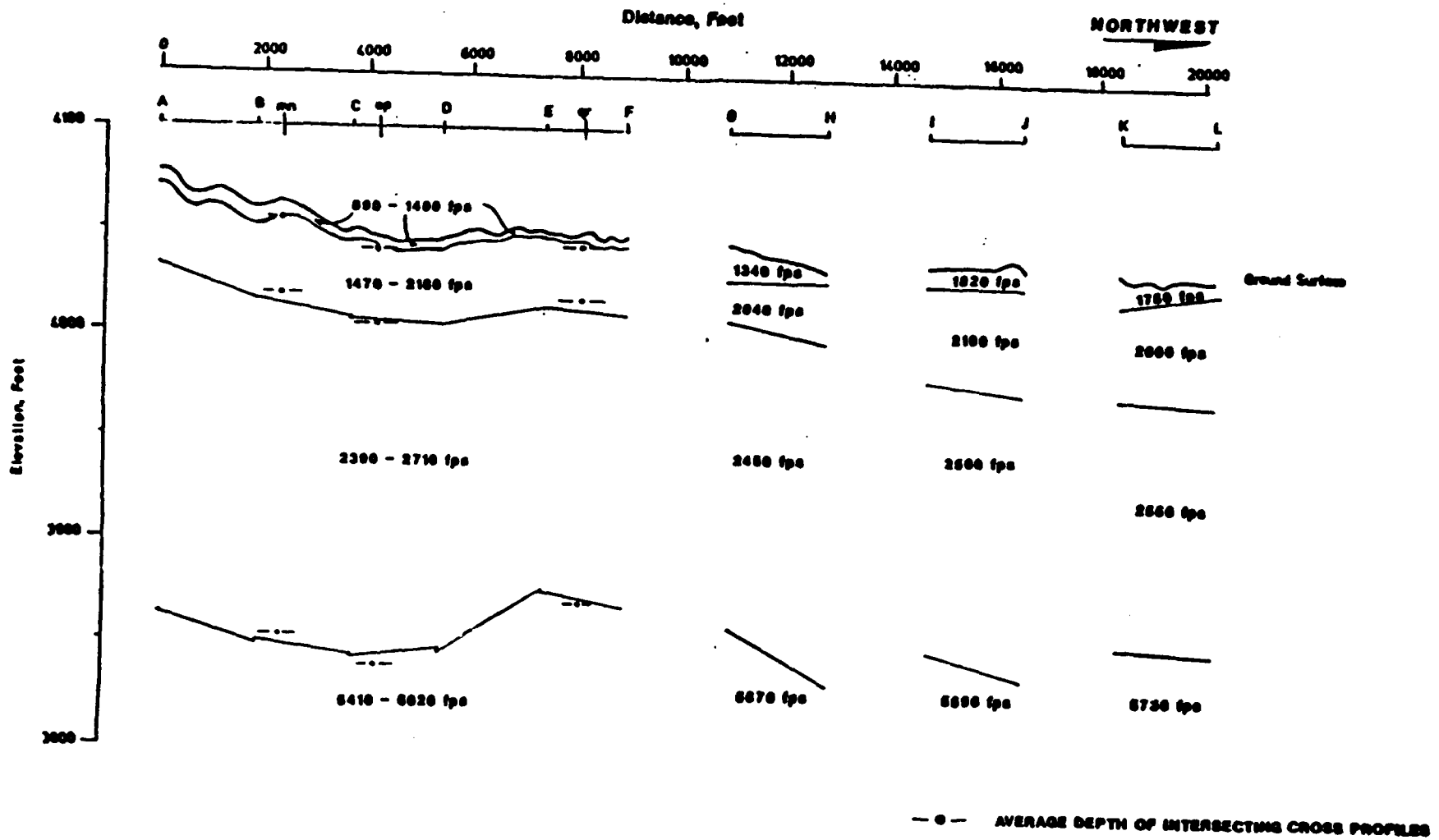

Figure 26. Typical seismic compression wave velocity profile from seismic refraction surveys

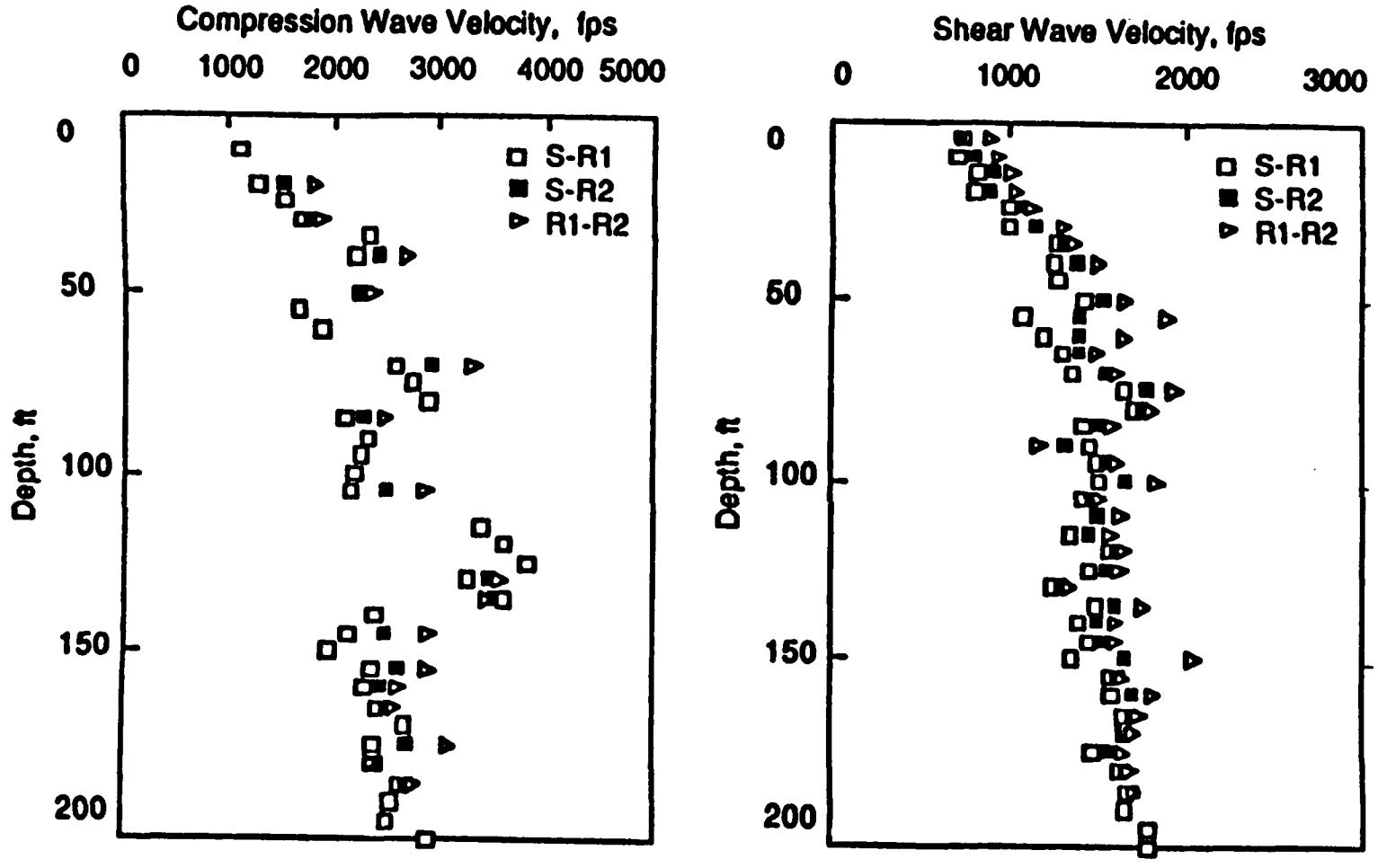

Figure 27. In-situ P- and S-wave velocities profiles from crosshole tests performed at the Orogrande site

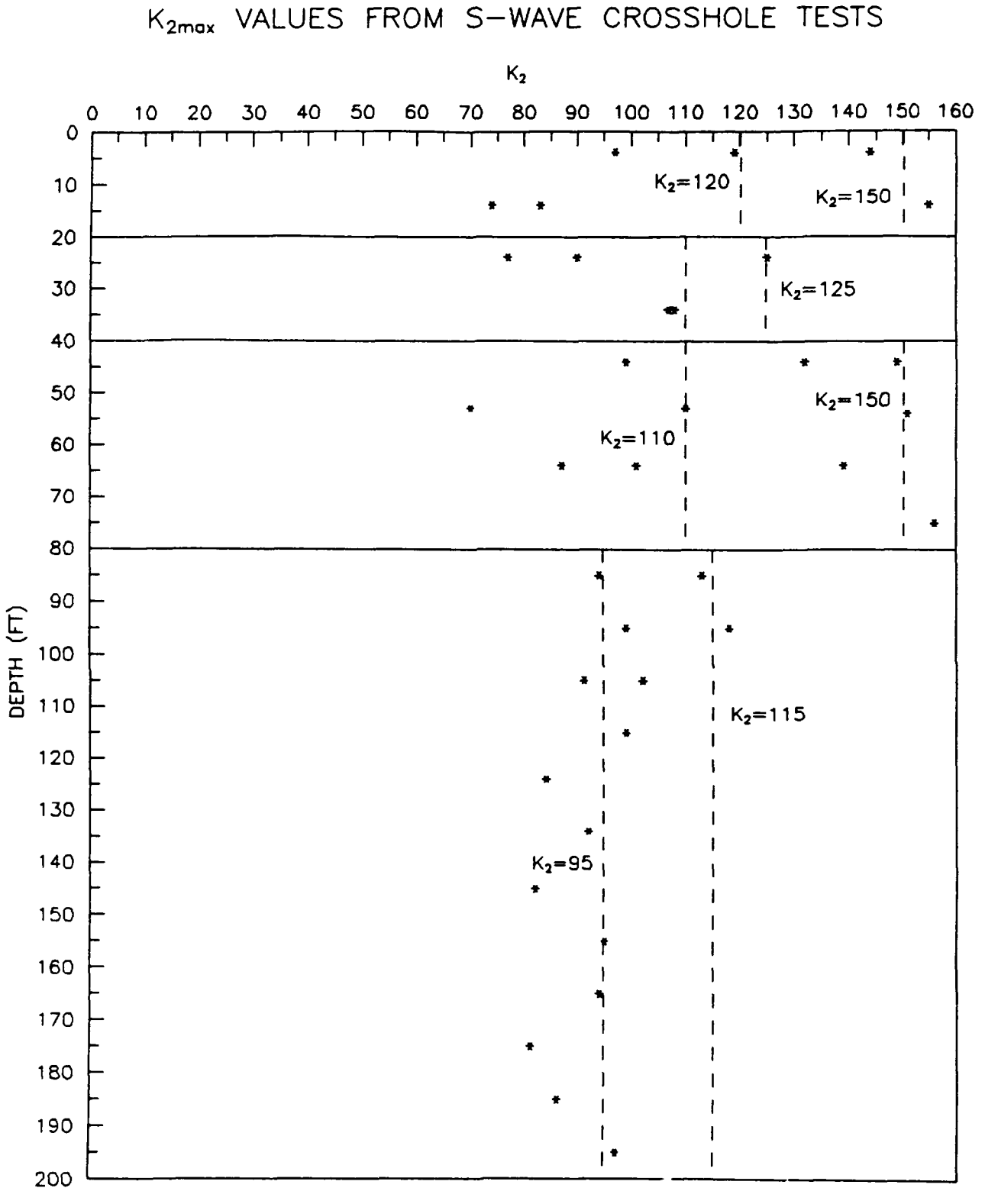

Figure 28. K_{2max} values from crosshole S-wave tests

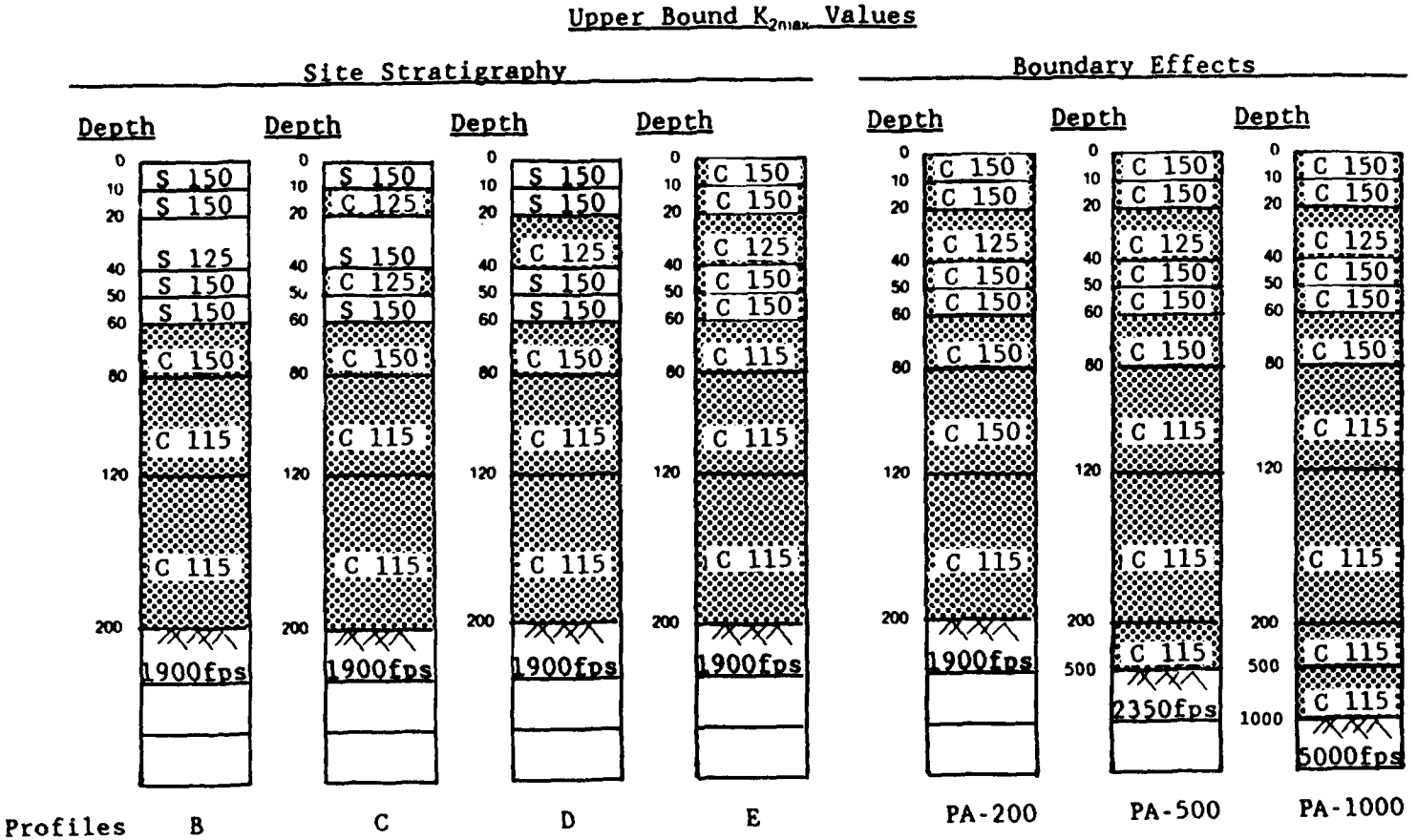

Figure 29. Upper bound stiffness profiles

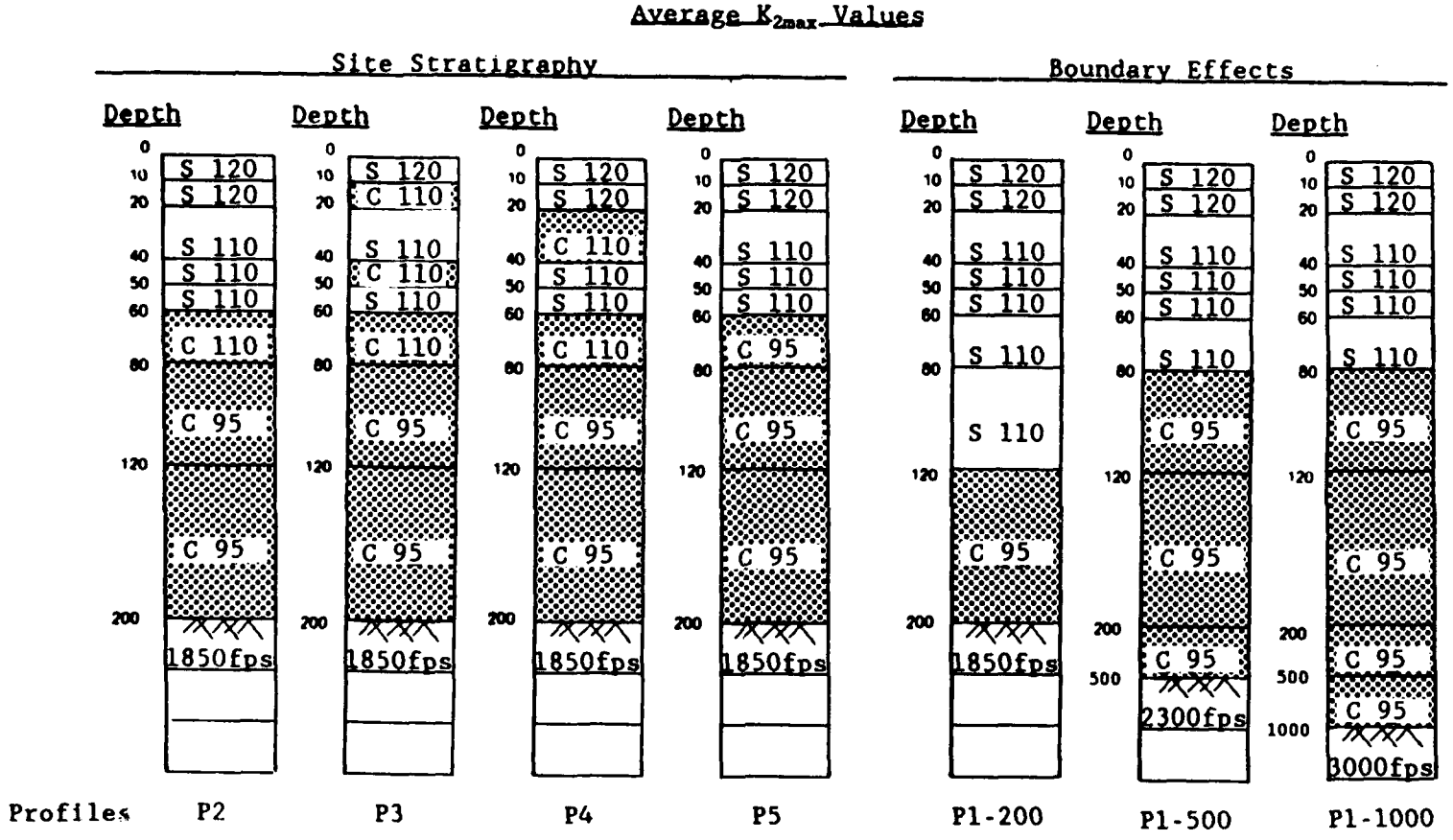

Figure 30. Average stiffness profiles

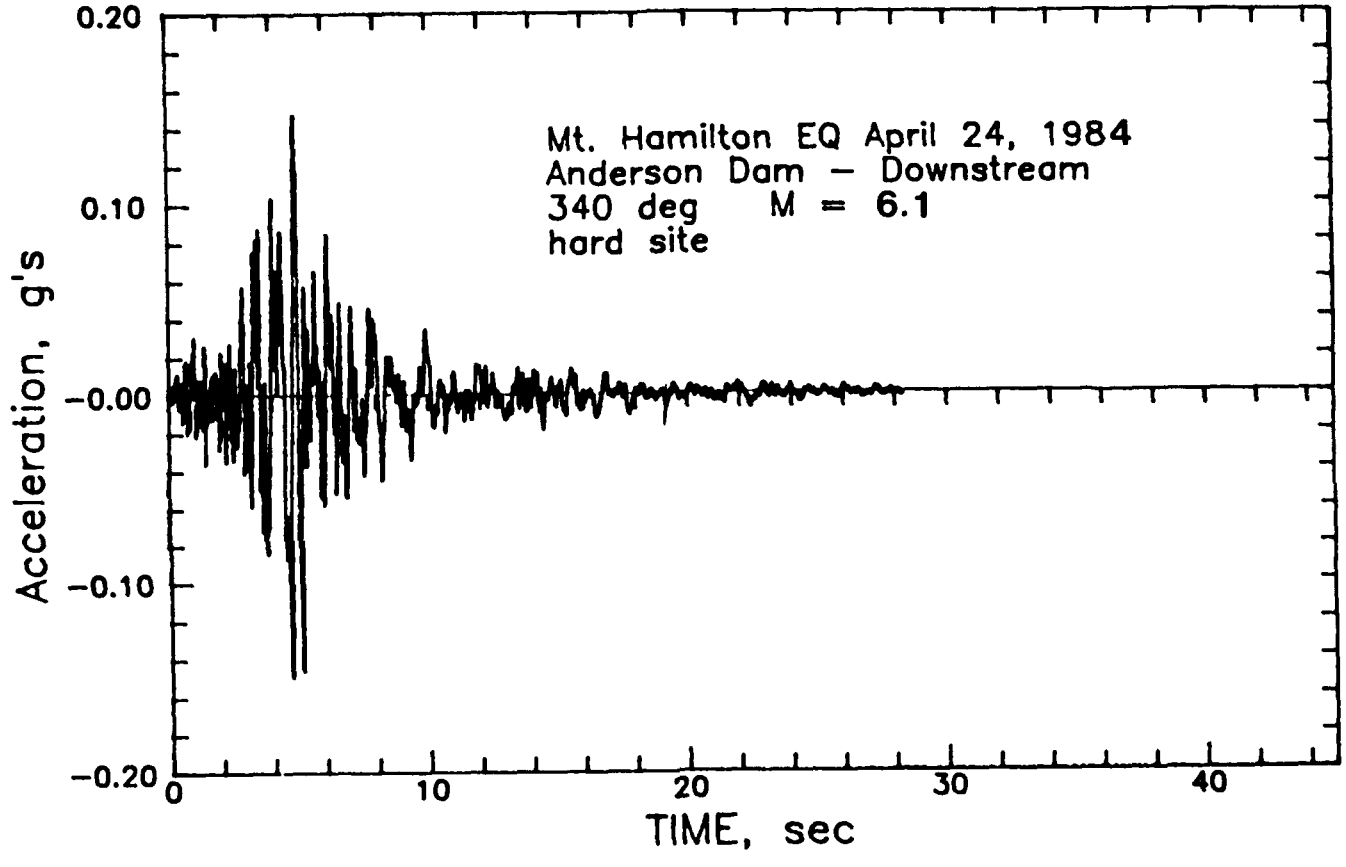

Figure 31. Accelerogram A

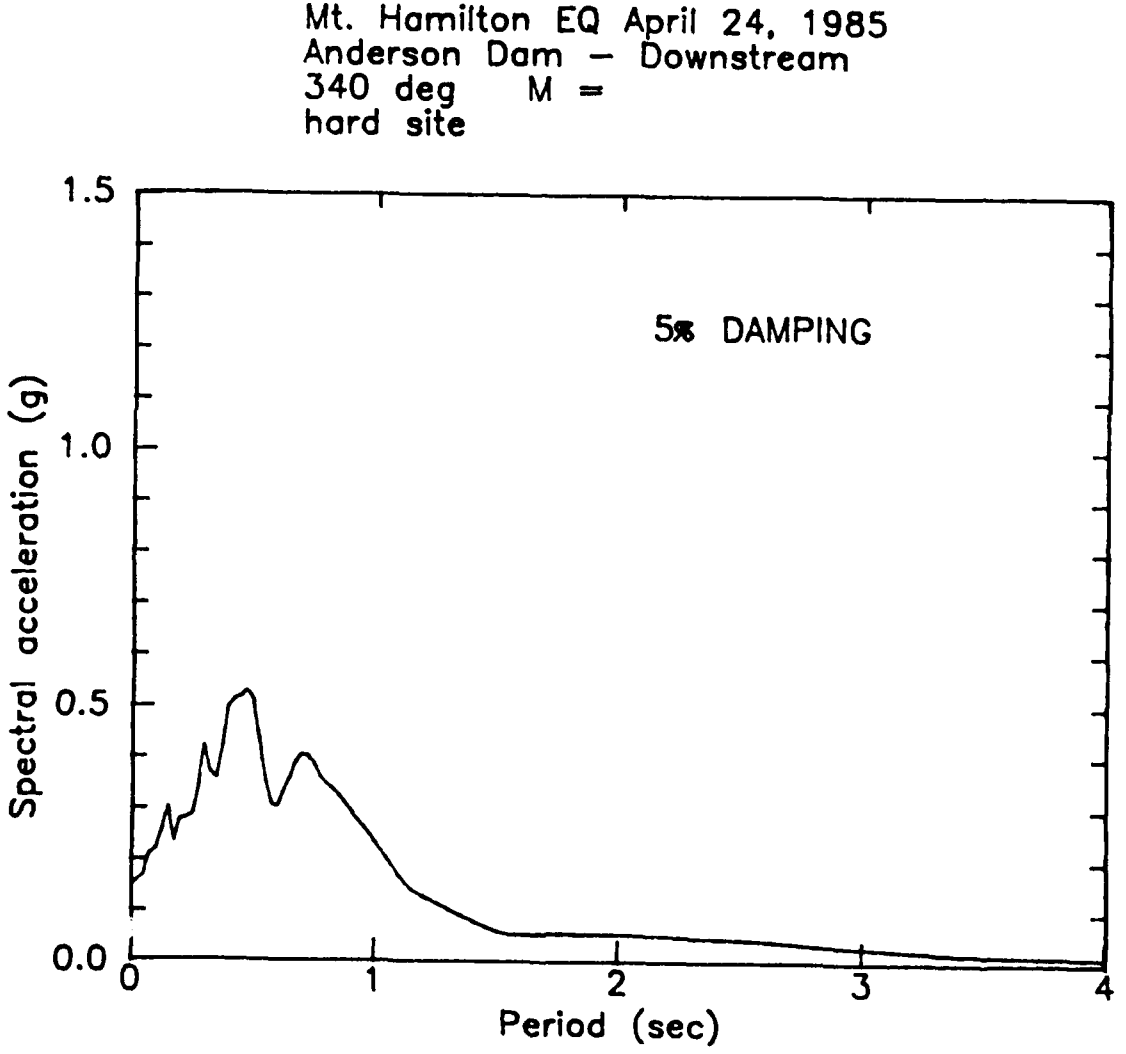

Figure 32. Response spectrum for accelerogram A

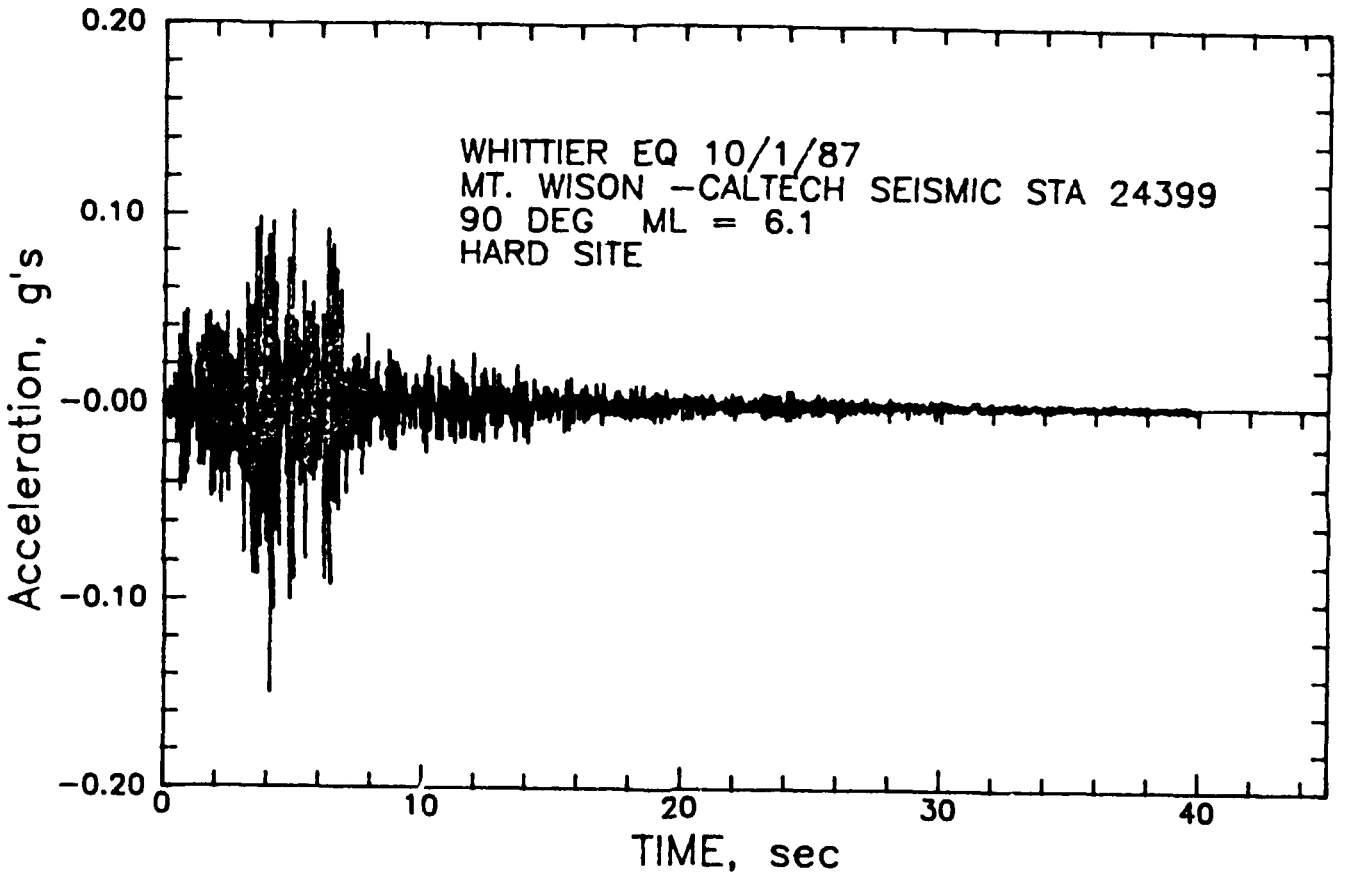

Figure 33. Accelerogram B

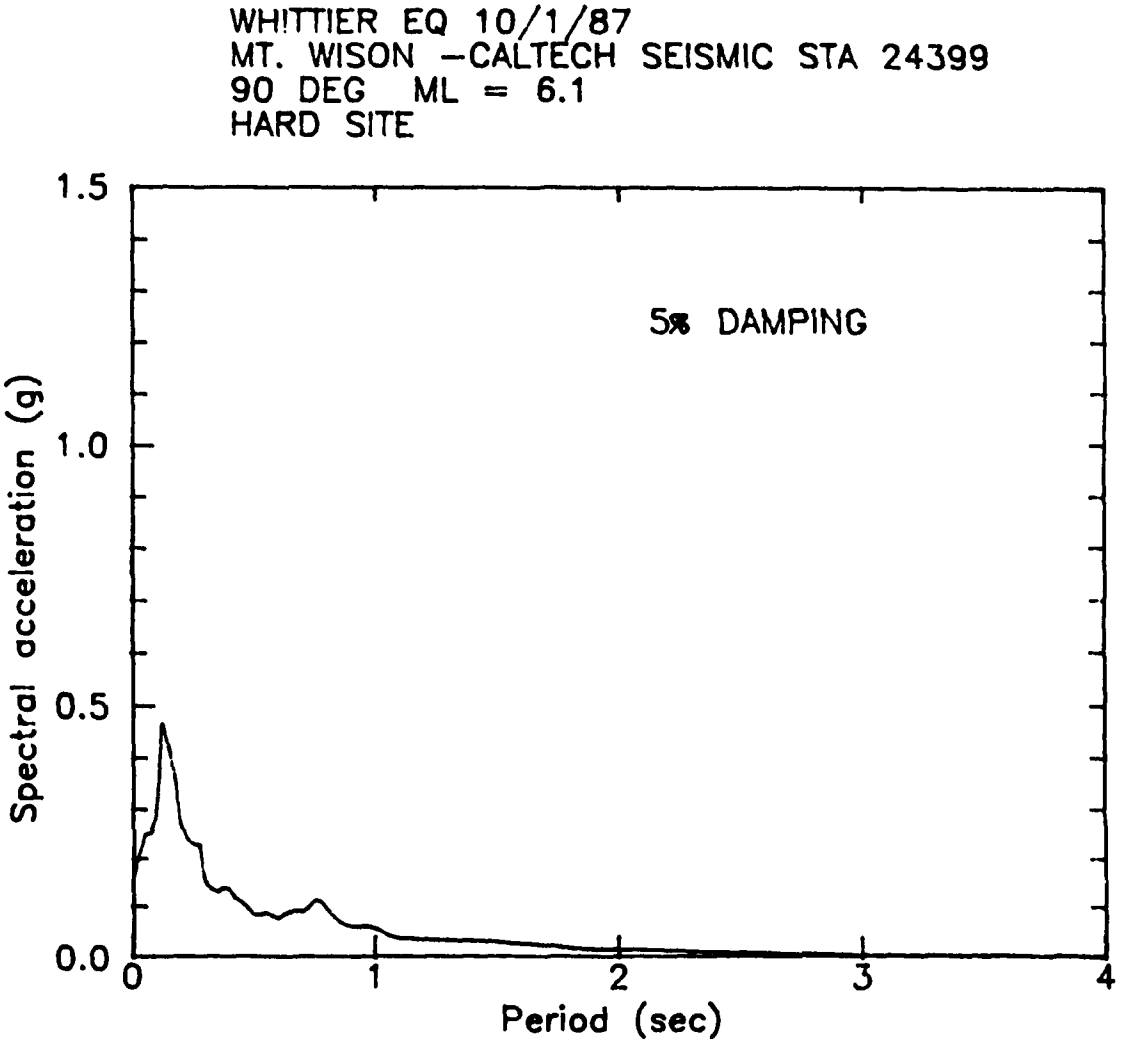

Figure 34. Response spectrum for accelerogram B

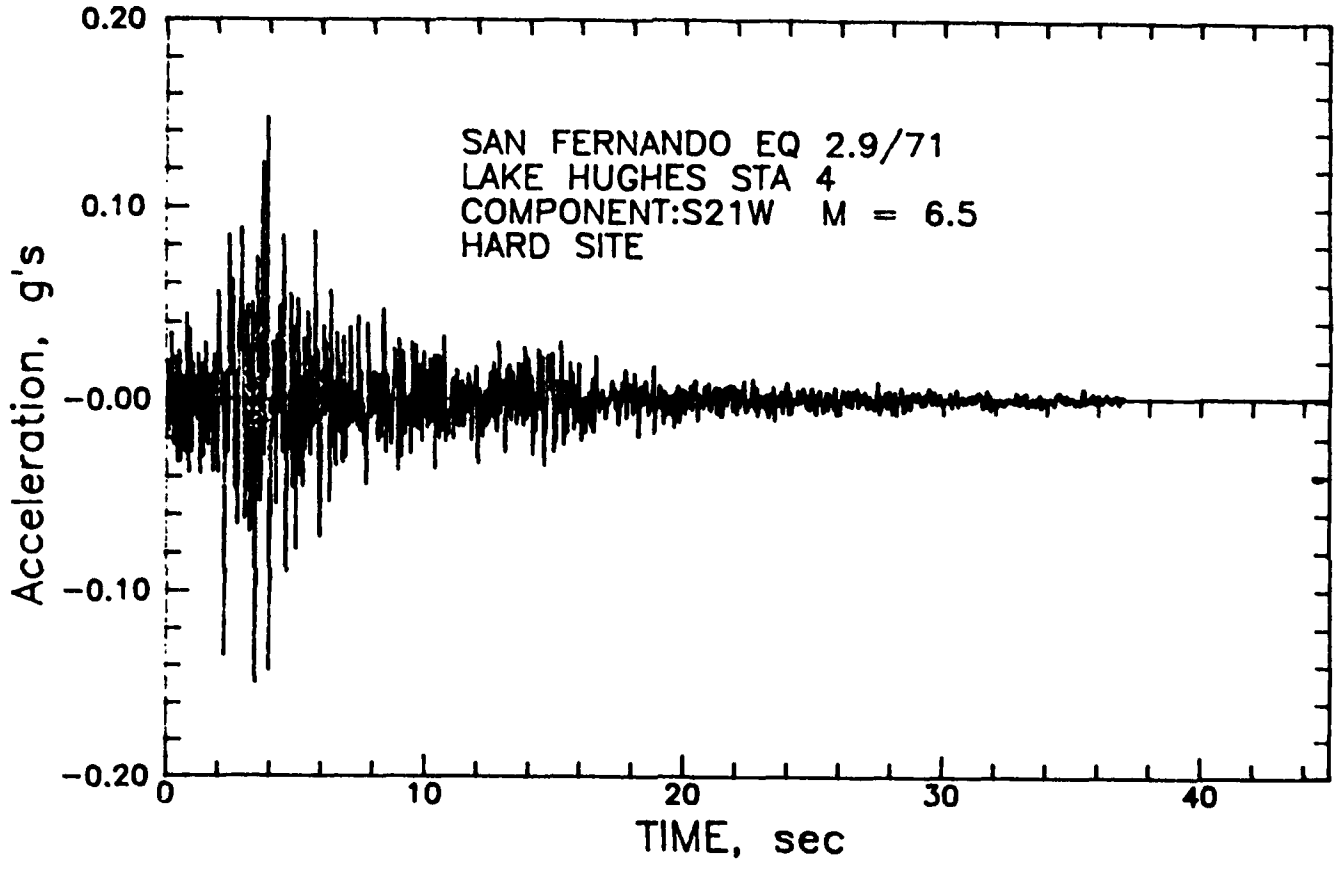

Figure 35. Accelerogram C

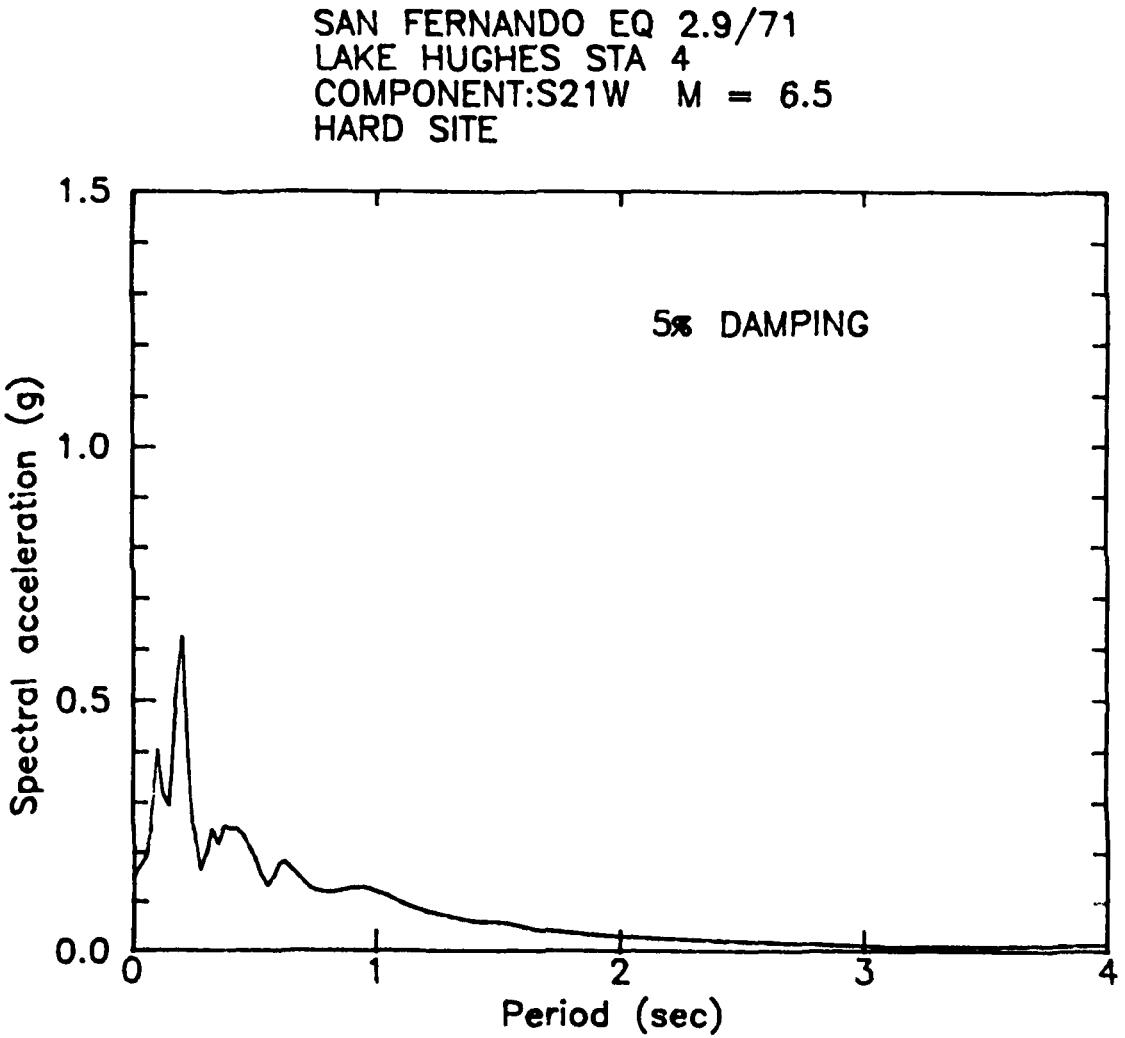

Figure 36. Response spectrum for accelerogram C

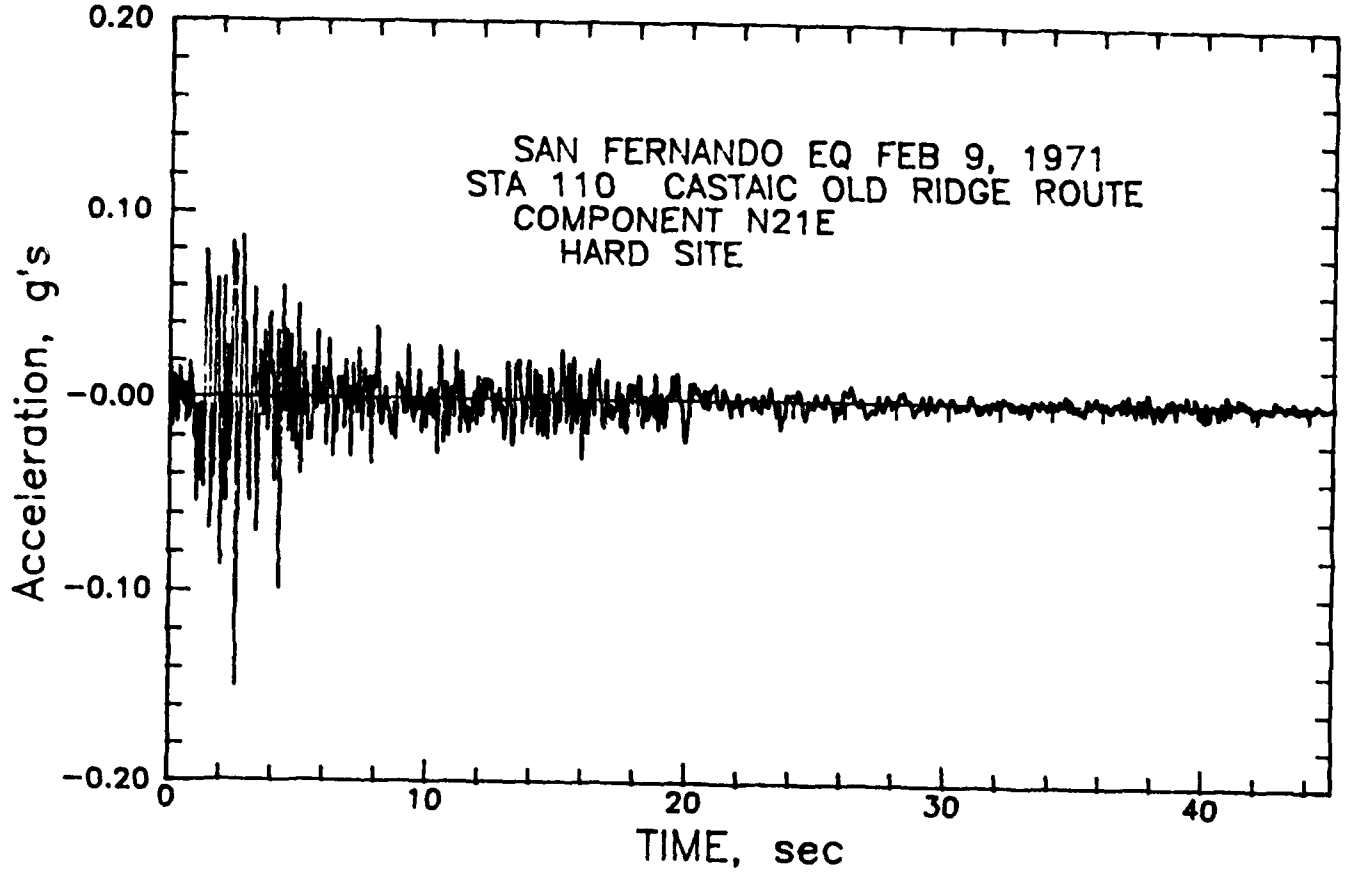

Figure 37. Accelerogram D

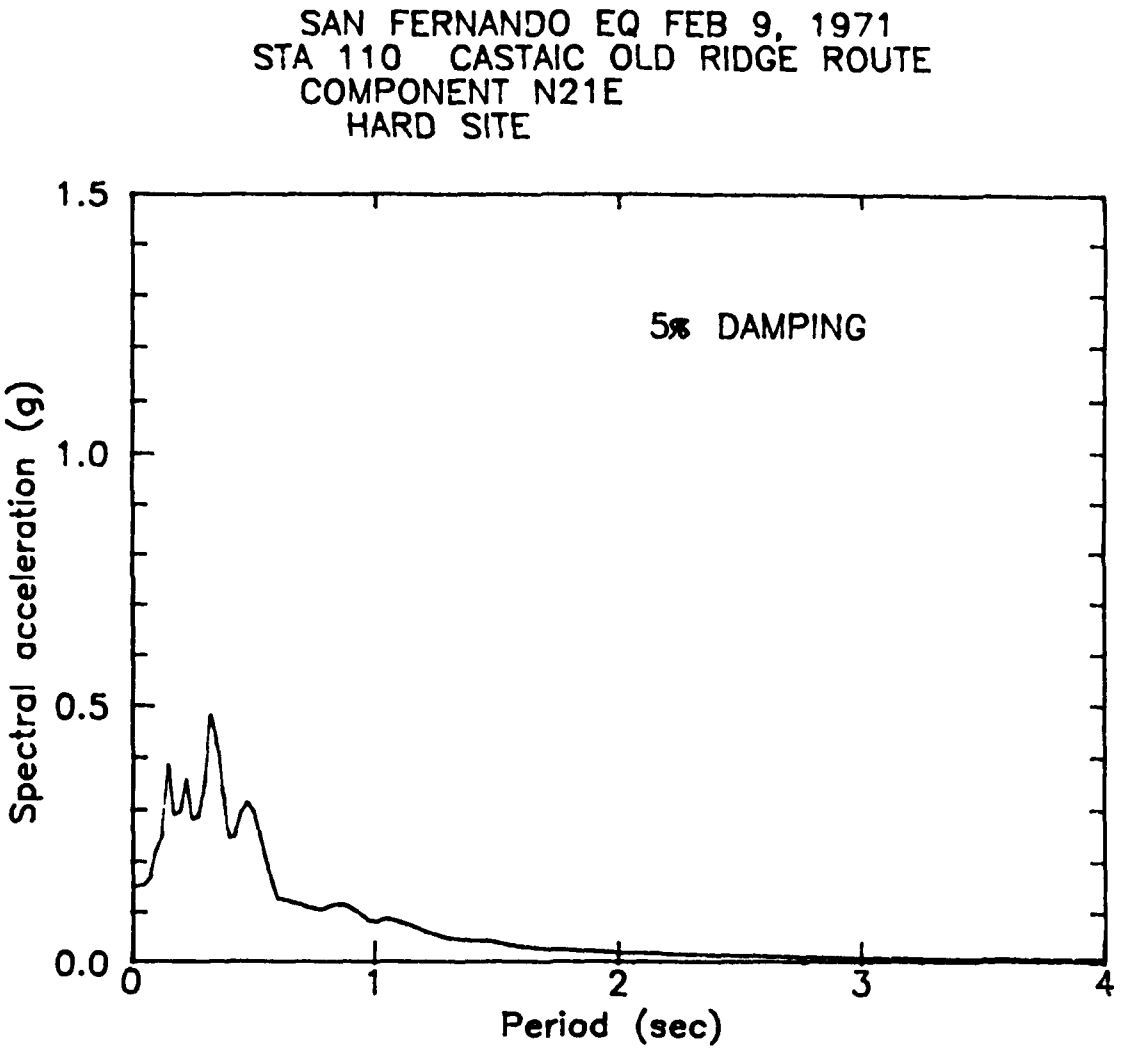

Figure 38. Response spectrum for accelerogram D

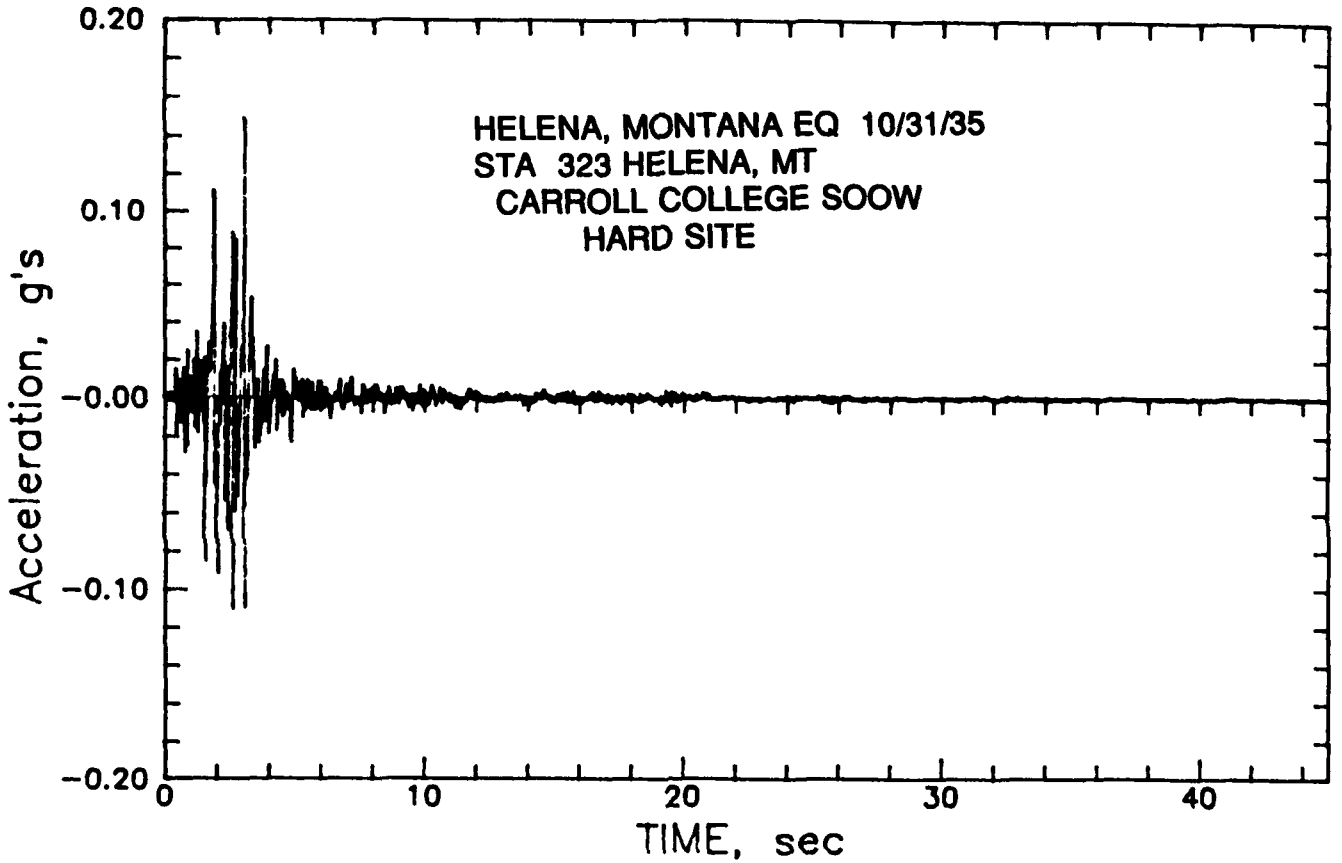

Figure 39. Accelerogram E

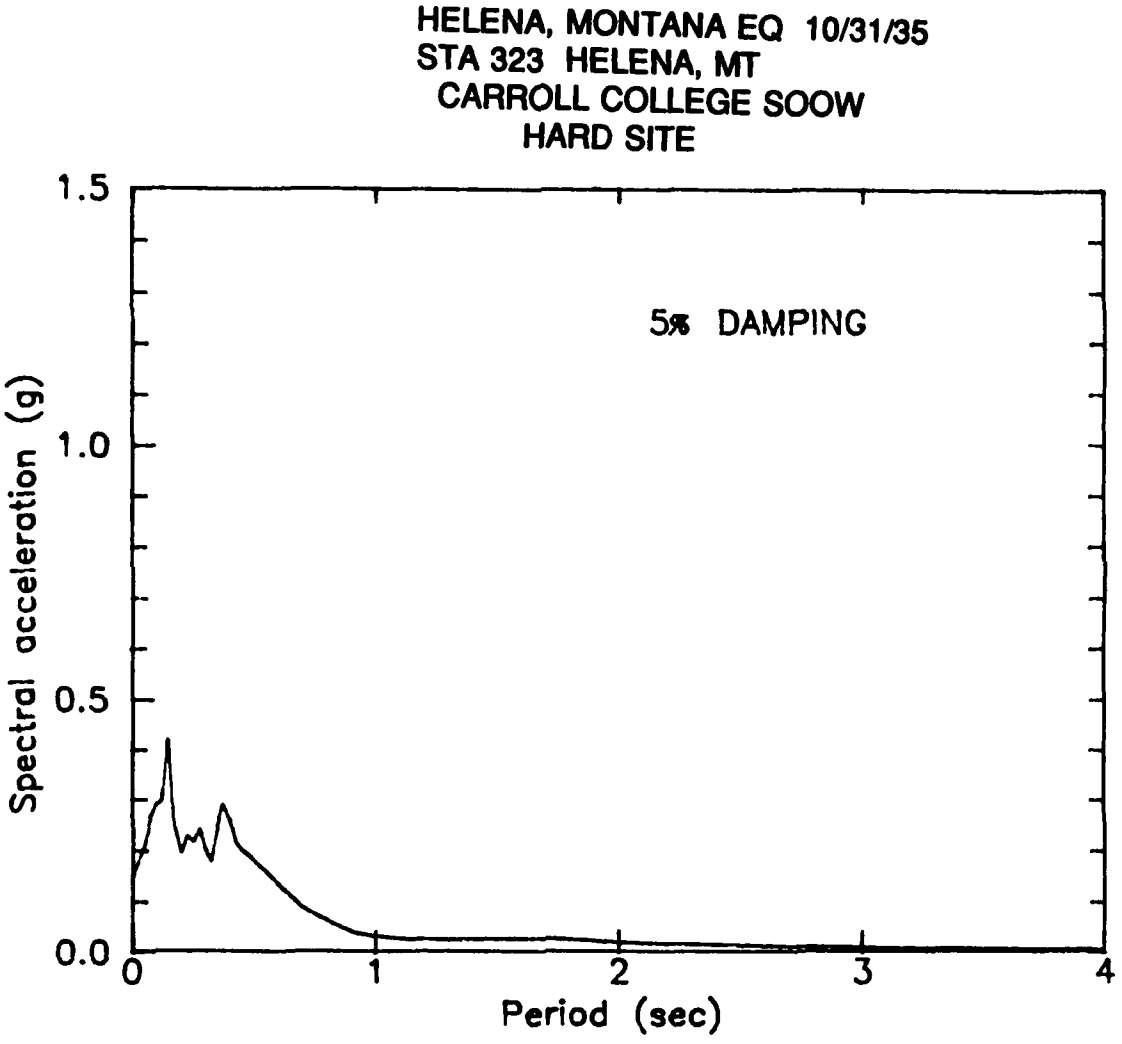

Figure 40. Response spectrum for accelerogram E

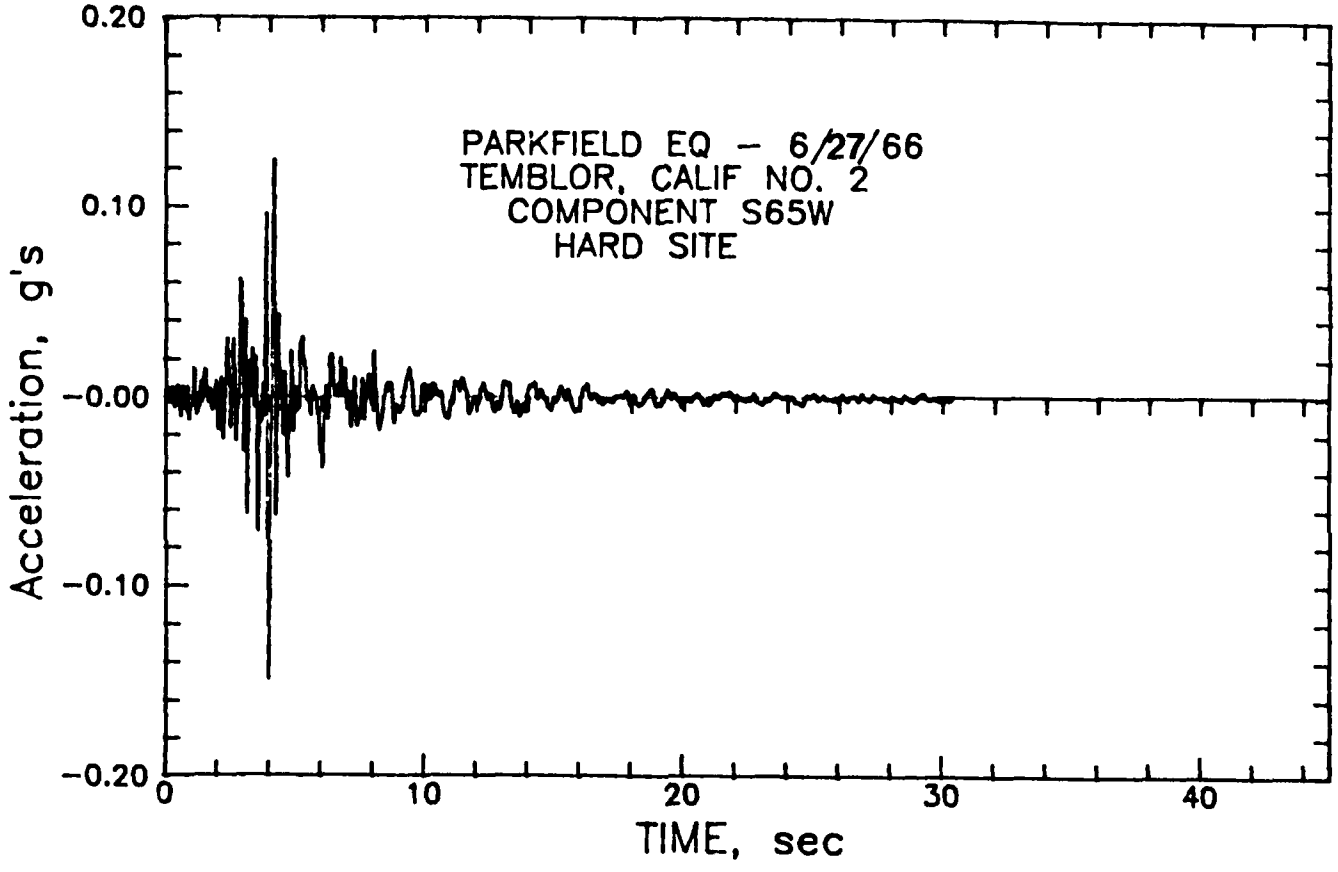

Figure 41. Accelerogram F

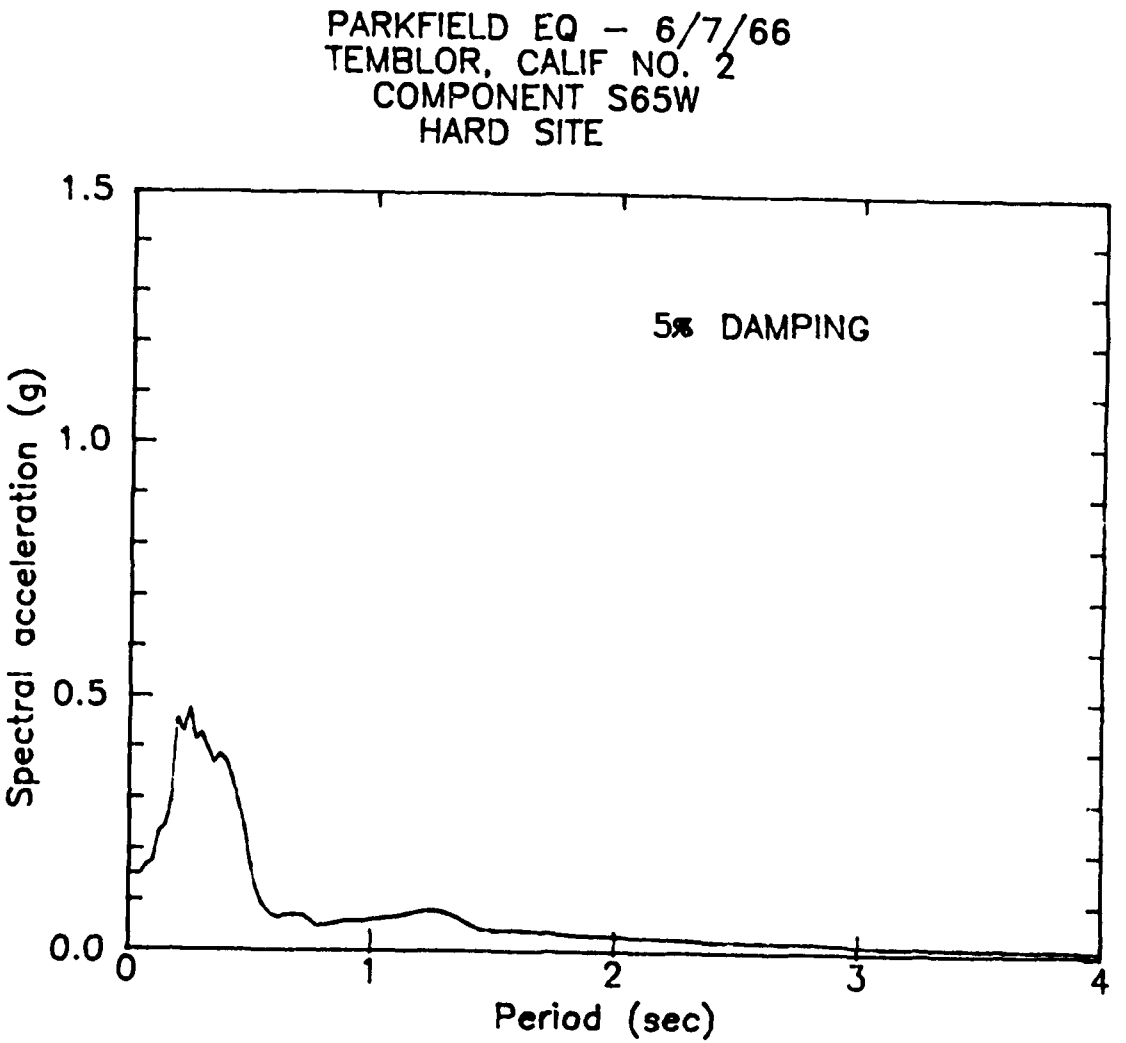

Figure 42. Response spectrum for accelerogram F

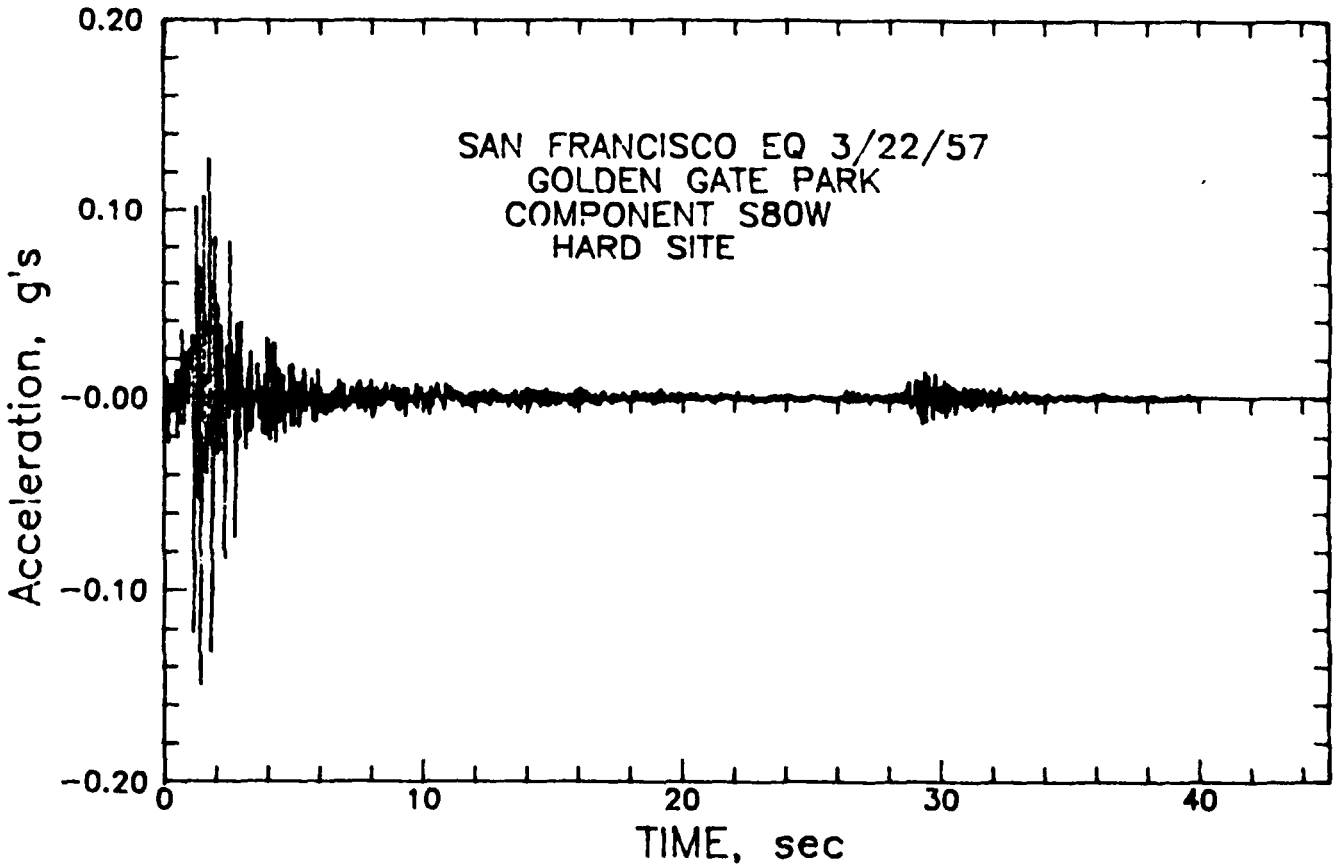

Figure 43. Accelerogram G

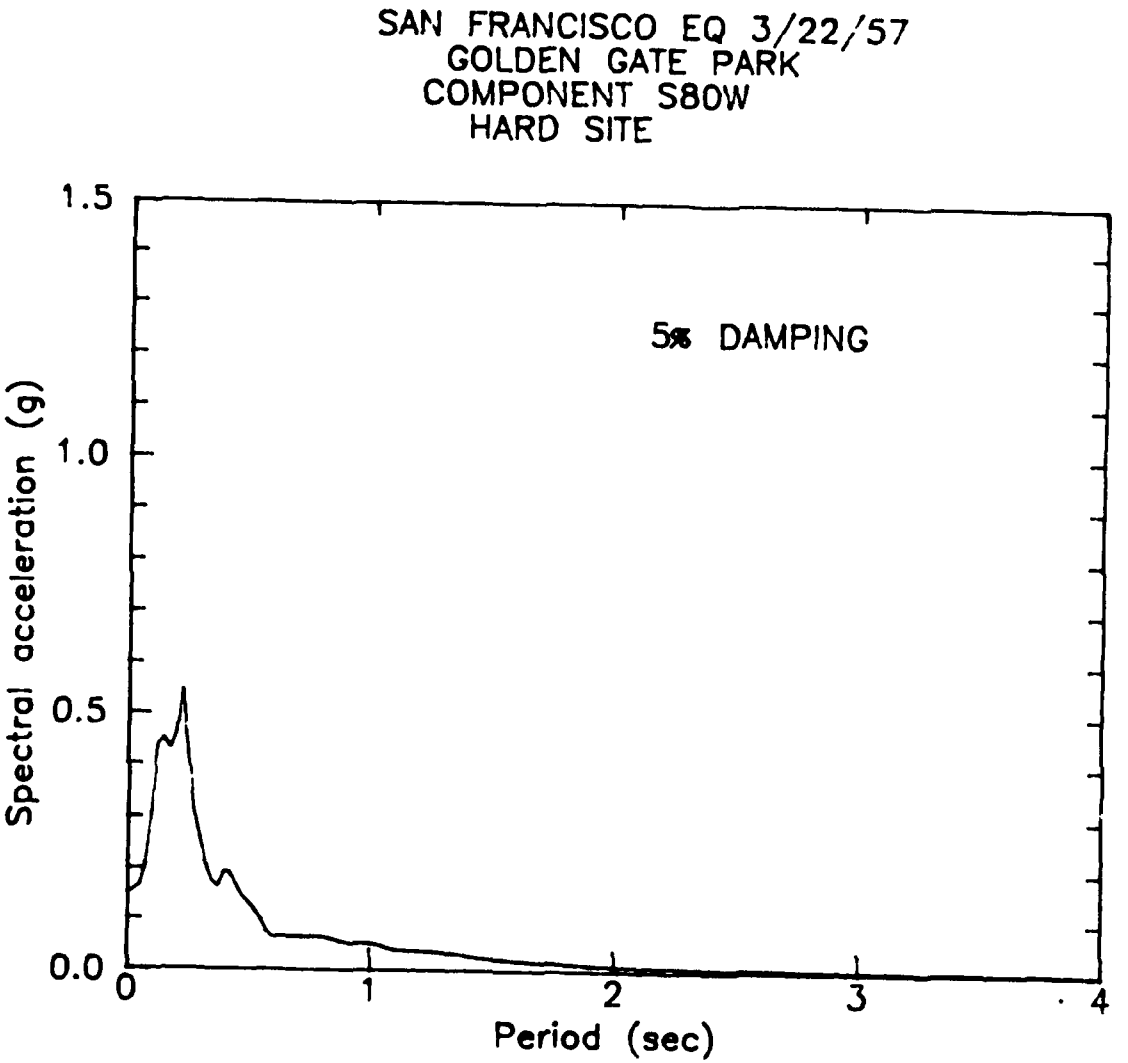

Figure 44. Response spectrum for accelerogram G

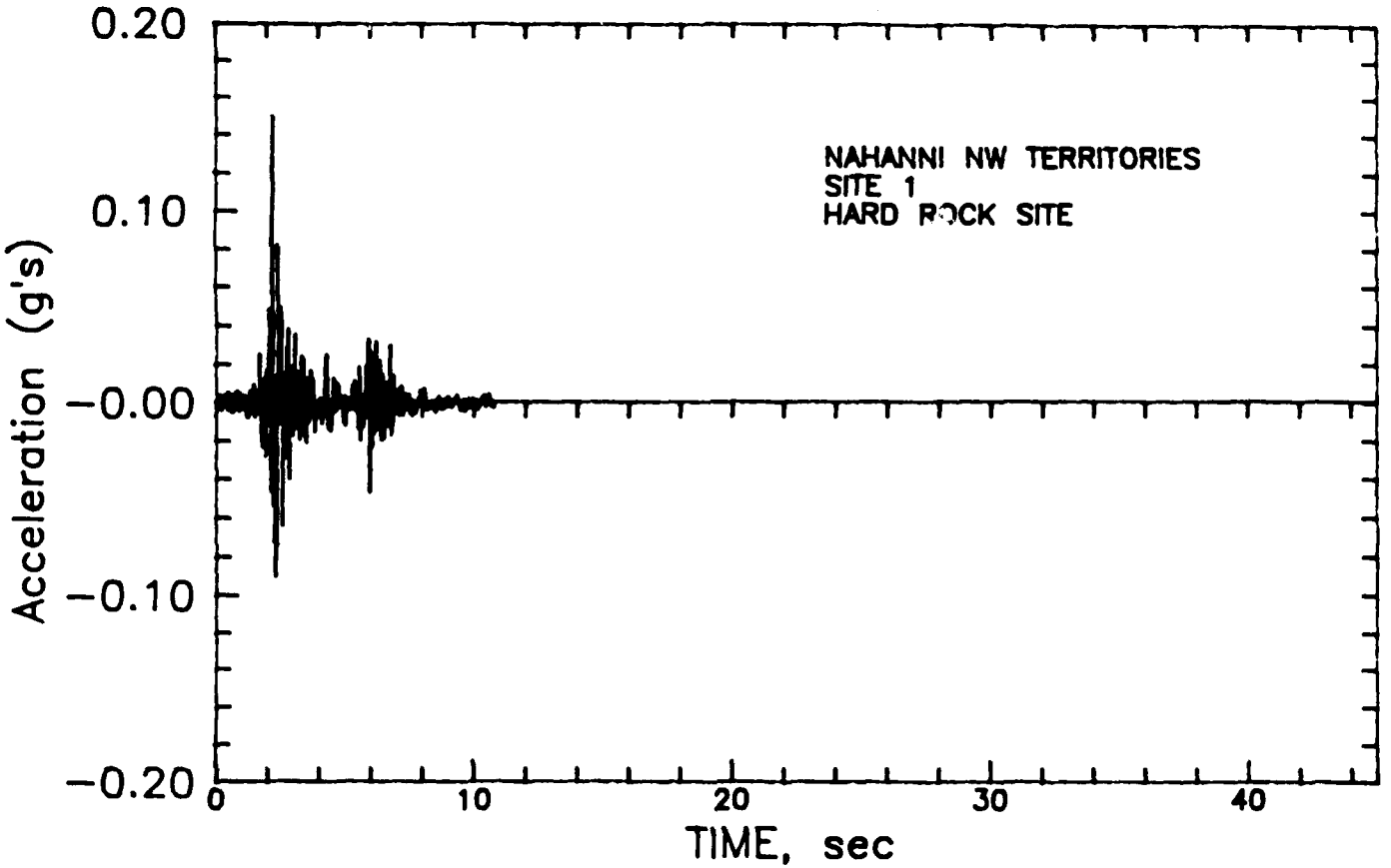

Figure 45. Accelerogram H

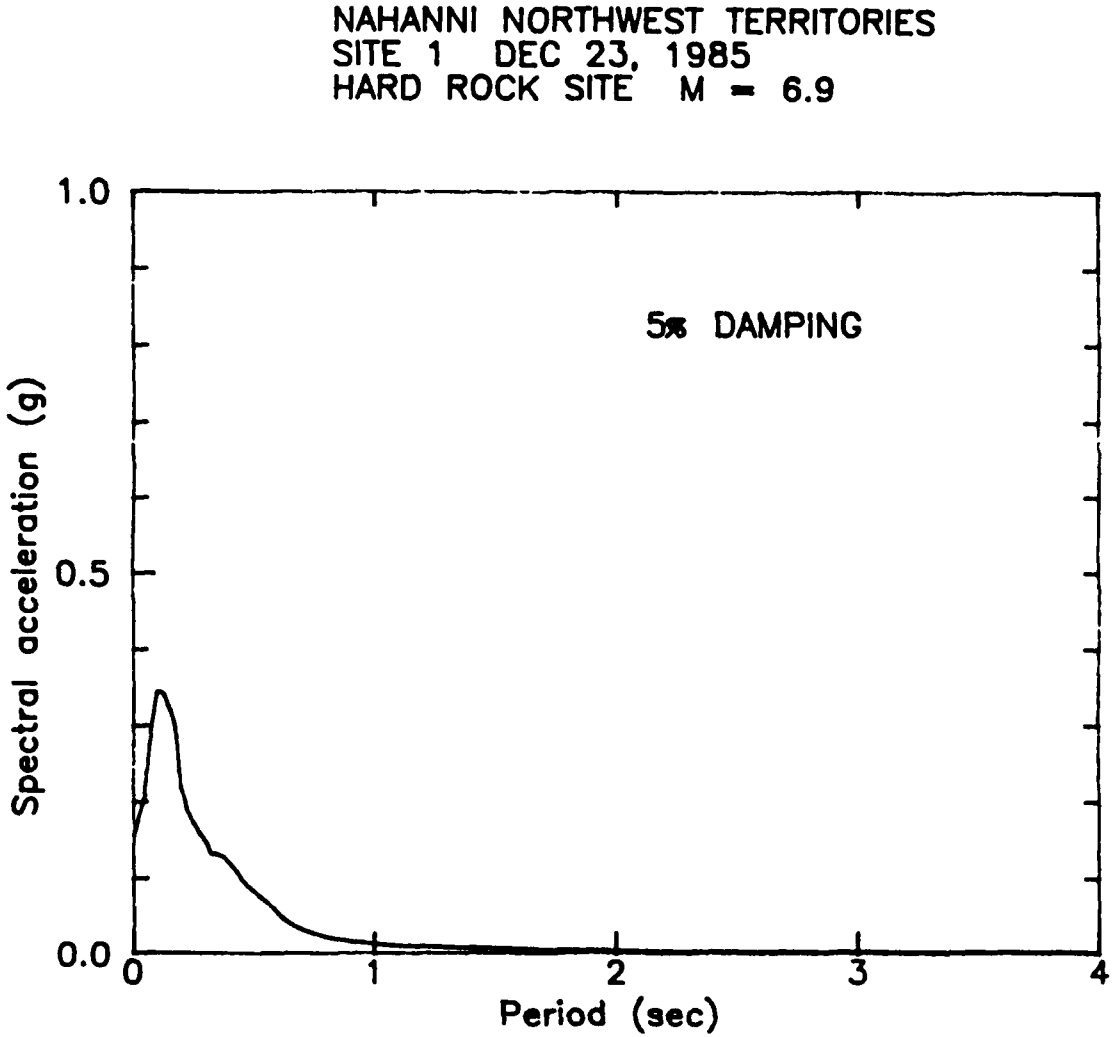

Figure 46. Response spectrum for accelerogram H

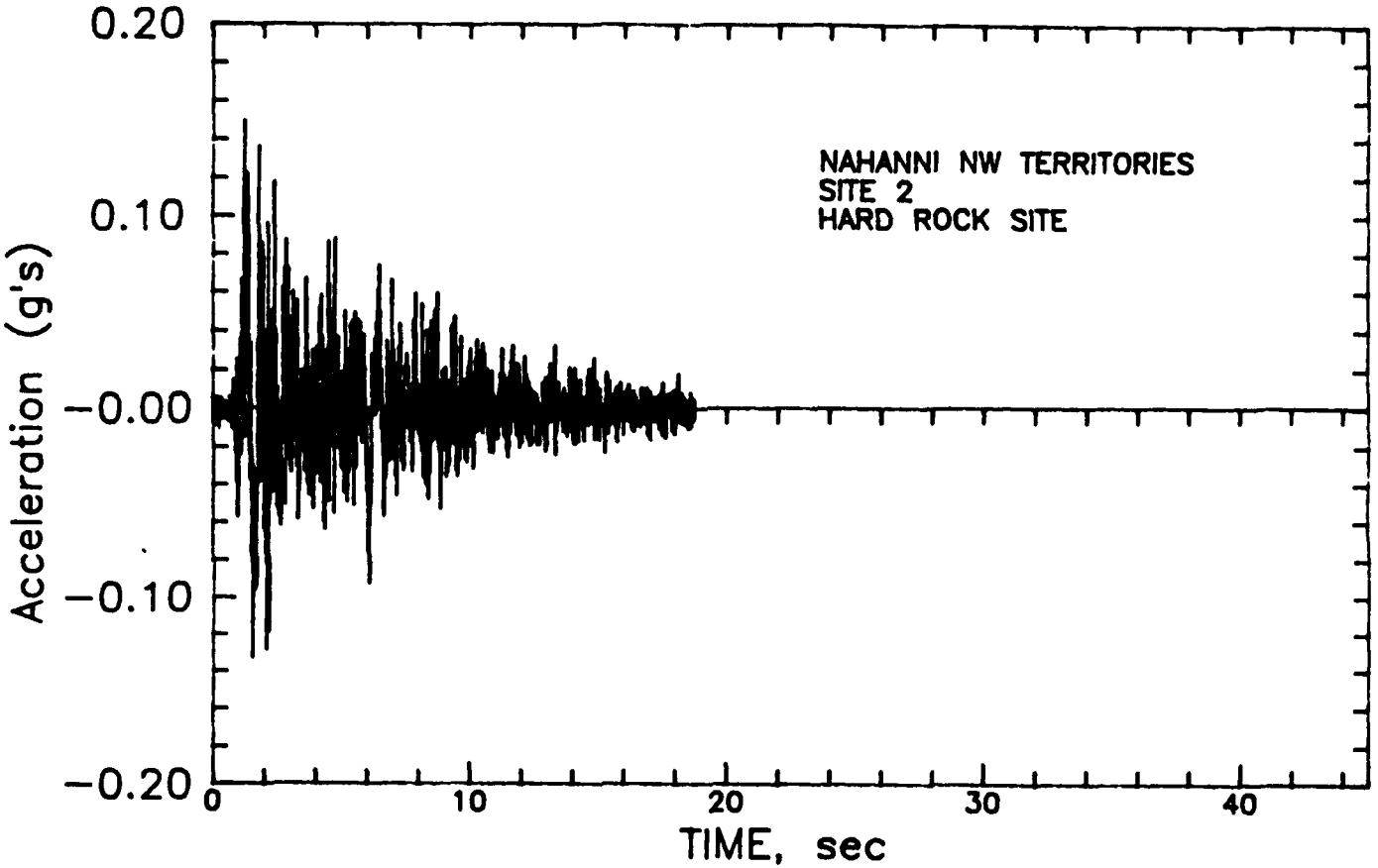

Figure 47. Accelerogram I

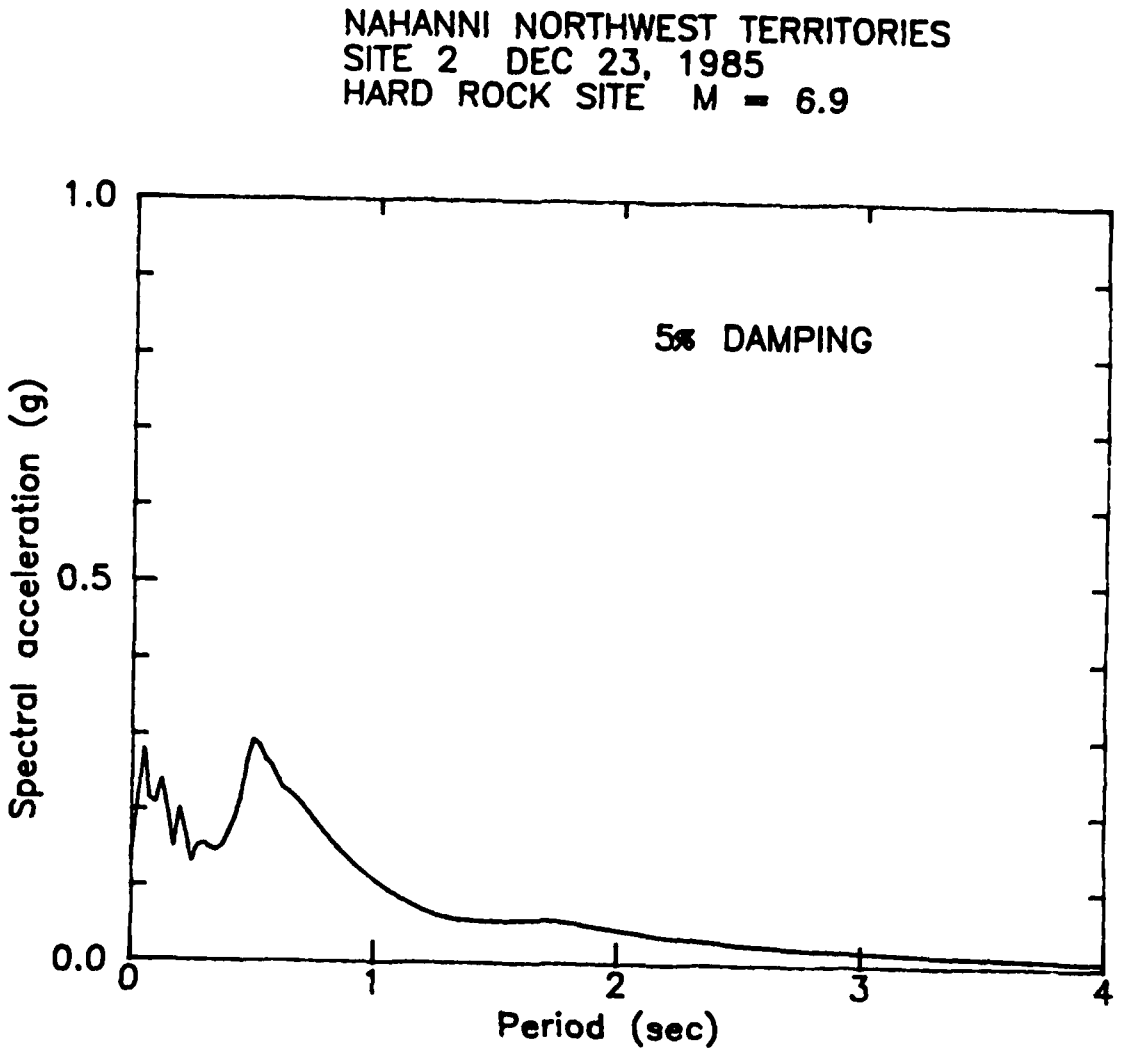

Figure 48. Response spectrum for accelerogram I

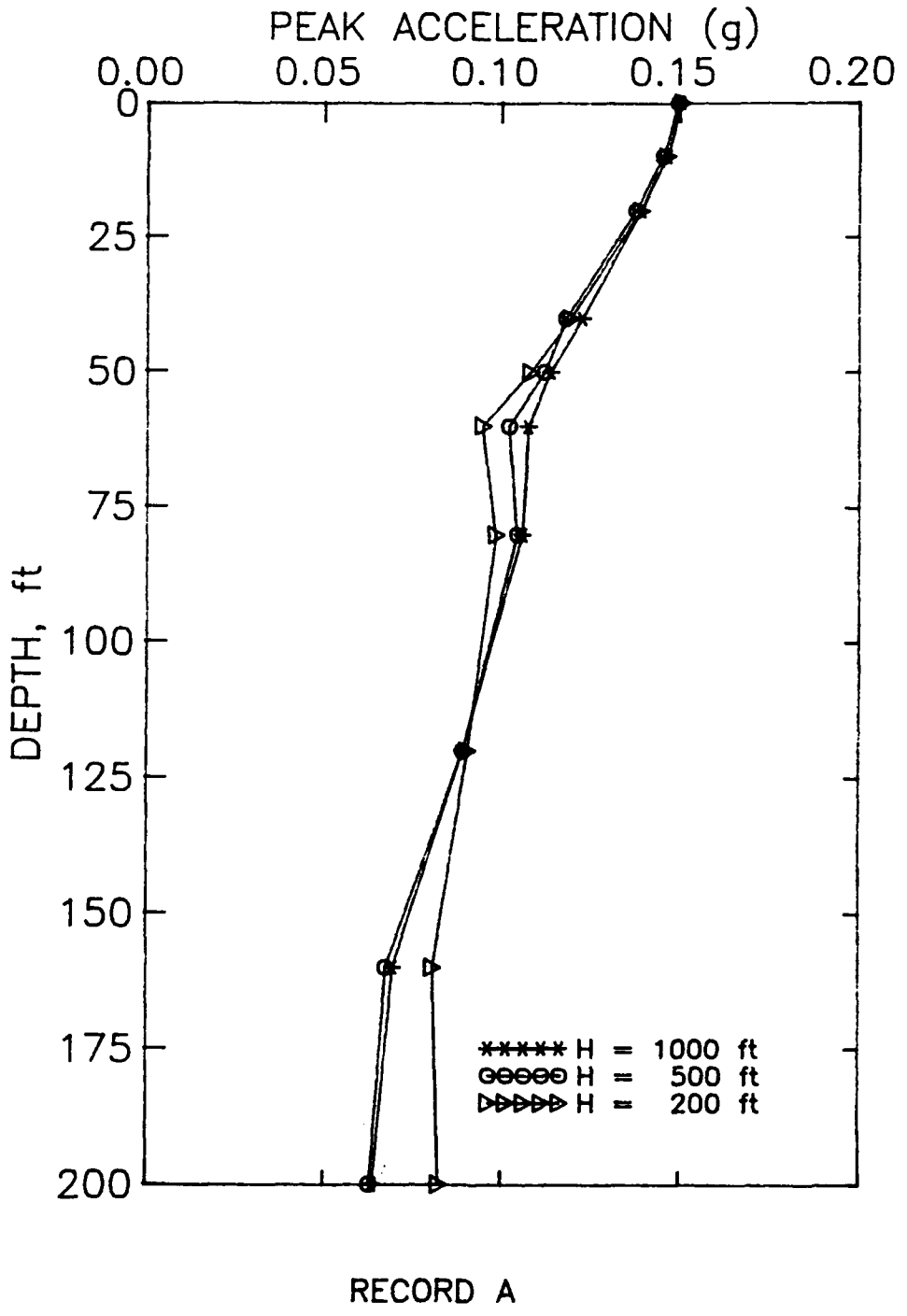

Figure 49. Peak acceleration versus depth for the upper-bound stiffness profiles with H = 200 ft, 500 ft, and 1,000 ft

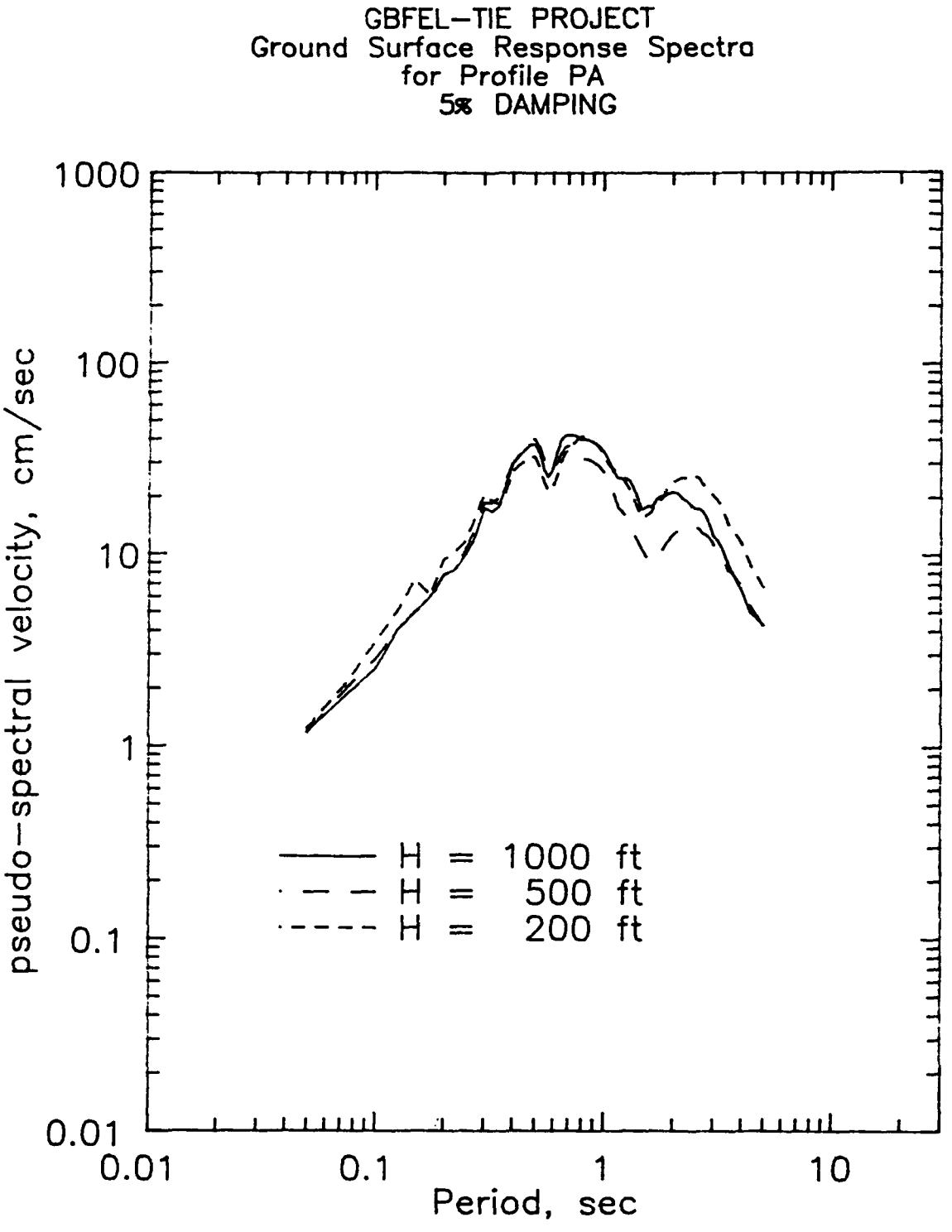

Figure 50. Response spectral comparisons for the upper-bound stiffness profiles with H = 200 ft, 500 ft, and 1,000 ft

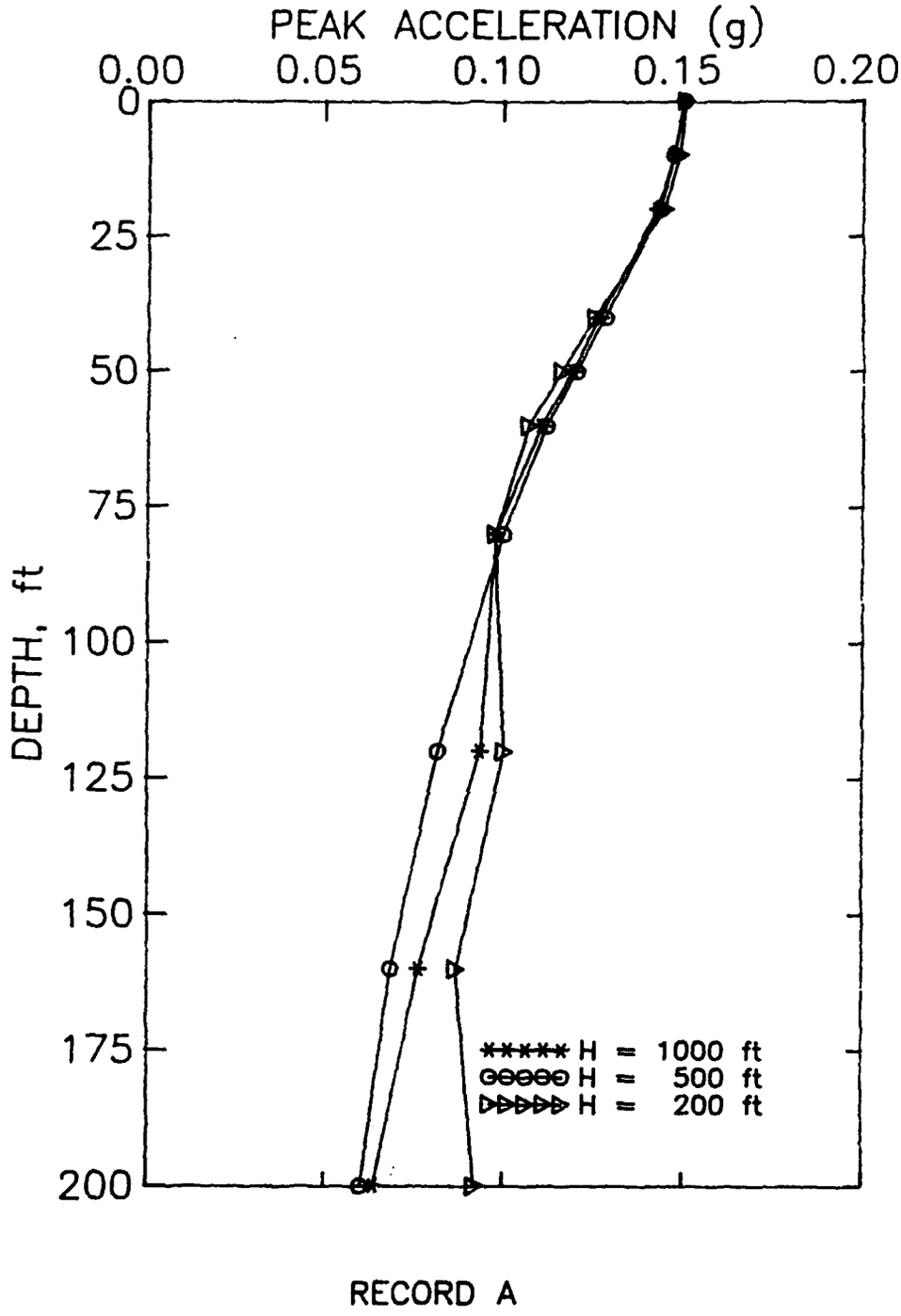

Figure 51. Peak acceleration versus depth for the average stiffness profiles with H = 200 ft, 500 ft, and 1,000 ft

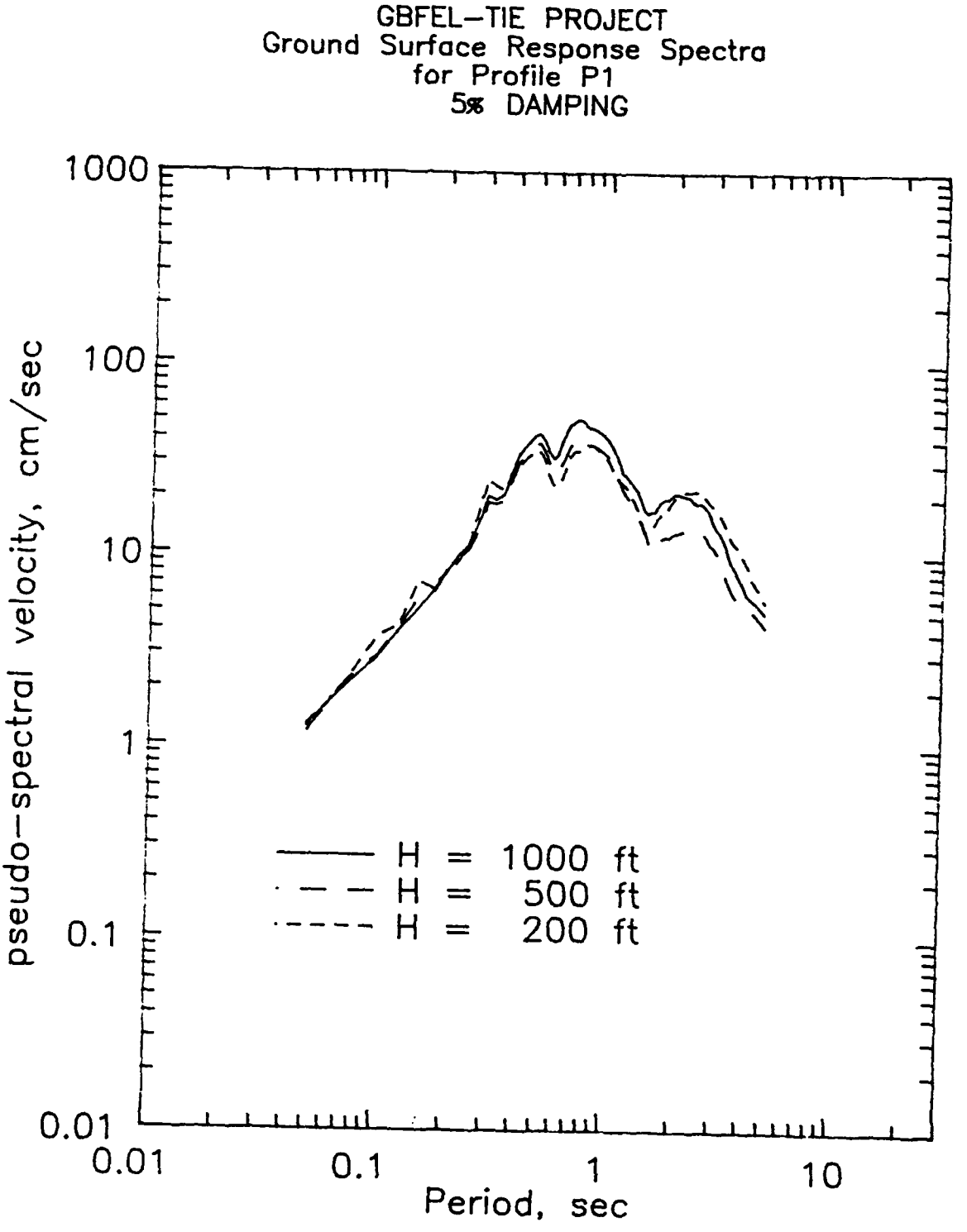

Figure 52. Response spectral comparisons for the average stiffness profiles with H = 200 ft, 500 ft, and 1,000 ft

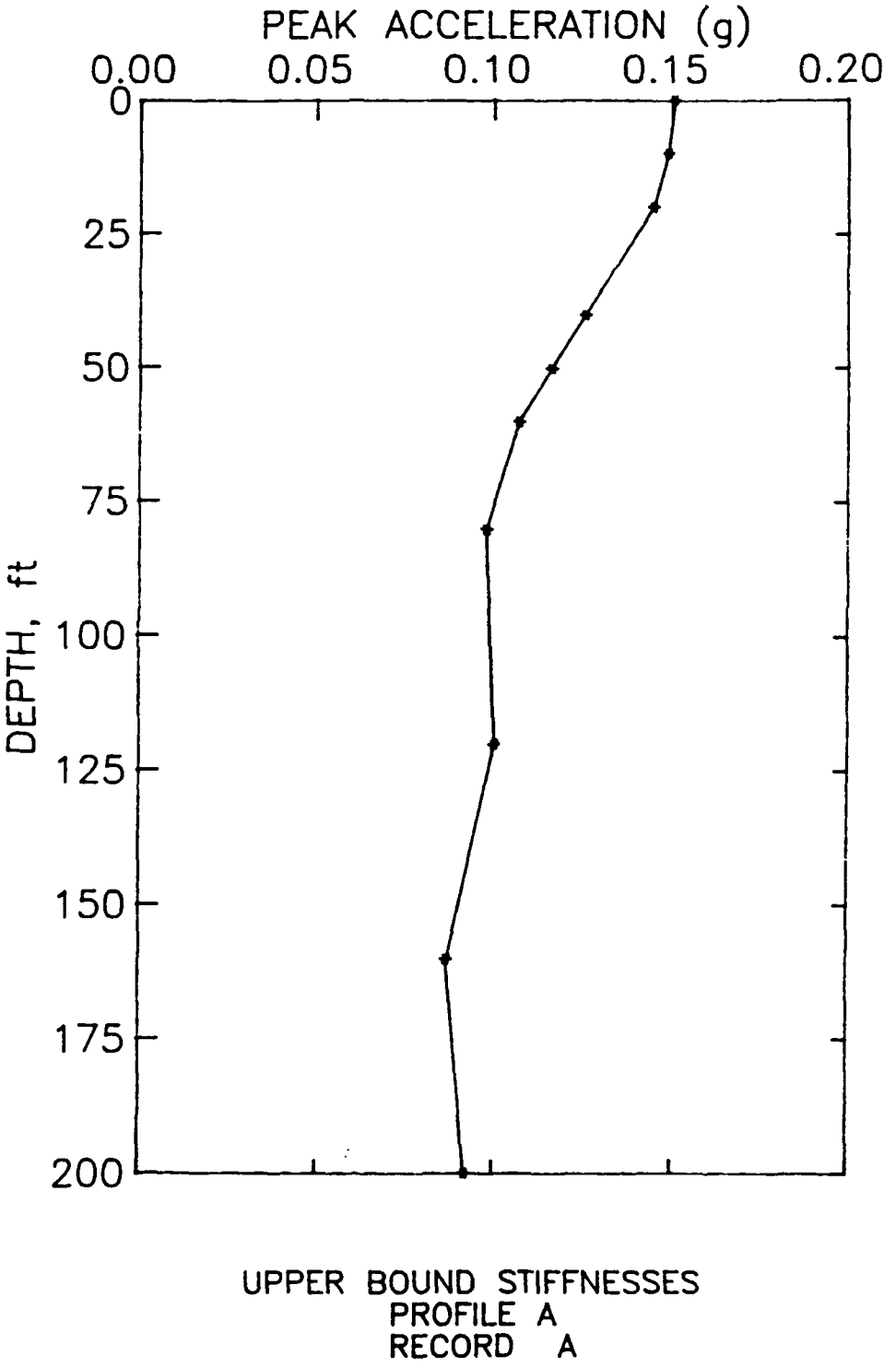

Figure 53. Upper bound sensitivity analysis to stratigraphy variation-Peak accelerations versus depth for Profile A due to Record A

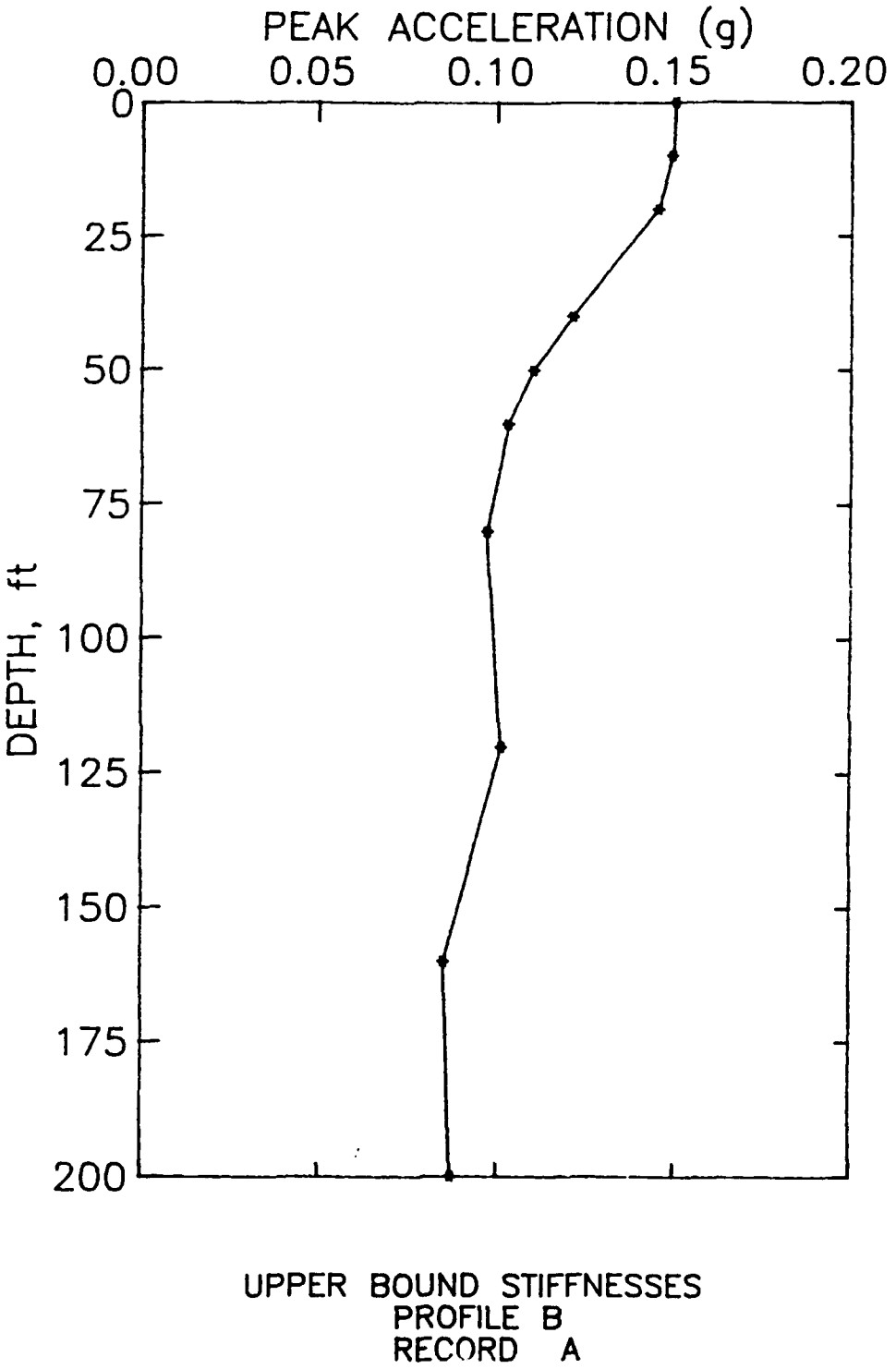

Figure 54. Upper bound sensitivity analysis to stratigraphy variation-Peak accelerations versus depth for Profile B due to Record A

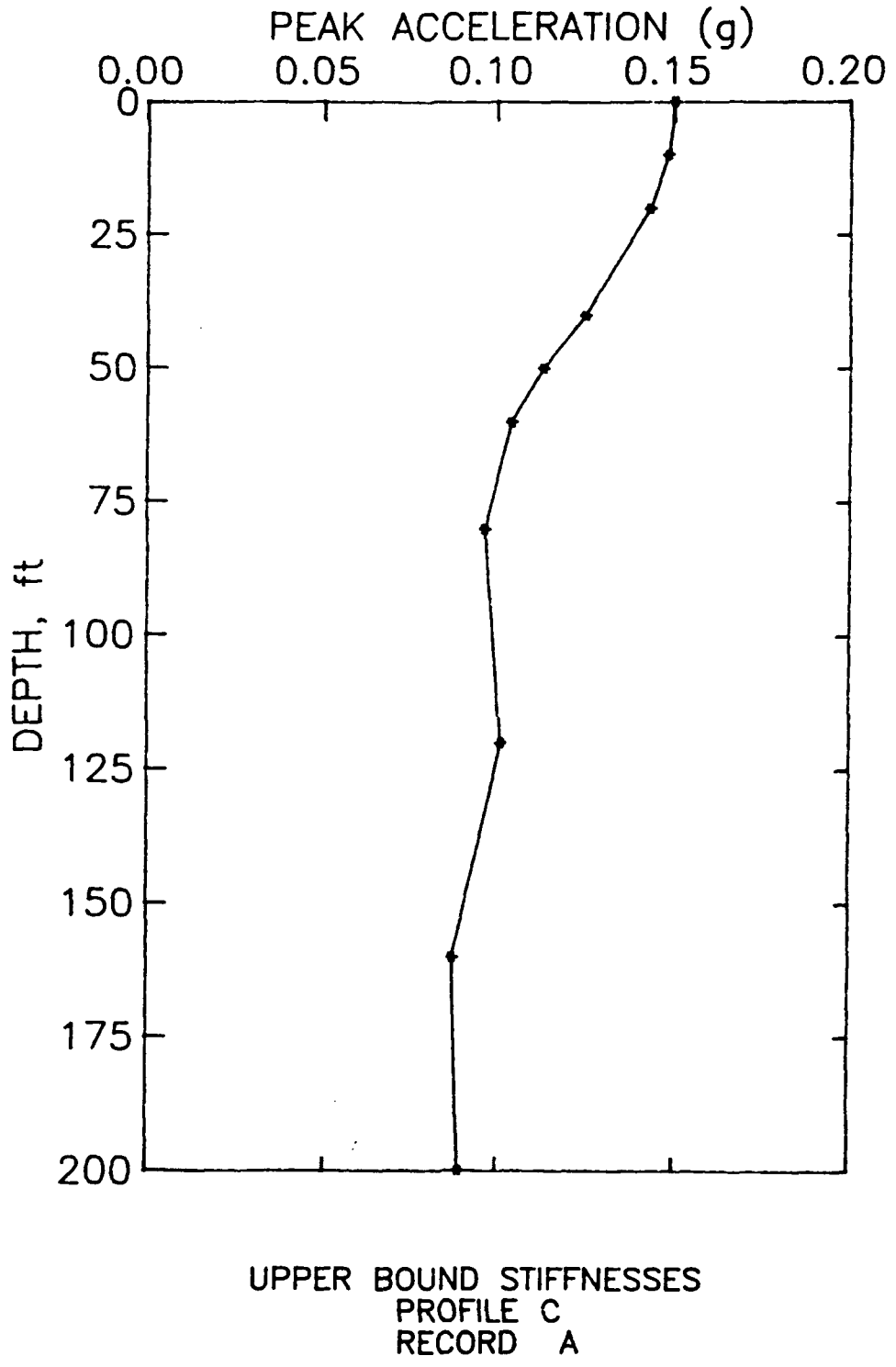

Figure 55. Upper bound sensitivity analysis to stratigraphy variation-Peak accelerations versus depth for Profile C due to Record A

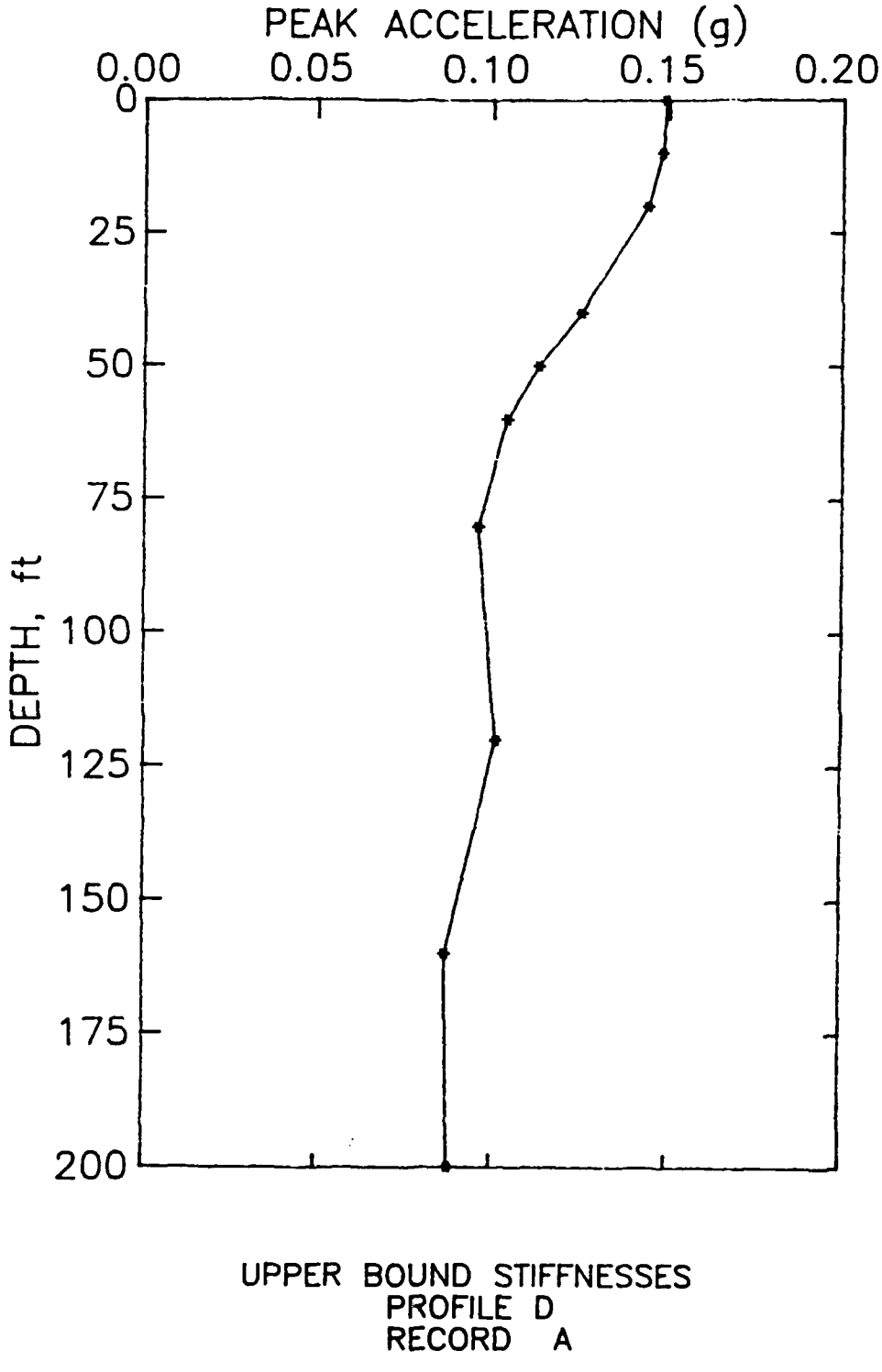

Figure 56. Upper bound sensitivity analysis to stratigraphy variation-Peak accelerations versus depth for Profile D due to Record A

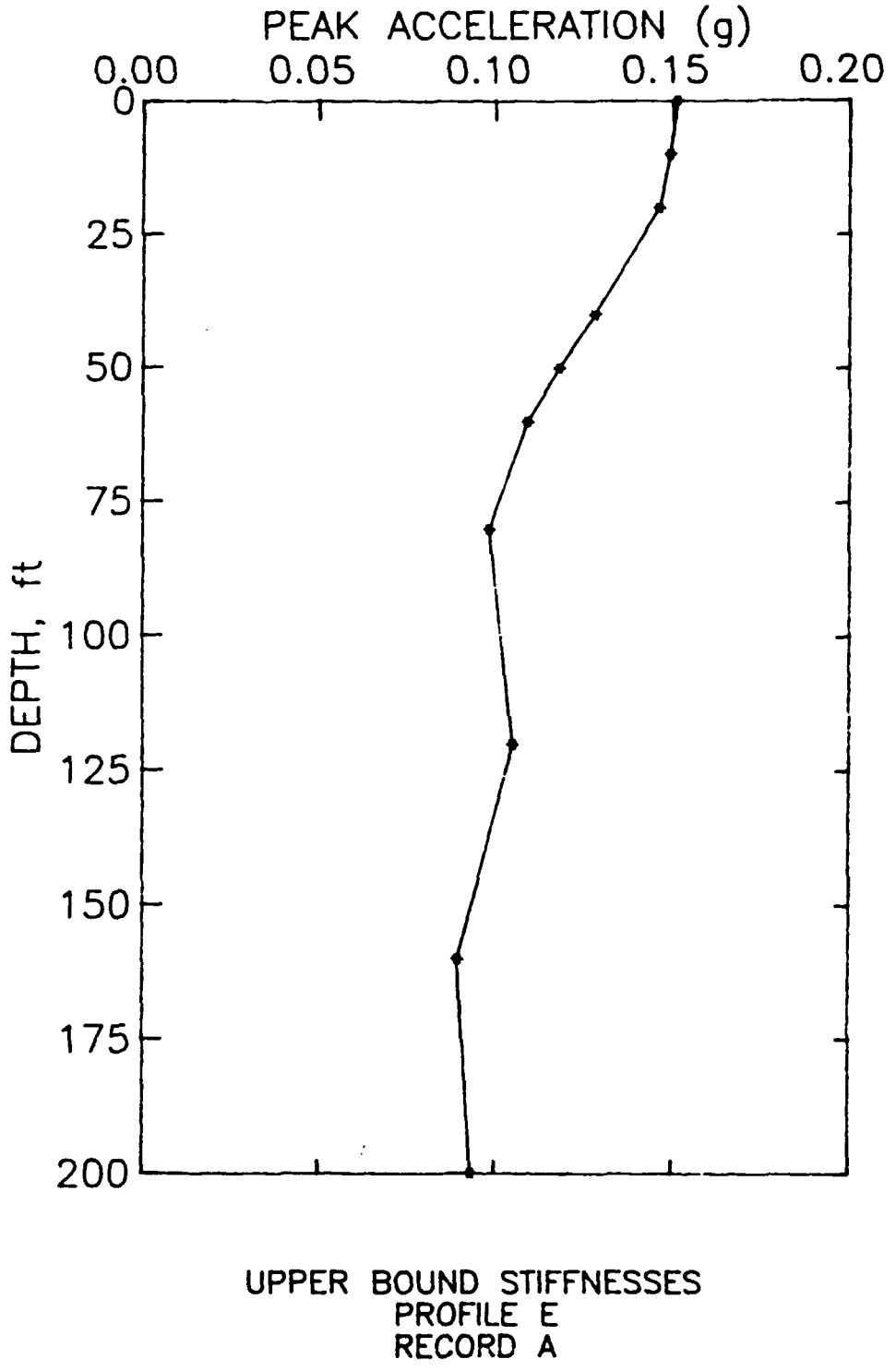

Figure 57. Upper bound sensitivity analysis to stratigraphy variation-Peak accelerations versus depth for Profile E due to Record A

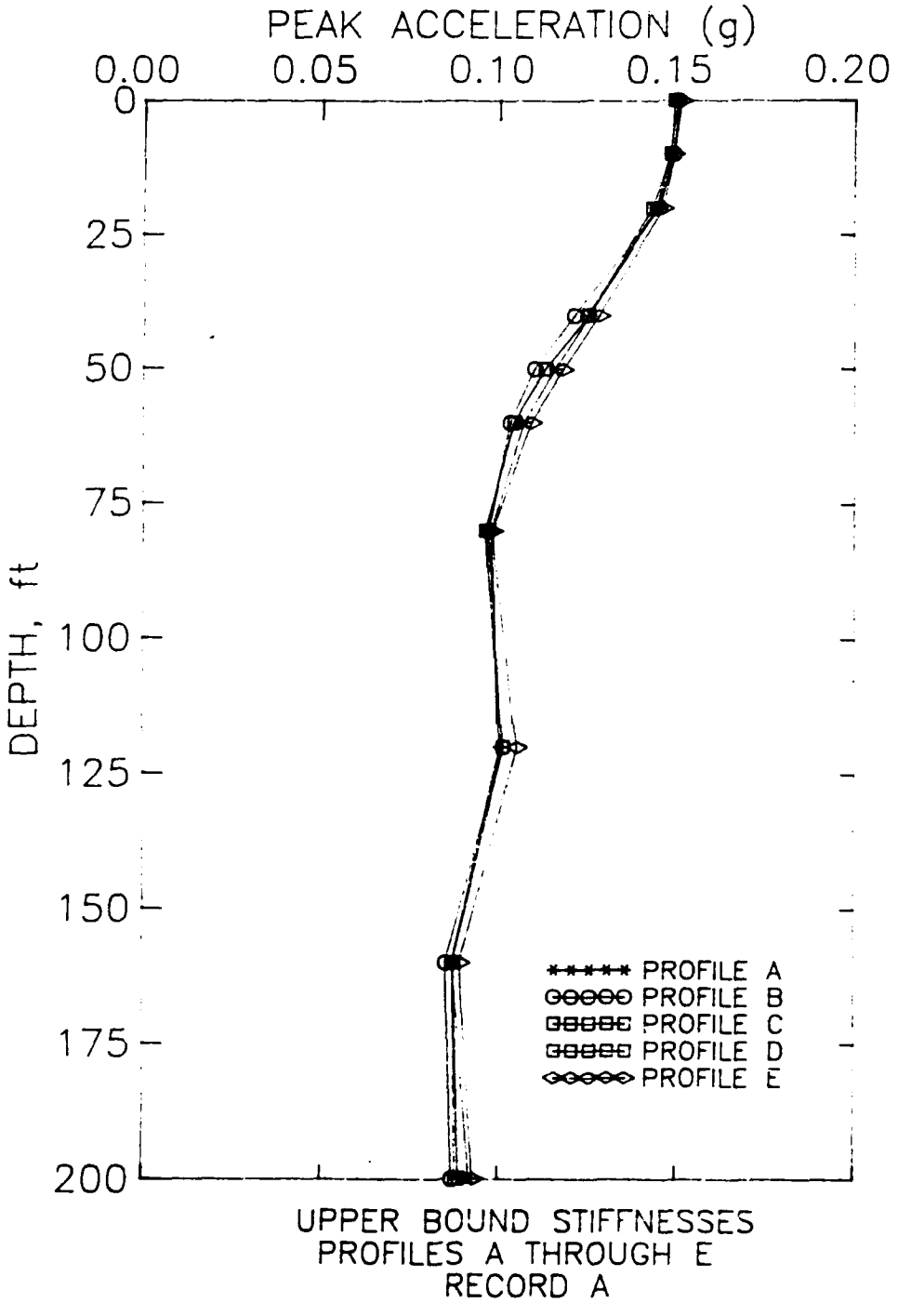

Figure 58. Sensitivity of dynamic response to stratigraphy variations-Comparison of peak acceleration for upper bound stiffness Profiles A through E

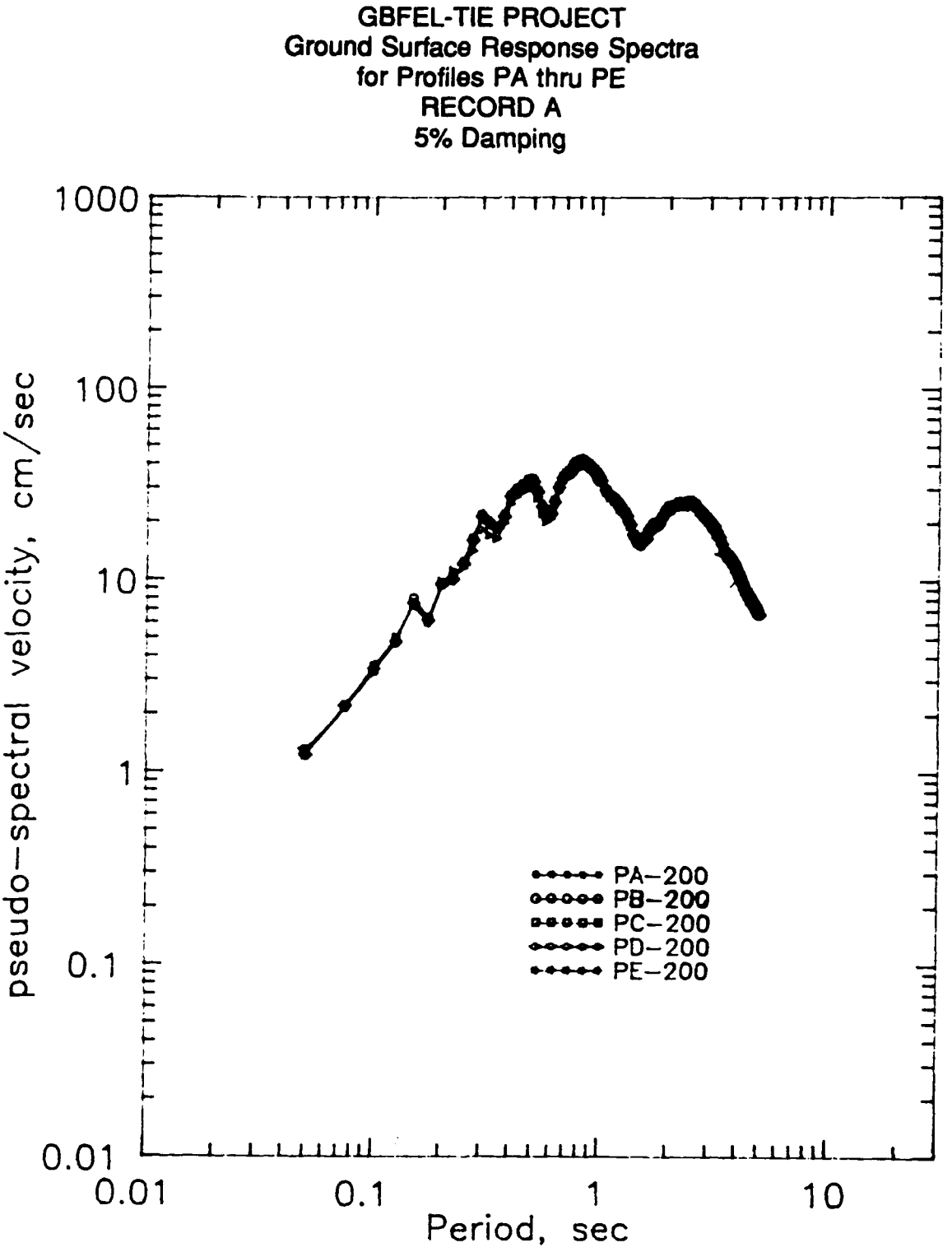

Figure 59. Sensitivity of dynamic response to stratigraphy variations-Comparison of response spectra for upper bound stiffness Profiles PA through PE

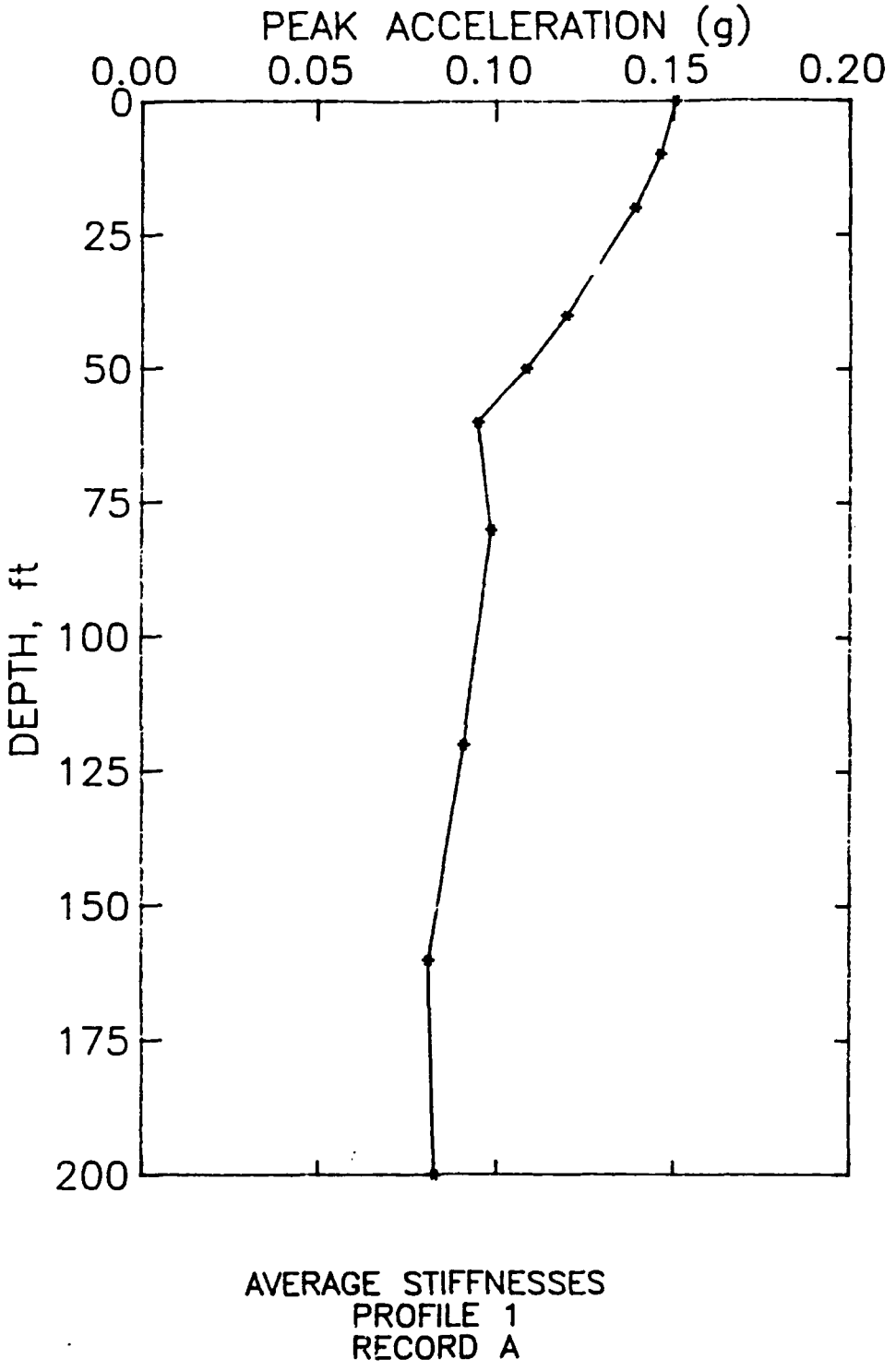

Figure 60. Upper bound sensitivity analysis to stratigraphy variation Peak accelerations versus depth for Profile I due to Record A

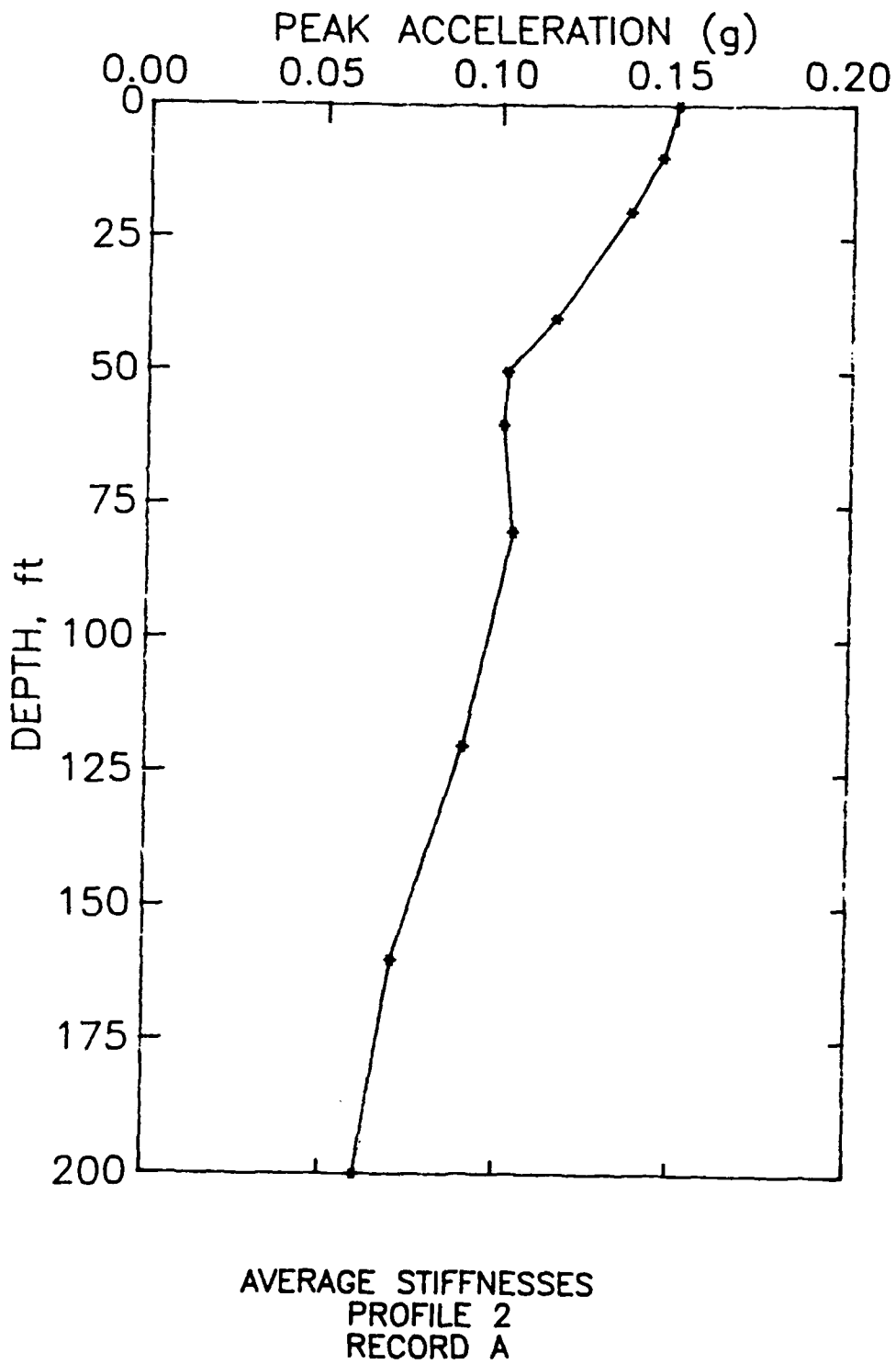

Figure 61. Sensitivity analysis to stratigraphy variation (average stiffnesses) - Peak accelerations versus depth for Profile 2 due to Record A

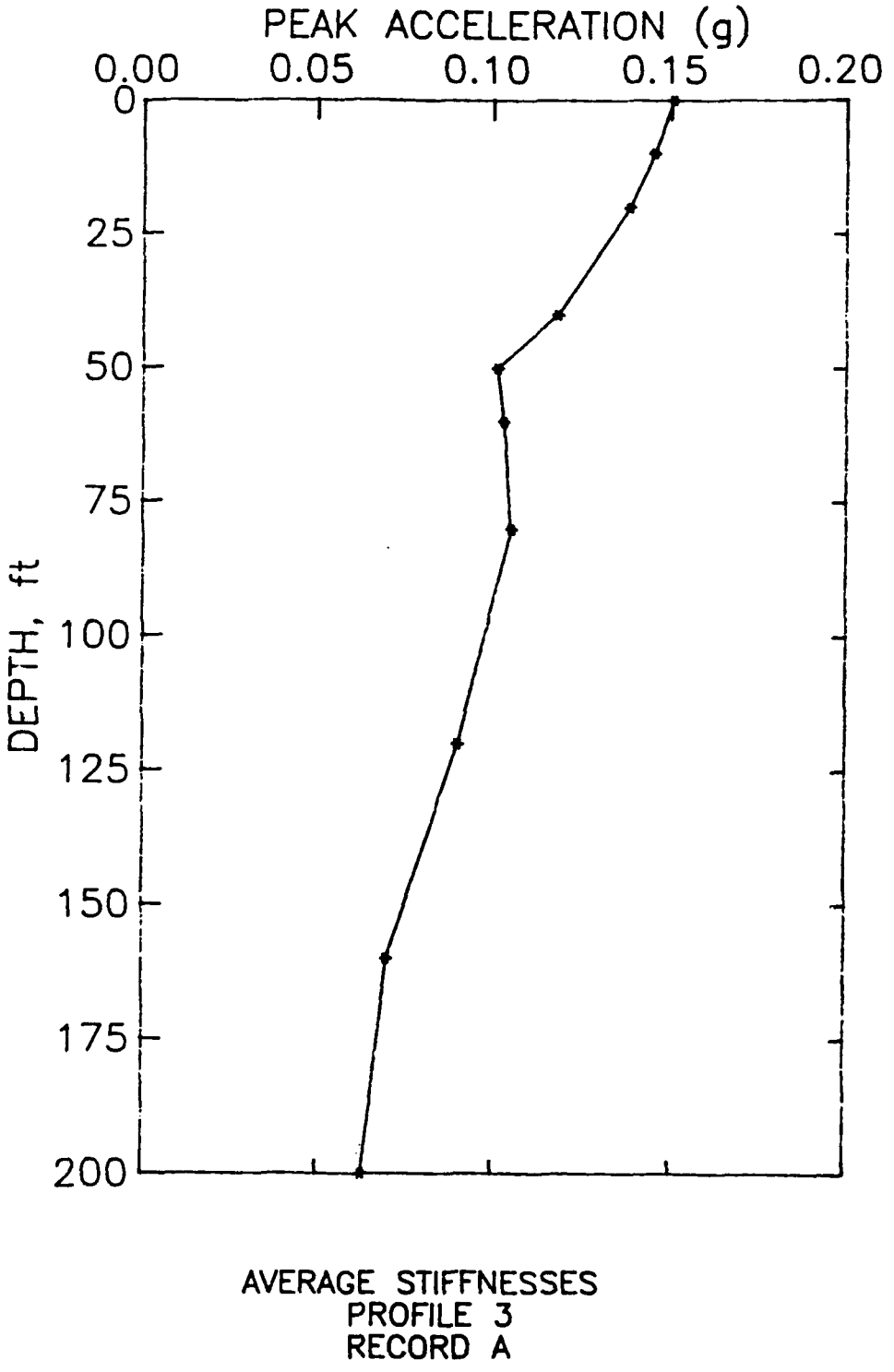

Figure 62. Sensitivity analysis to stratigraphy variation (average stiffnesses) - Peak accelerations versus depth for Profile 3 due to Record A

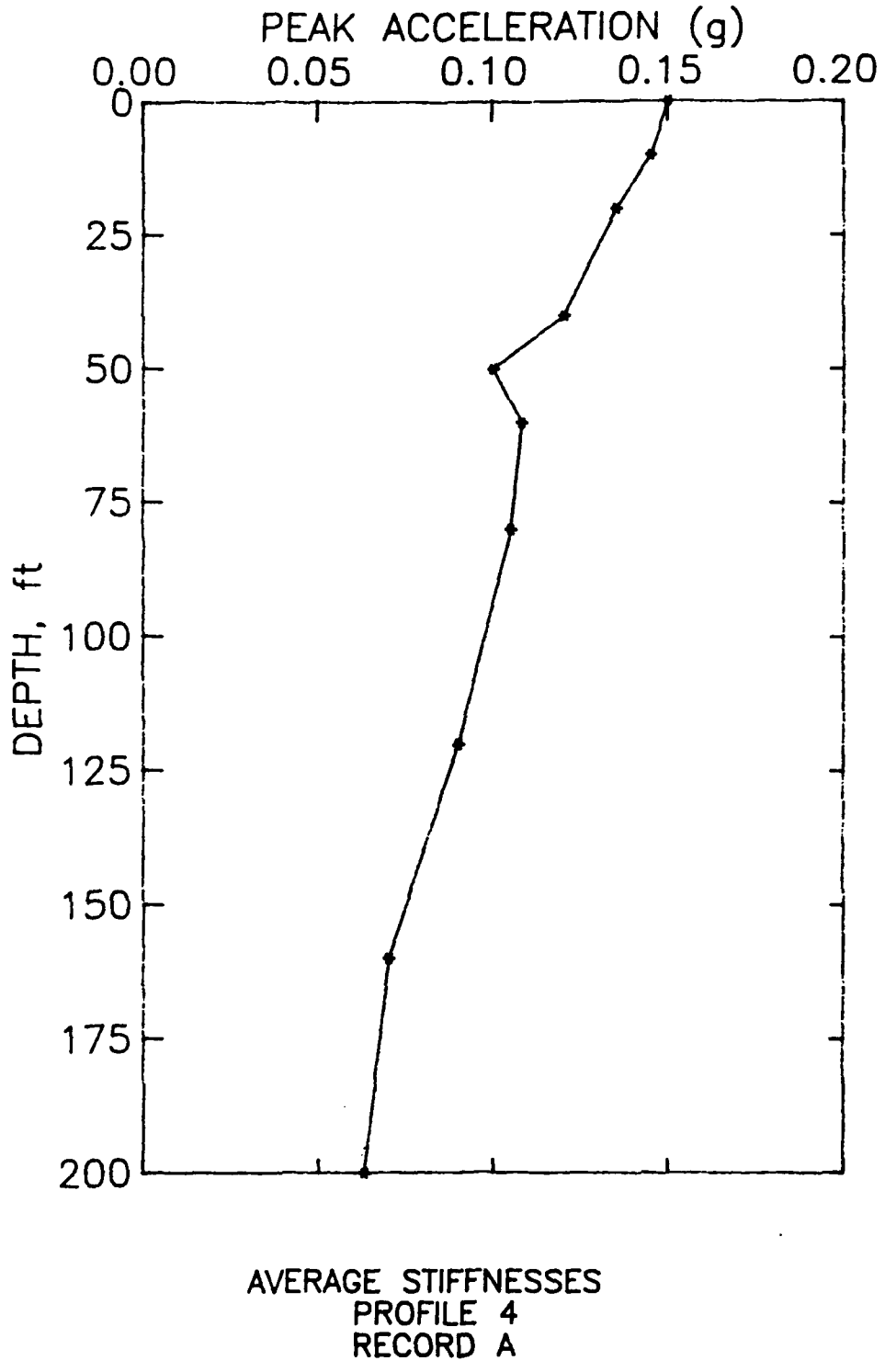

Figure 63. Sensitivity analysis to stratigraphy variation (average stiffnesses) - Peak accelerations versus depth for Profile 4 due to Record A

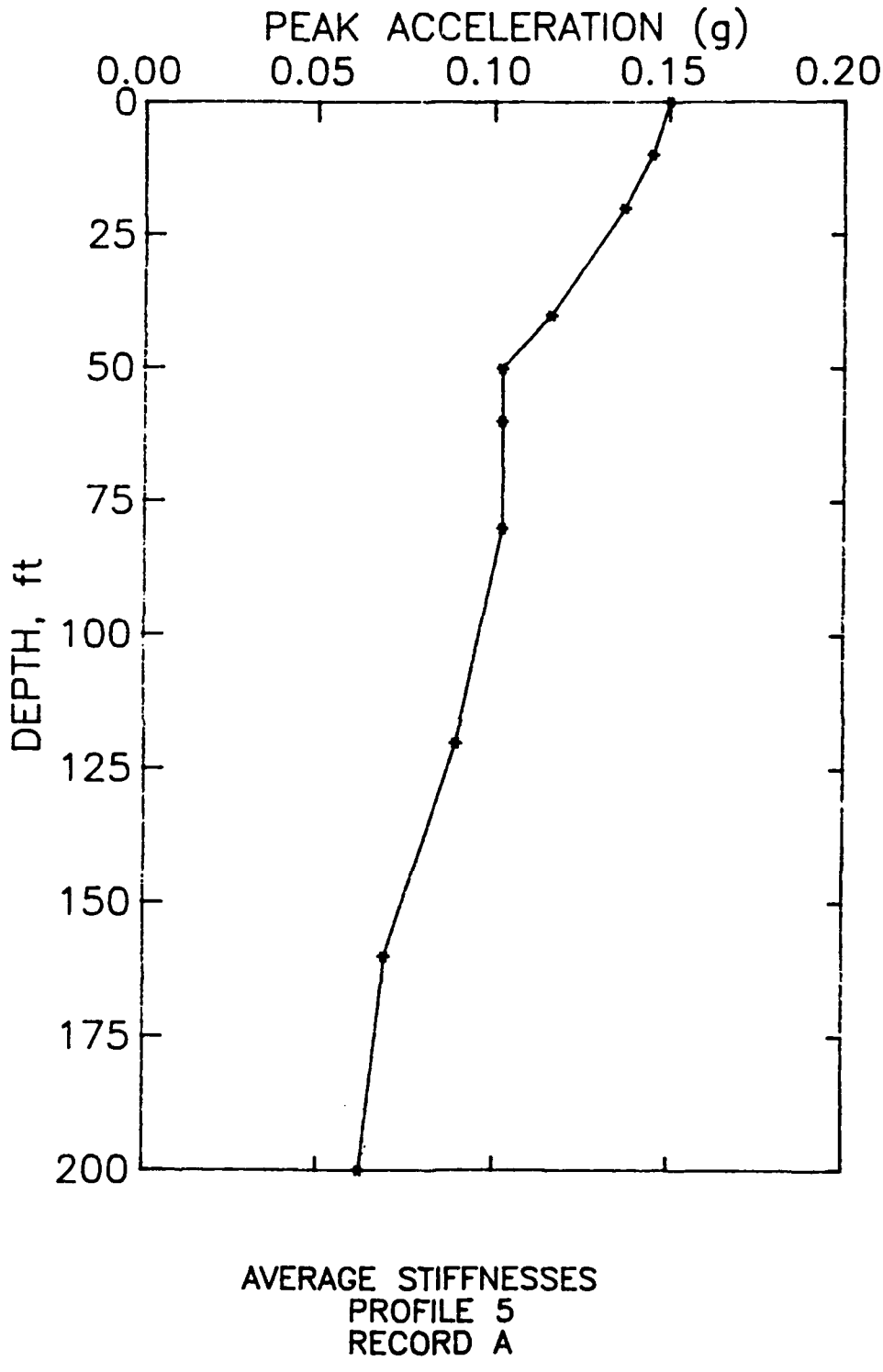

Figure 64. Upper bound sensitivity analysis to stratigraphy variation (average stiffnesses) - Peak accelerations versus depth for Profile 5 due to Record A

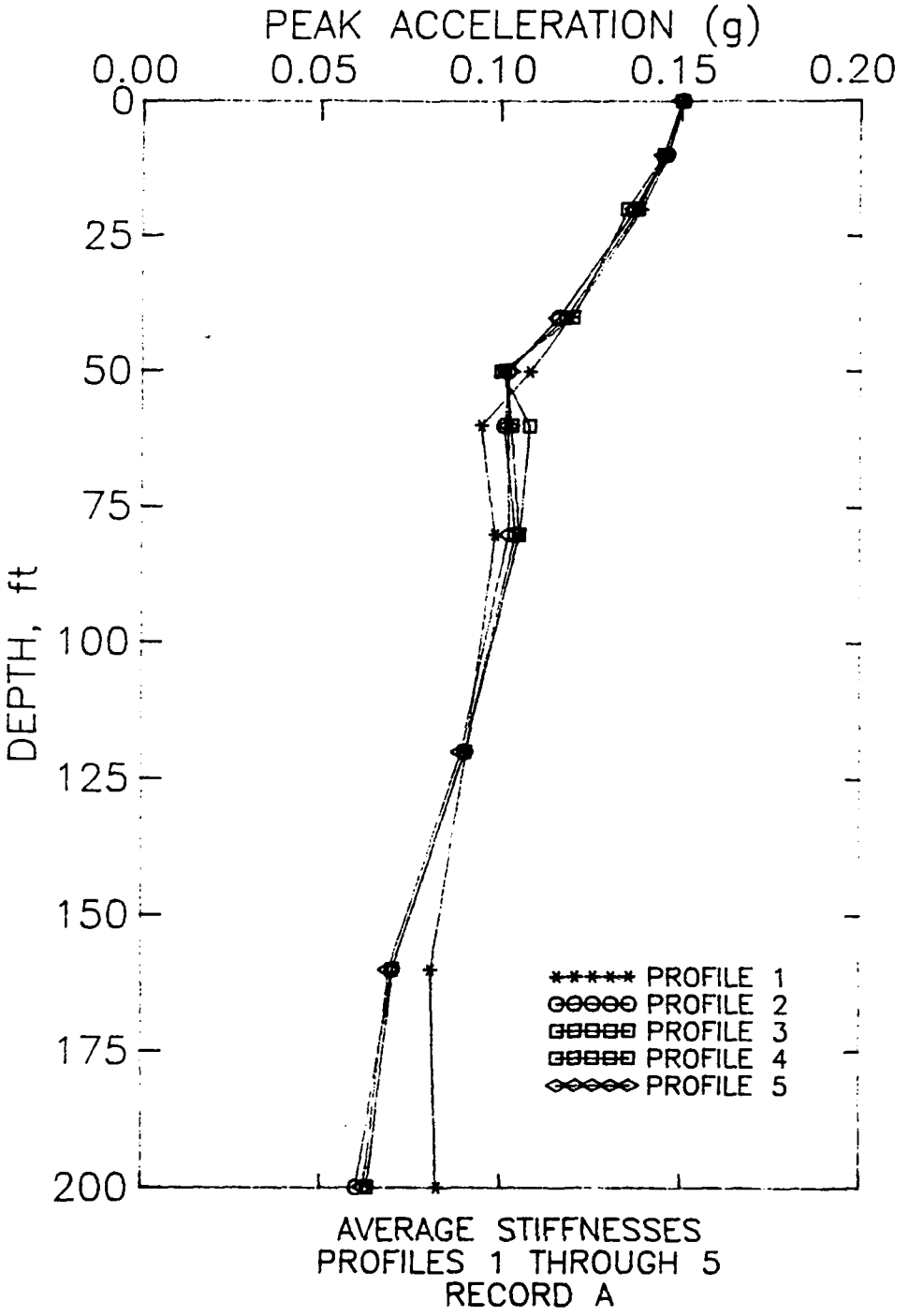

Figure 65. Sensitivity of dynamic response to stratigraphy variation - Comparison of response spectra for upper bound stiffness Profiles 1 through 5

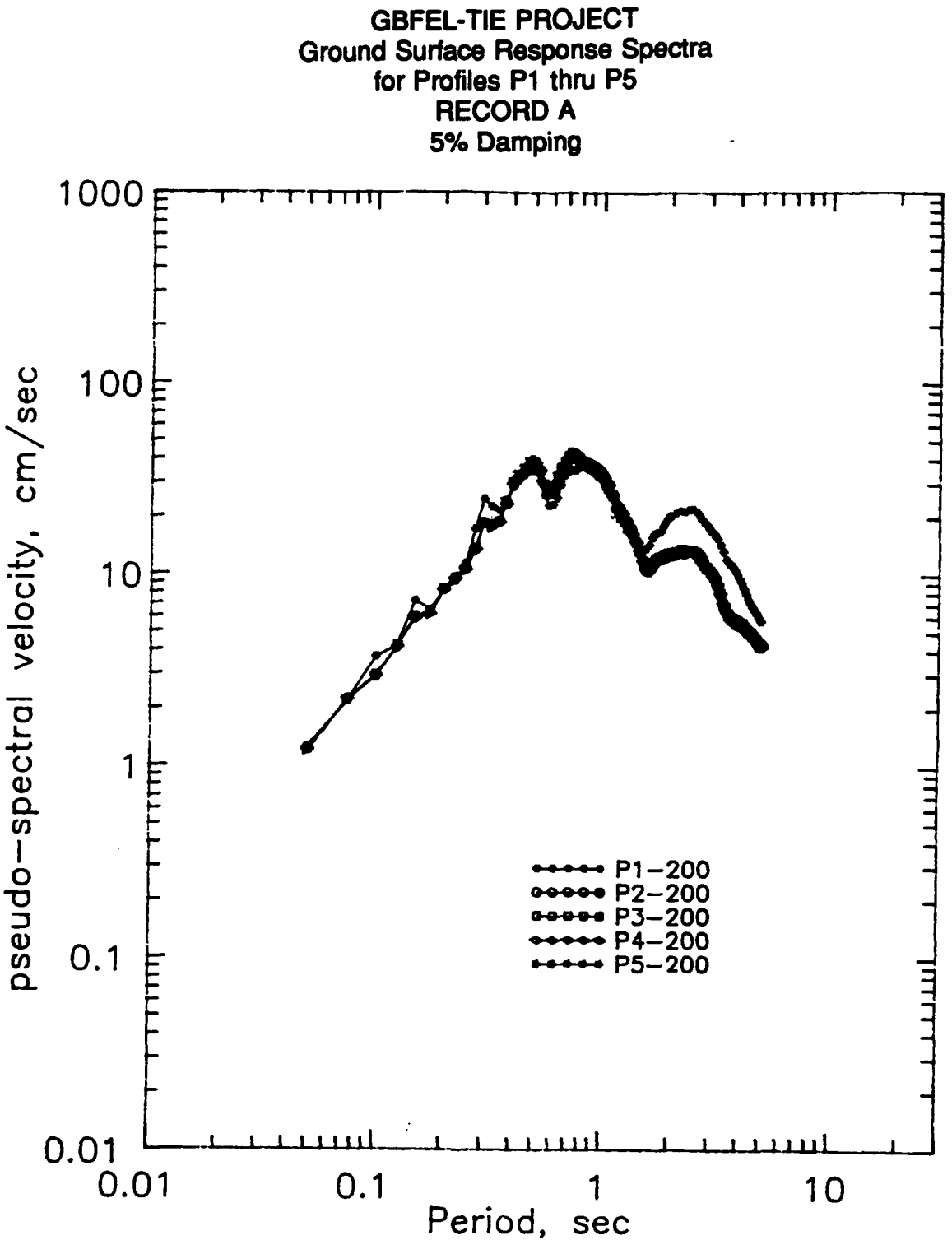

Figure 66. Sensitivity of dynamic response to stratigraphy variation - Comparison of response spectra for average stiffness Profiles P1 through P5

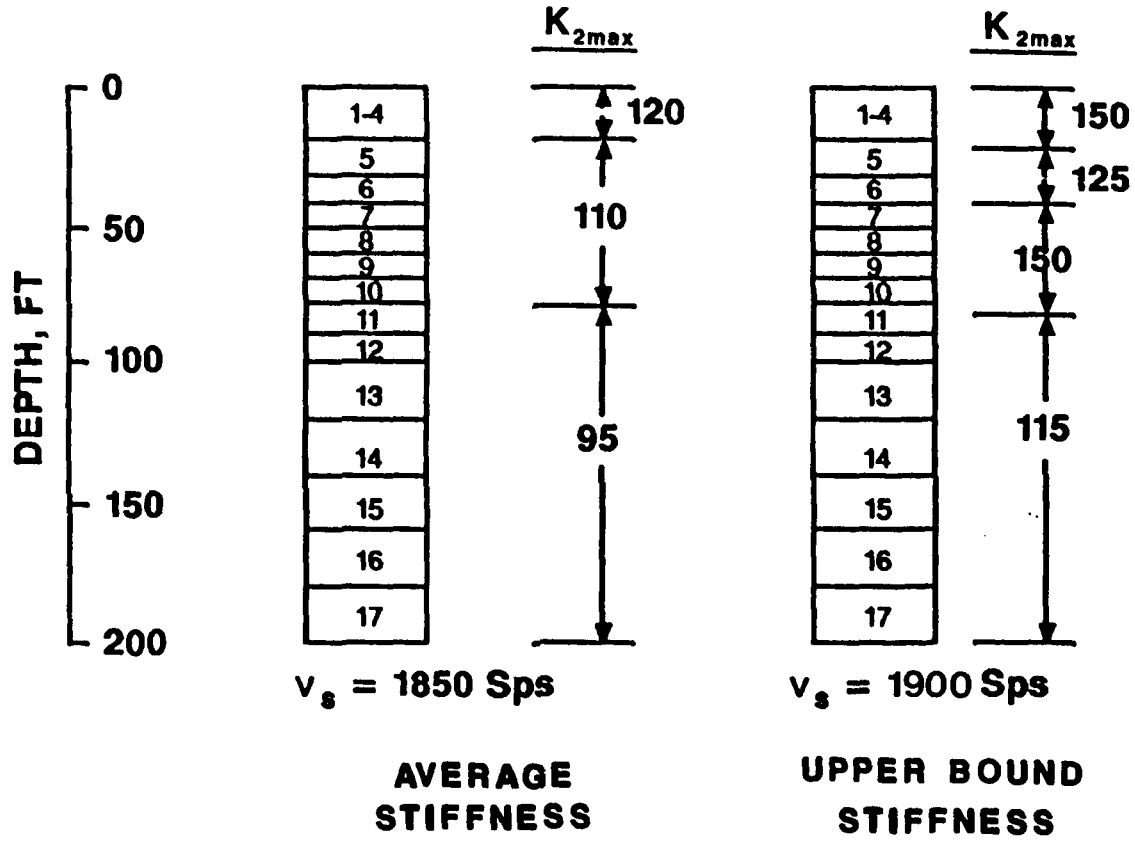

Figure 67. Truncated SHAKE profiles

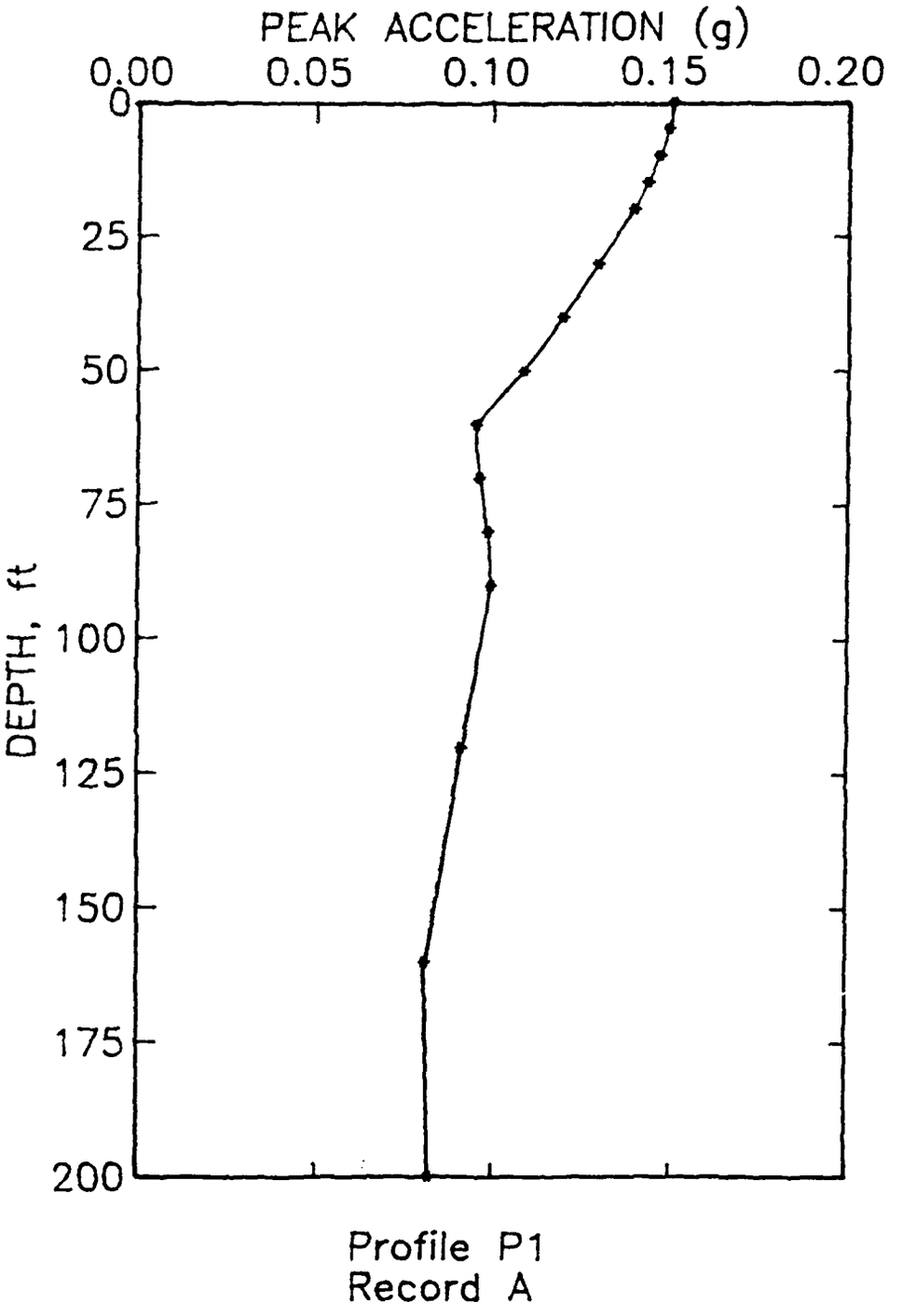

Figure 68. Acceleration versus depth for Profile P1 excited by Record A

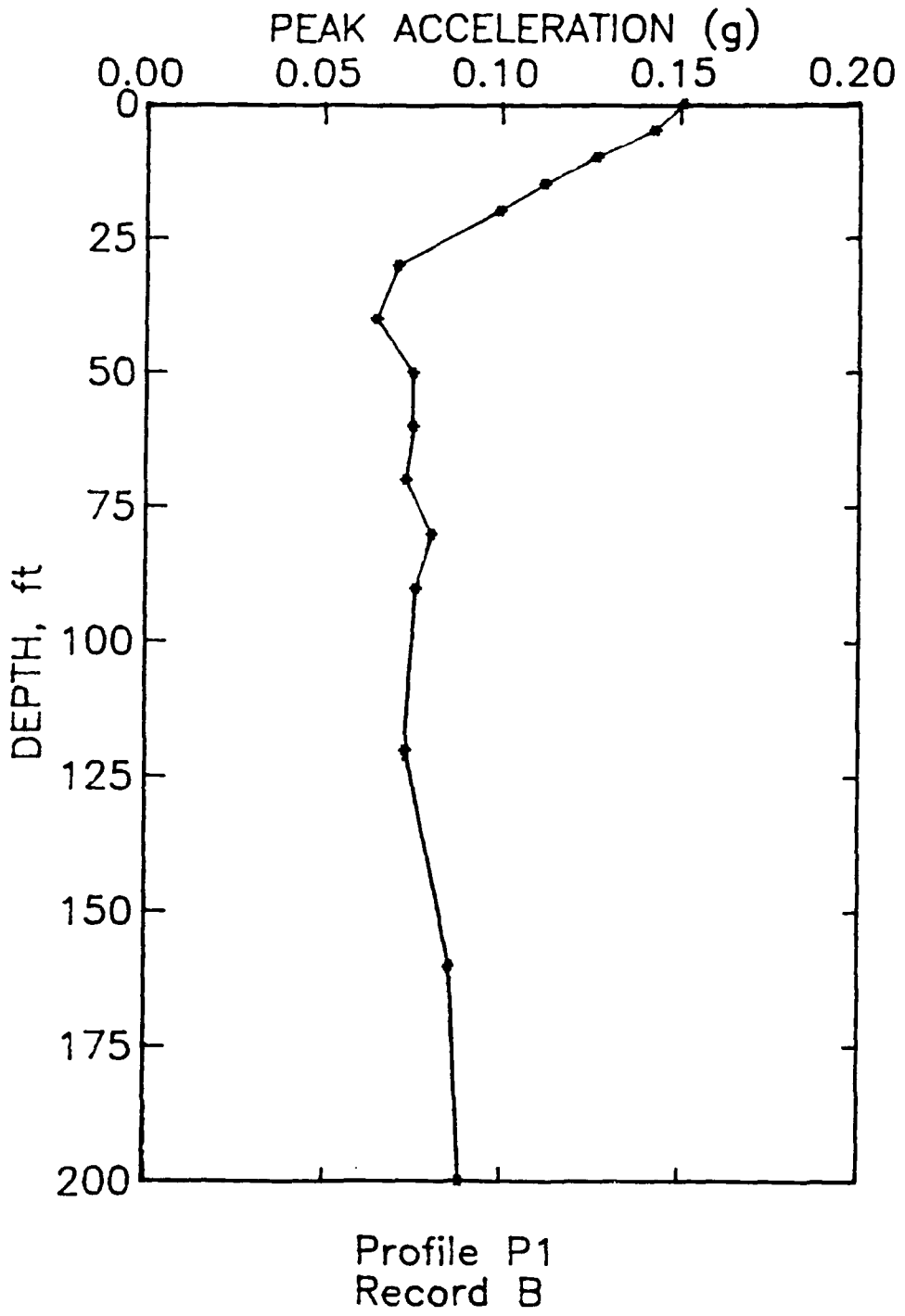

Figure 69. Acceleration versus depth for Profile P1 excited by Record B

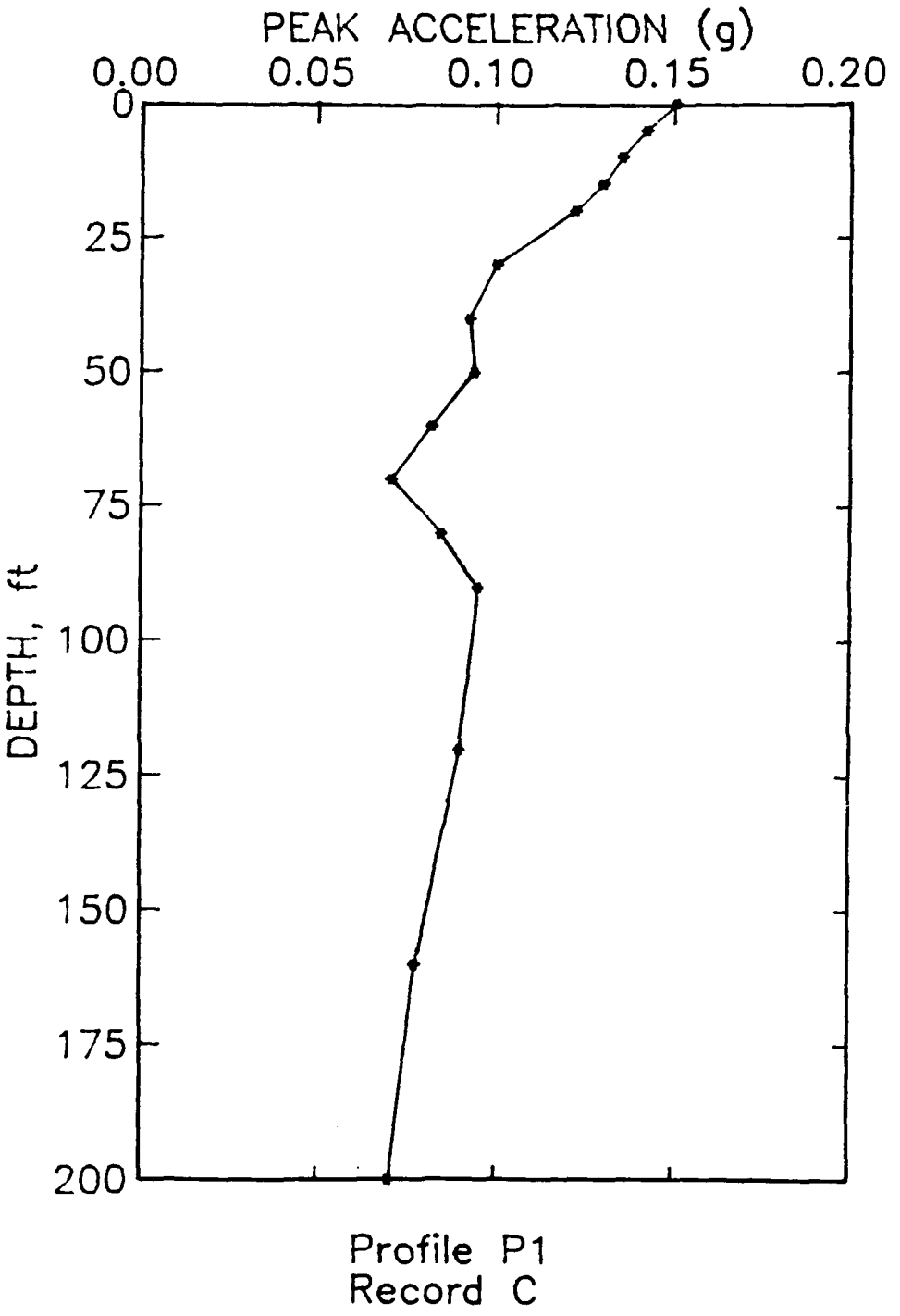

Figure 70. Acceleration versus depth for Profile P1 excited by Record C

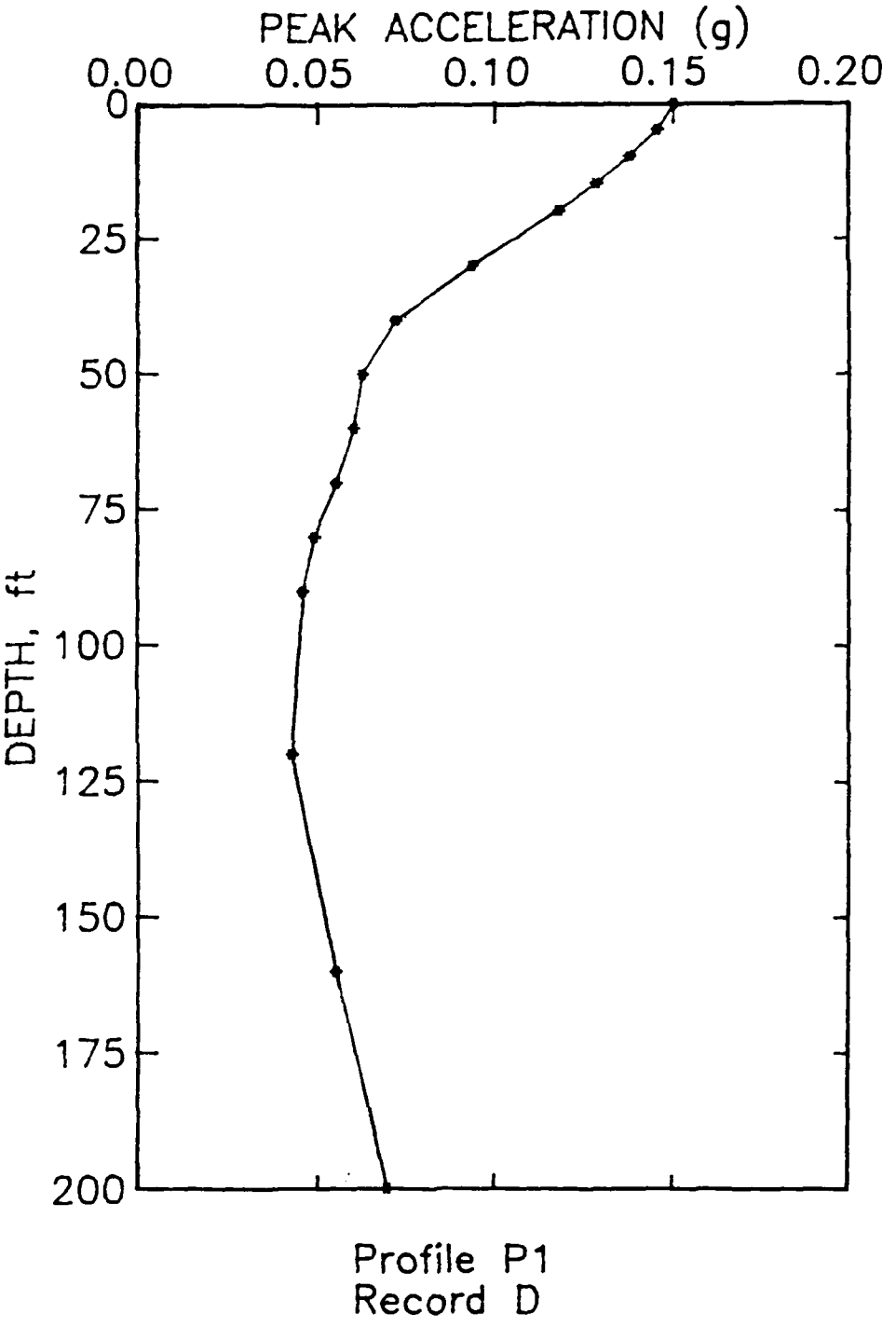

Figure 71. Acceleration versus depth for Profile P1 excited by Record D

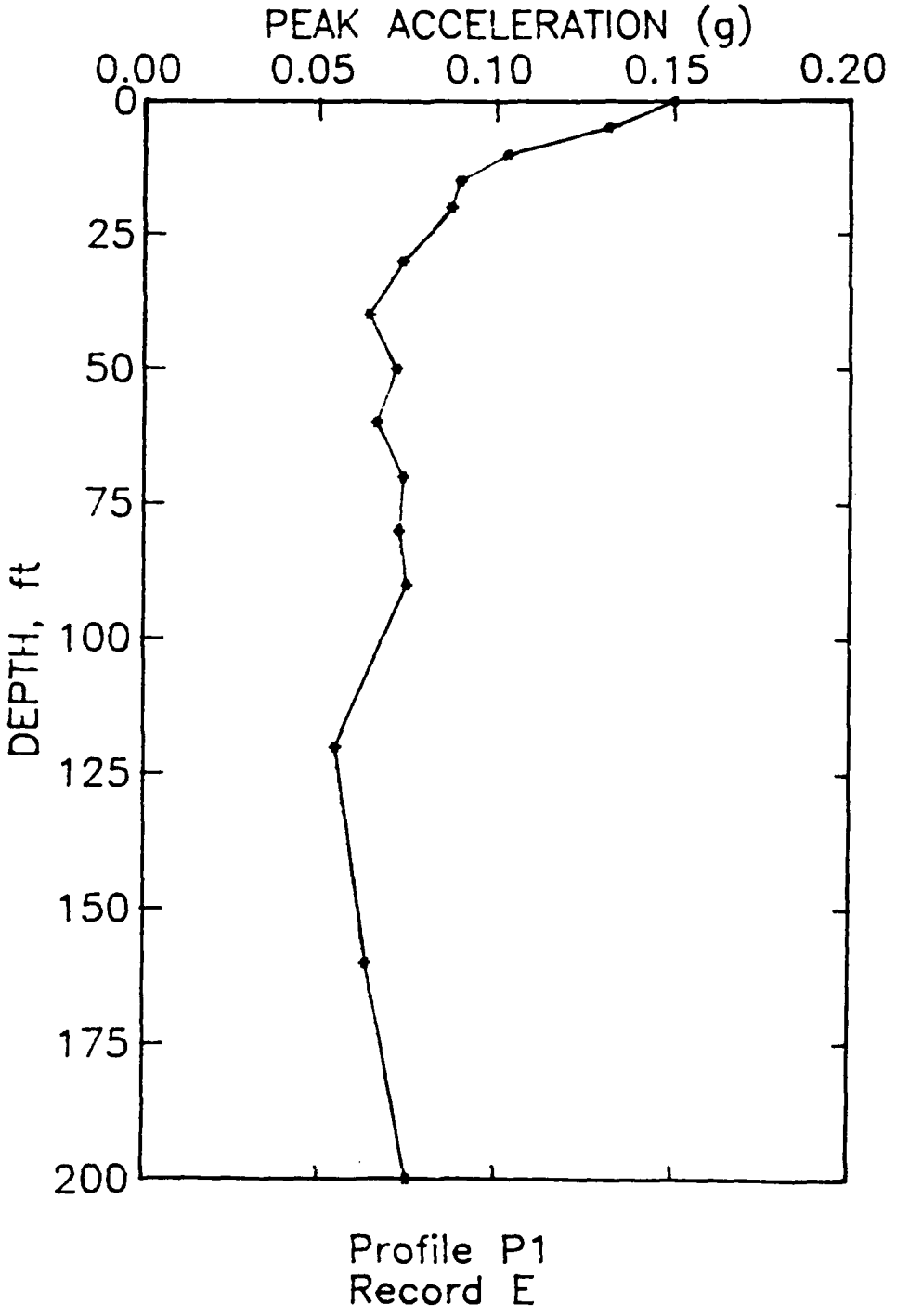

Figure 72. Acceleration versus depth for Profile P1 excited by Record E

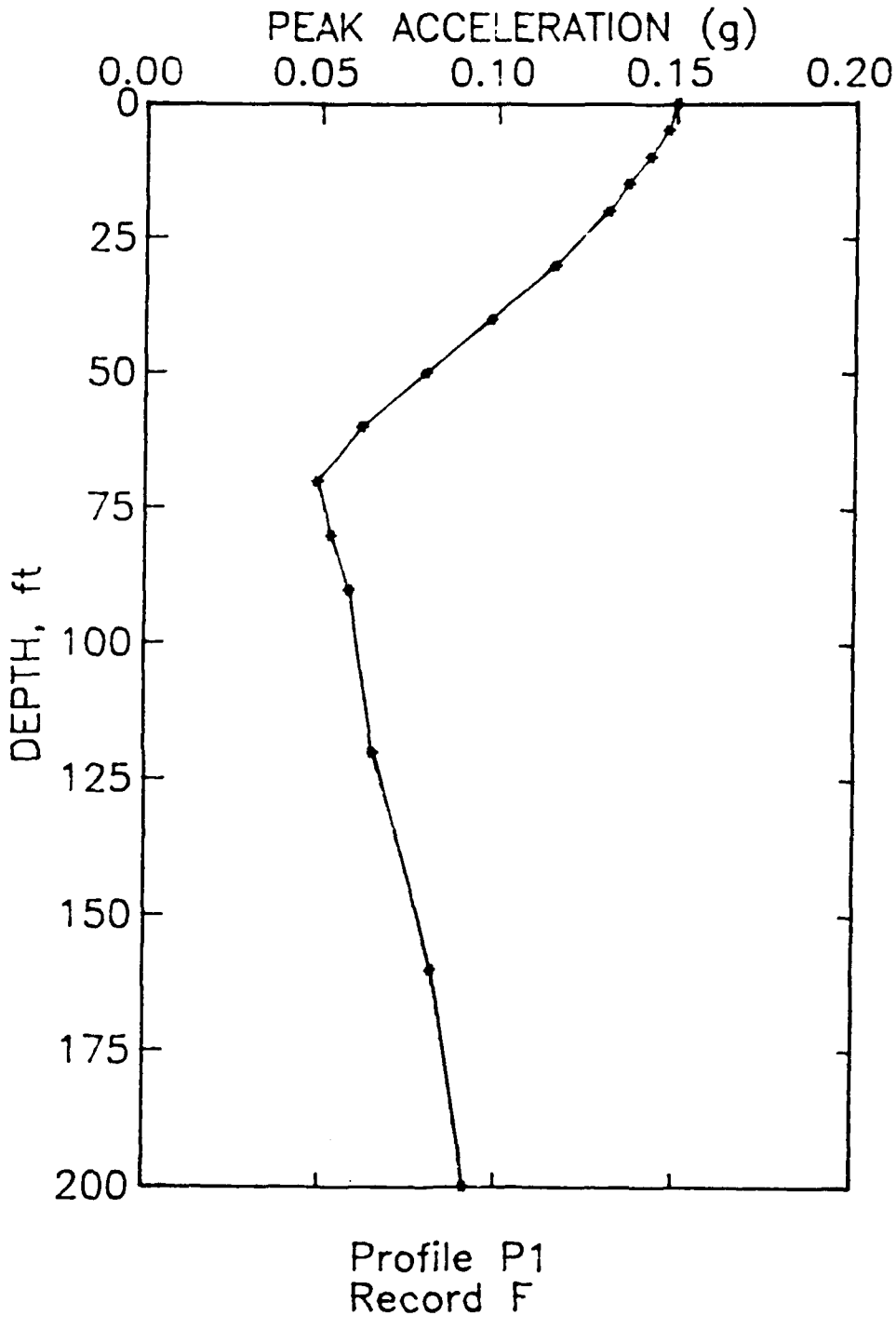

Figure 73. Acceleration versus depth for Profile P1 excited by Record F

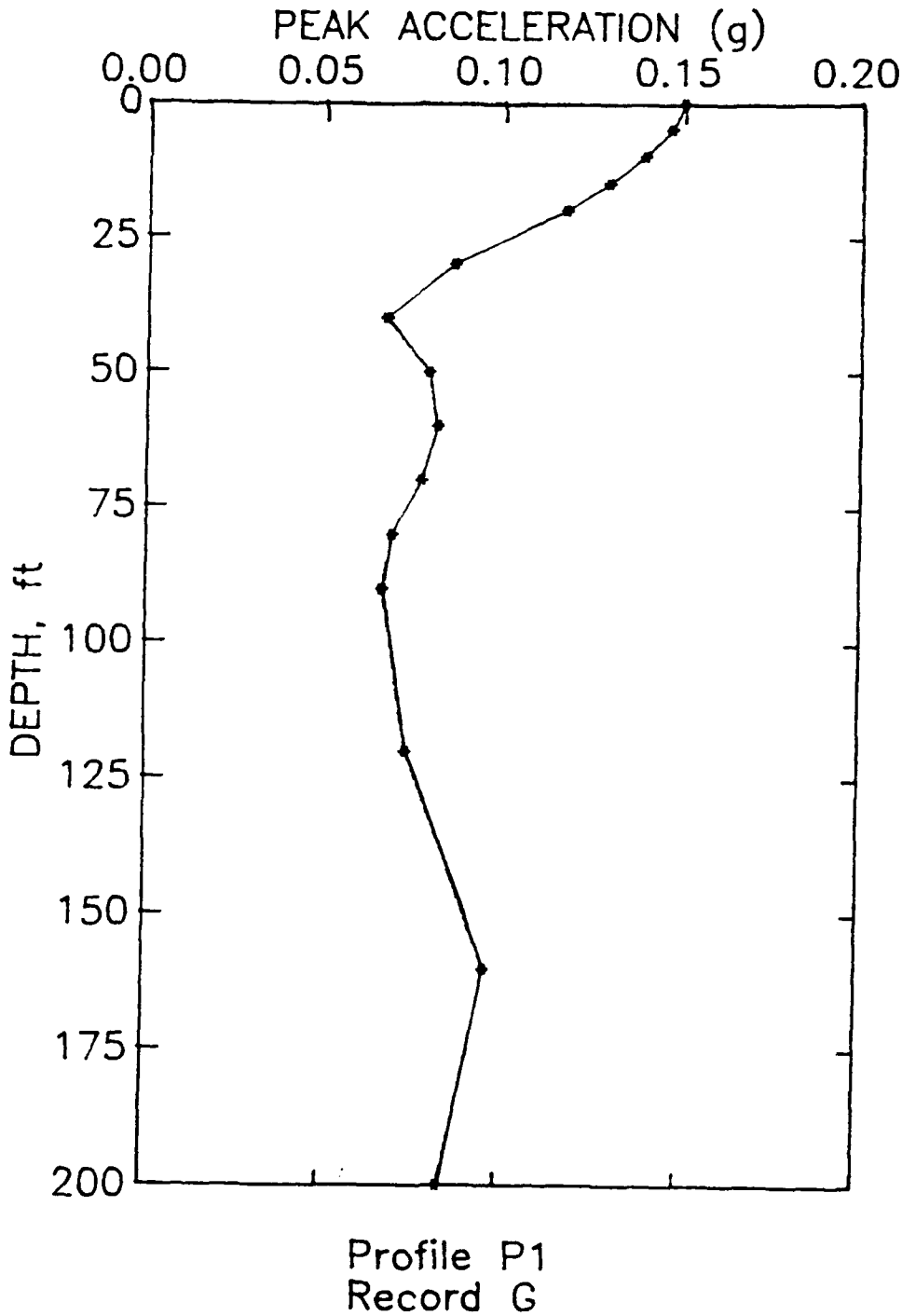

Figure 74. Acceleration versus depth for Profile P1 excited by Record G

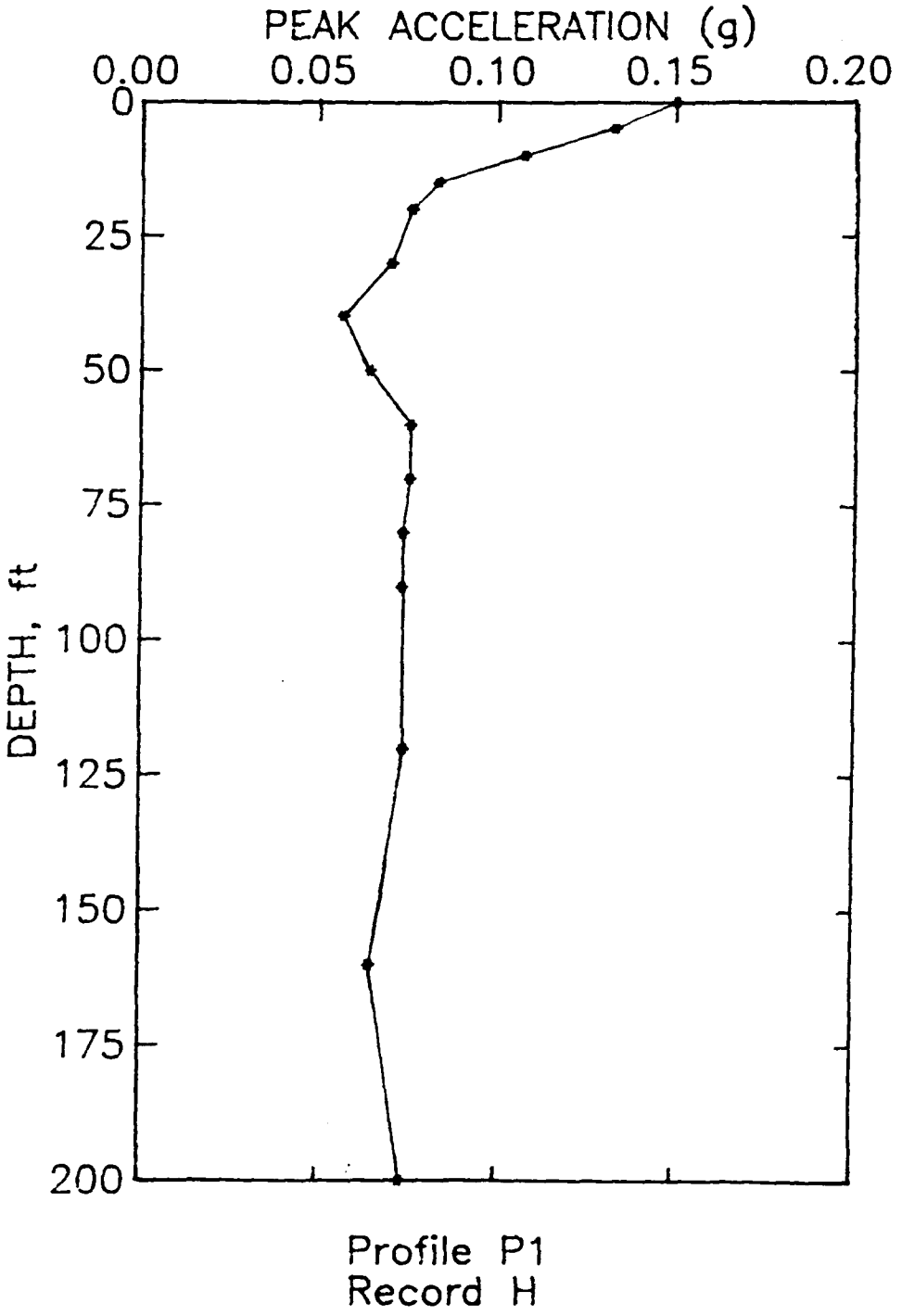

Figure 75. Acceleration versus depth for Profile P1 excited by Record H

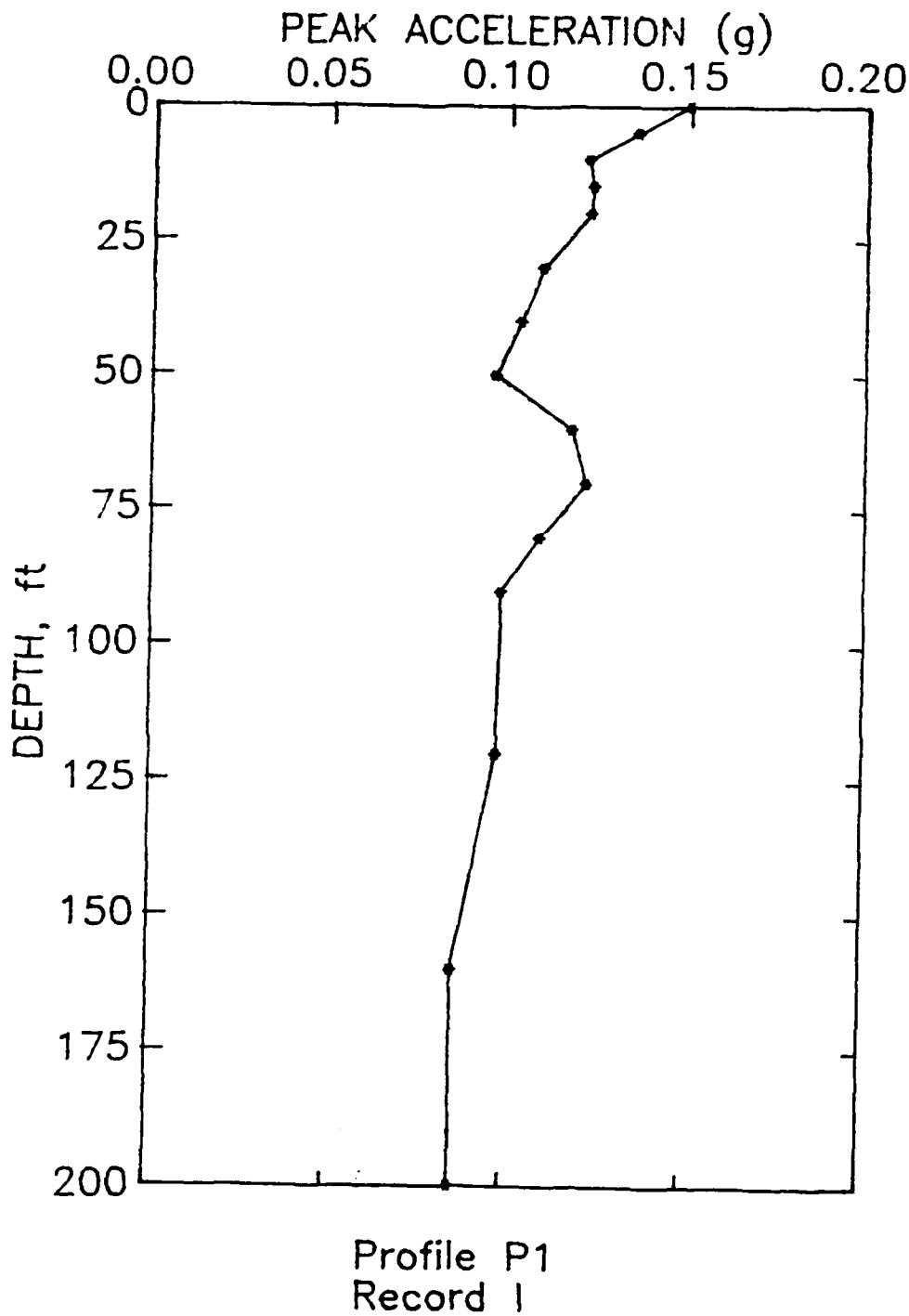

Figure 76. Acceleration versus depth for Profile P1 excited by Record I

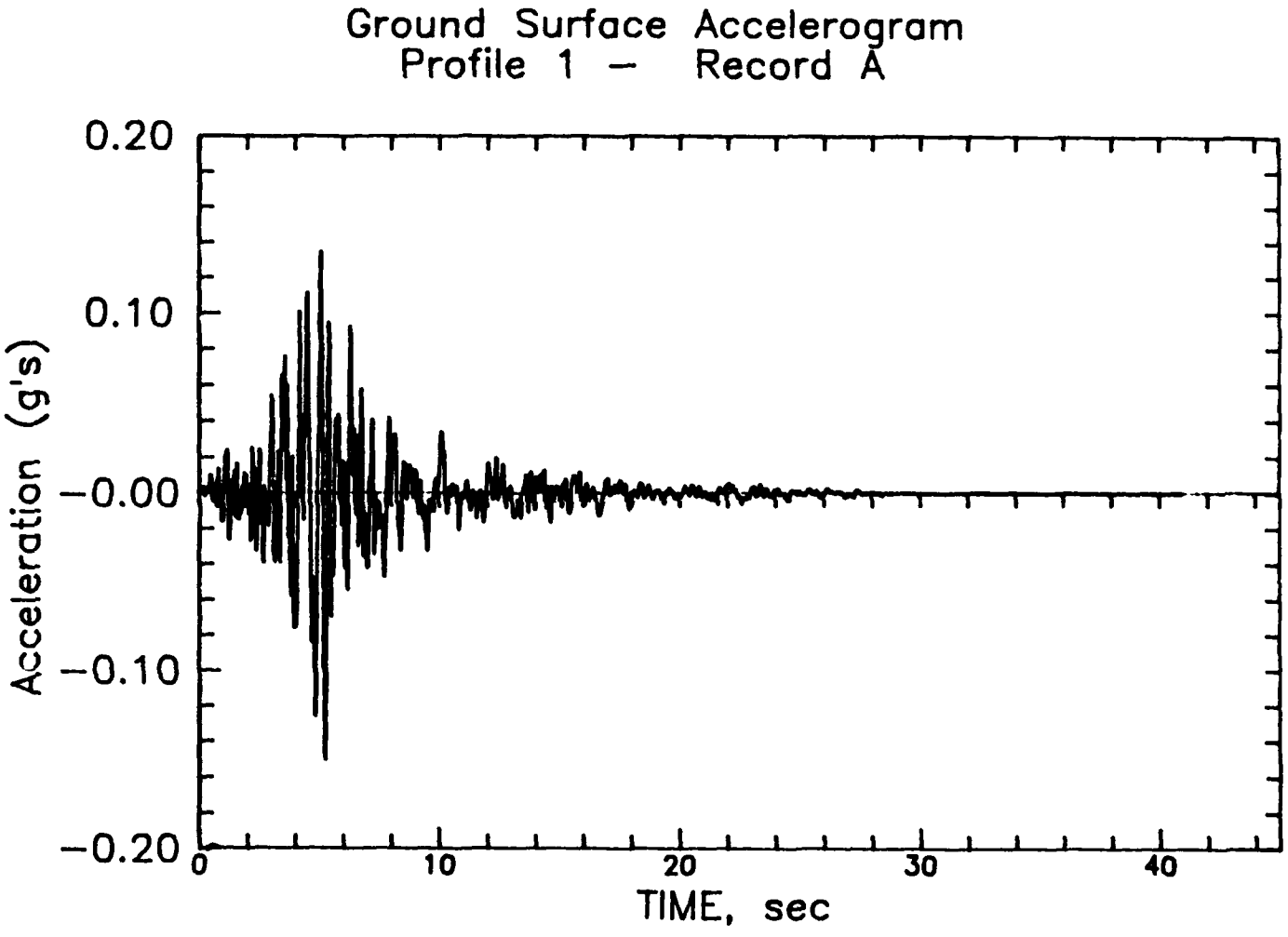

Figure 77. Ground surface accelerogram for Profile P1 derived from Record A

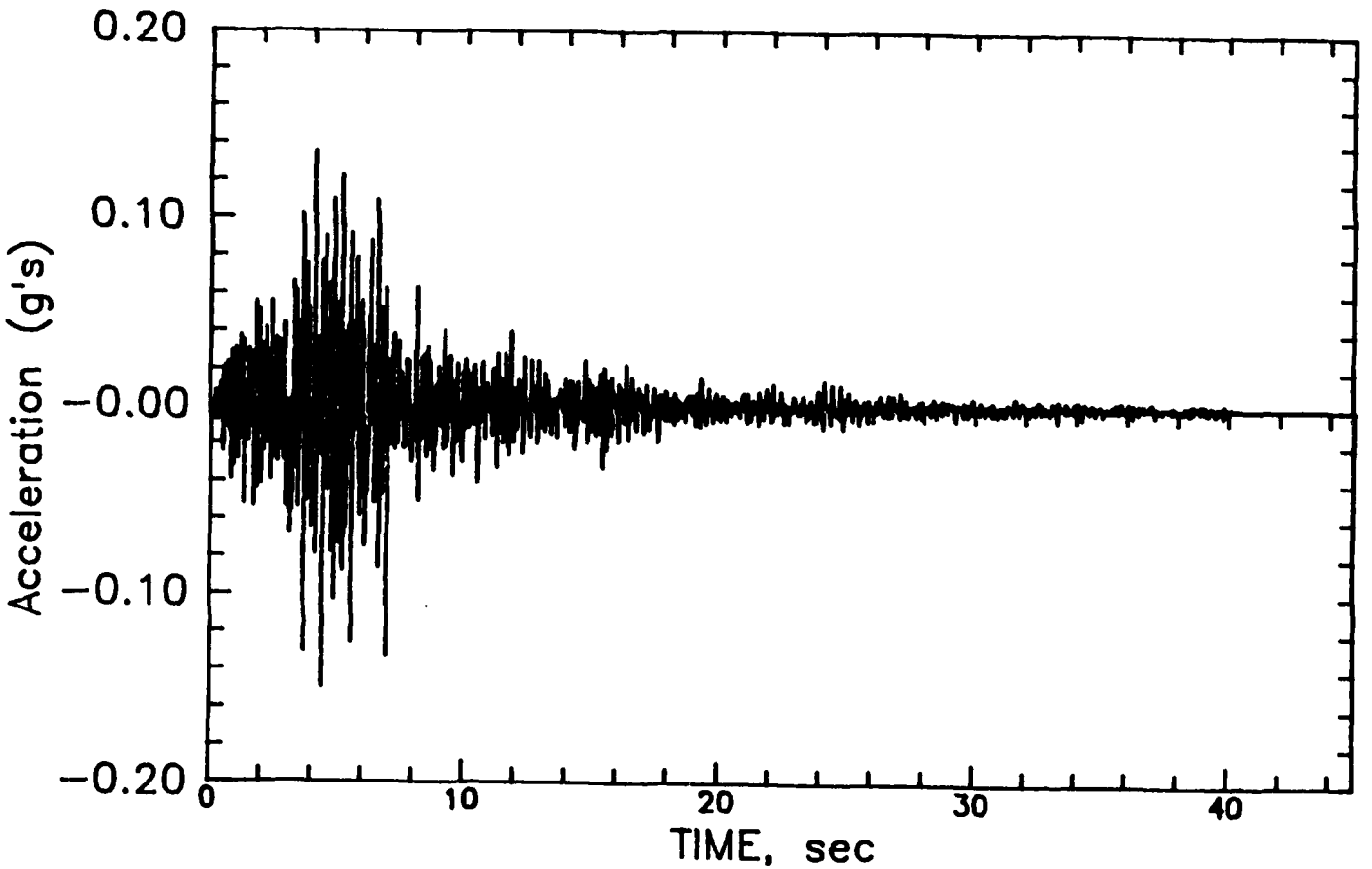

Figure 78. Ground surface accelerogram for Profile P1 derived from Record B

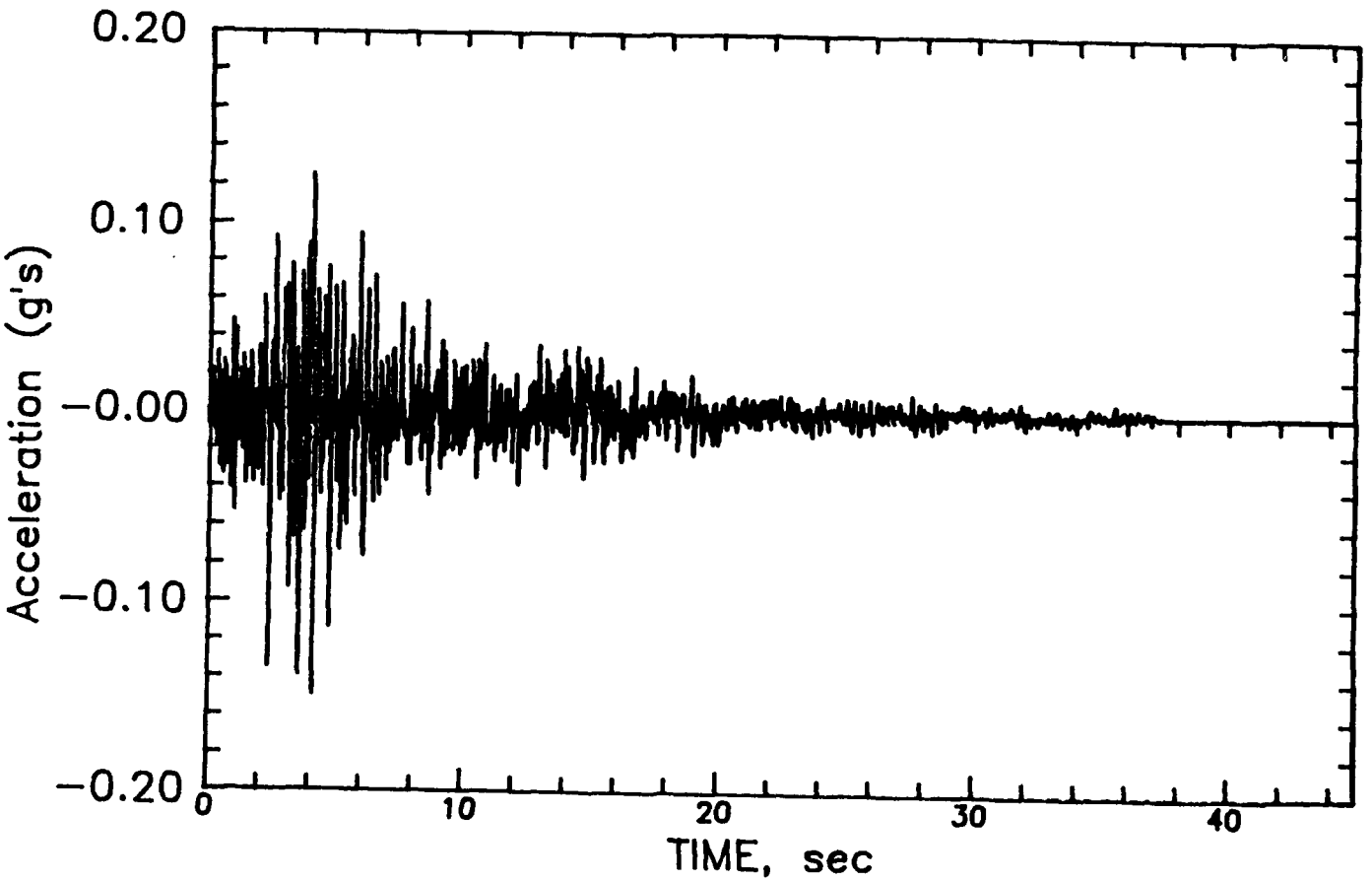

Figure 79. Ground surface accelerogram for Profile P1 derived from Record C

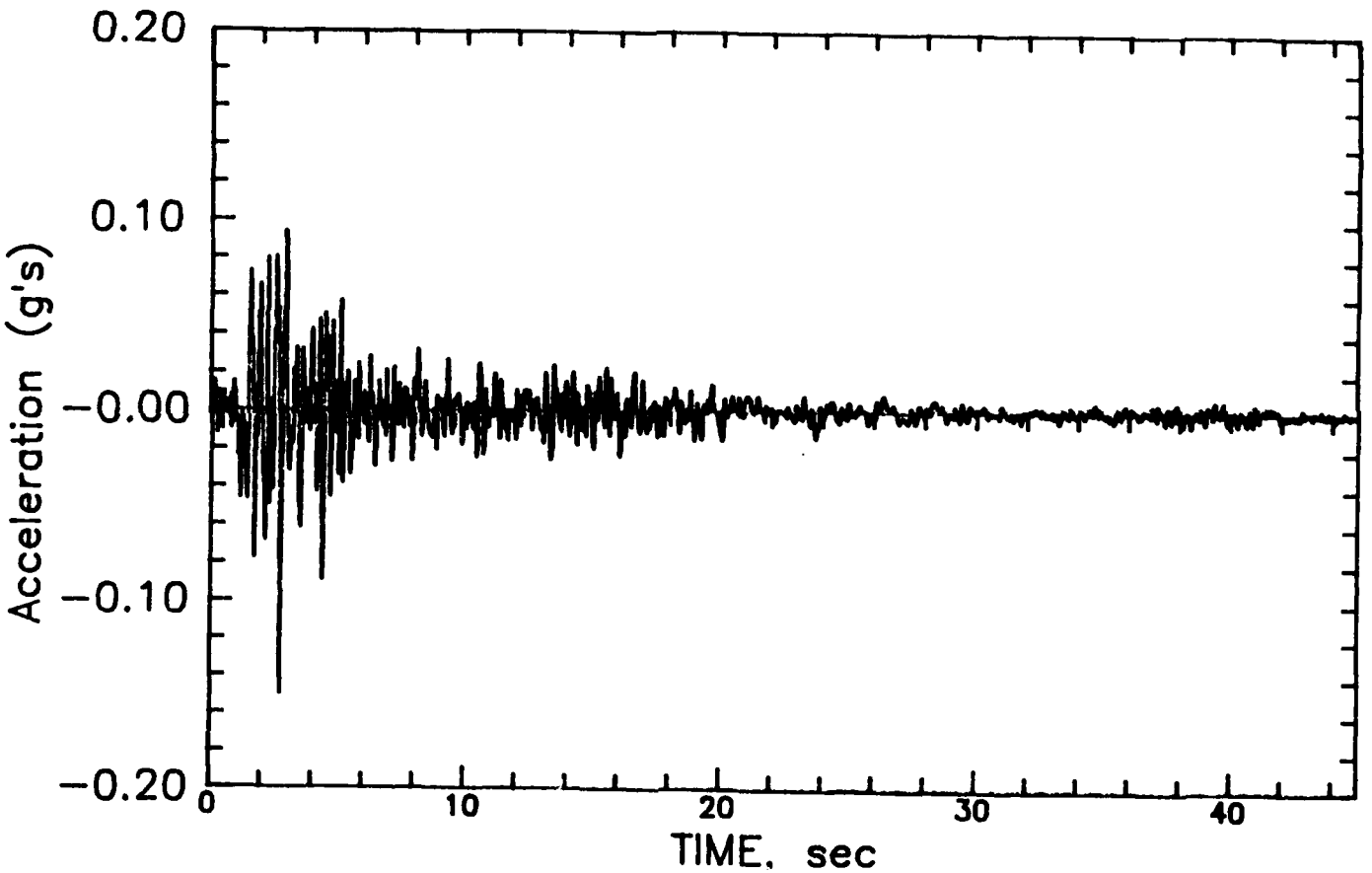

Figure 80. Ground surface accelerogram for Profile P1 derived from Record D

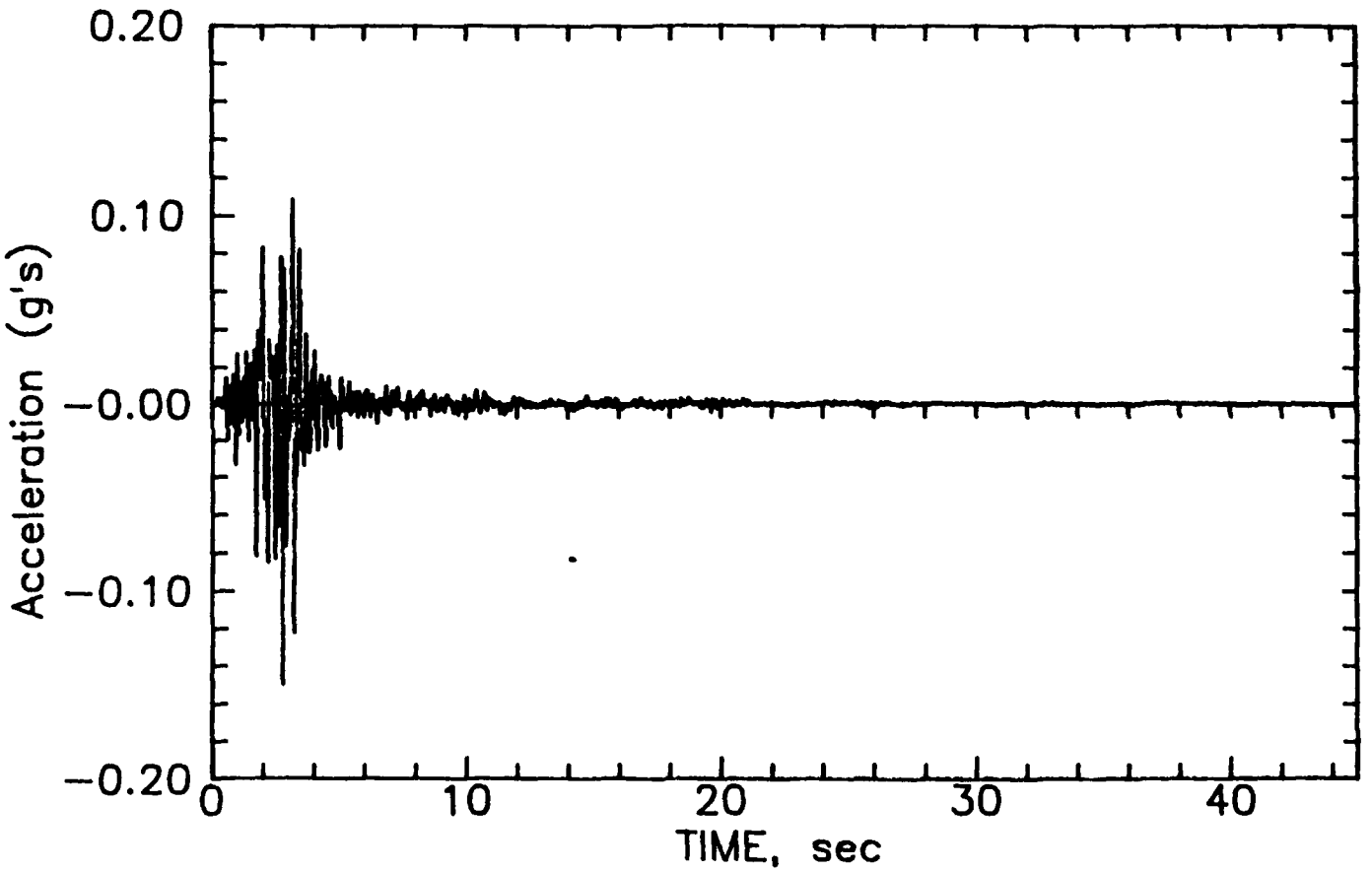

Figure 81. Ground surface accelerogram for Profile P1 derived from Record E

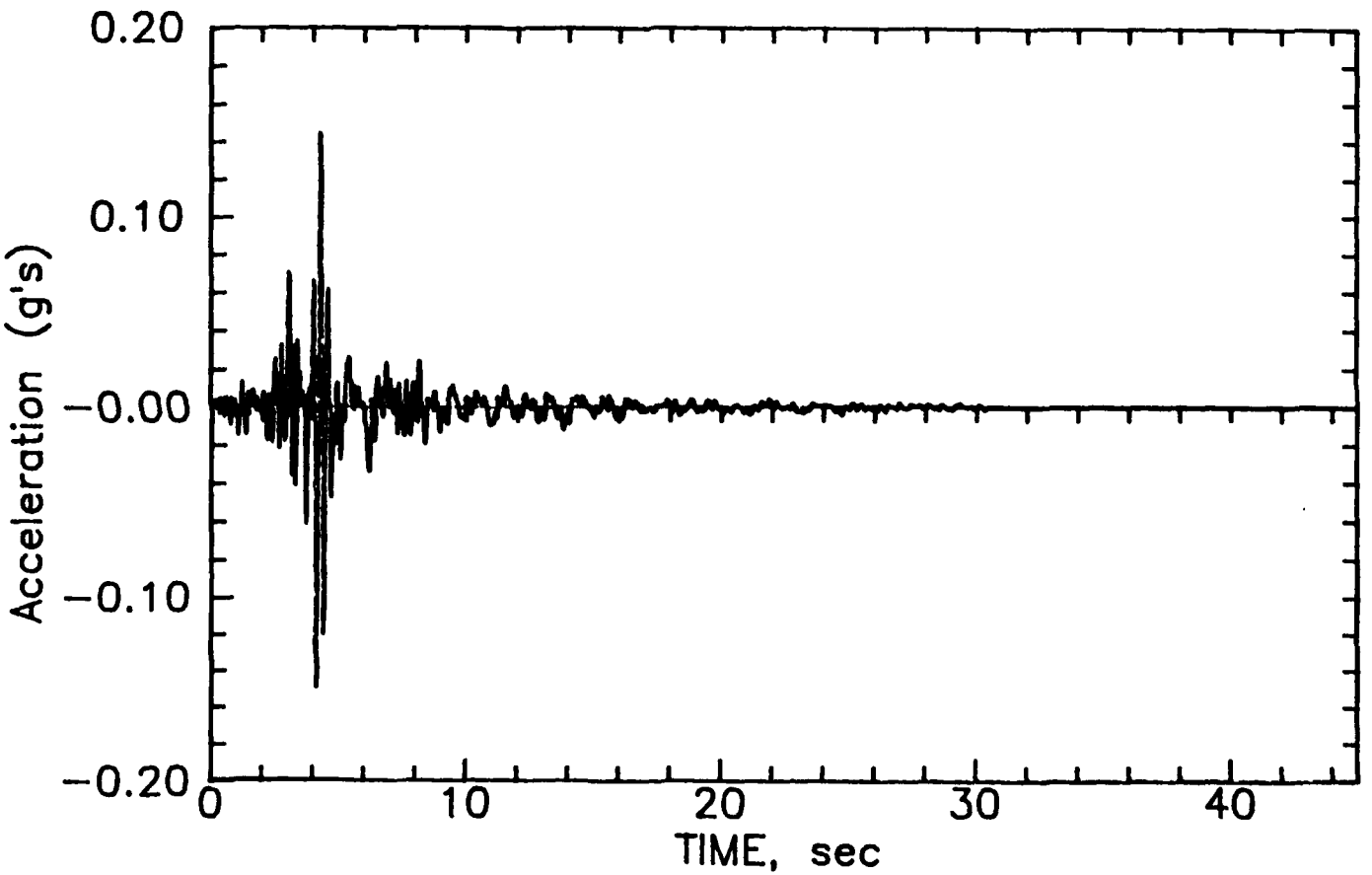

Figure 82. Ground surface accelerogram for Profile P1 derived from Record F

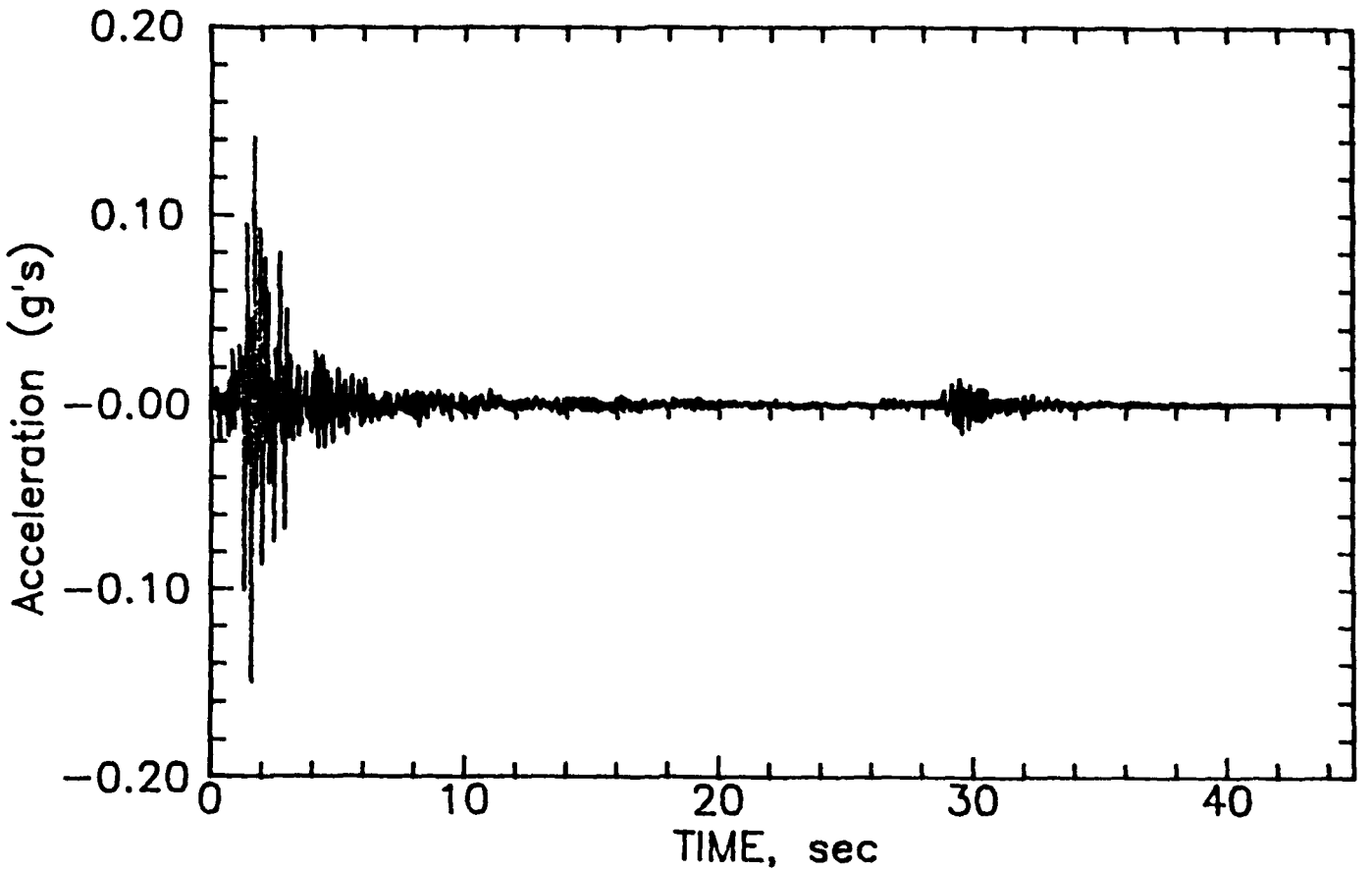

Figure 83. Ground surface accelerogram for Profile P1 derived from Record G

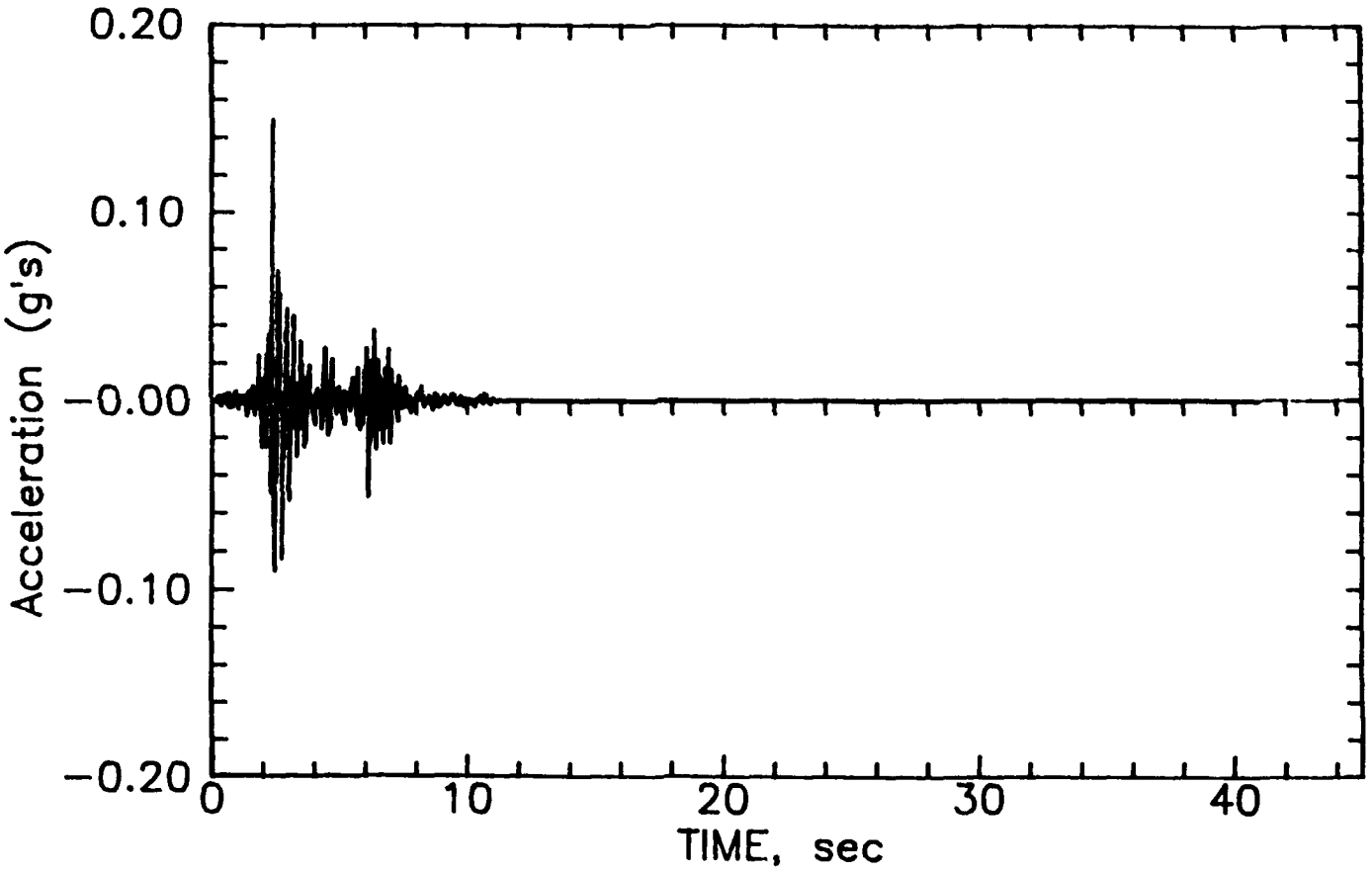

Figure 84. Ground surface accelerogram for Profile P1 derived from Record H

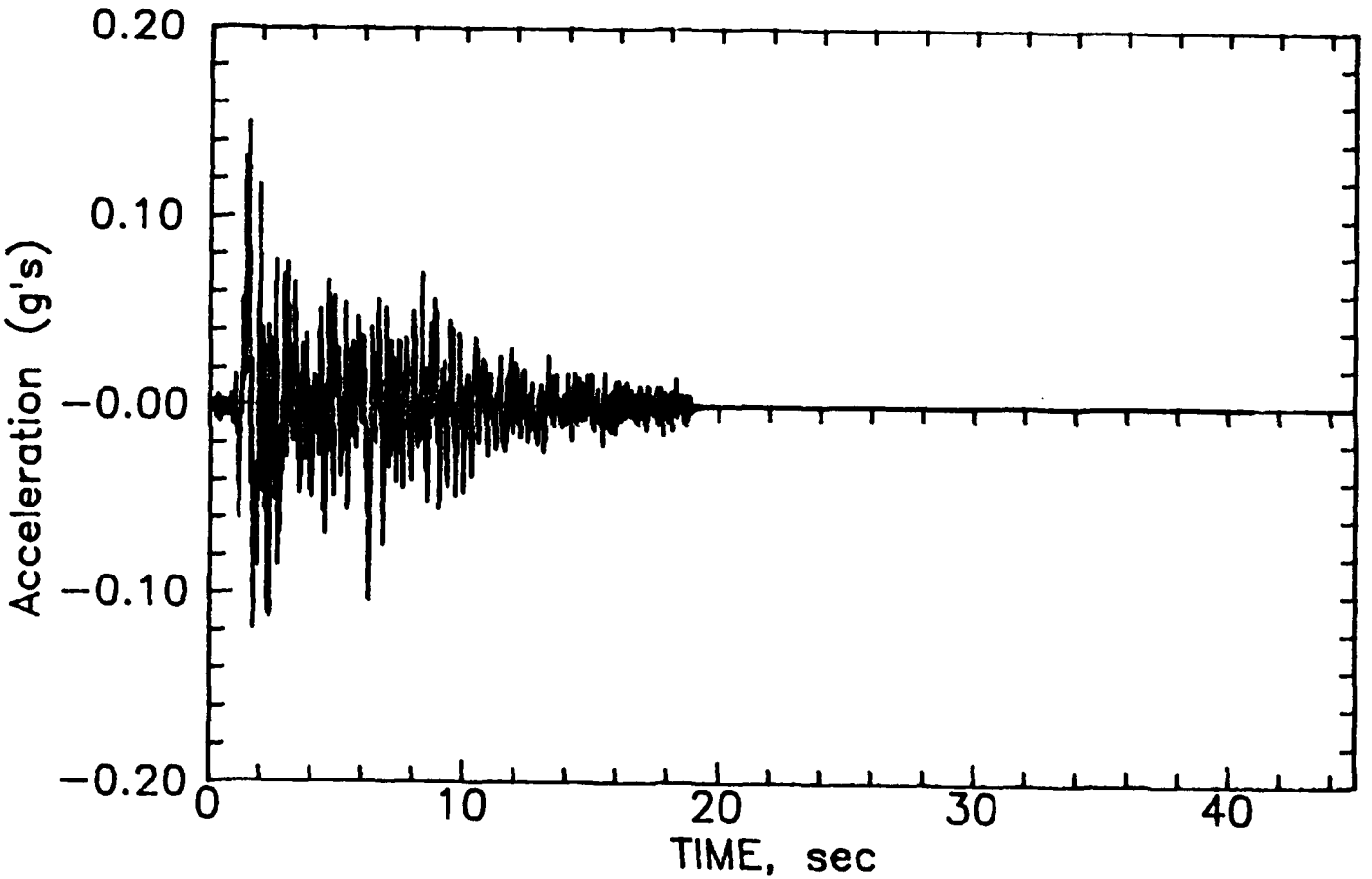

Figure 85. Ground surface accelerogram for Profile P1 derived from Record I

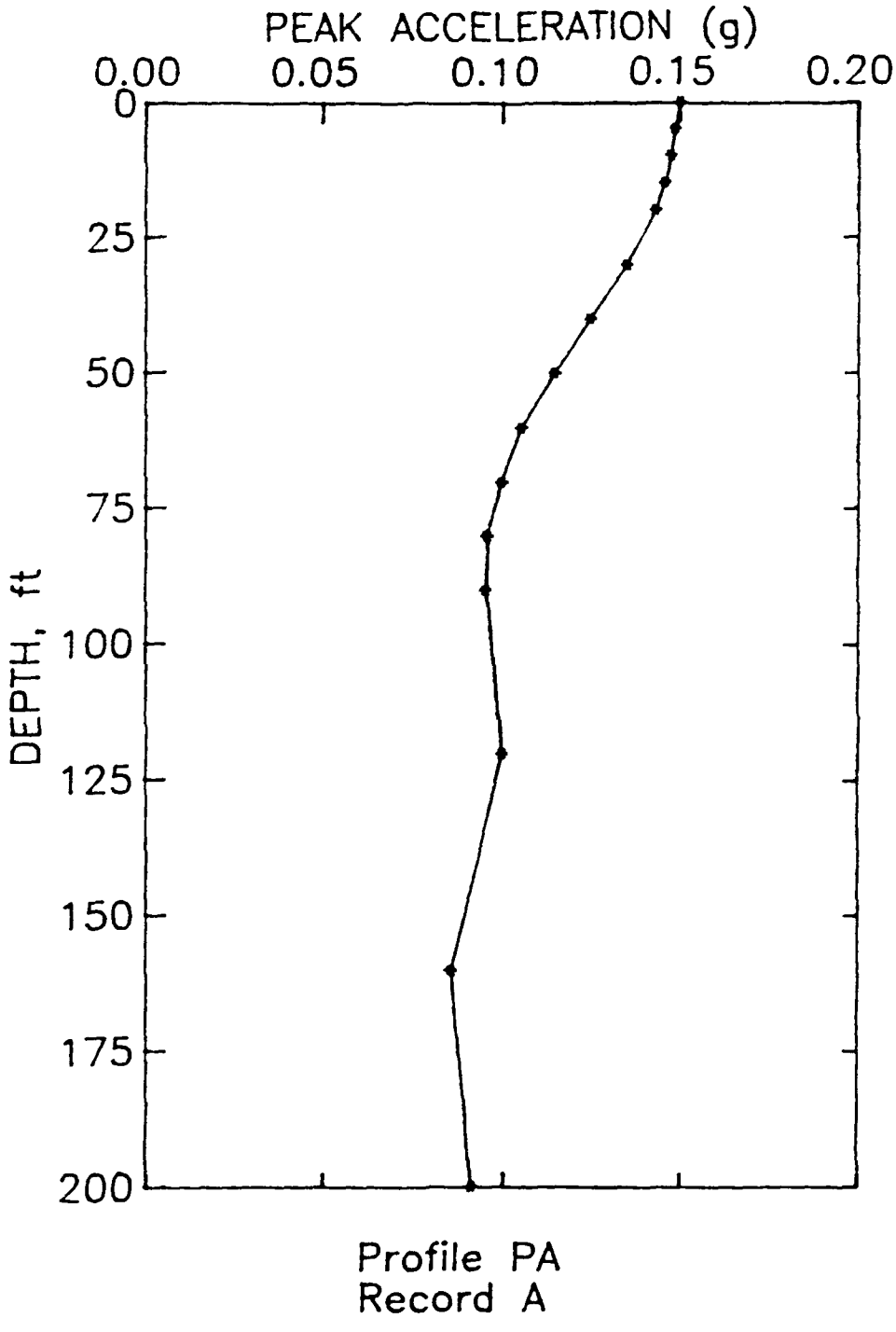

Figure 86. Peak acceleration versus depth for Profile PA excited by Record A

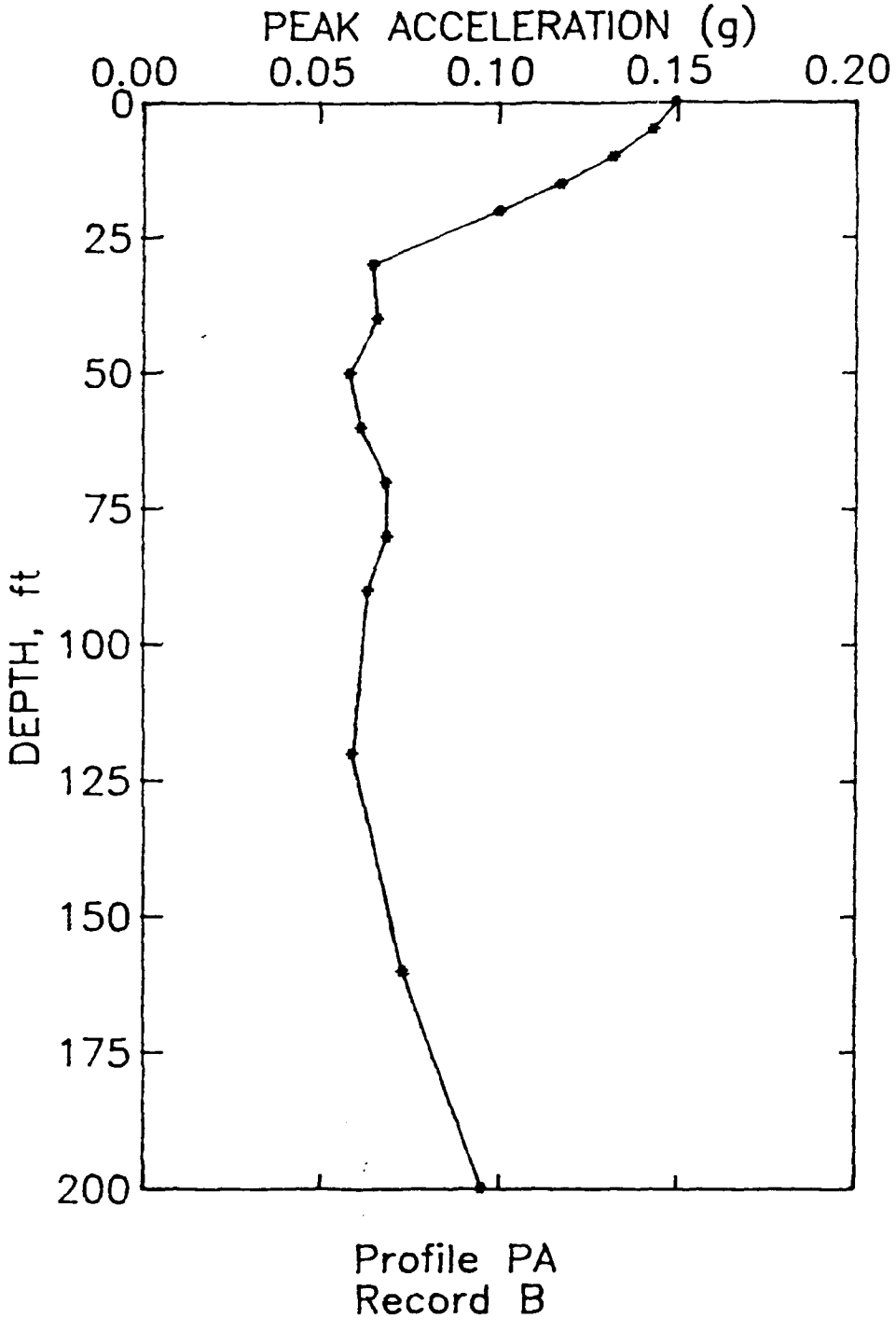

Figure 87. Peak acceleration versus depth for Profile PA excited by Record B

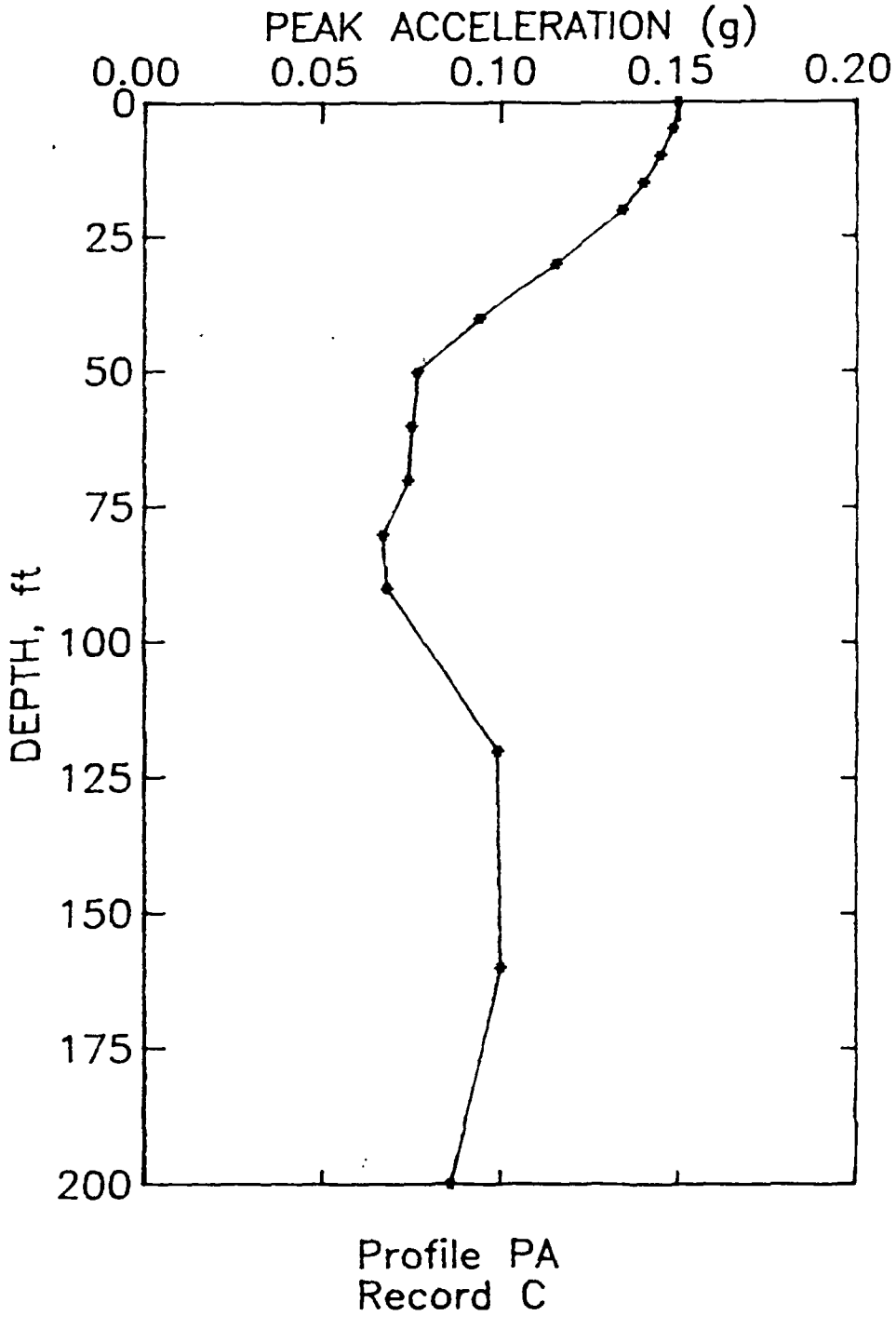

Figure 88. Peak acceleration versus depth for Profile PA excited by Record C

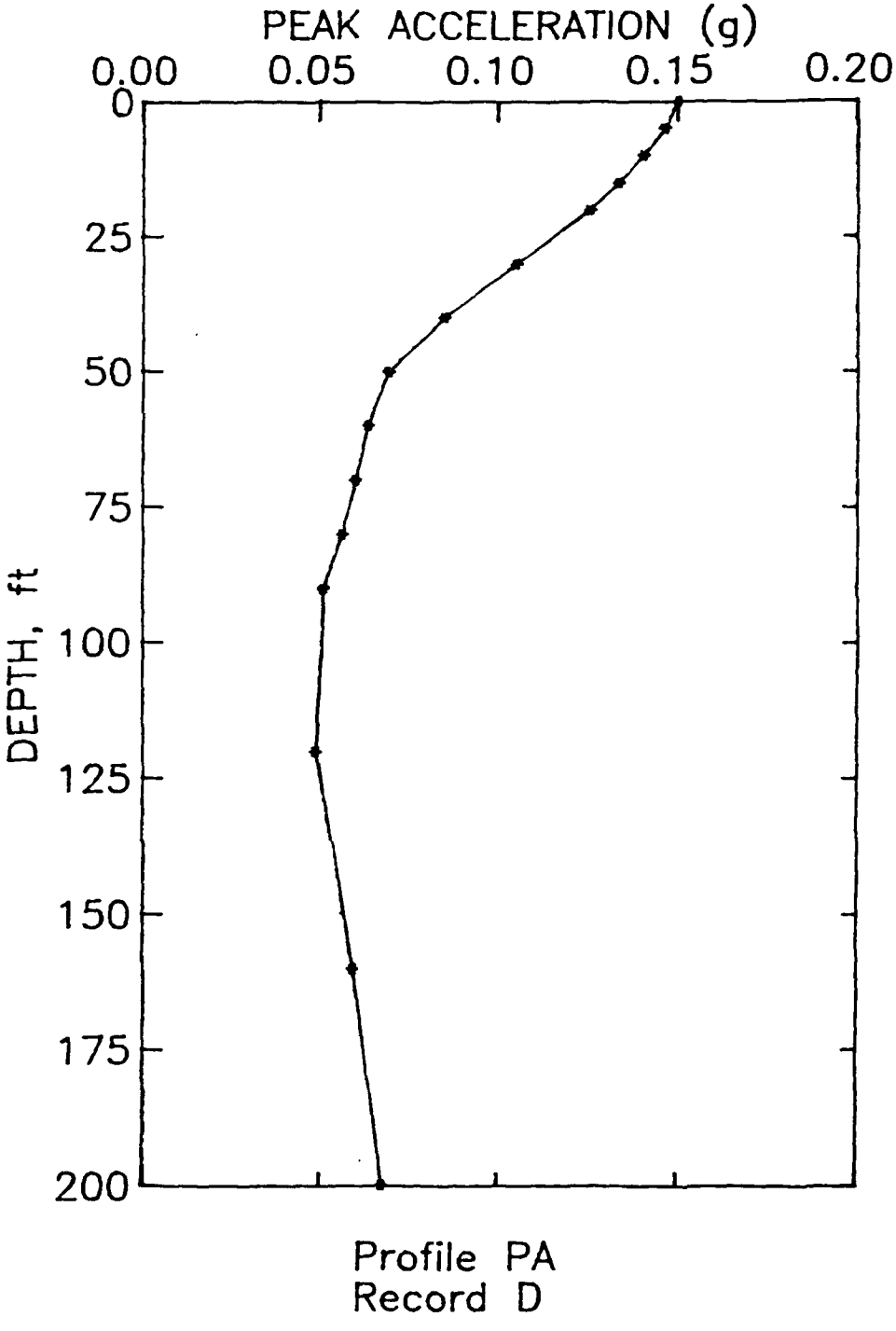

Figure 89. Peak acceleration versus depth for Profile PA excited by Record D

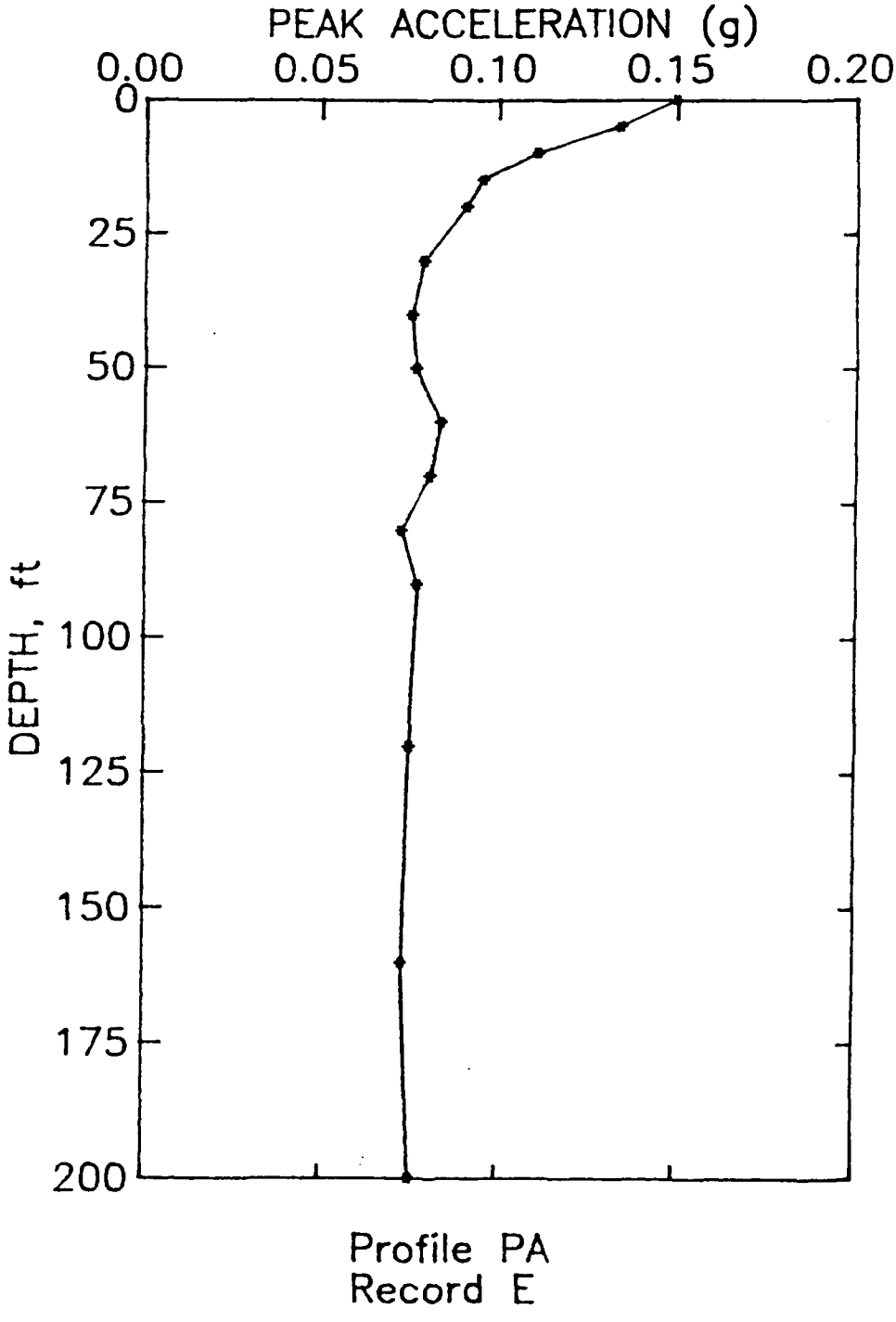

Figure 90. Peak acceleration versus depth for Profile PA excited by Record E

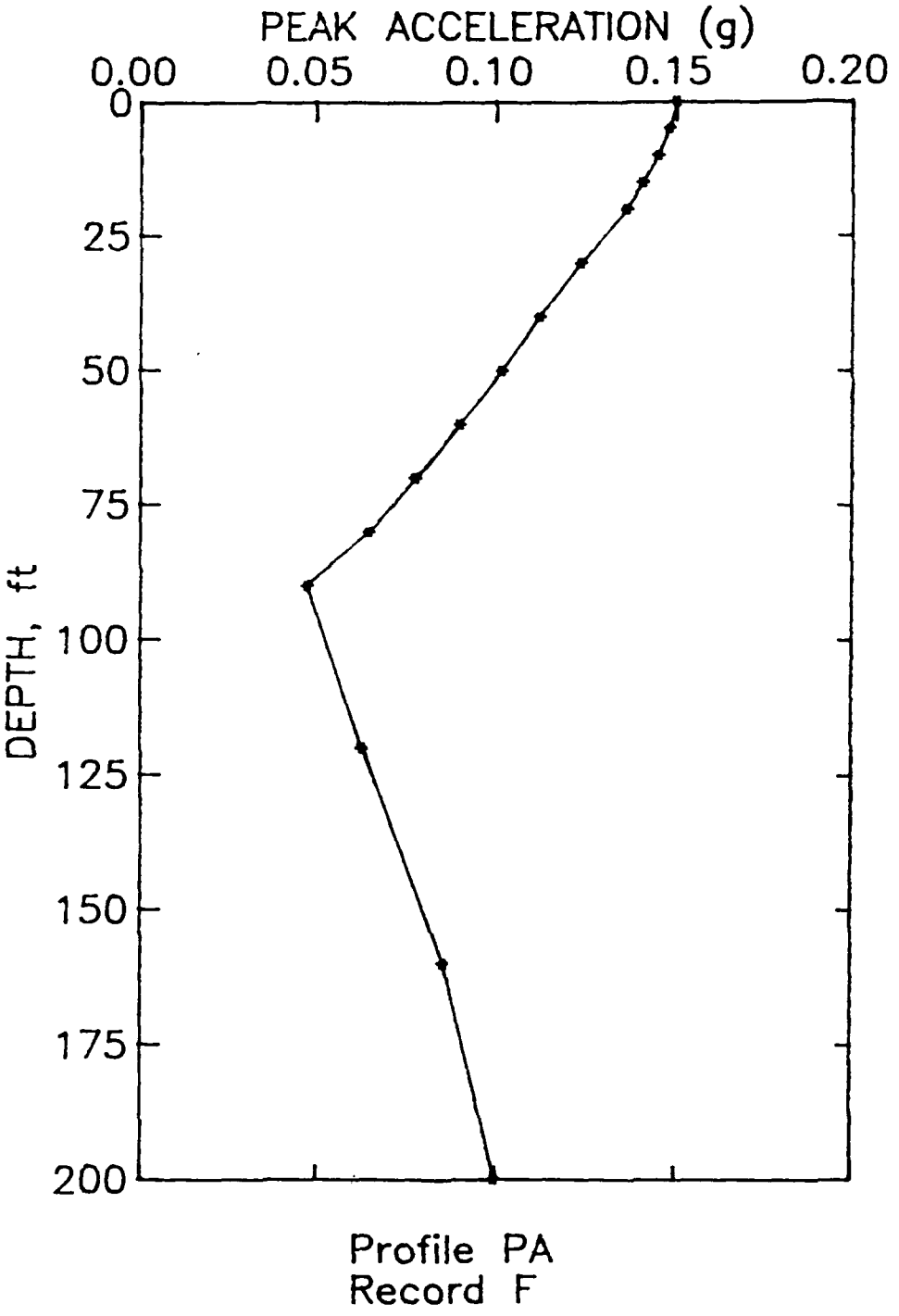

Figure 91. Peak acceleration versus depth for Profile PA excited by Record F

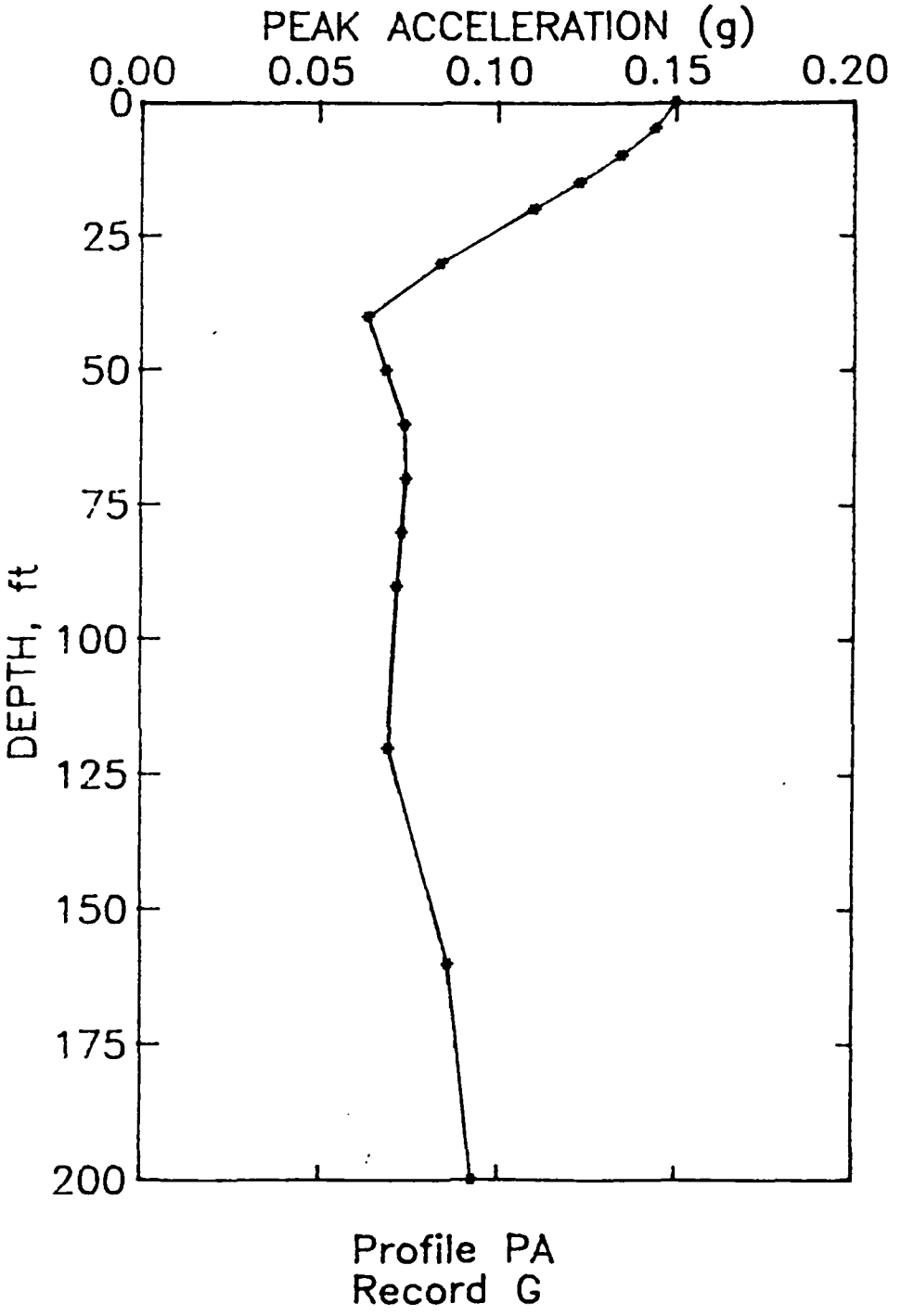

Figure 92. Peak acceleration versus depth for Profile PA excited by Record G

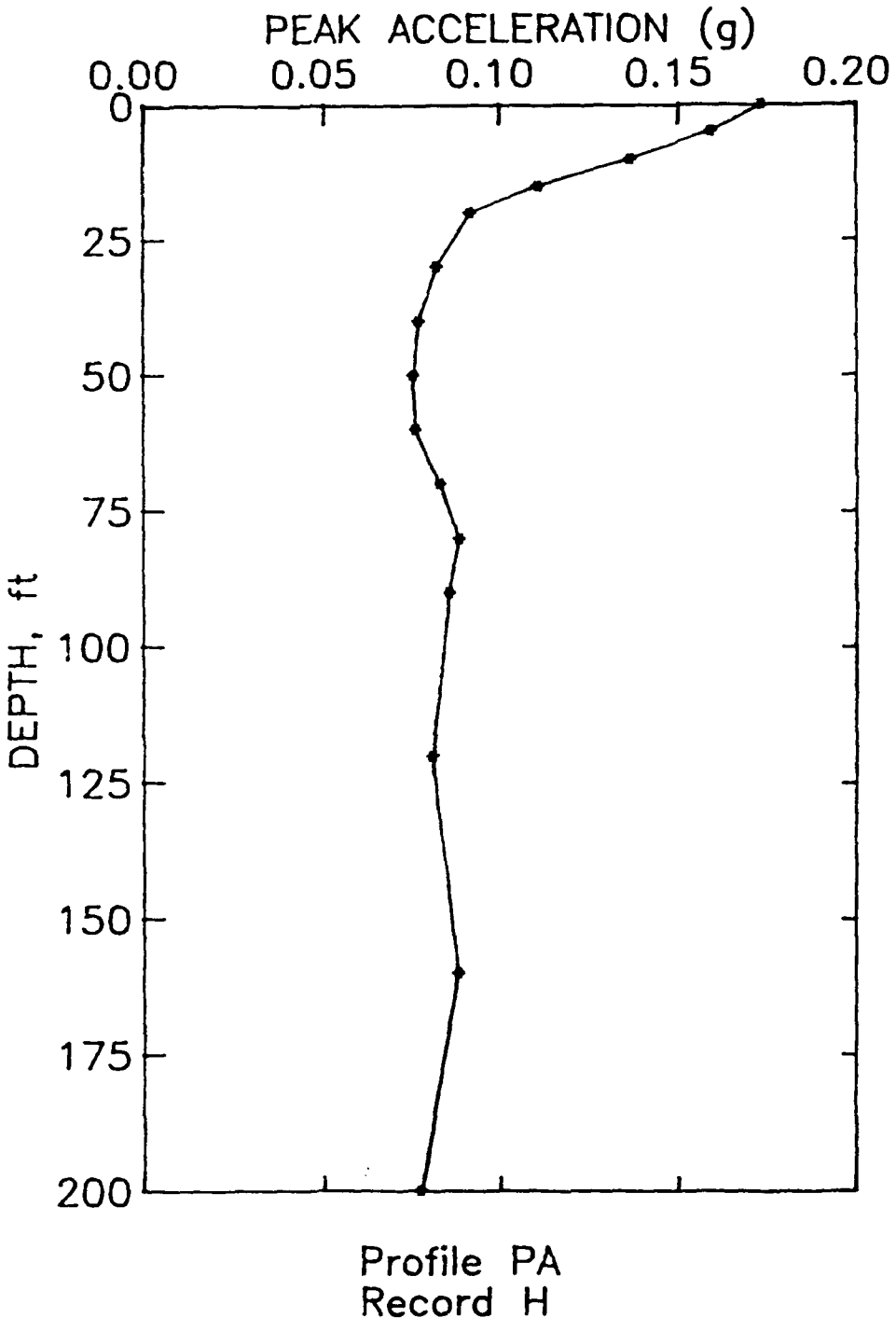

Figure 93. Peak acceleration versus depth for Profile PA excited by Record H

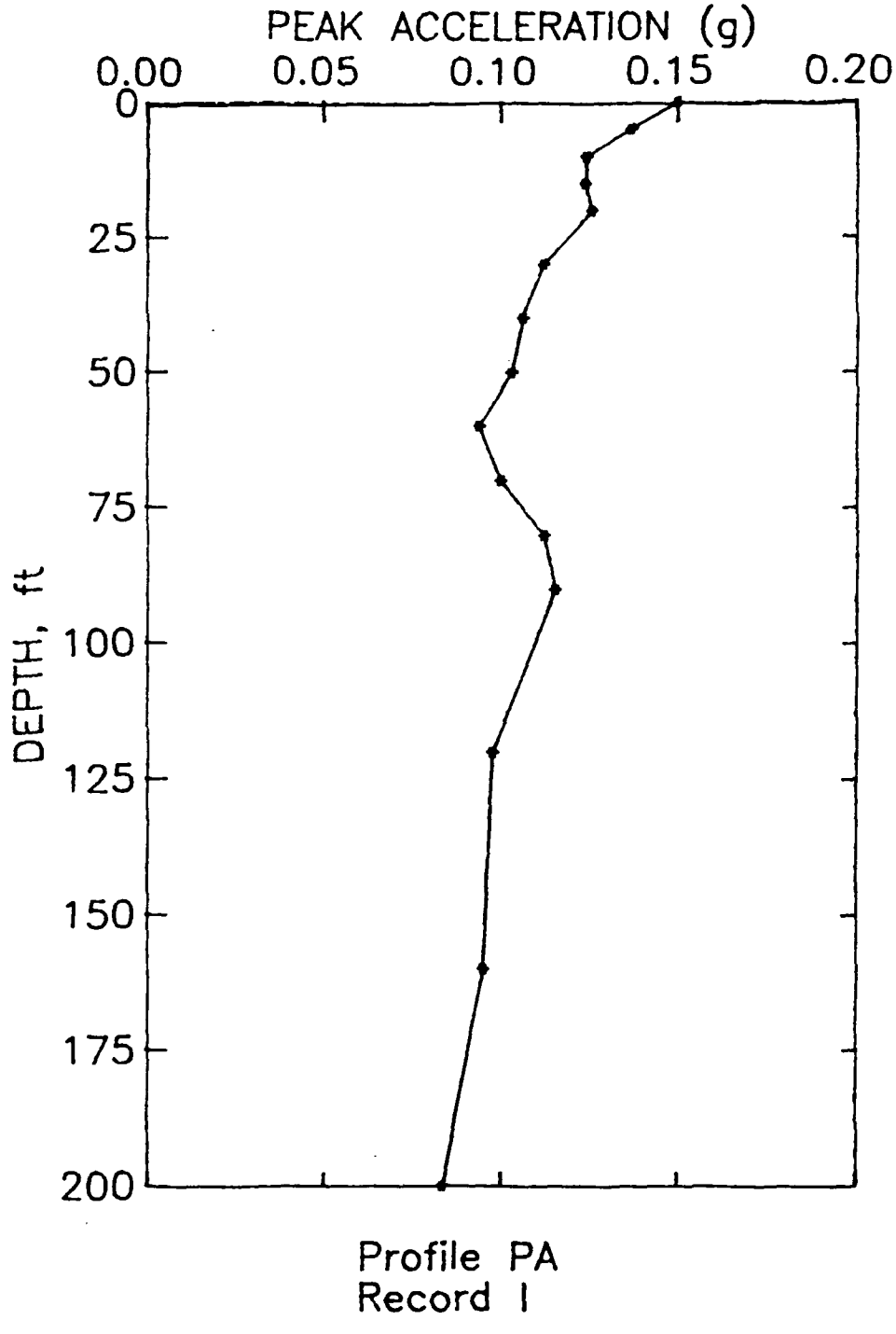

Figure 94. Peak acceleration versus depth for Profile PA excited by Record I

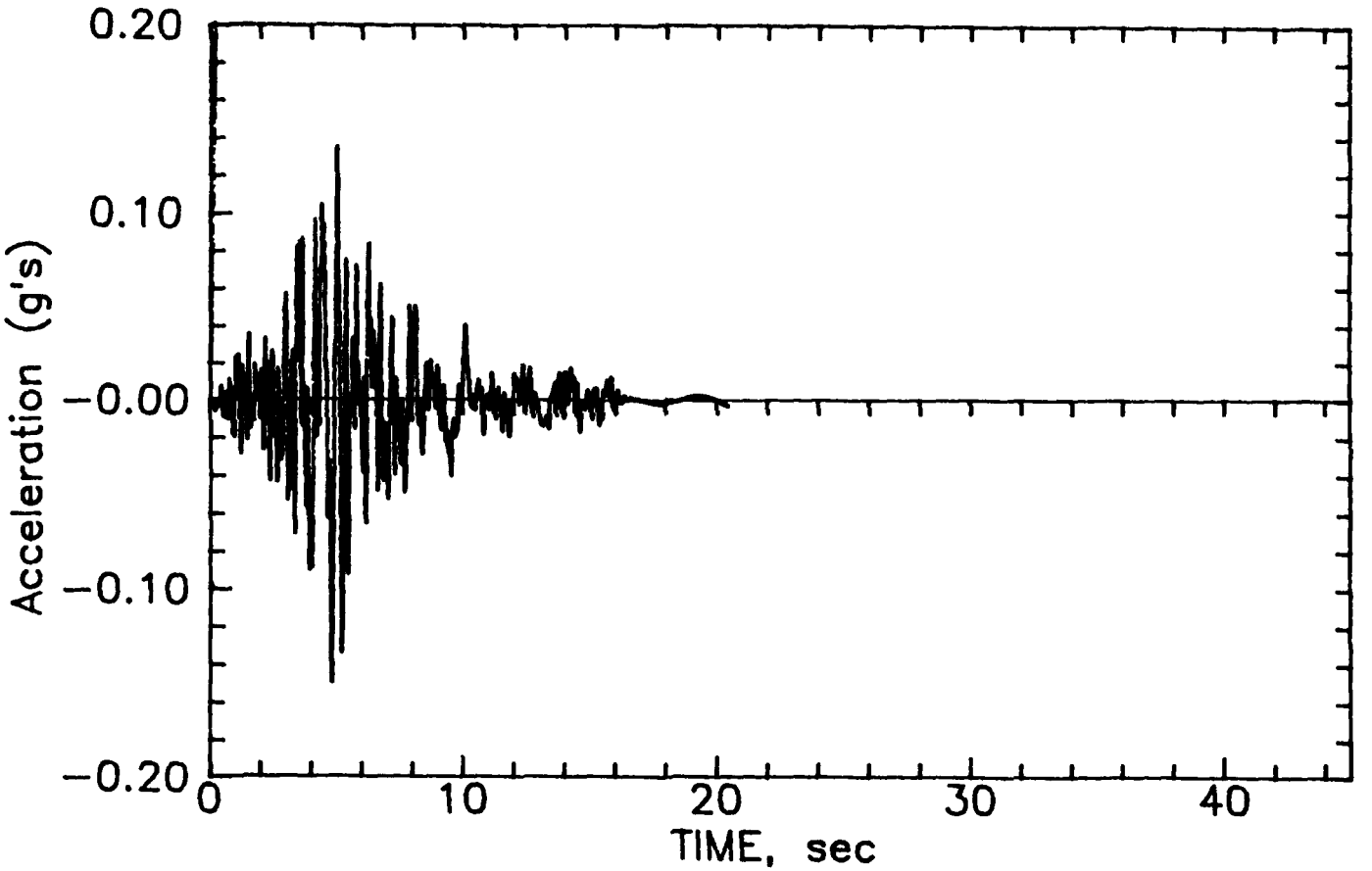

Figure 95. Ground surface accelerogram for Profile PA derived from Record A

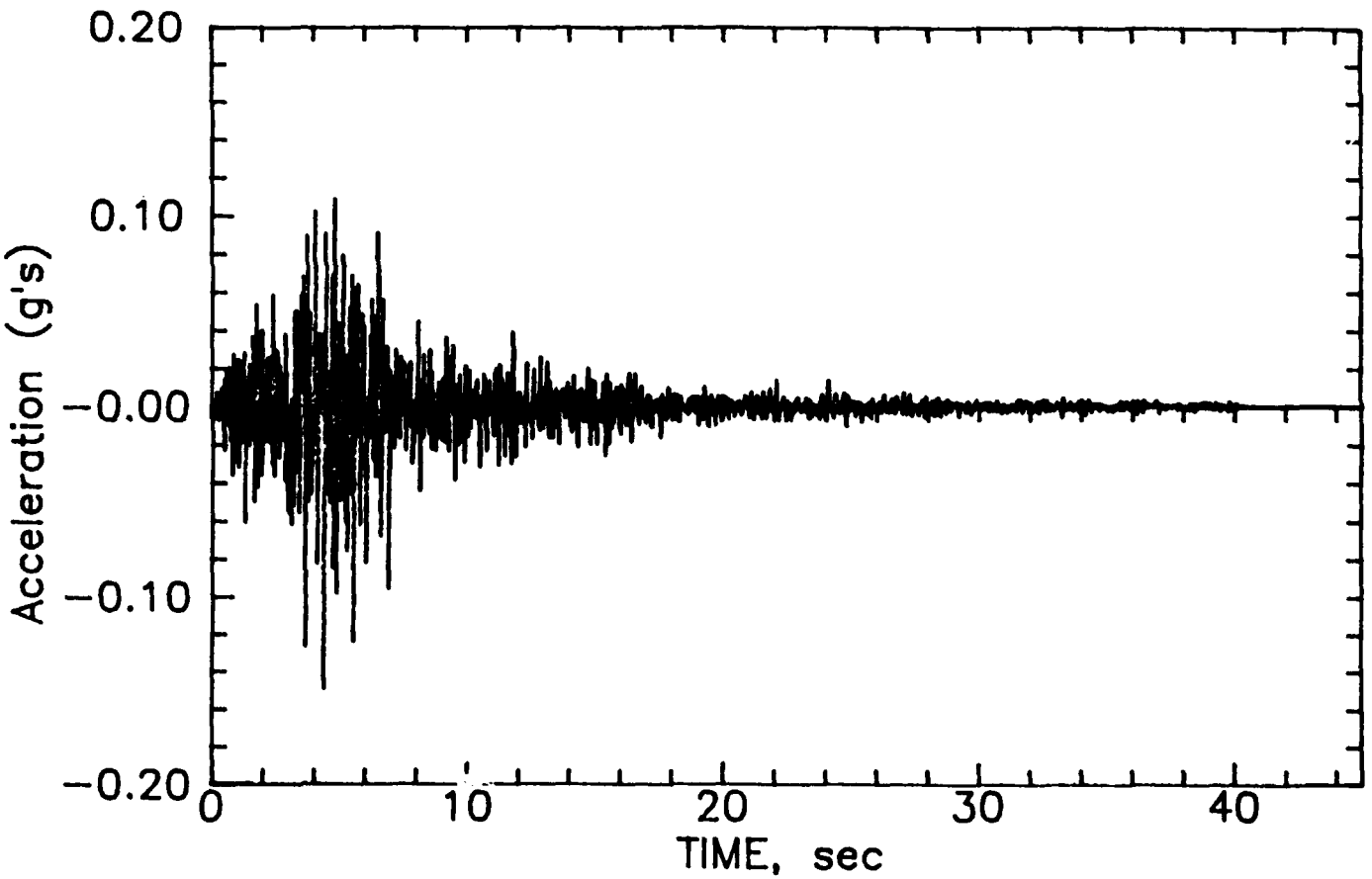

Figure 96. Ground surface accelerogram for Profile PA derived from Record B

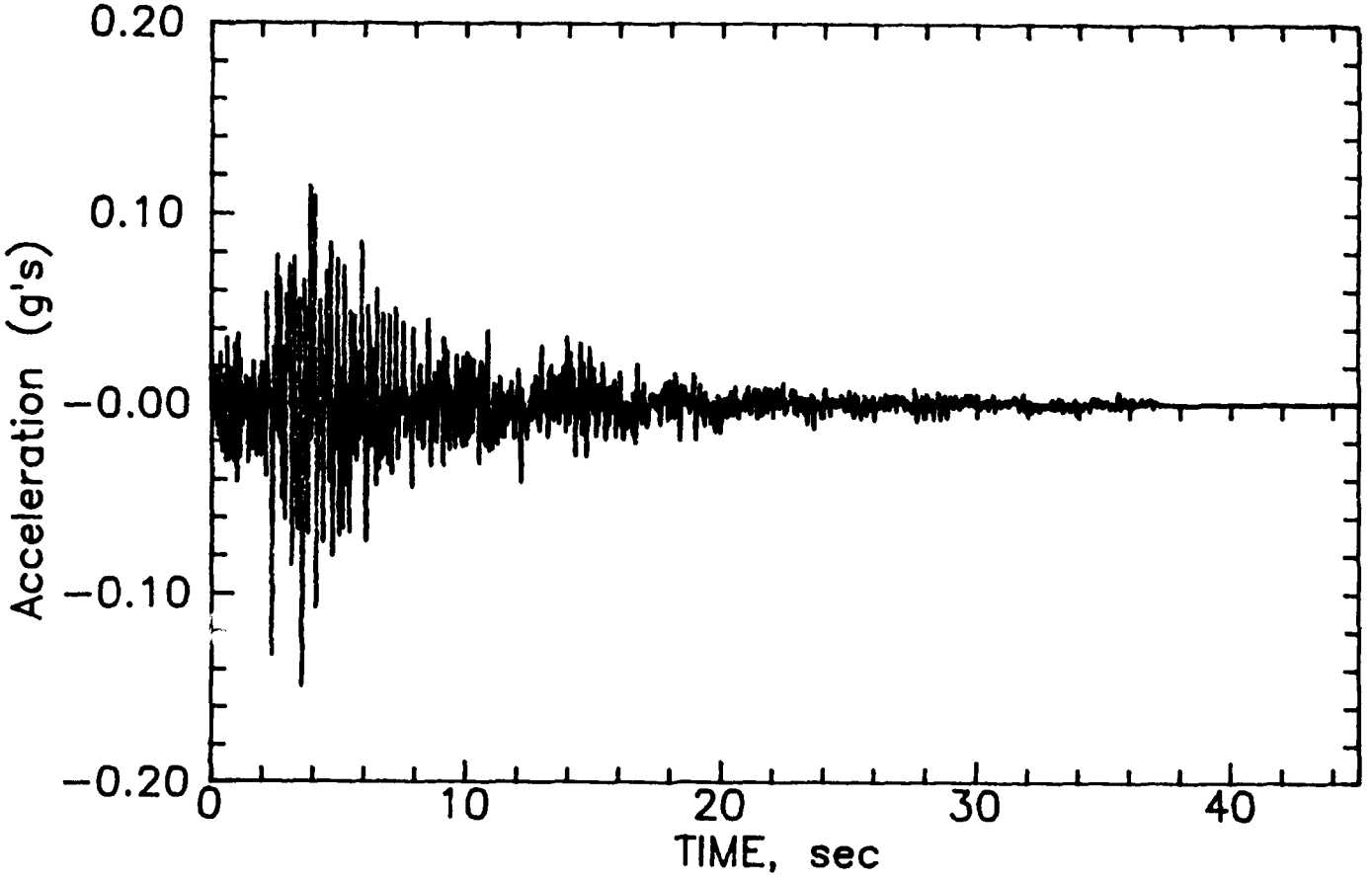

Figure 97. Ground surface accelerogram for Profile PA derived from Record C

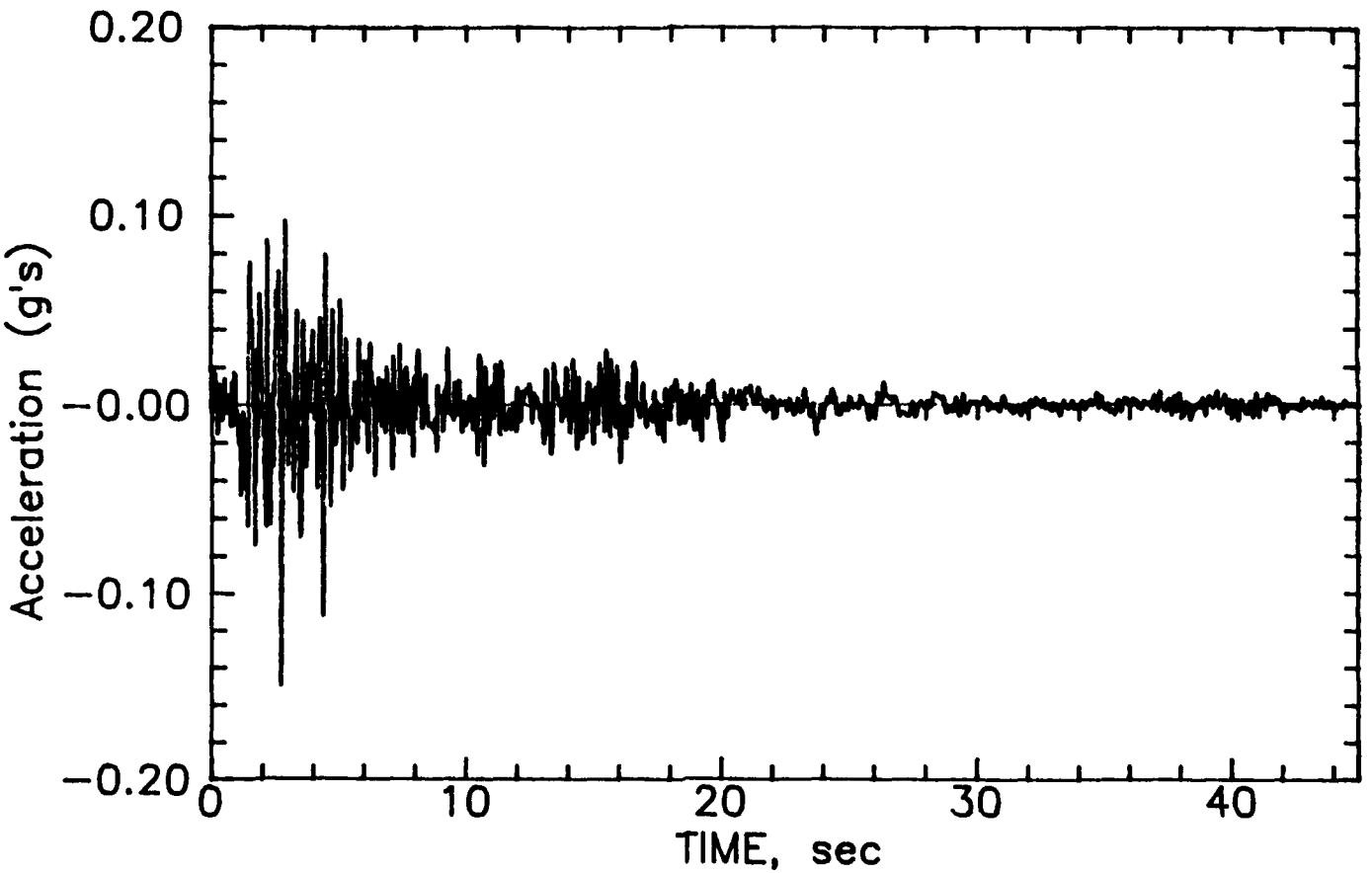

Figure 98. Ground surface accelerogram for Profile PA derived from Record D

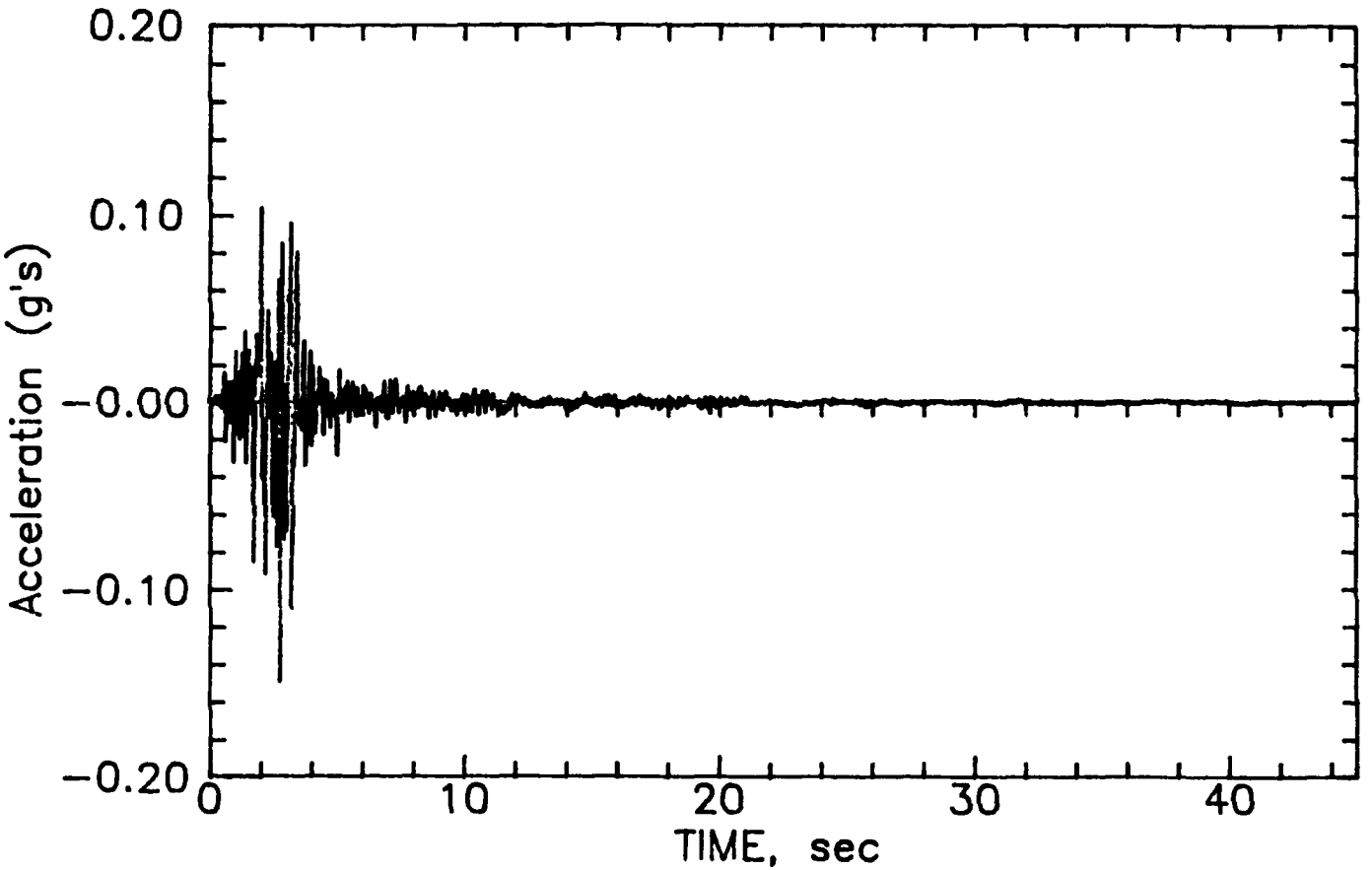

Figure 99. Ground surface accelerogram for Profile PA derived from Record E

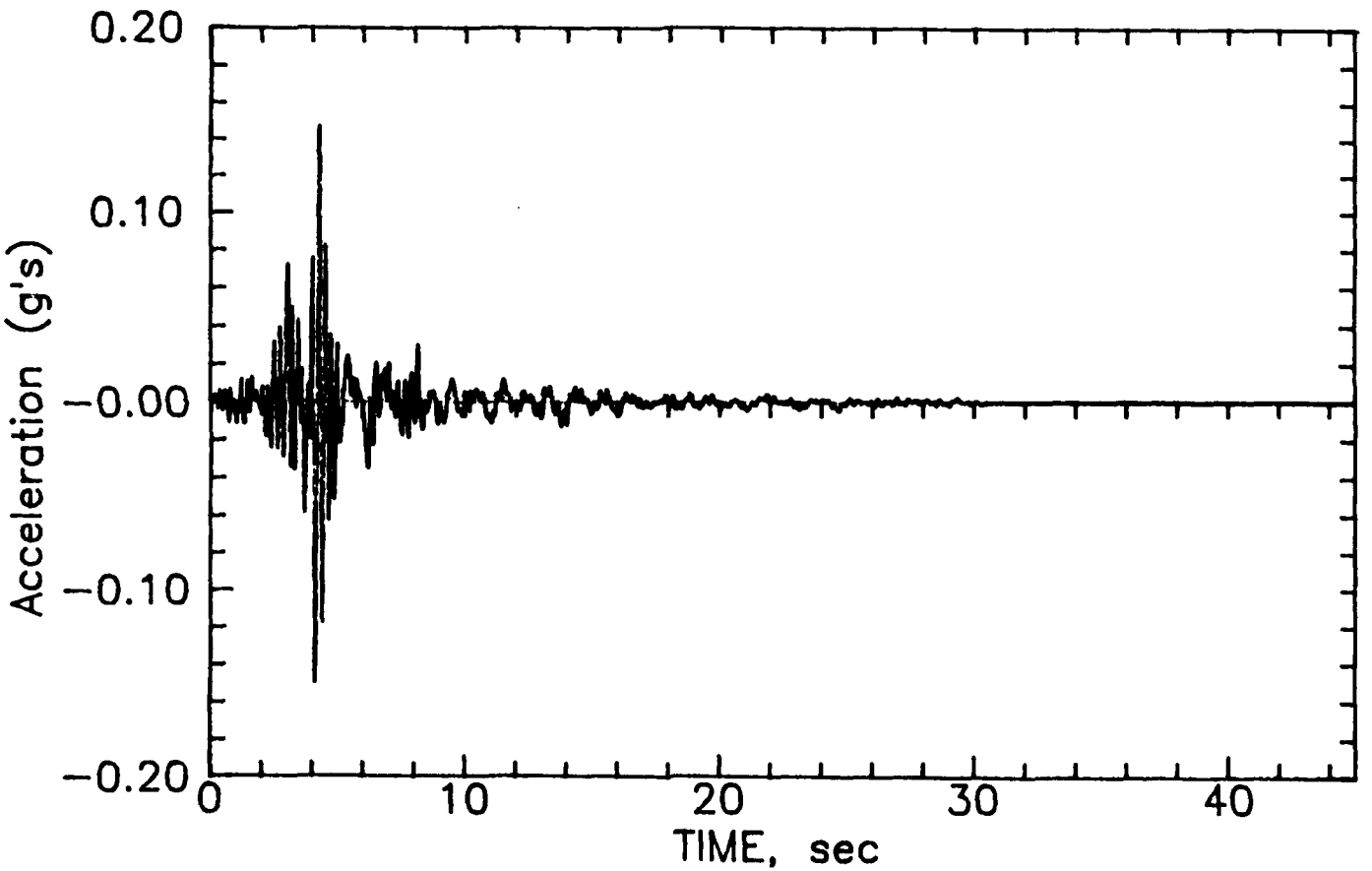

Figure 100. Ground surface accelerogram for Profile PA derived from Record F

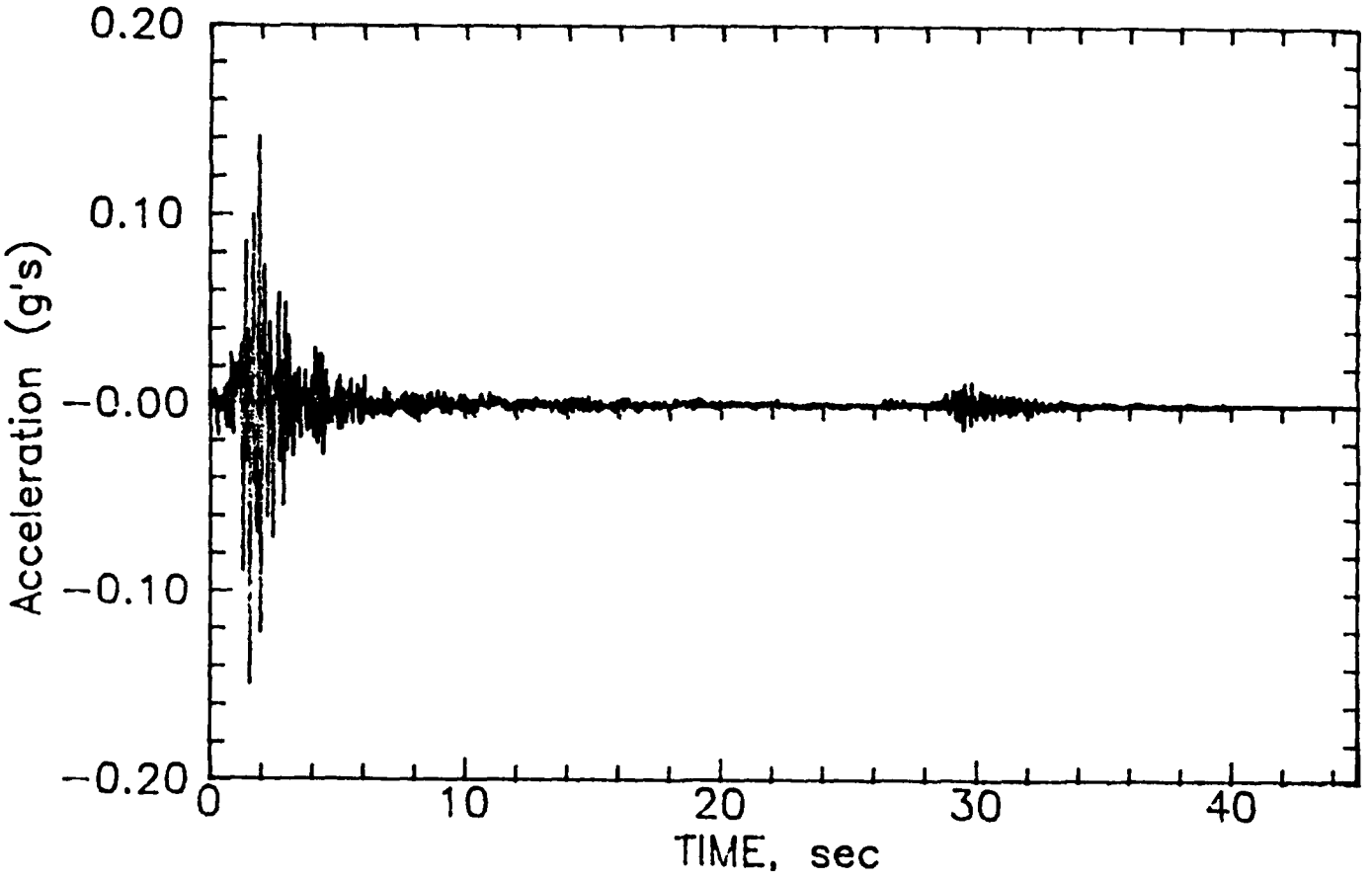

Figure 101. Ground surface accelerogram for Profile PA derived from Record G

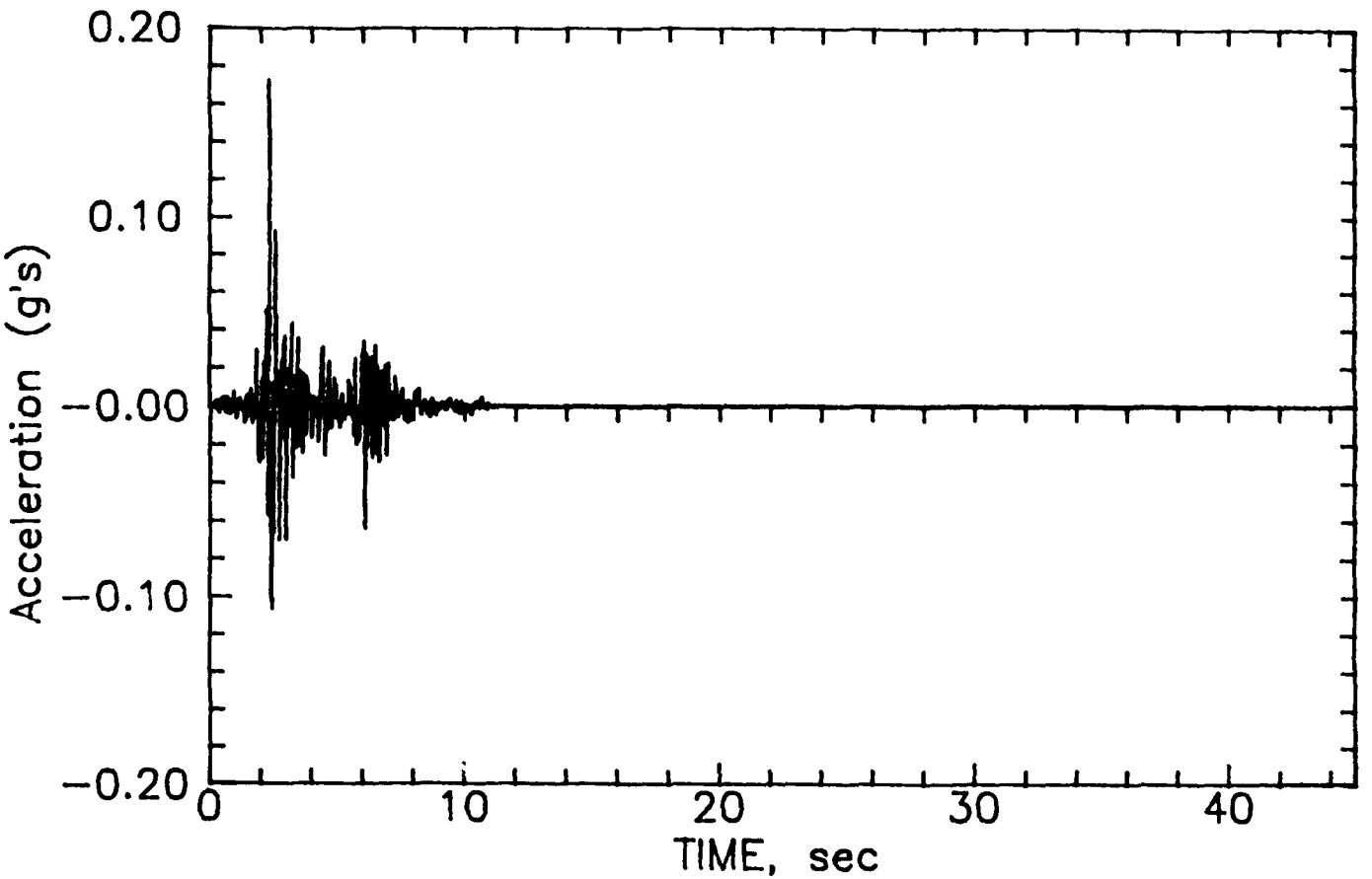

Figure 102. Ground surface accelerogram for Profile PA derived from Record H

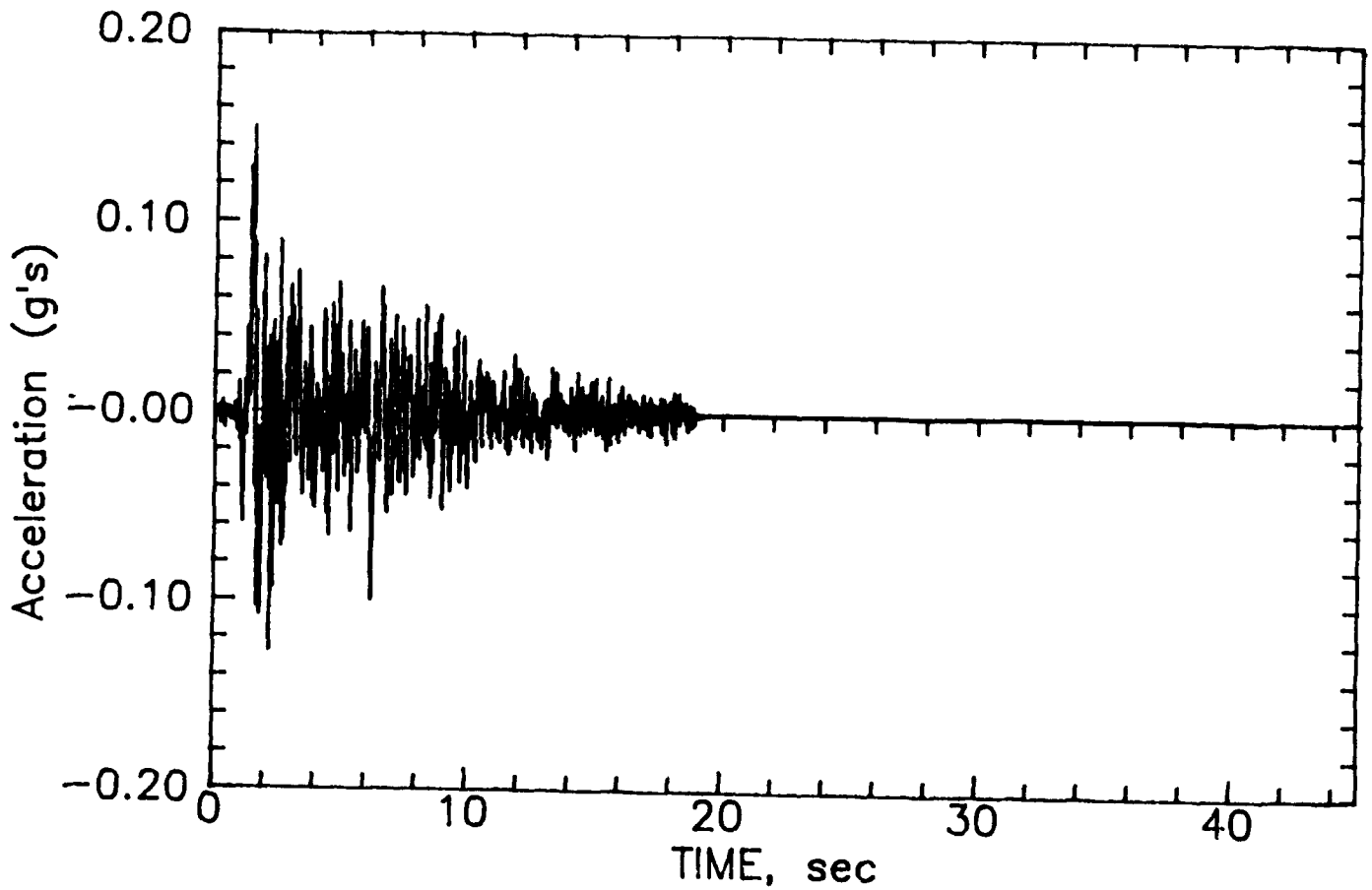

Figure 103. Ground surface accelerogram for Profile PA derived from Record I

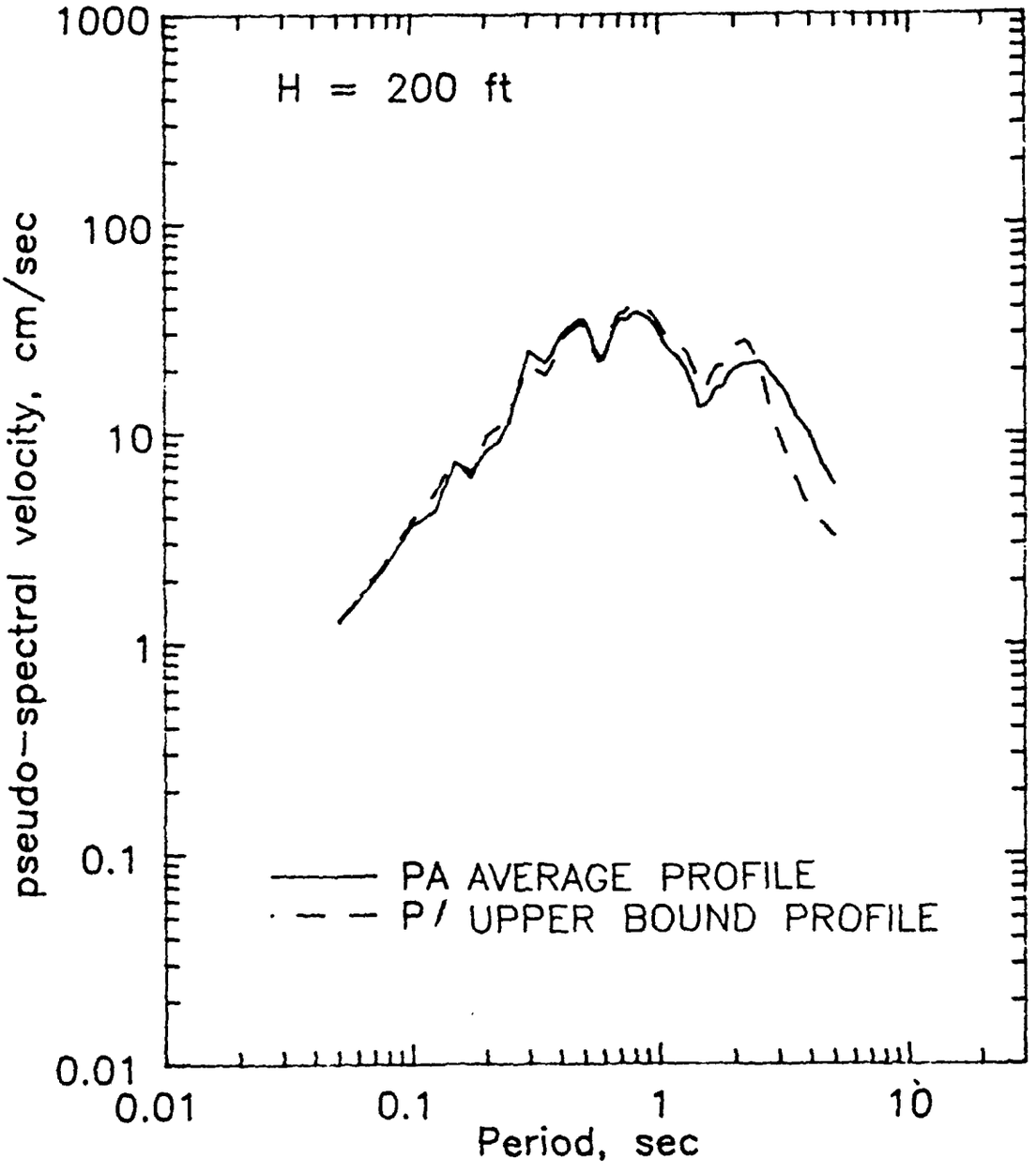

Figure 104. Comparison of ground surface velocity response spectra for Profiles PA and Pl excited by Record A

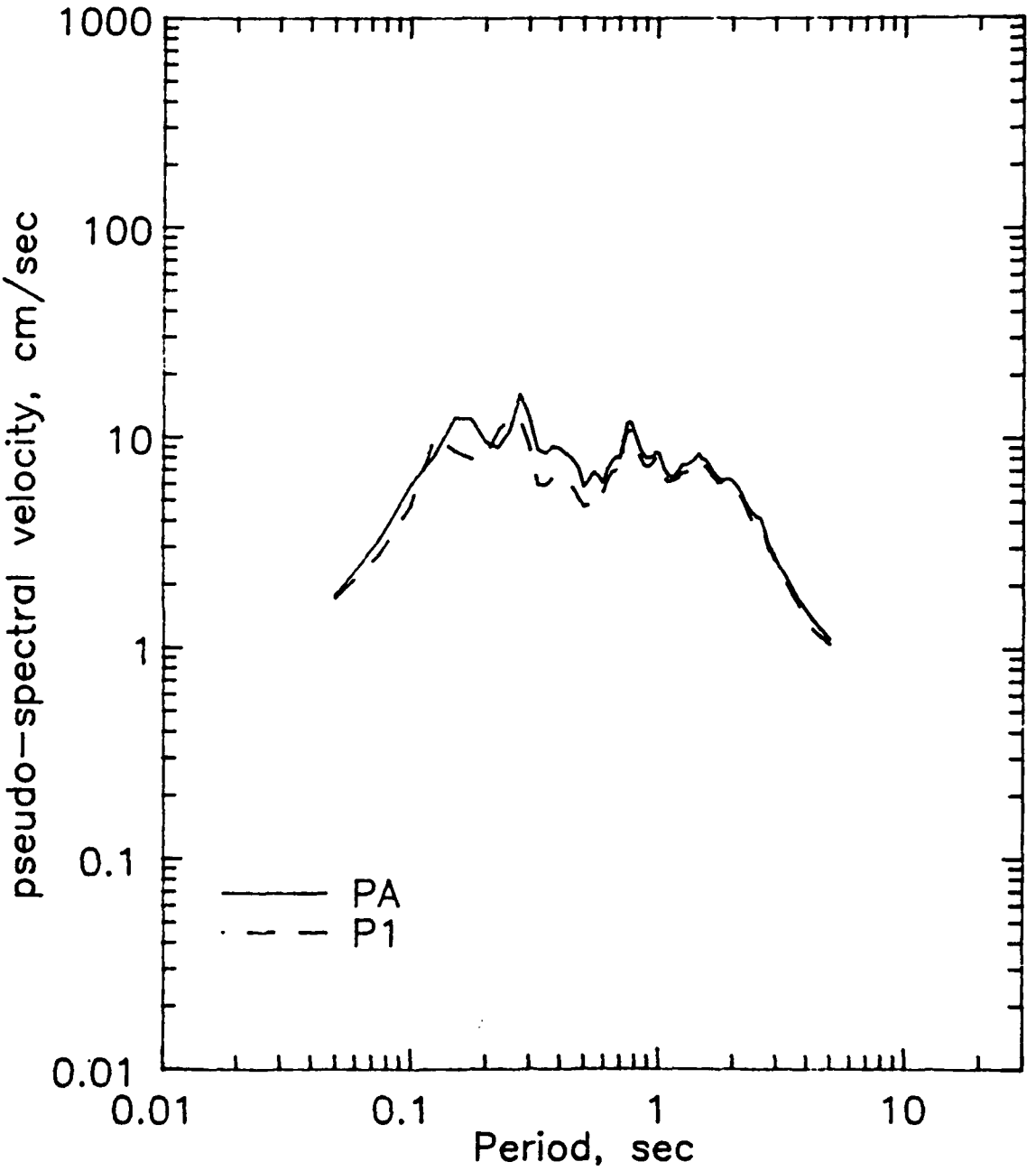

Figure 105. Comparison of ground surface velocity response spectra for Profiles PA and P1 excited by Record B

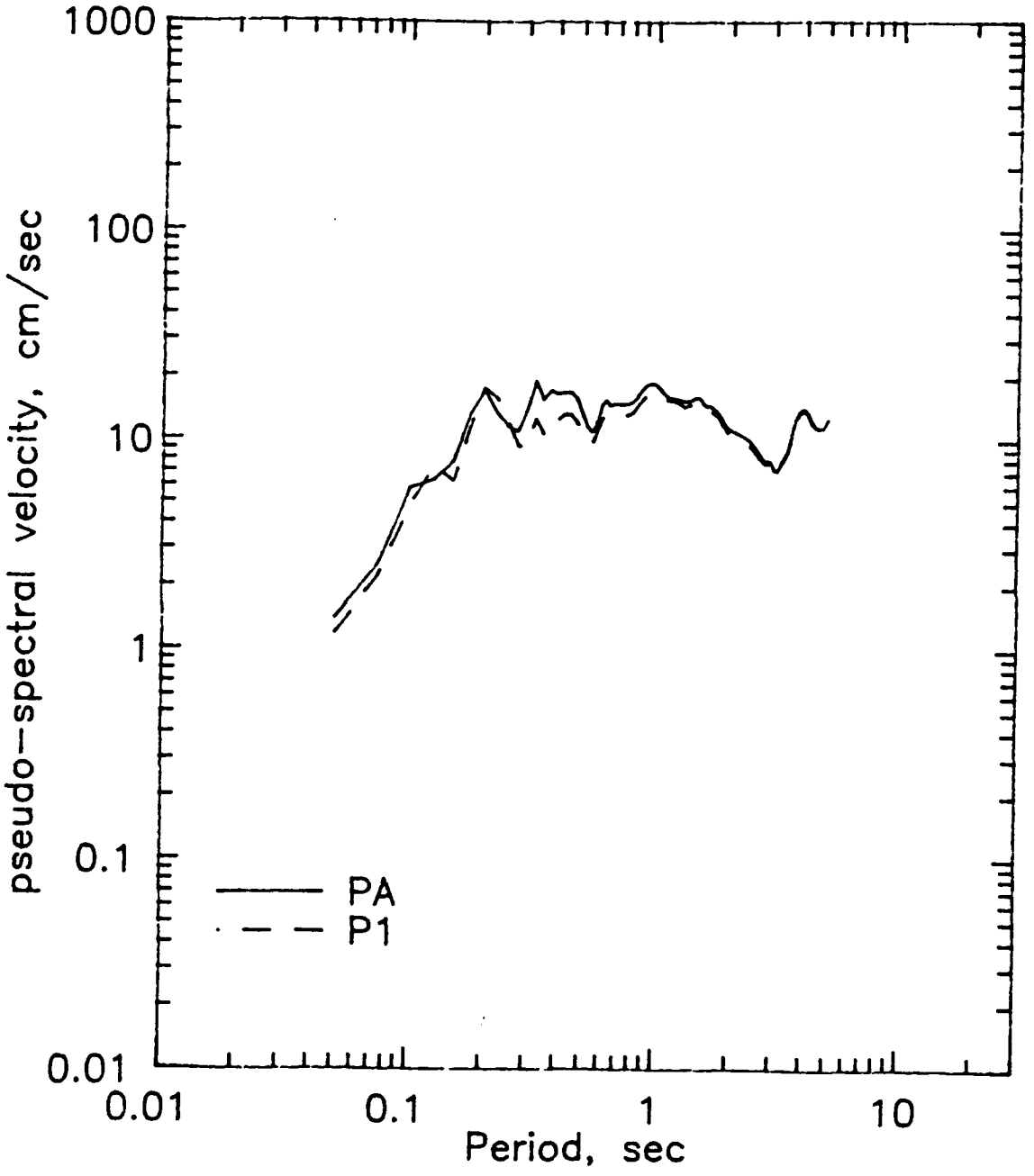

Figure 106. Comparison of ground surface velocity response spectra for Profiles PA and P1 excited by Record C

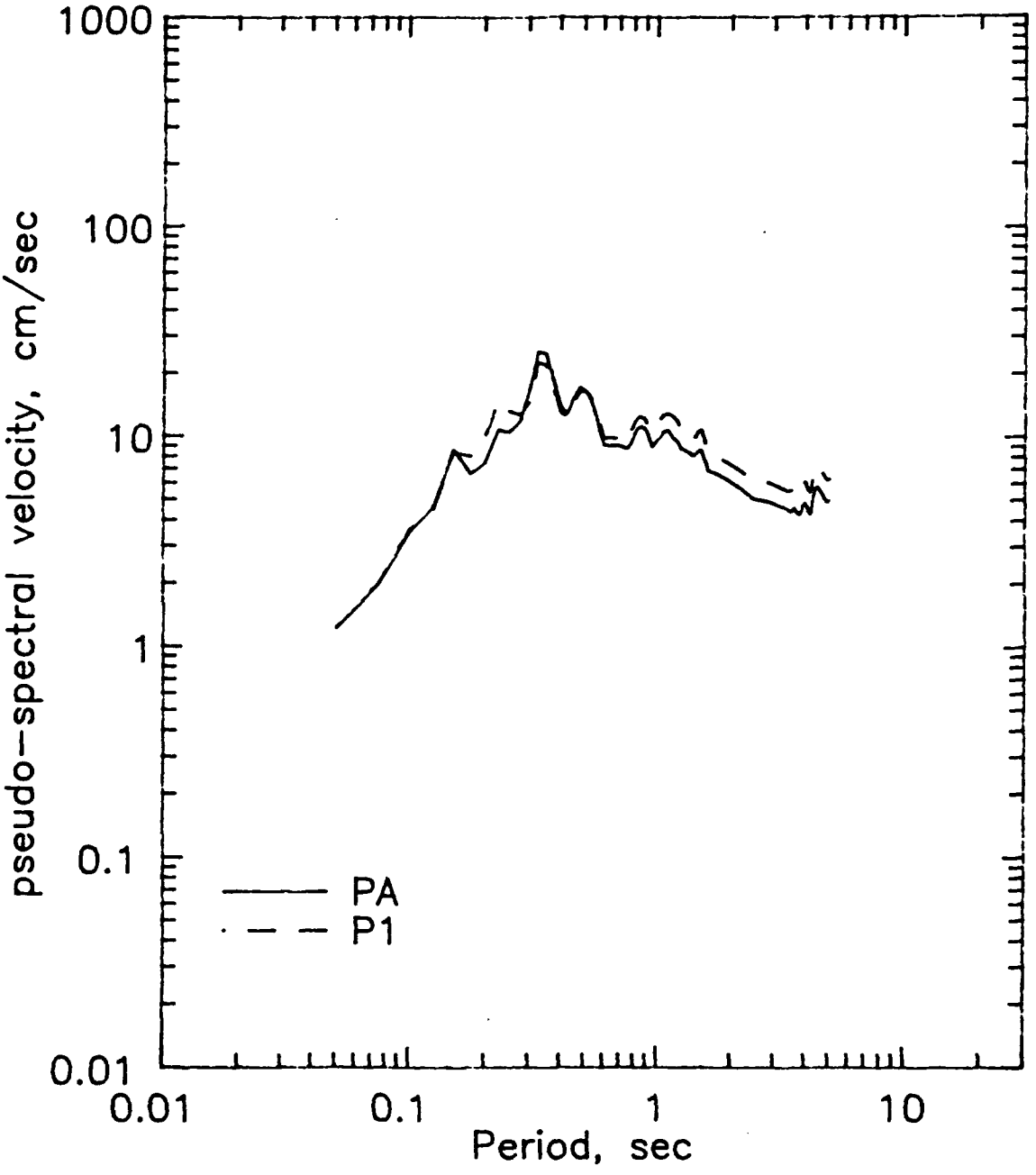

Figure 107. Comparison of ground surface velocity response spectra for Profiles PA and P1 excited by Record D

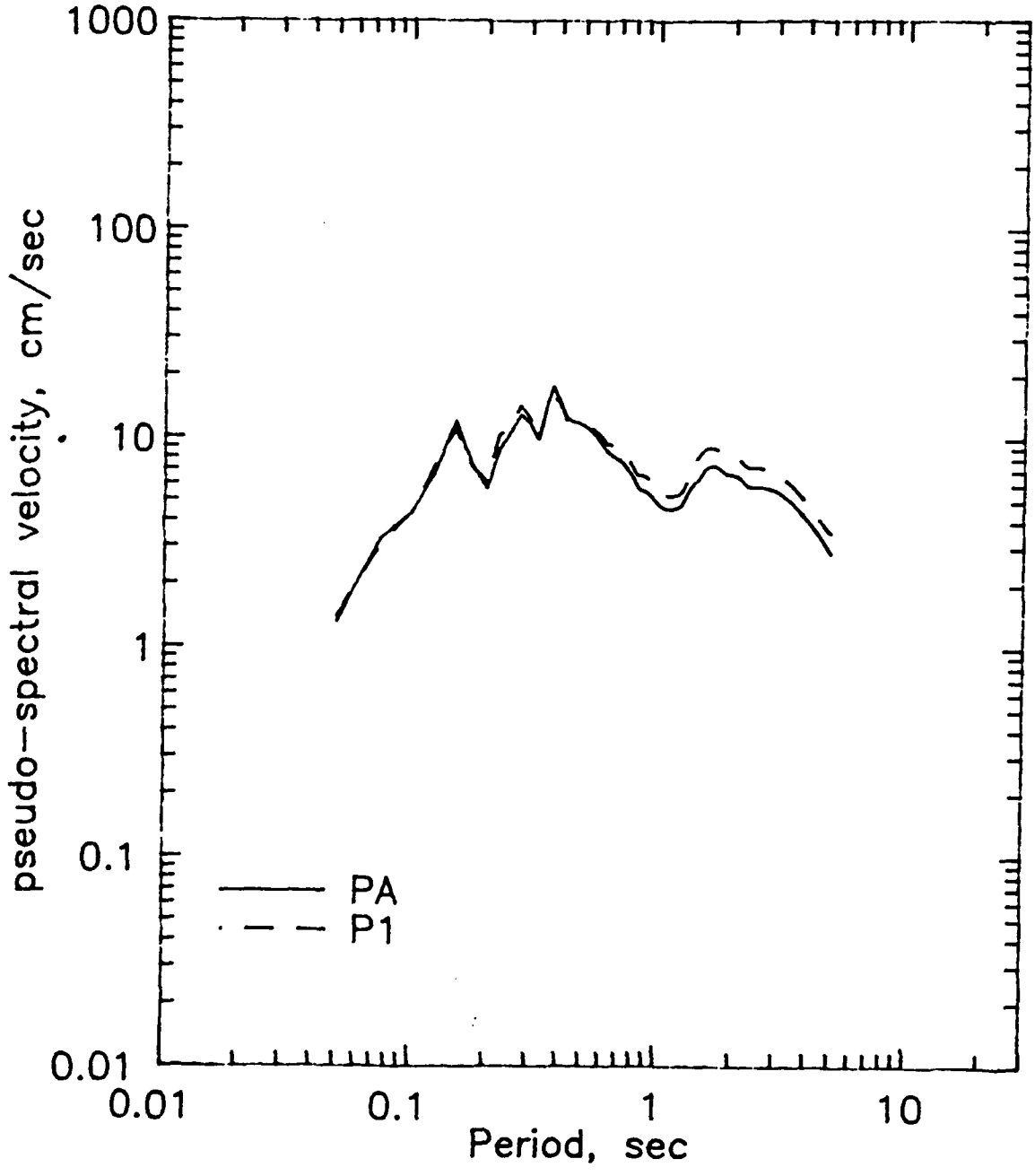

Figure 108. Comparison of ground surface velocity response spectra for Profiles PA and P1 excited by Record E

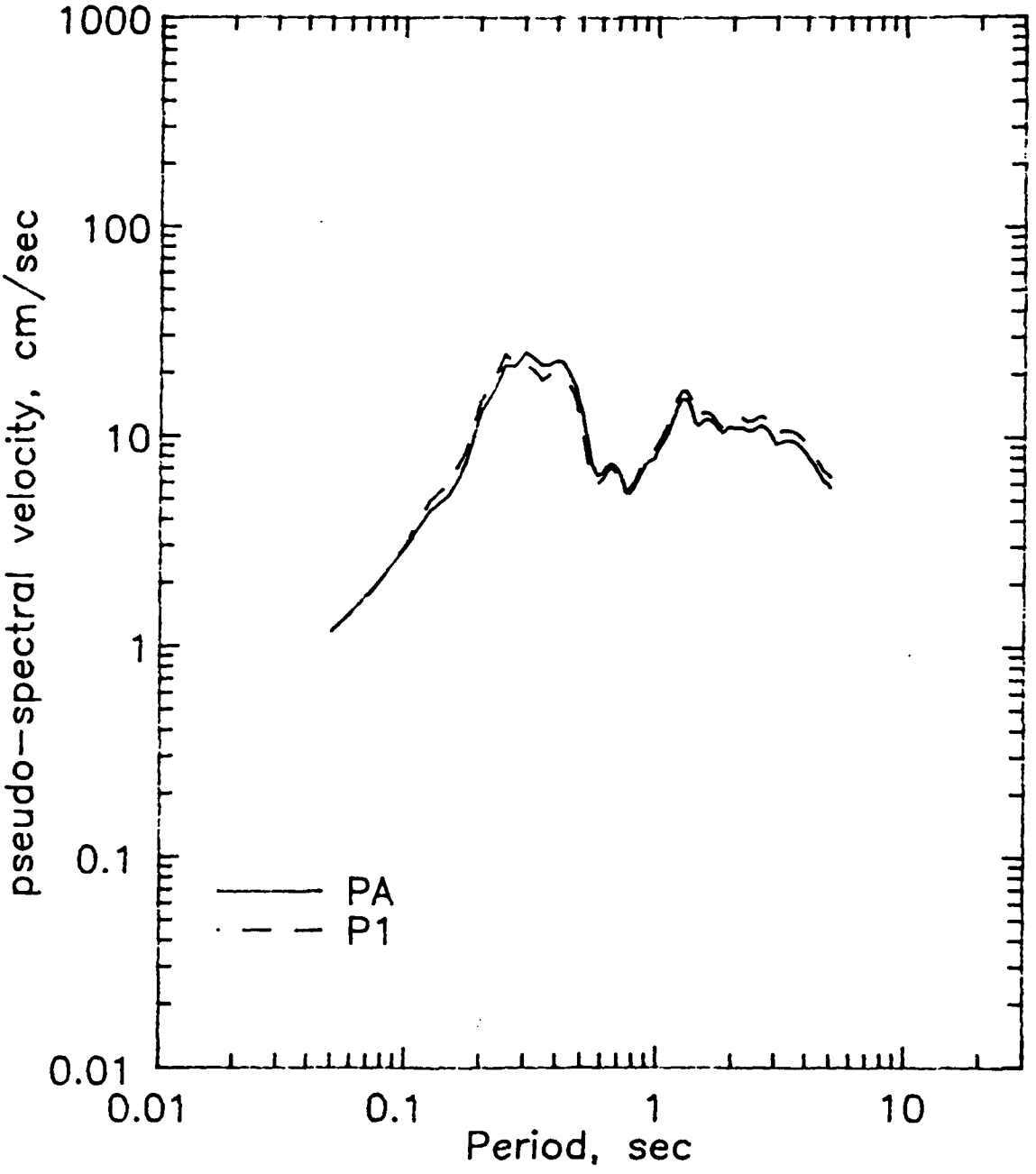

Figure 109. Comparison of ground surface velocity response spectra for Profiles PA and P1 excited by Record F

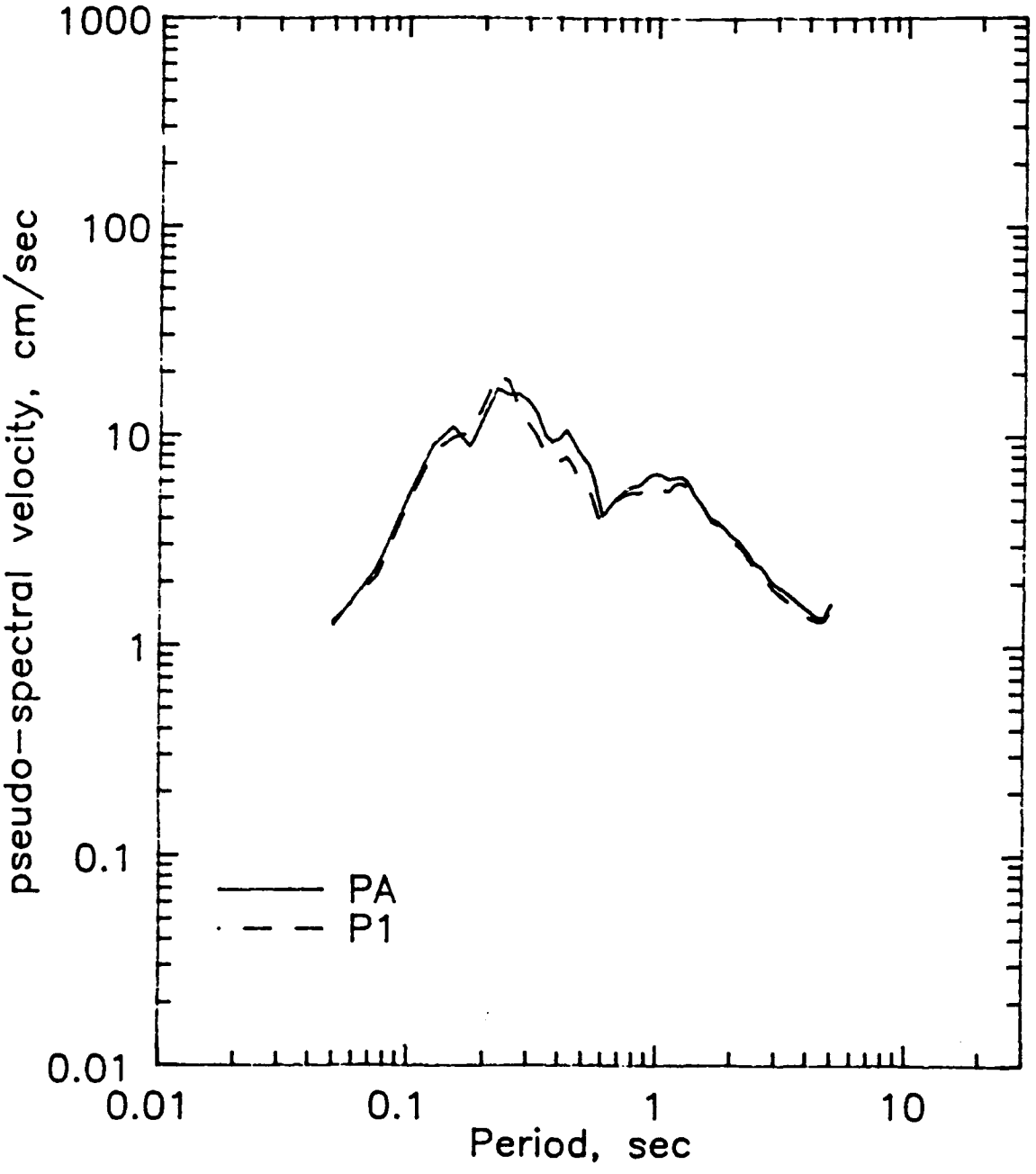

Figure 110. Comparison of ground surface velocity response spectra for Profiles PA and P1 excited by Record G

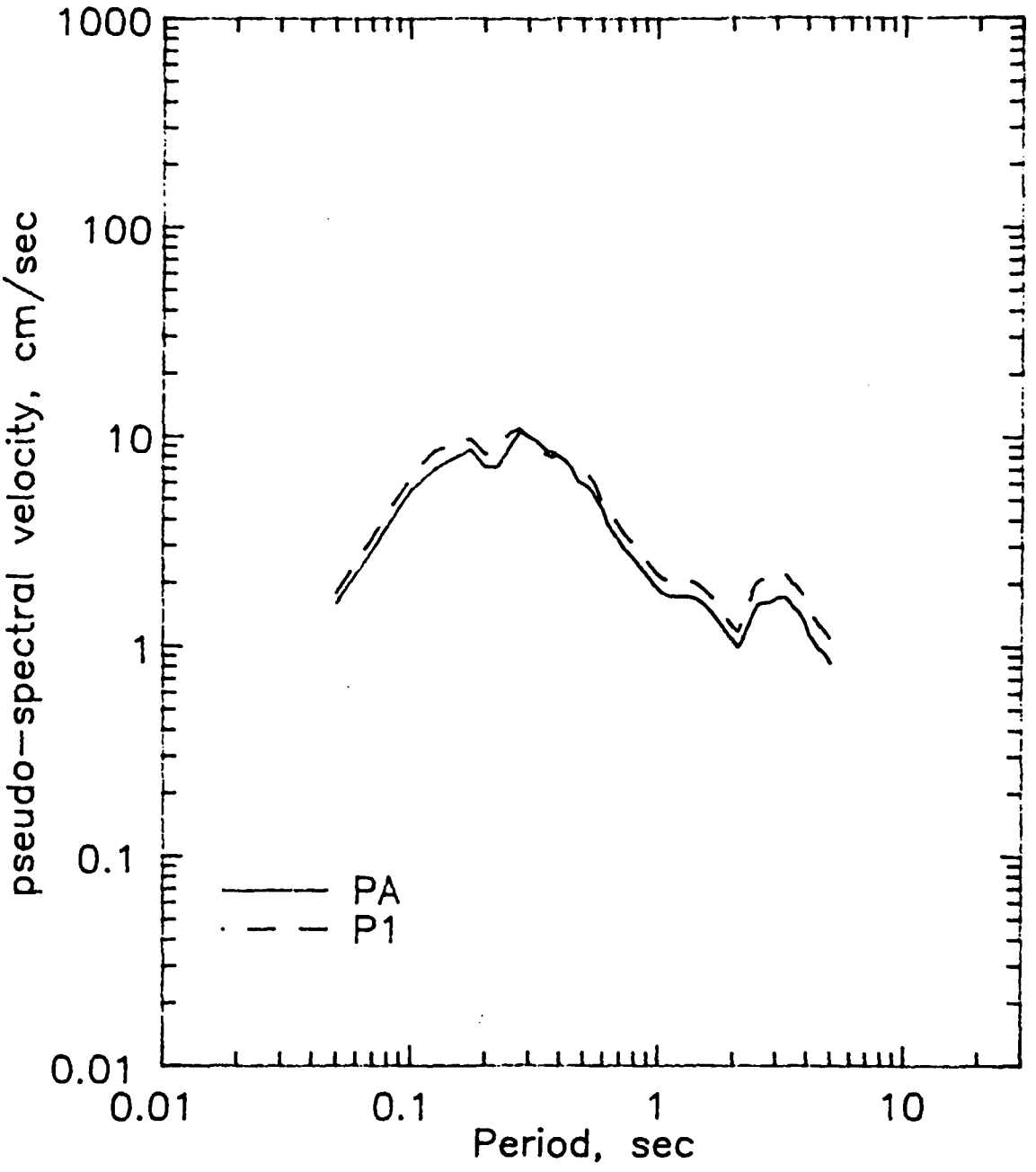

Figure 111. Comparison of ground surface velocity response spectra for Profiles PA and P1 excited by Record H

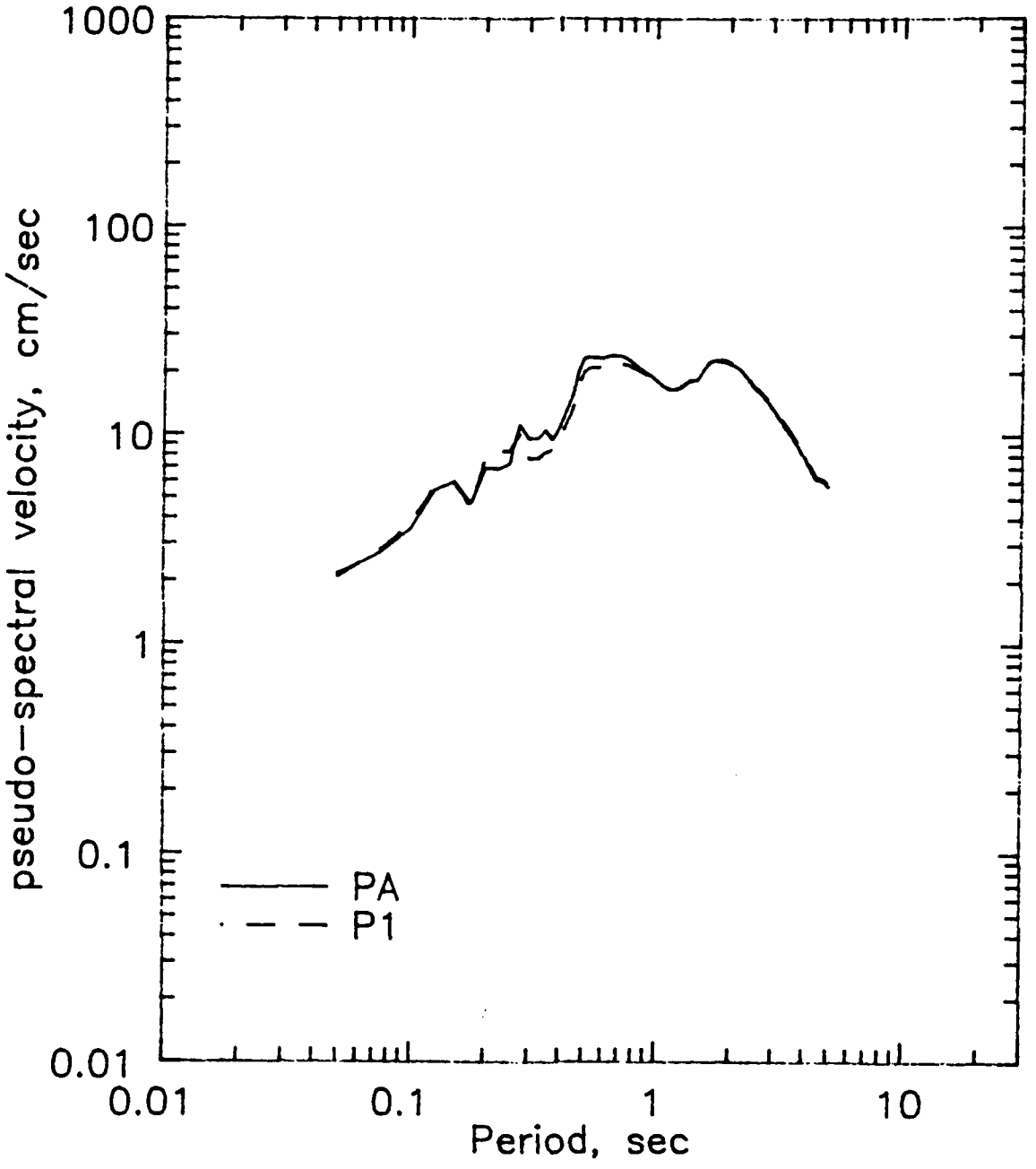

Figure 112. Comparison of ground surface velocity response spectra for Profiles PA and P1 excited by Record I

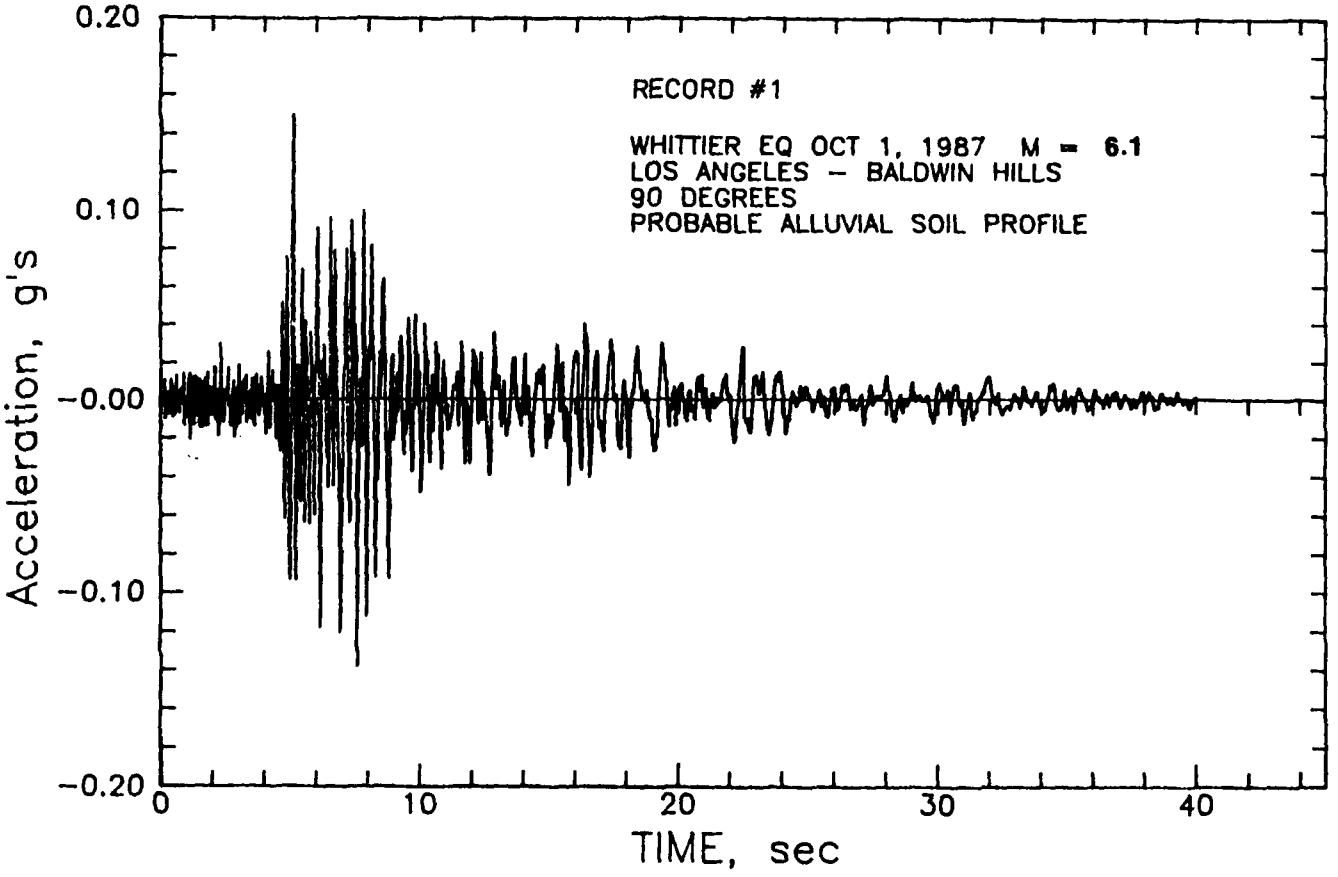

Figure 113. Acceleration history for Record #1

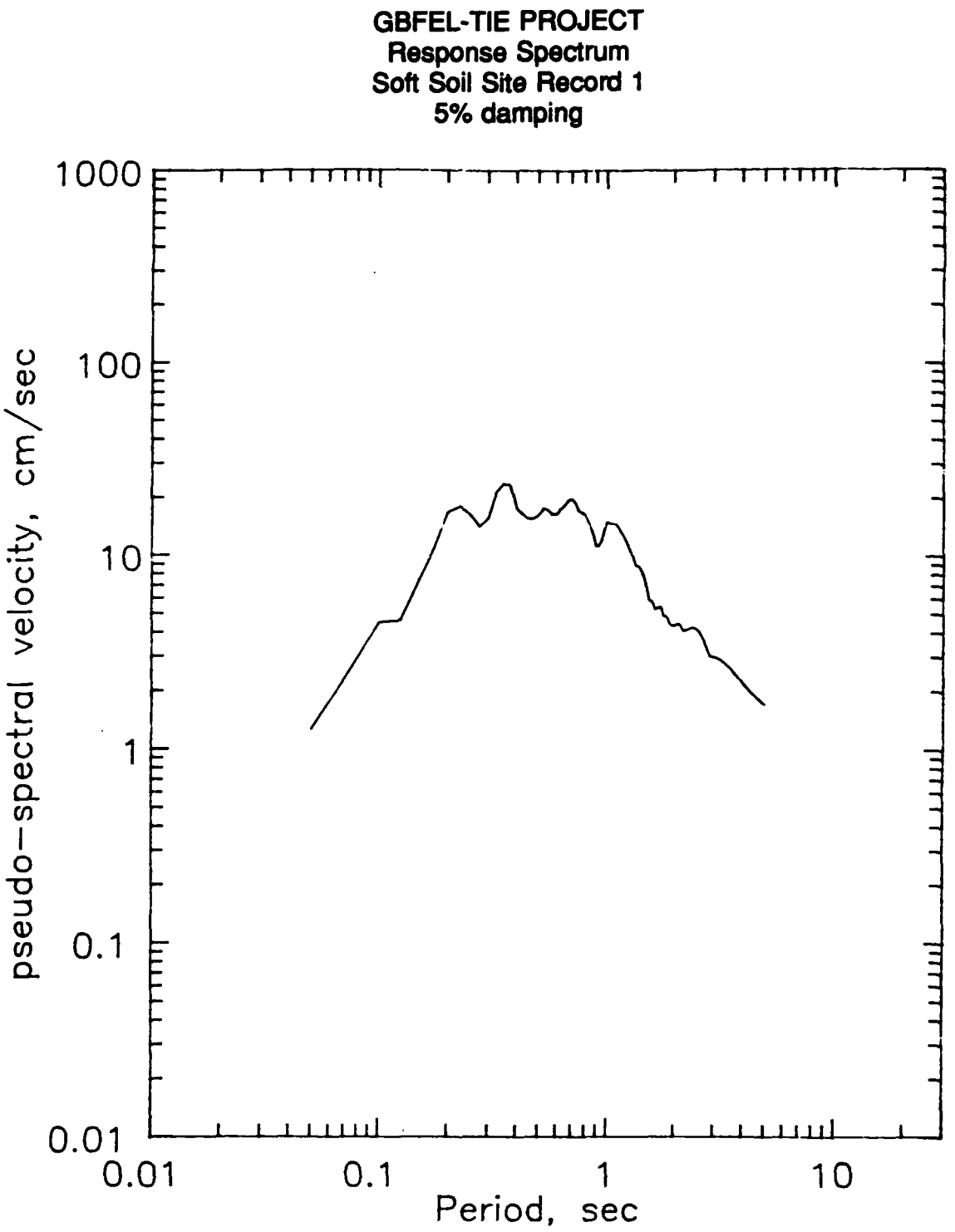

Figure 114. Response spectrum at 5-percent damping for Record 1

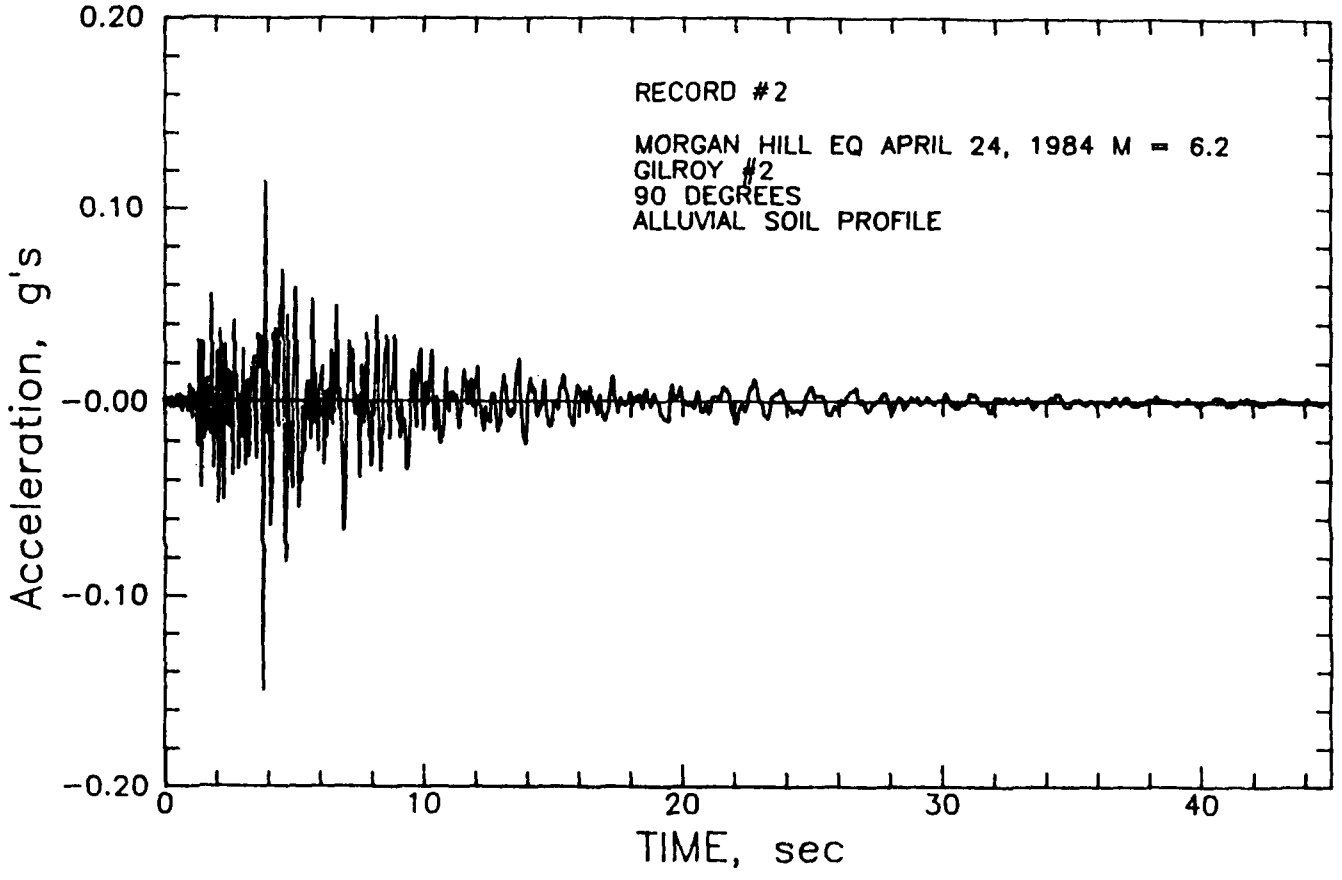

Figure 115. Acceleration history for Record 2

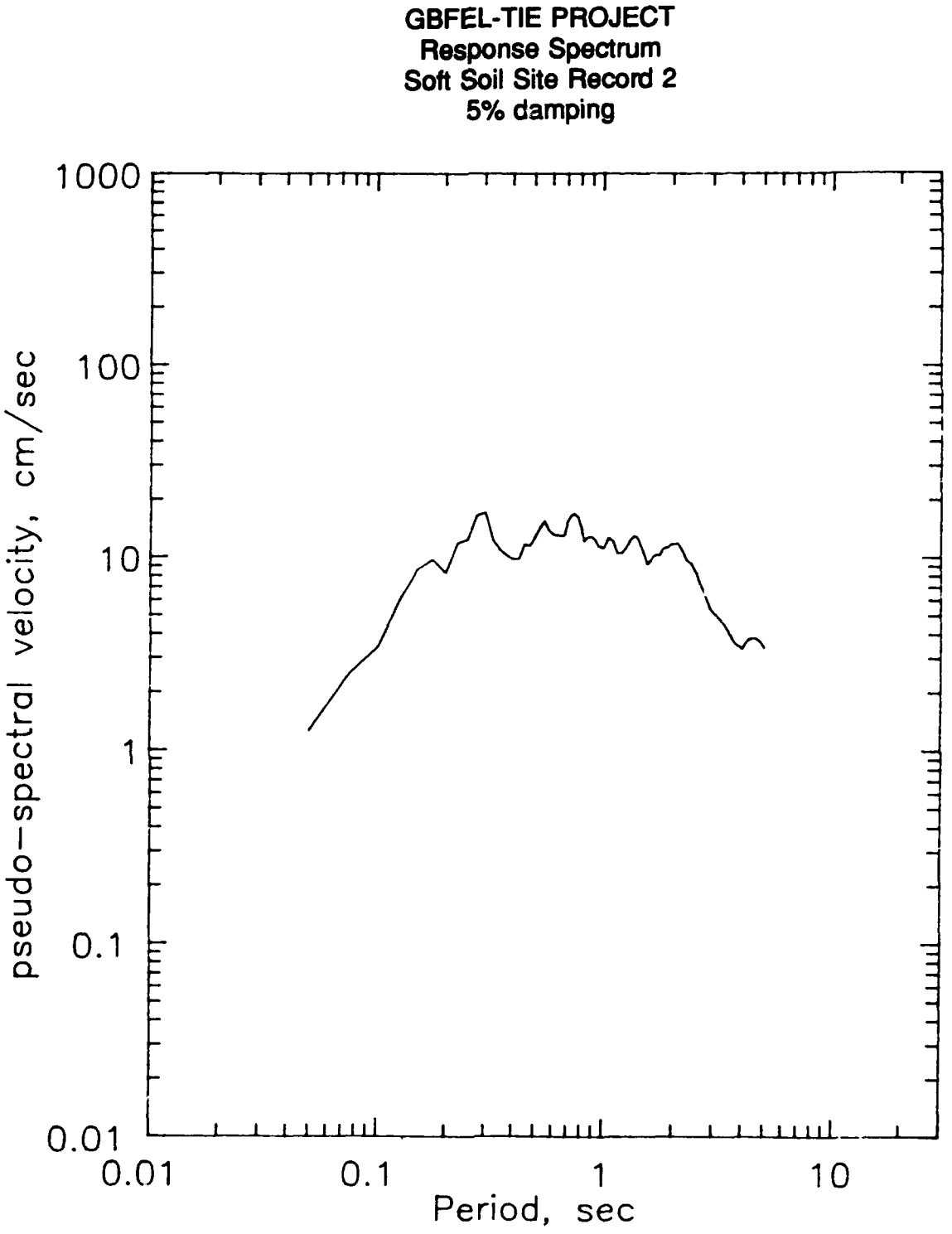

Figure 116. Response spectrum at 5-percent damping for Record 2

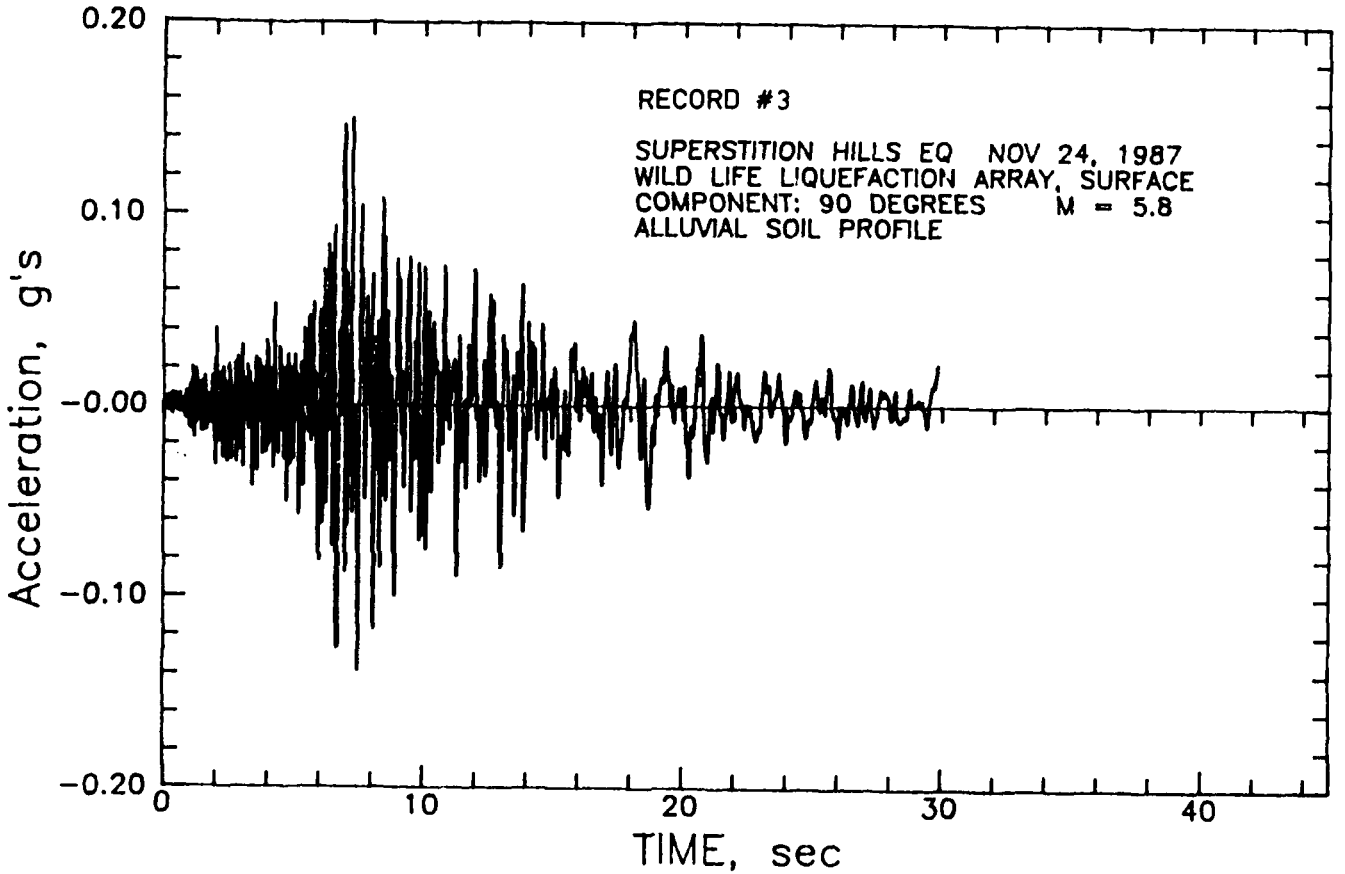

Figure 117. Acceleration history for Record 3

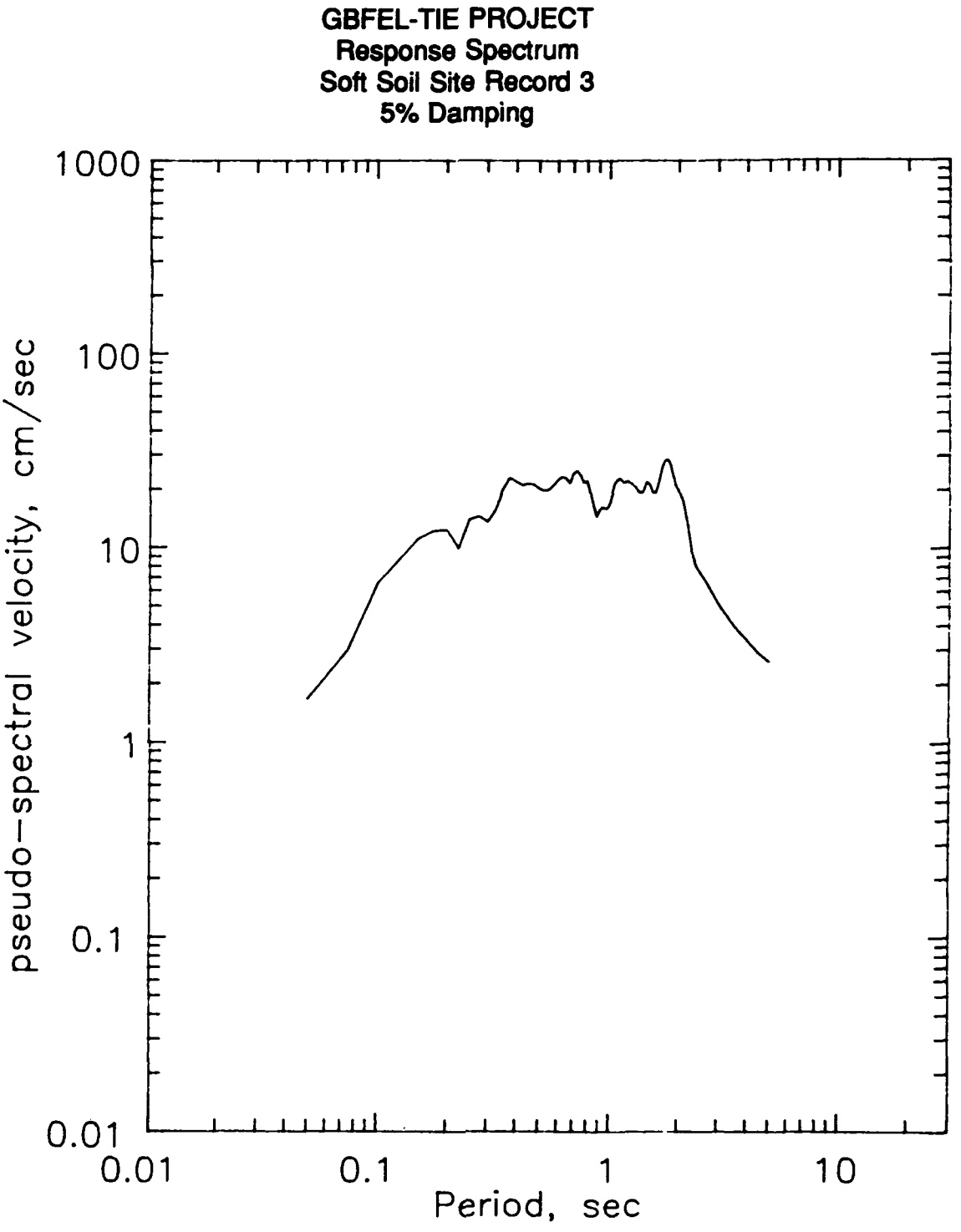

Figure 118. Response spectrum at 5-percent damping for Record 3

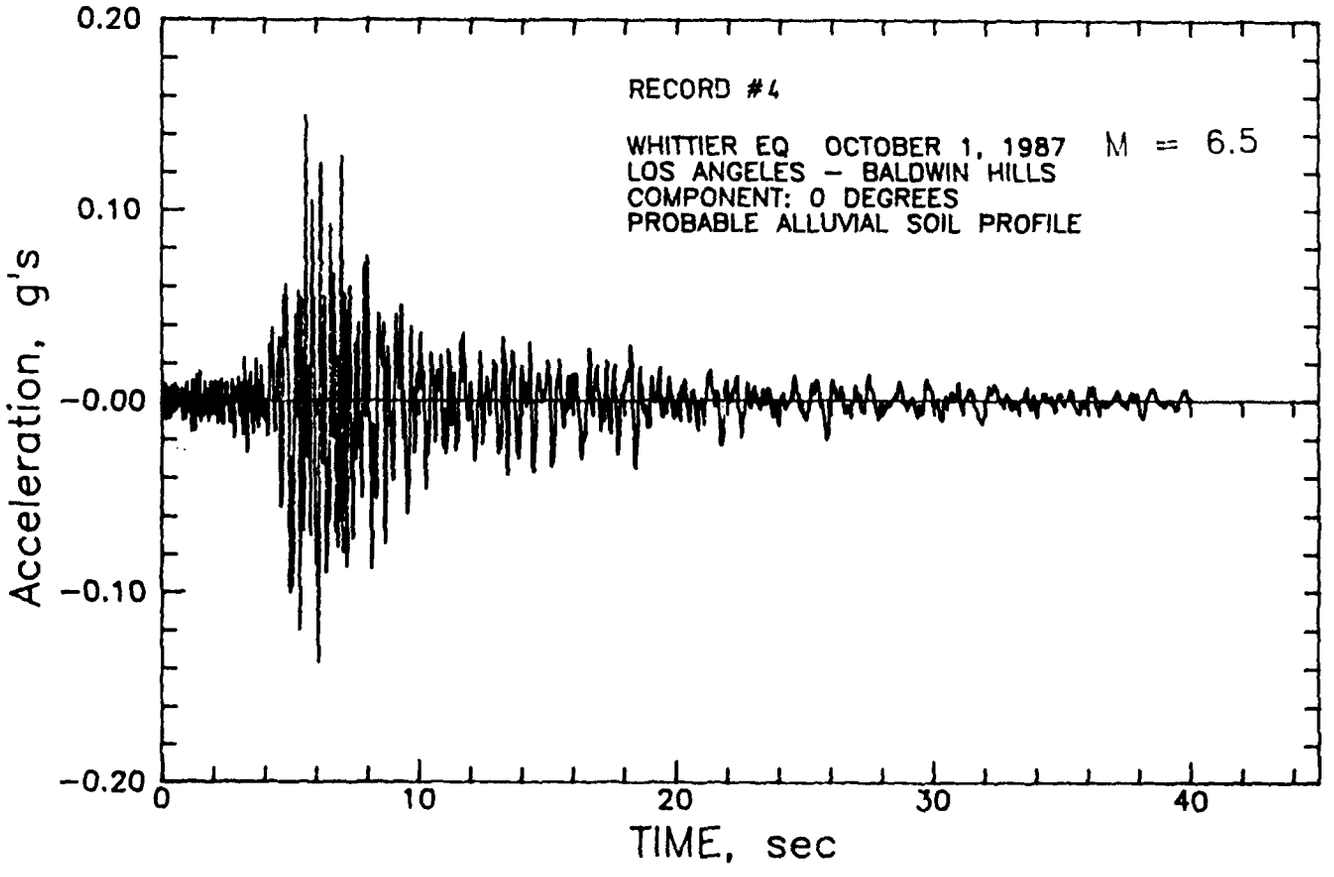

Figure 119. Acceleration history for Record 4

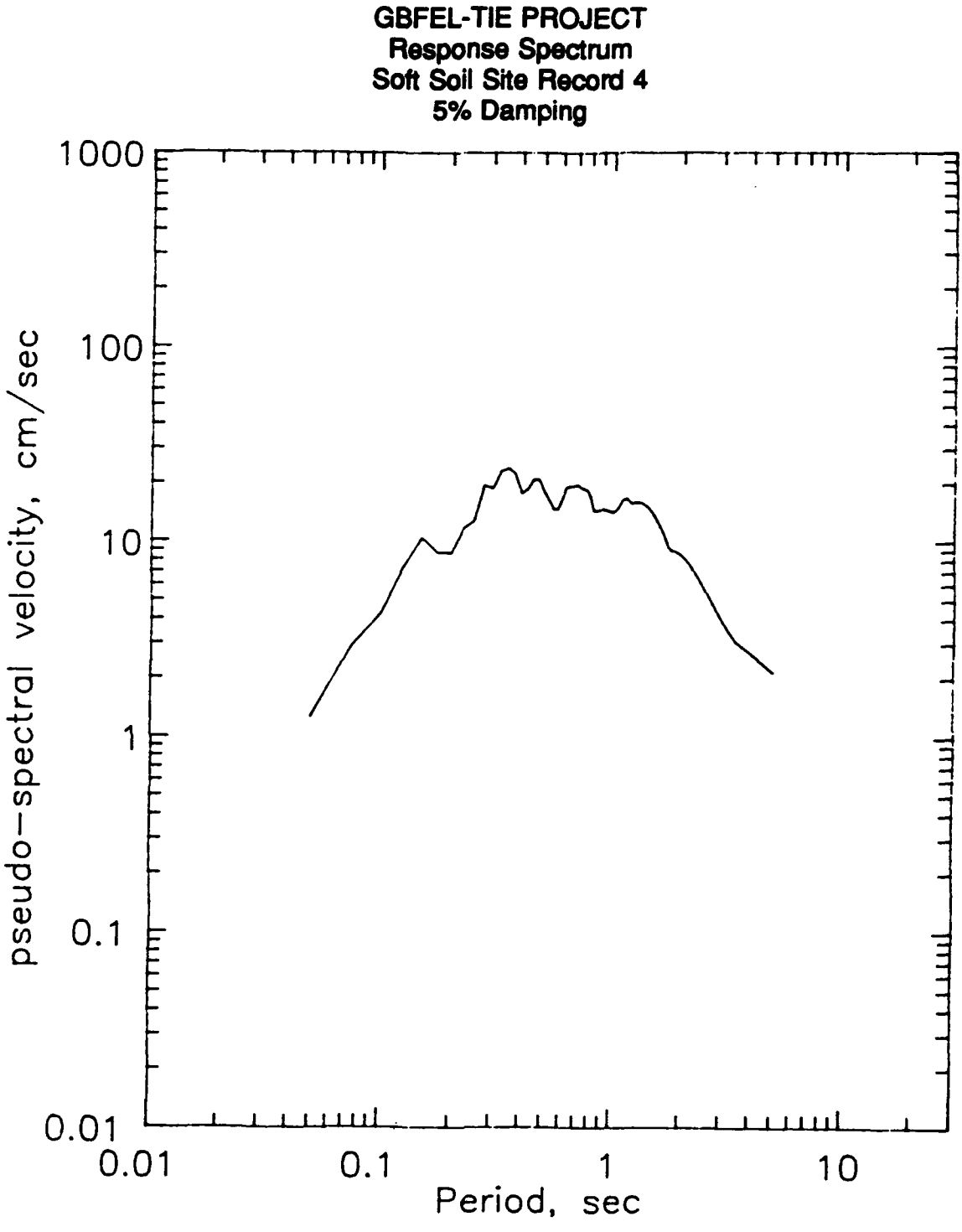

Figure 120. Response spectrum at 5-percent damping for Record 4

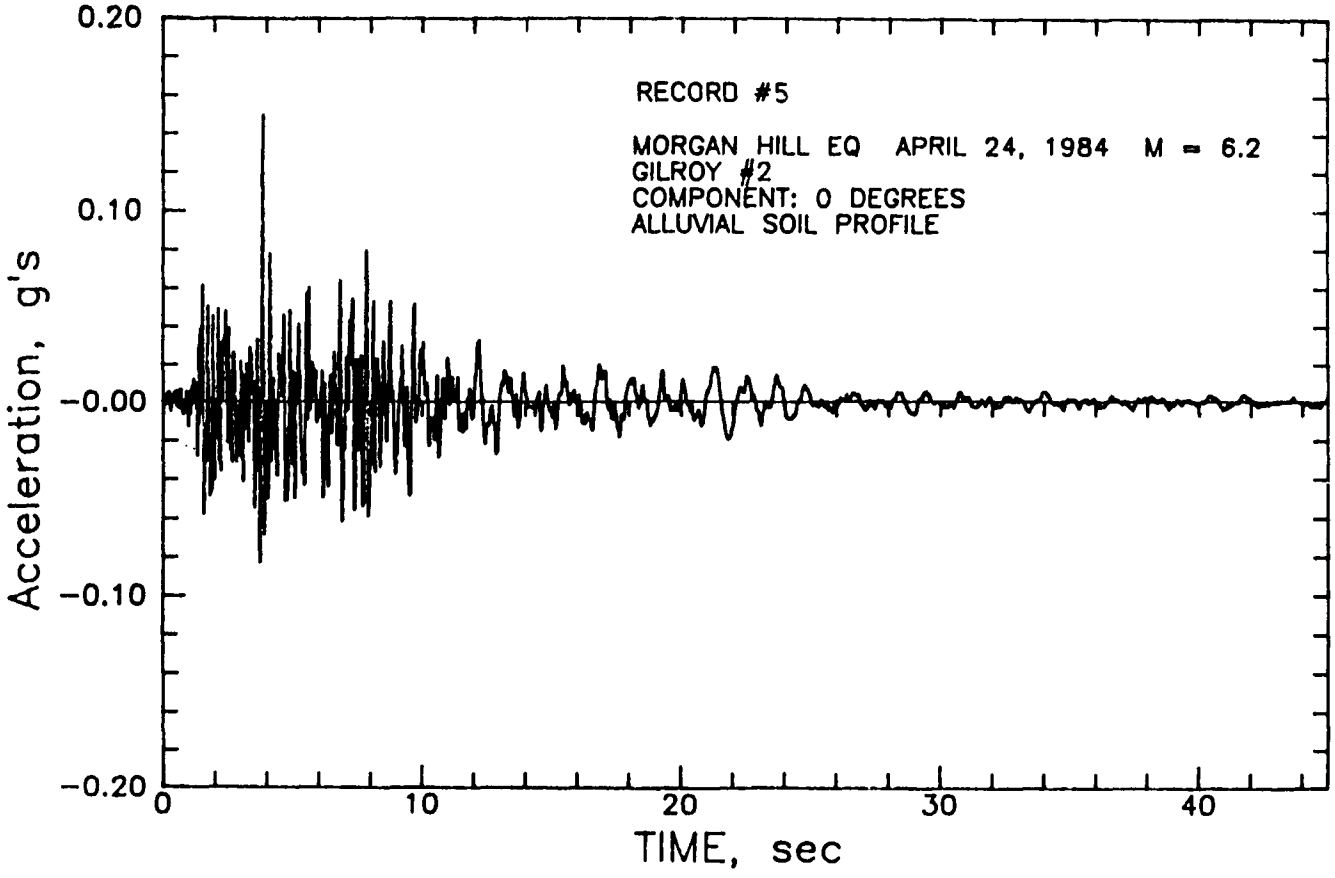

Figure 121. Acceleration history for Record 5

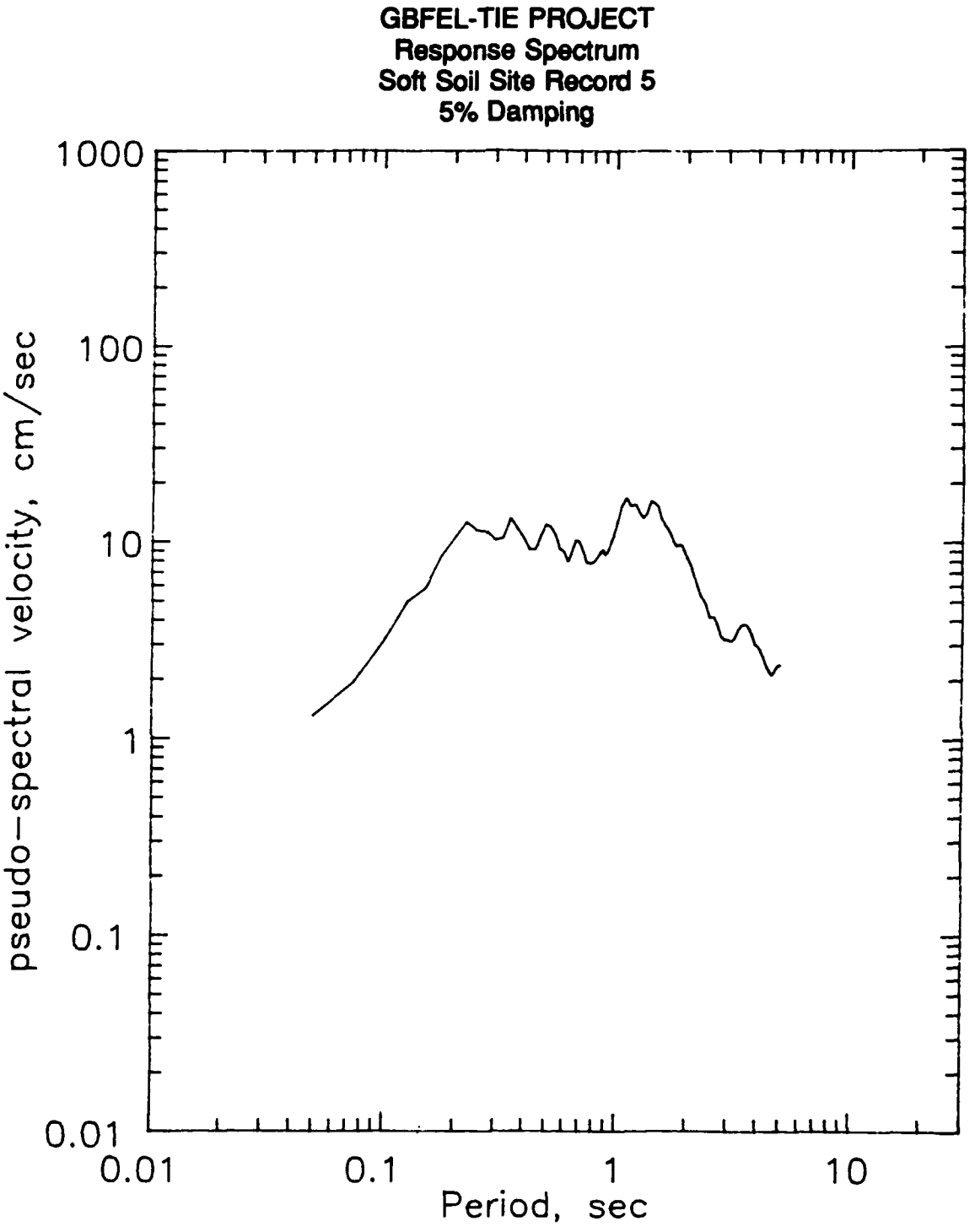

Figure 122. Response spectrum at 5-percent damping for Record 5

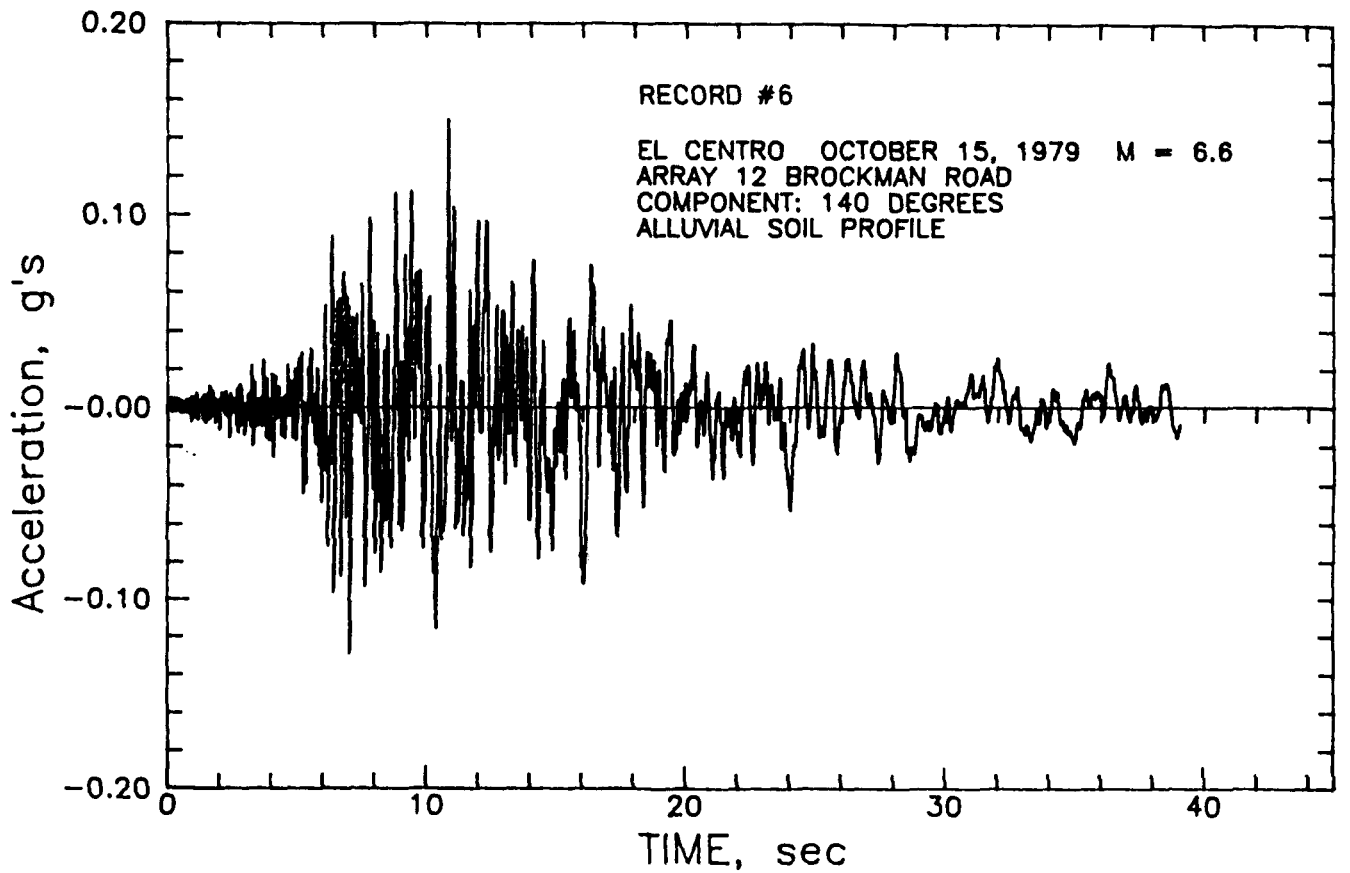

Figure 123. Acceleration history for Record 6

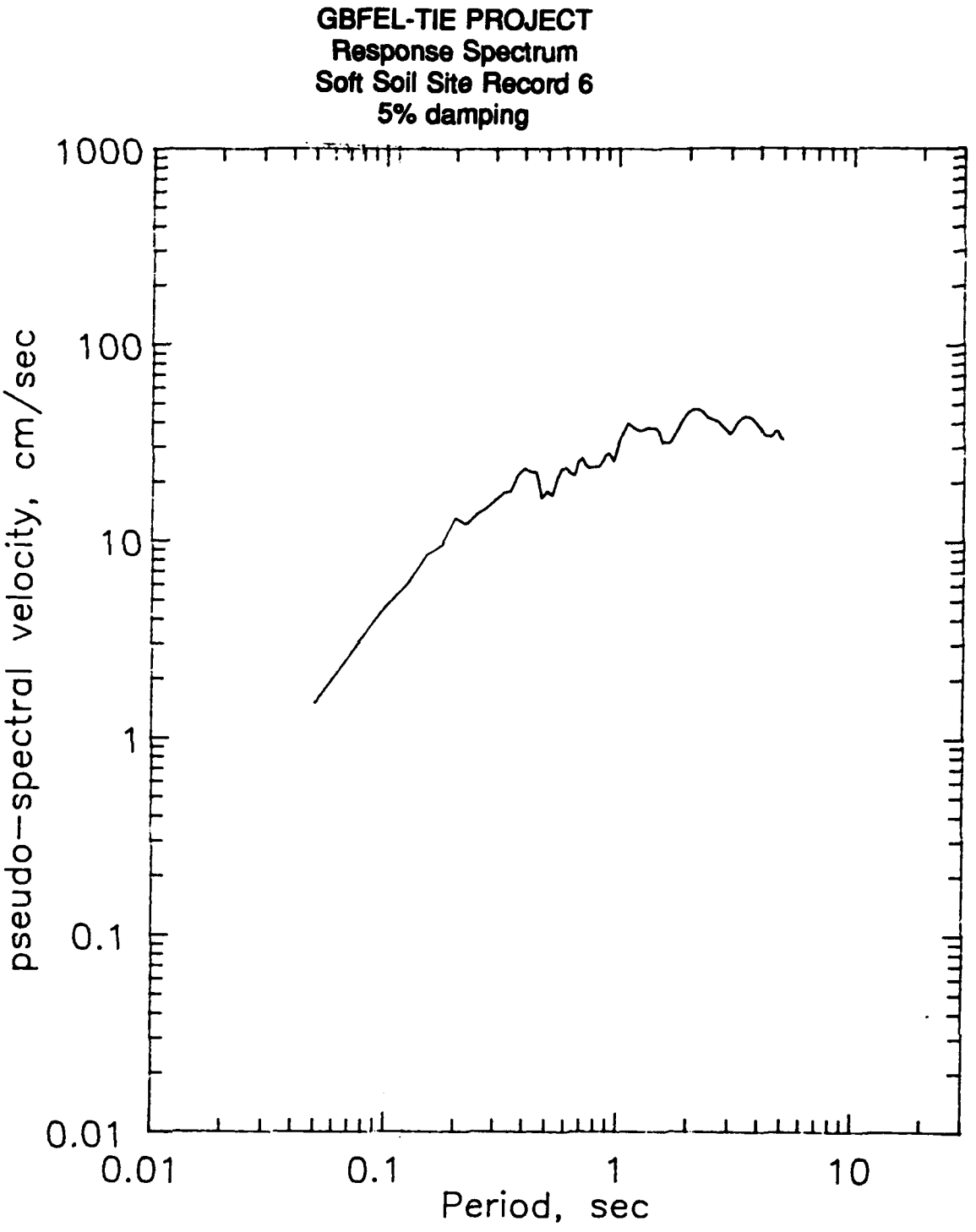

Figure 124. Response spectrum at 5-percent damping for Record 6

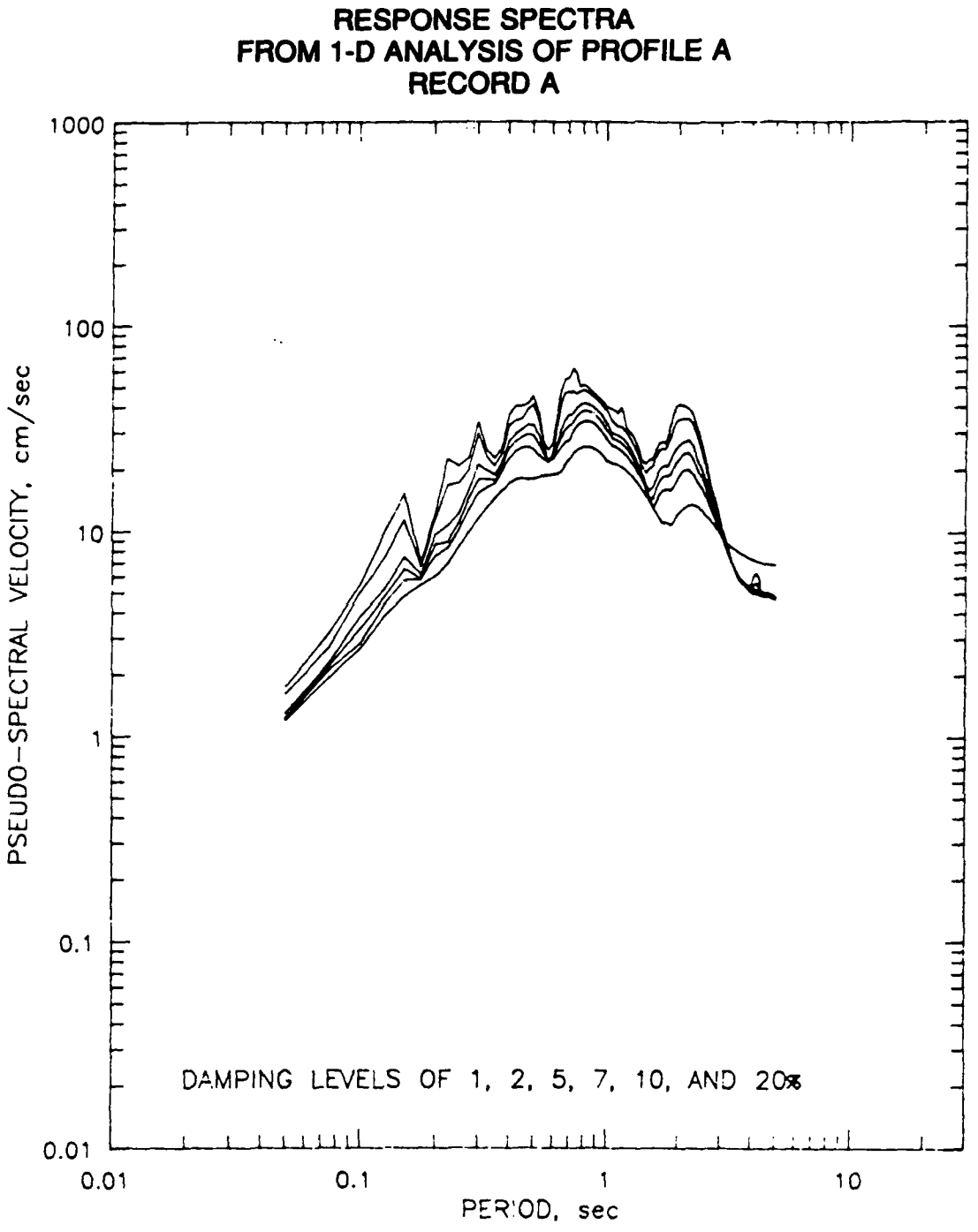

Figure 125. Response spectra of ground surface acceleration history of Profile A excited by Record A

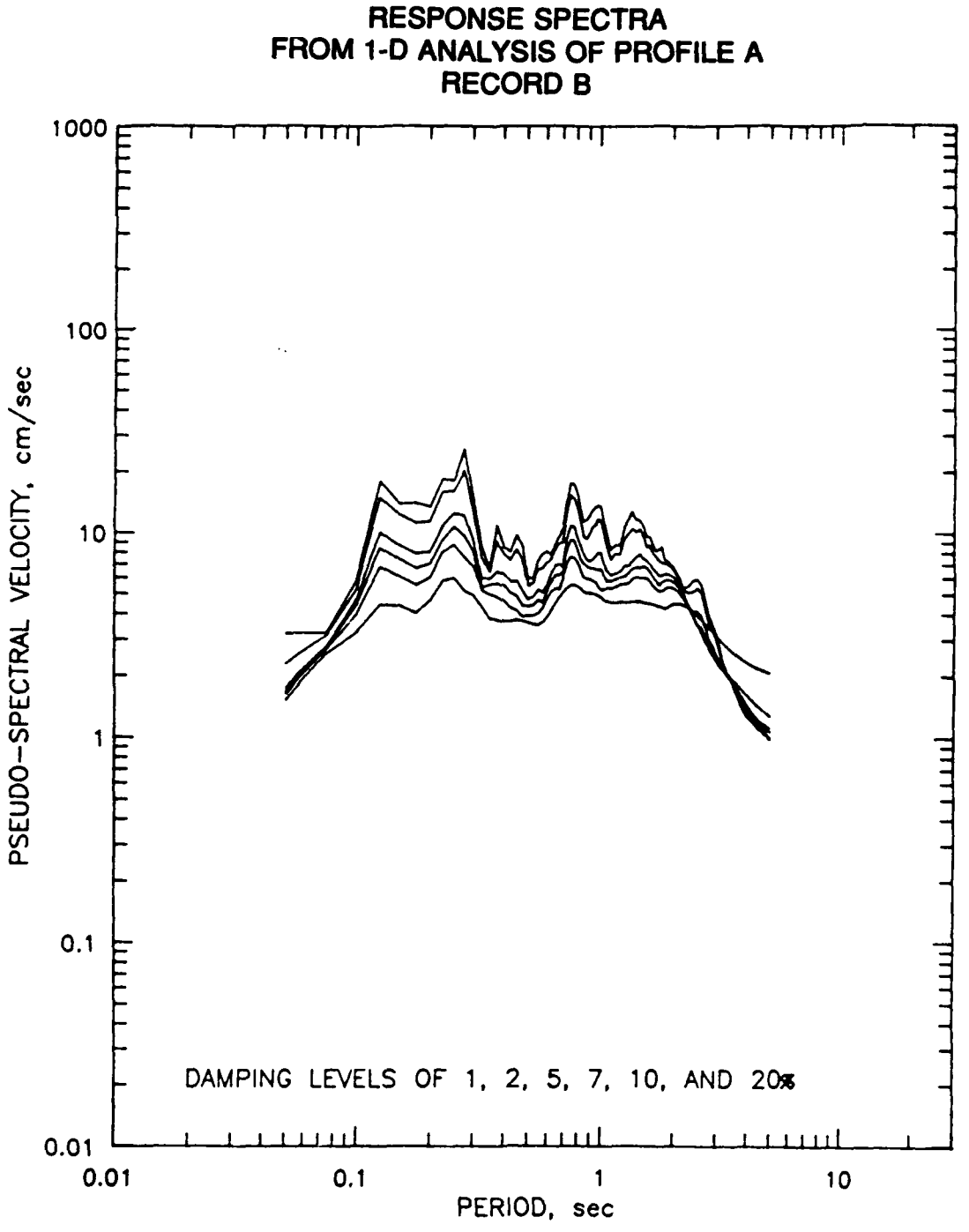

Figure 126. Response spectra of ground surface acceleration history of Profile A excited by Record B

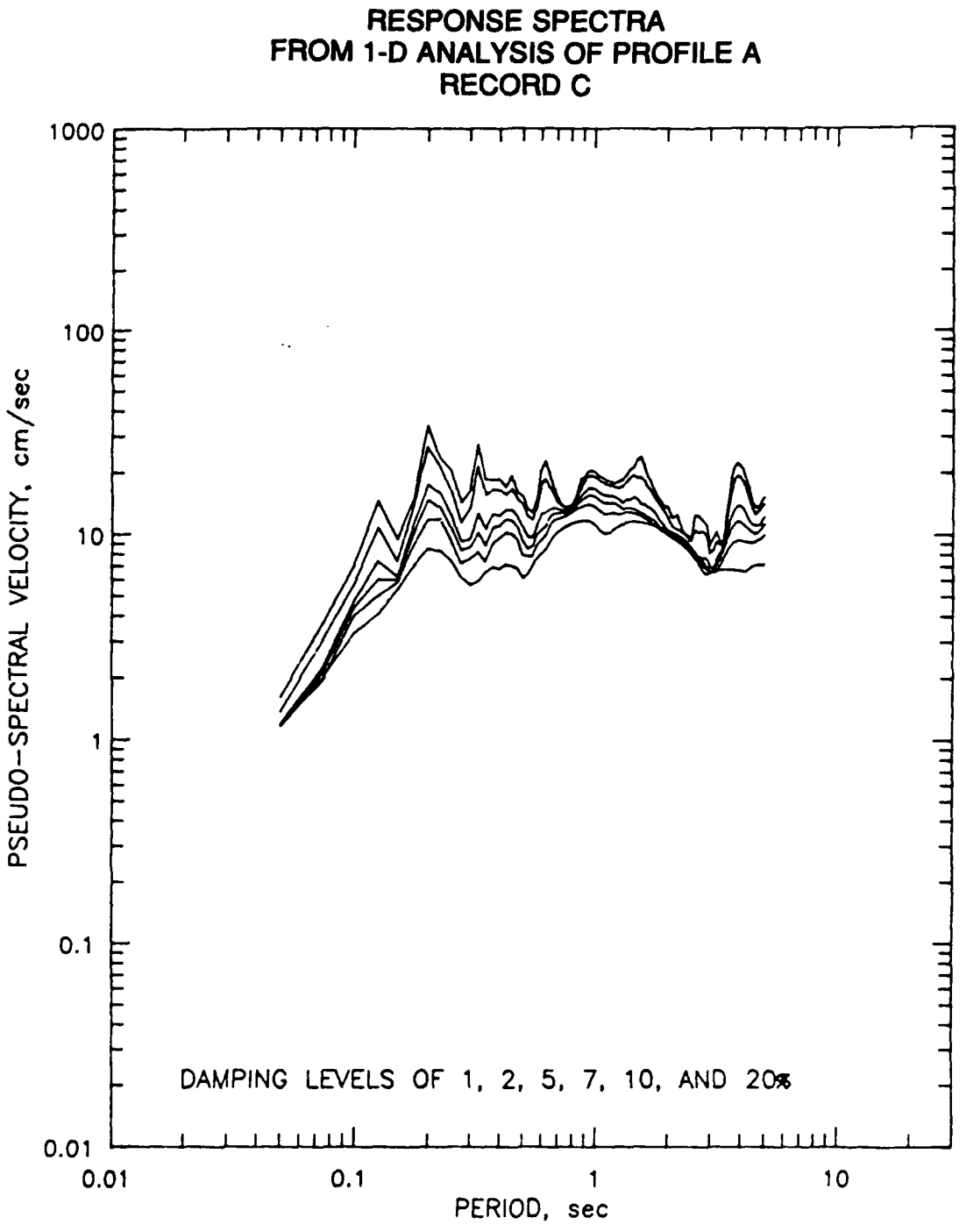

Figure 127. Response spectra of ground surface acceleration history of Profile A excited by Record C

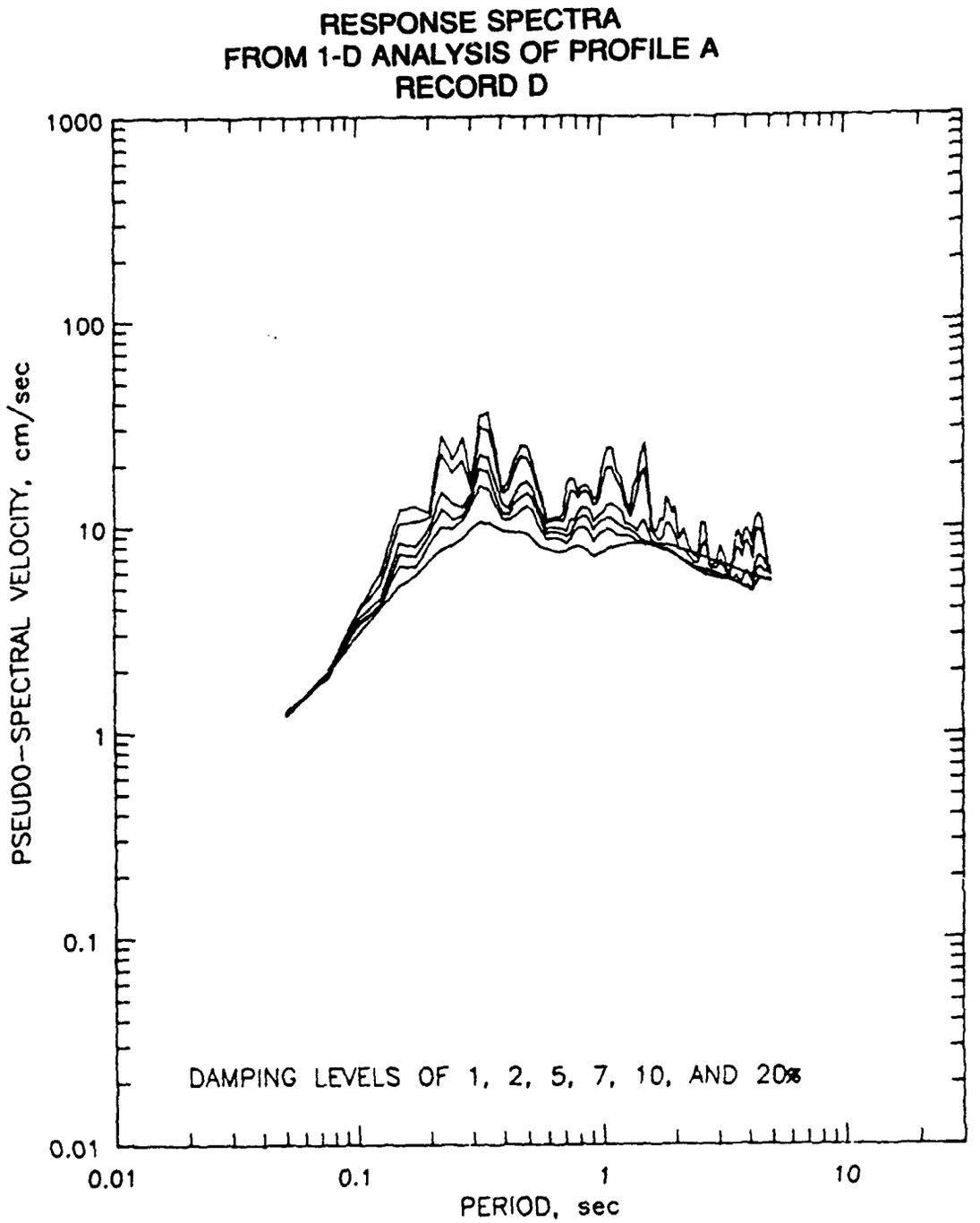

Figure 128. Response spectra of ground surface acceleration history of Profile A excited by Record D

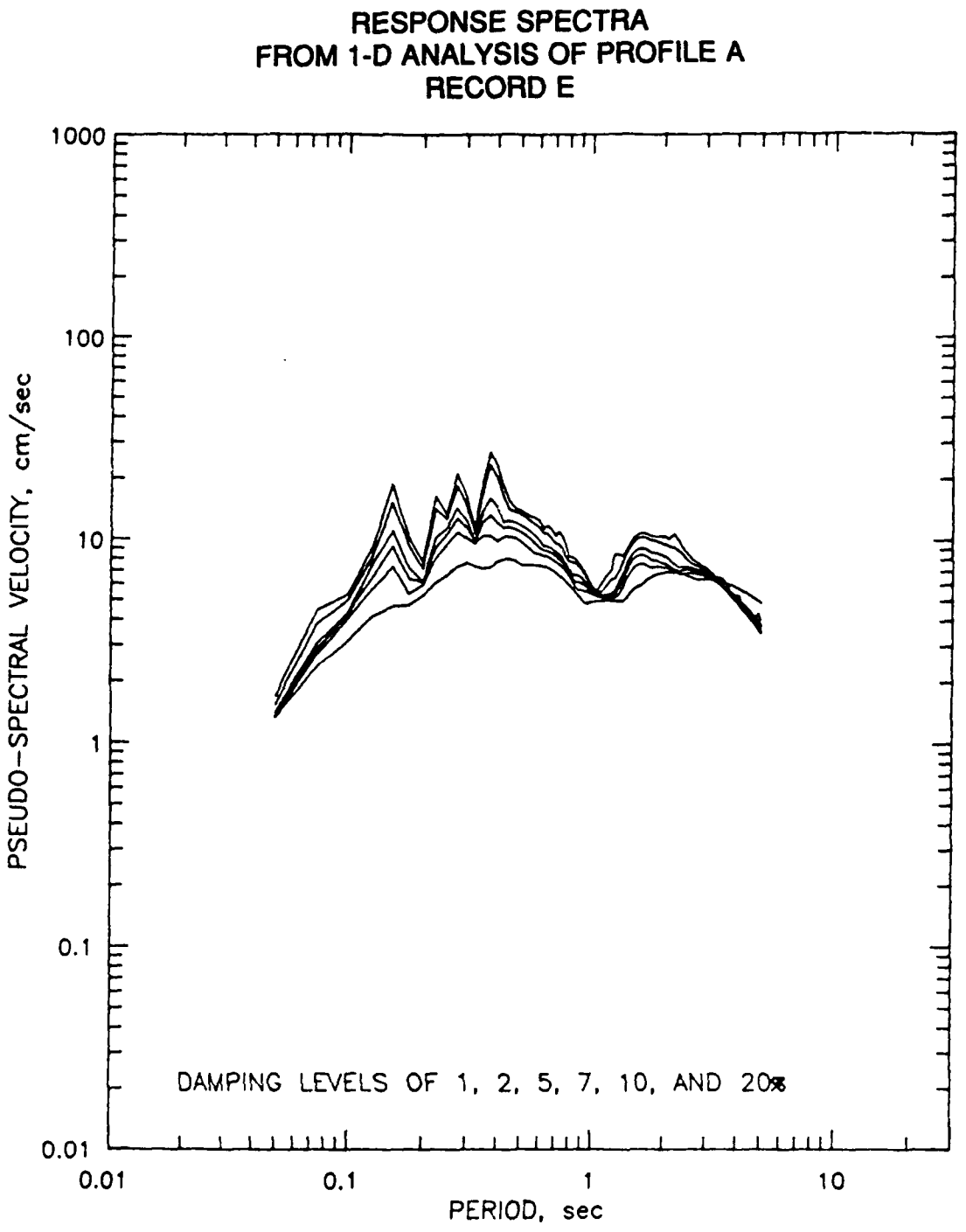

Figure 129. Response spectra of ground surface acceleration history of Profile A excited by Record E

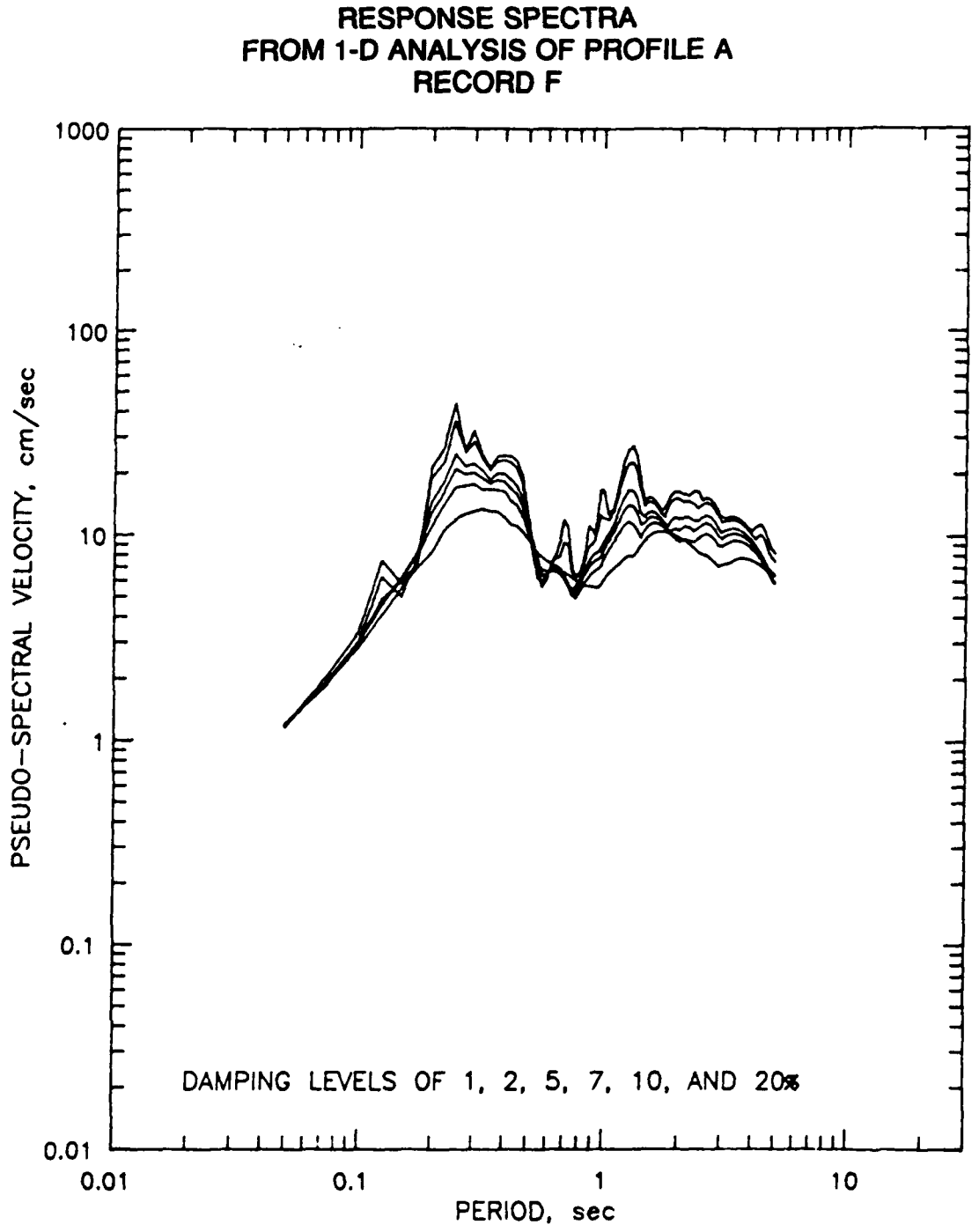

Figure 130. Response spectra of ground surface acceleration history of Profile A excited by Record F

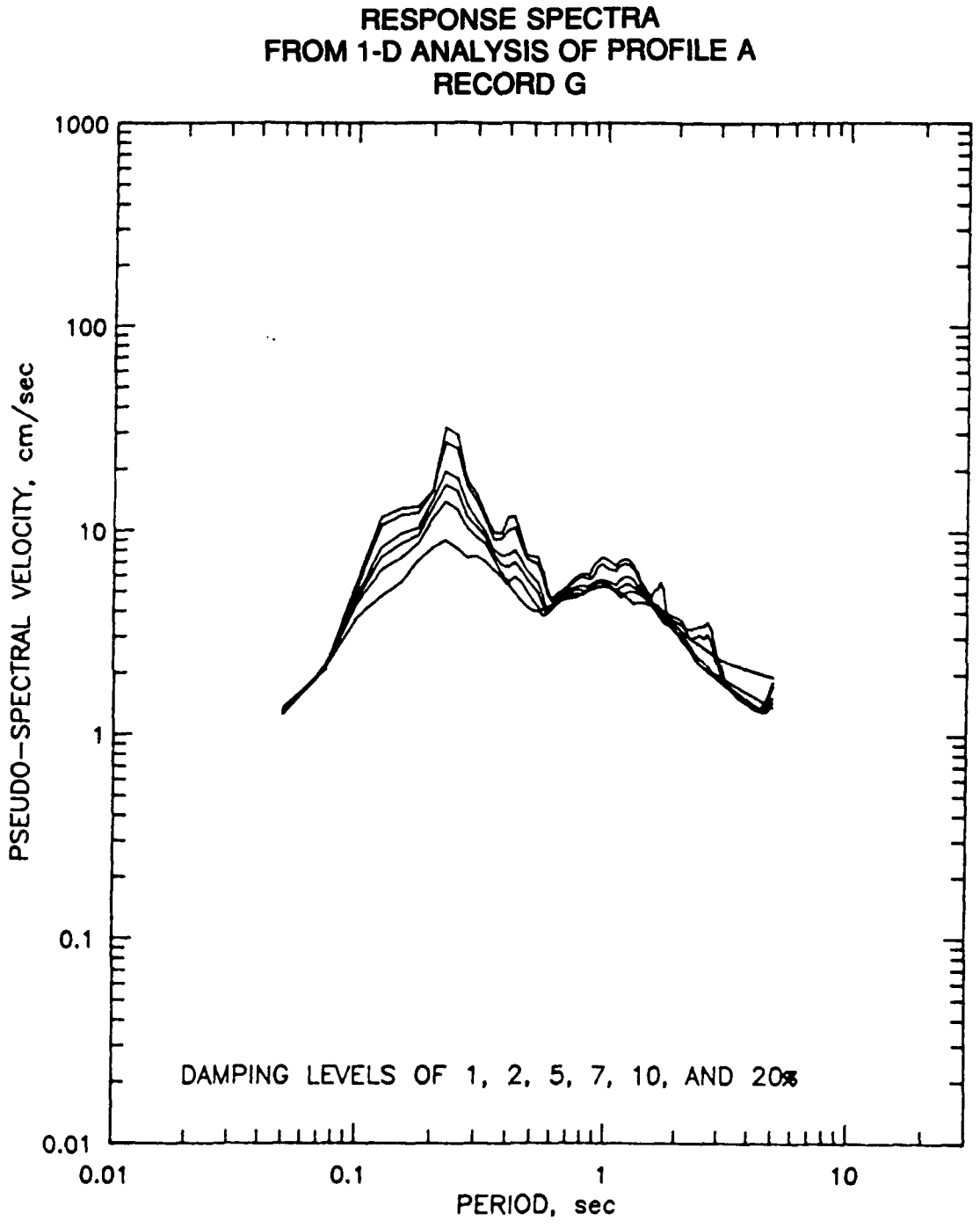

Figure 131. Response spectra of ground surface acceleration history of Profile A excited by Record G

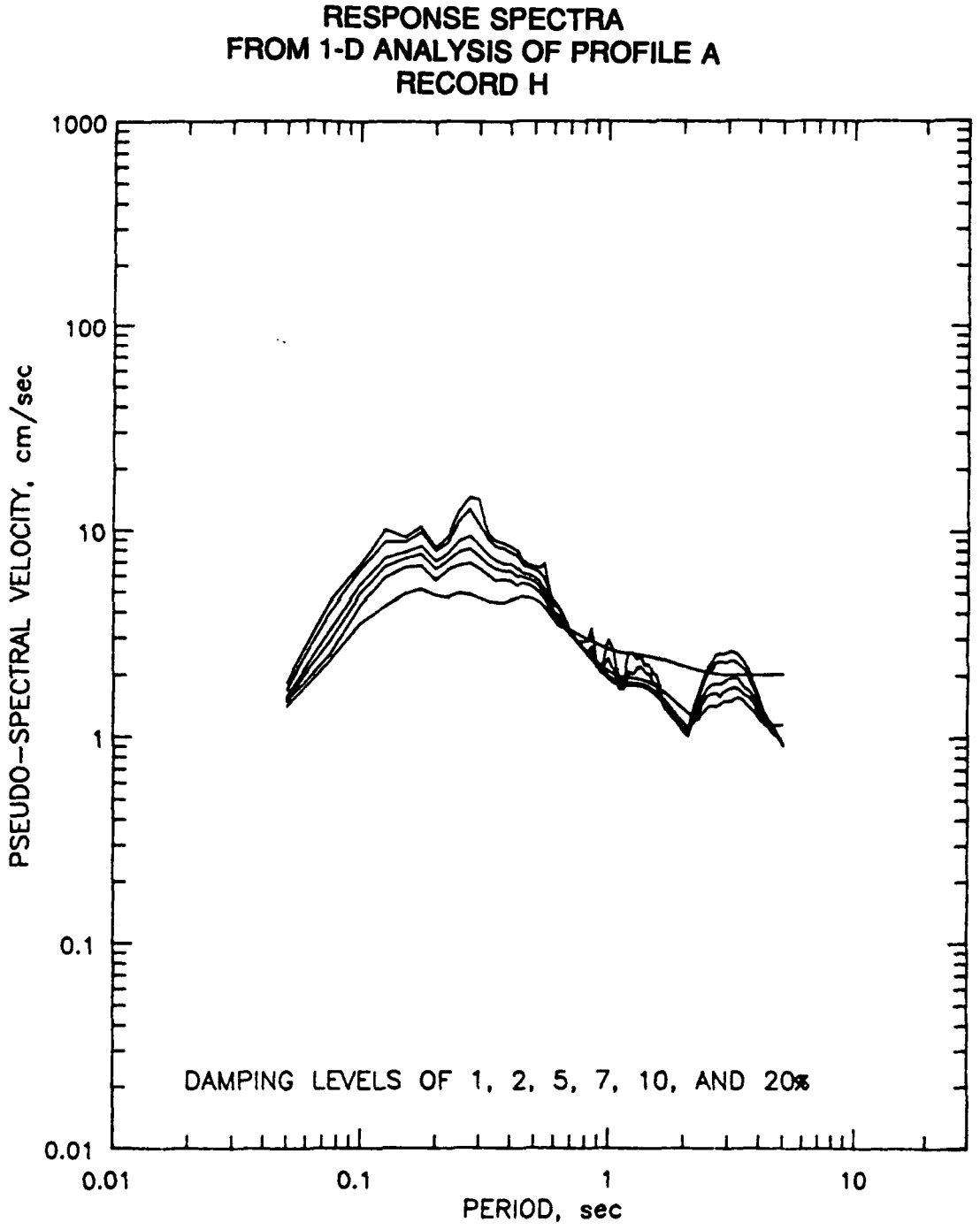

Figure 132. Response spectra of ground surface acceleration history of Profile A excited by Record H

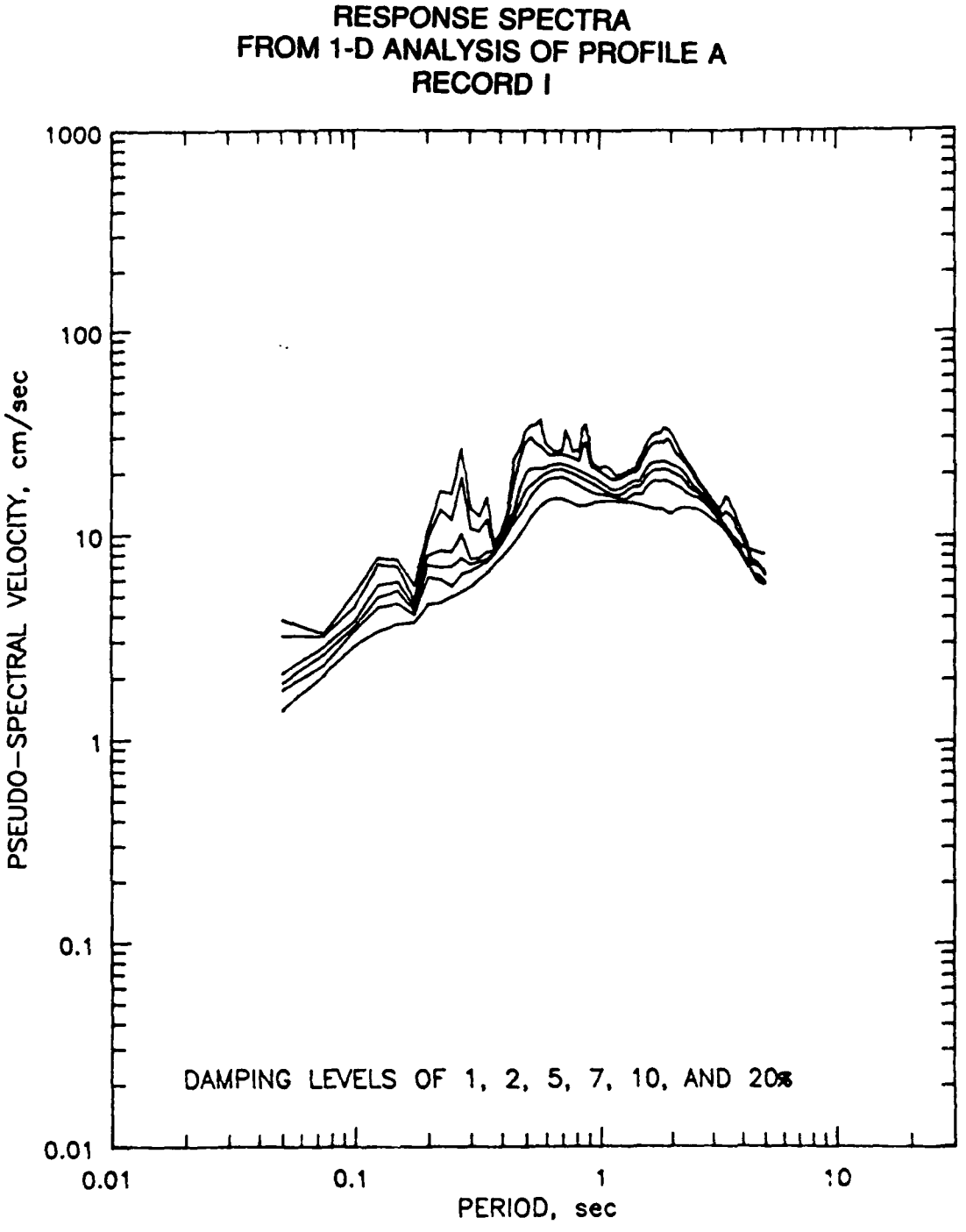

Figure 133. Response spectra of ground surface acceleration history of Profile A excited by Record I

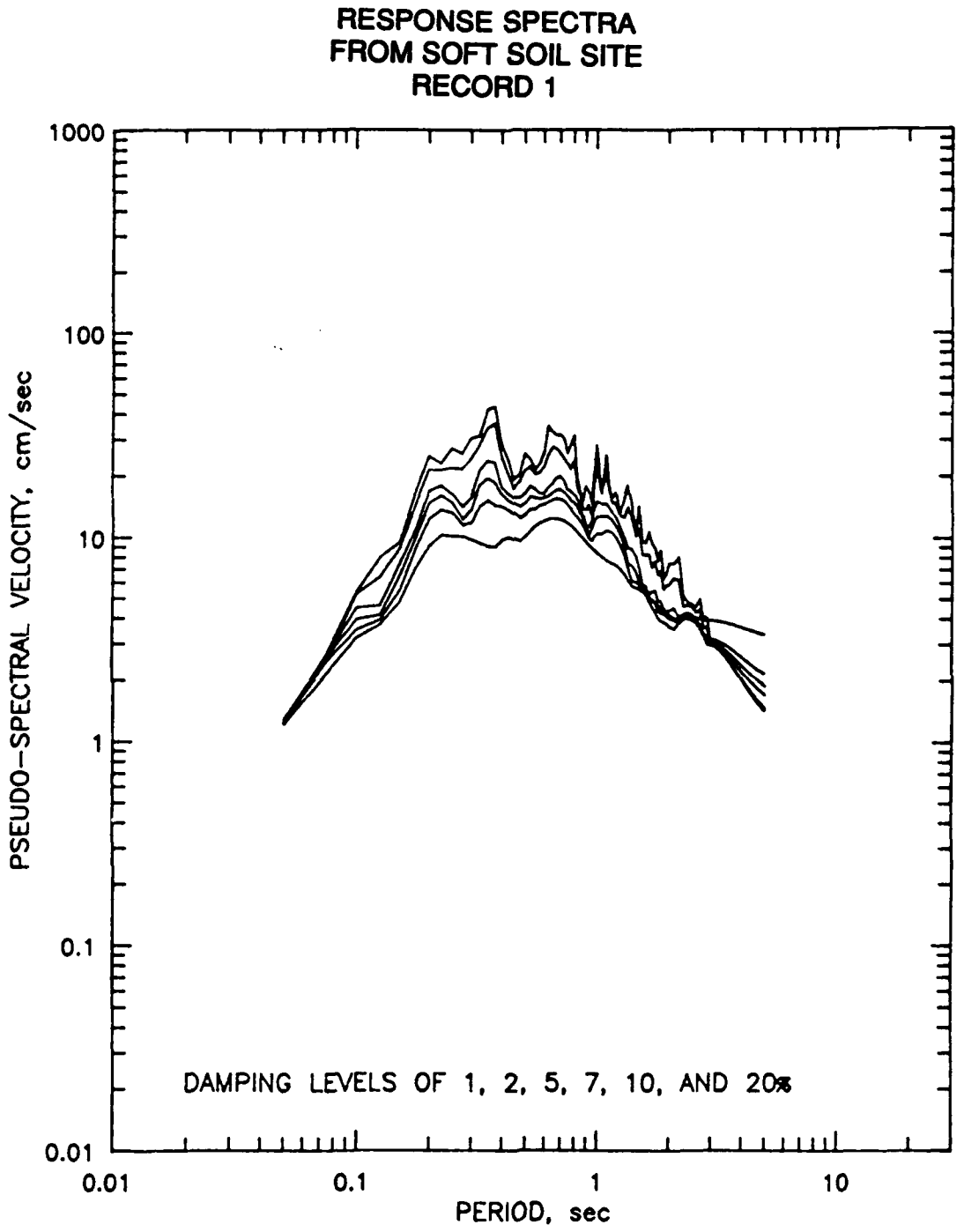

Figure 134. Response spectra of firm soil site Record 1

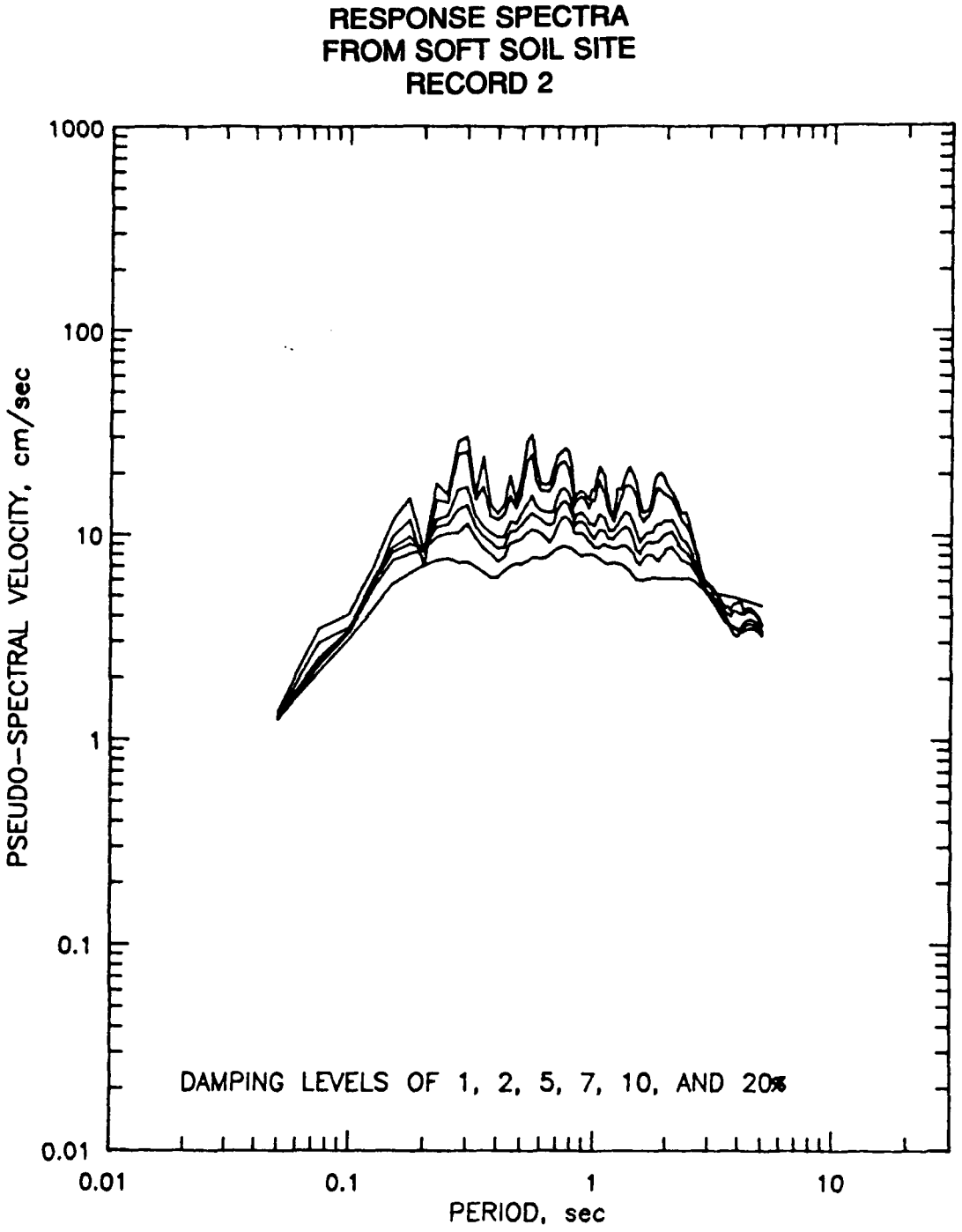

Figure 135. Response spectra of firm soil site Record 2

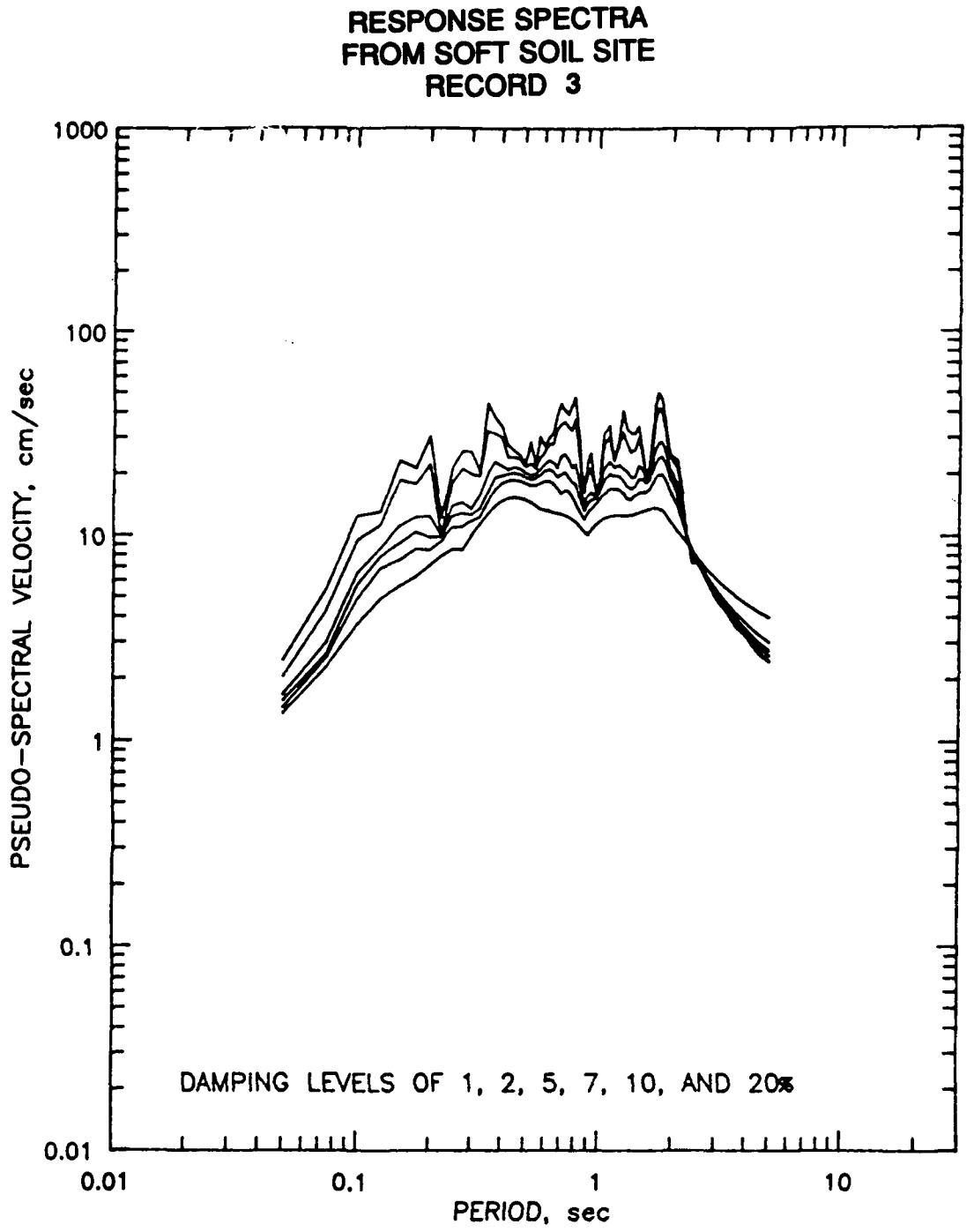

Figure 136. Response spectra of firm soil site Record #3

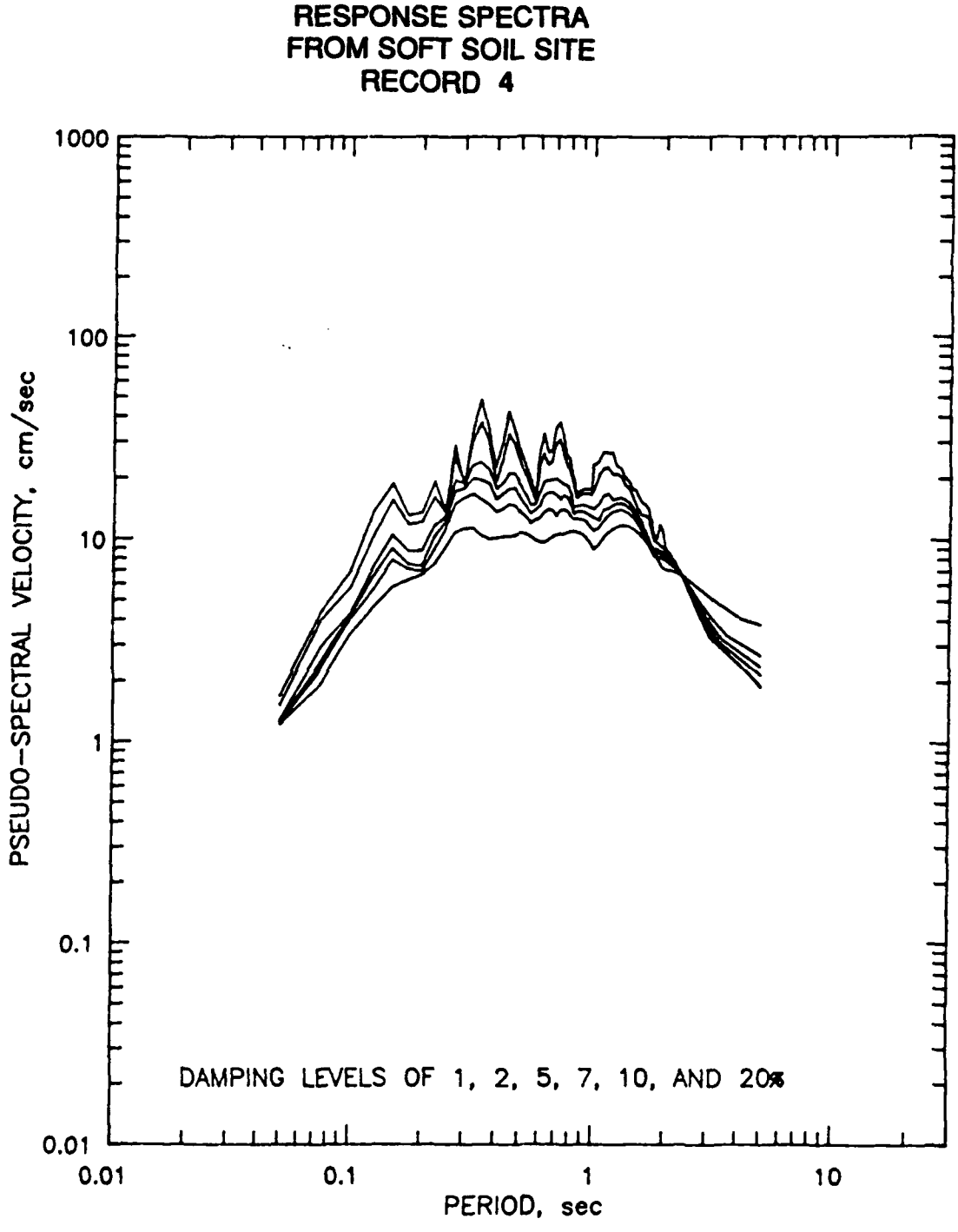

Figure 137. Response spectra of firm soil site Record #4

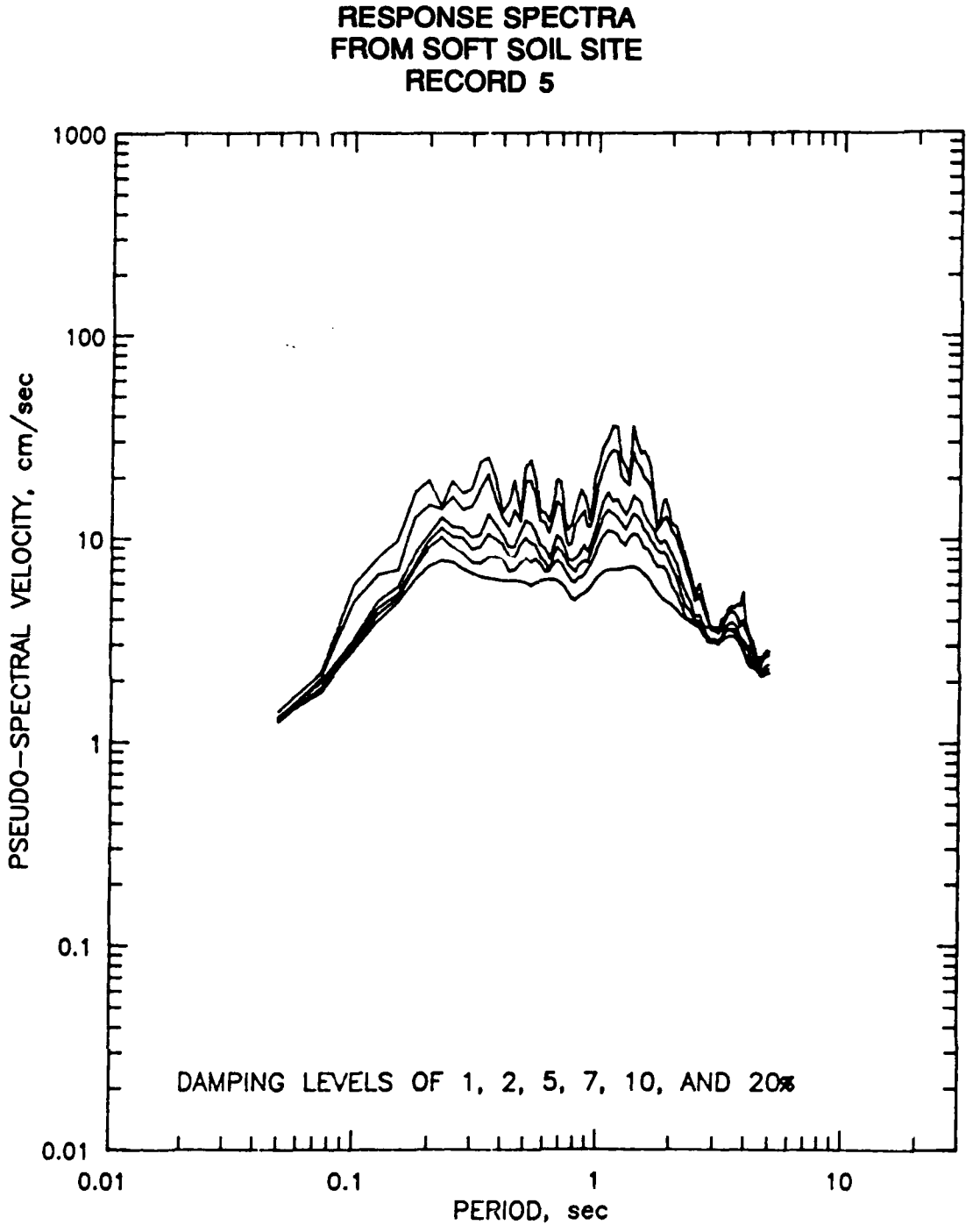

Figure 138. Response spectra of firm soil site Record #5

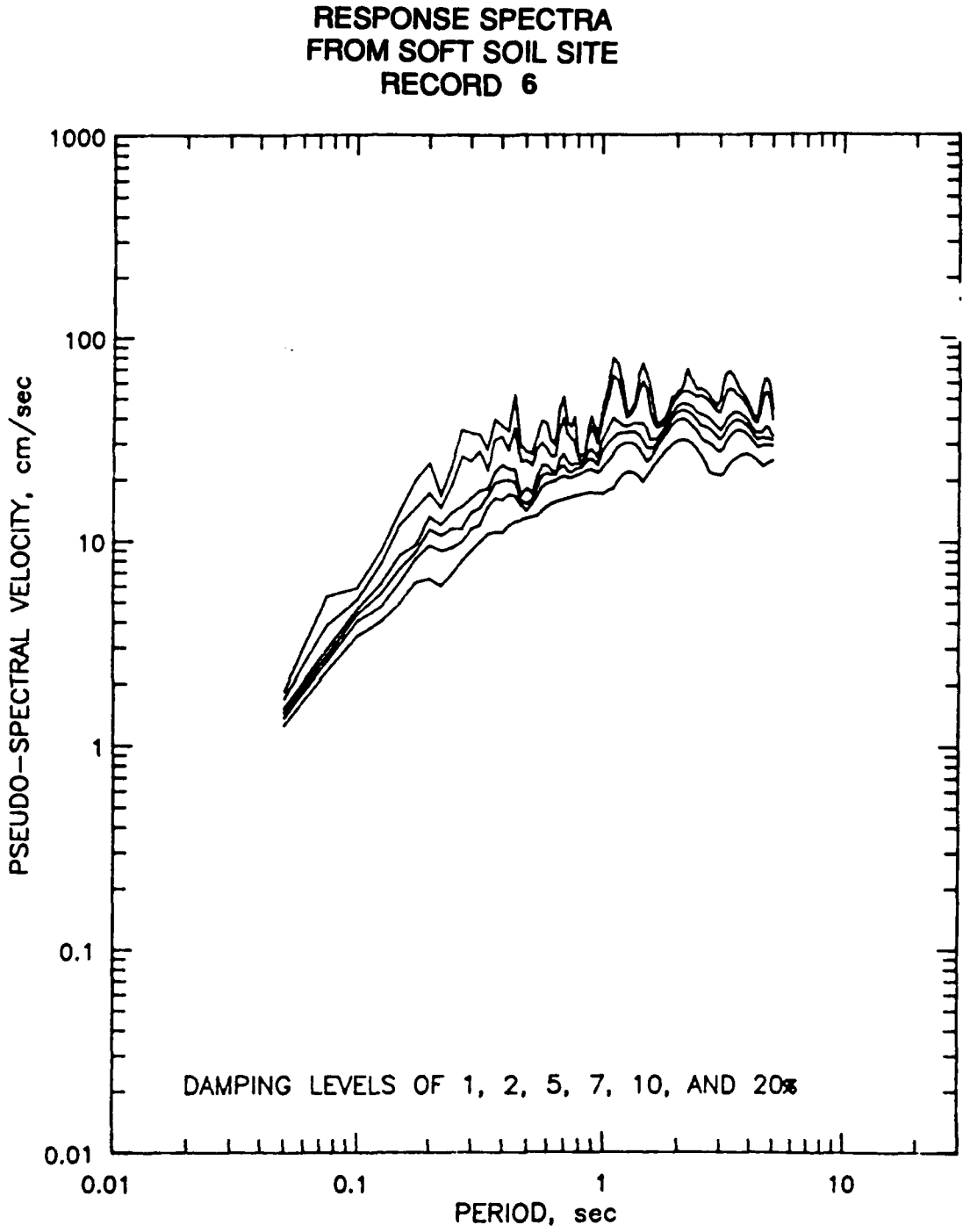

Figure 139. Response spectra of firm soil site Record #6

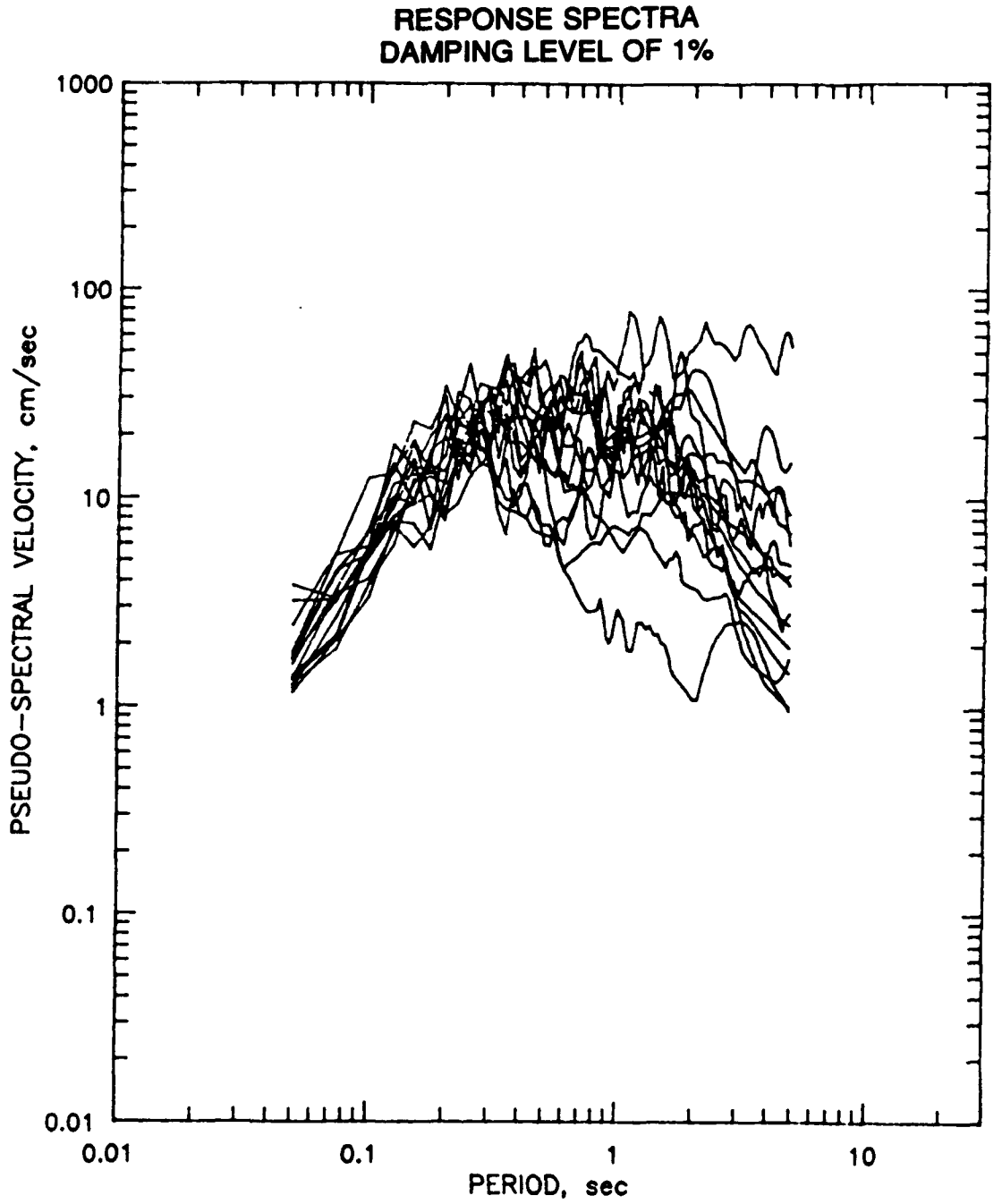

Figure 140. Composite of response spectra for all ground surface accelerograms used in this study at 1-percent damping level

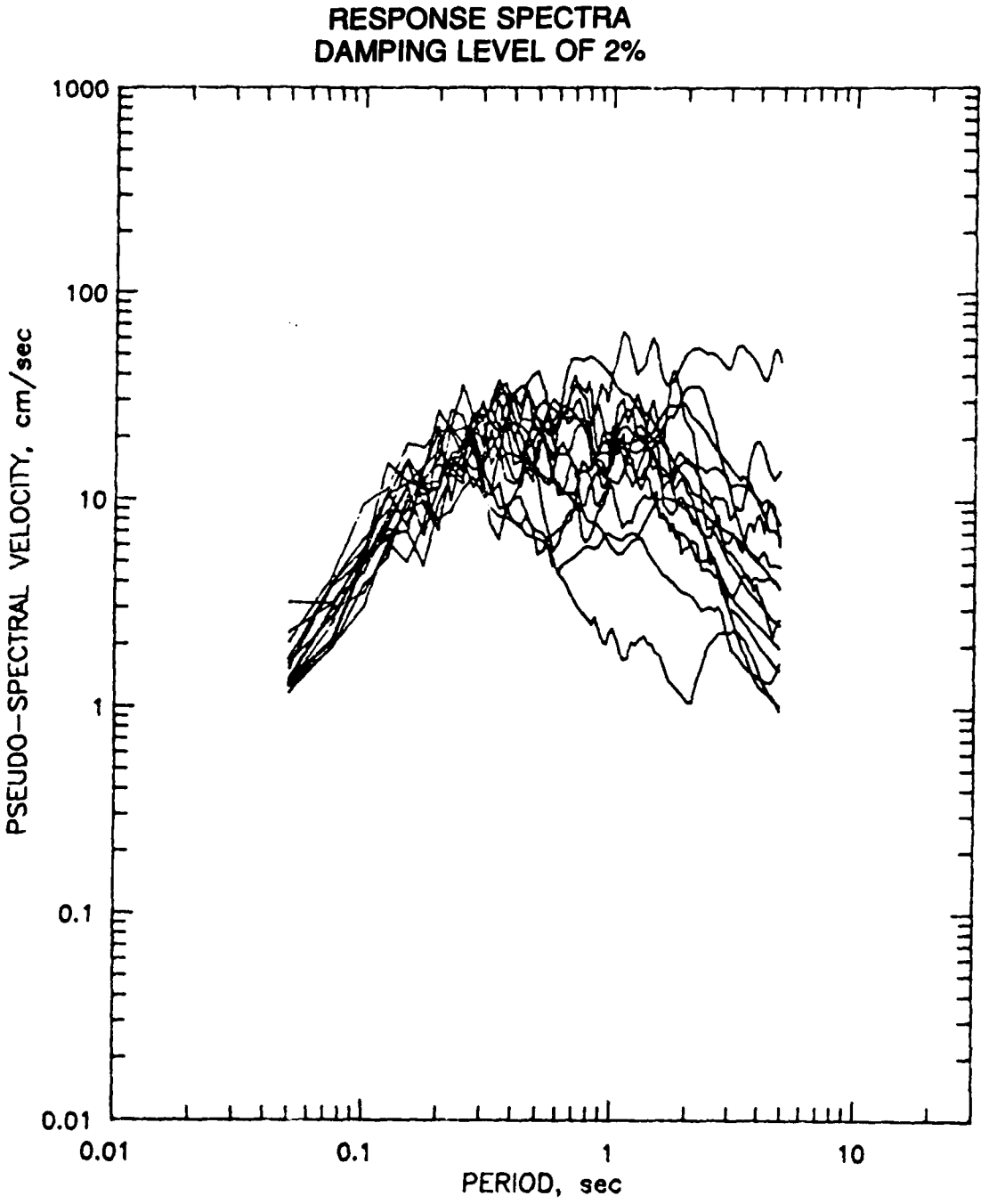

Figure 141. Composite of response spectra for all ground surface accelerograms used in this study at 2-percent damping level

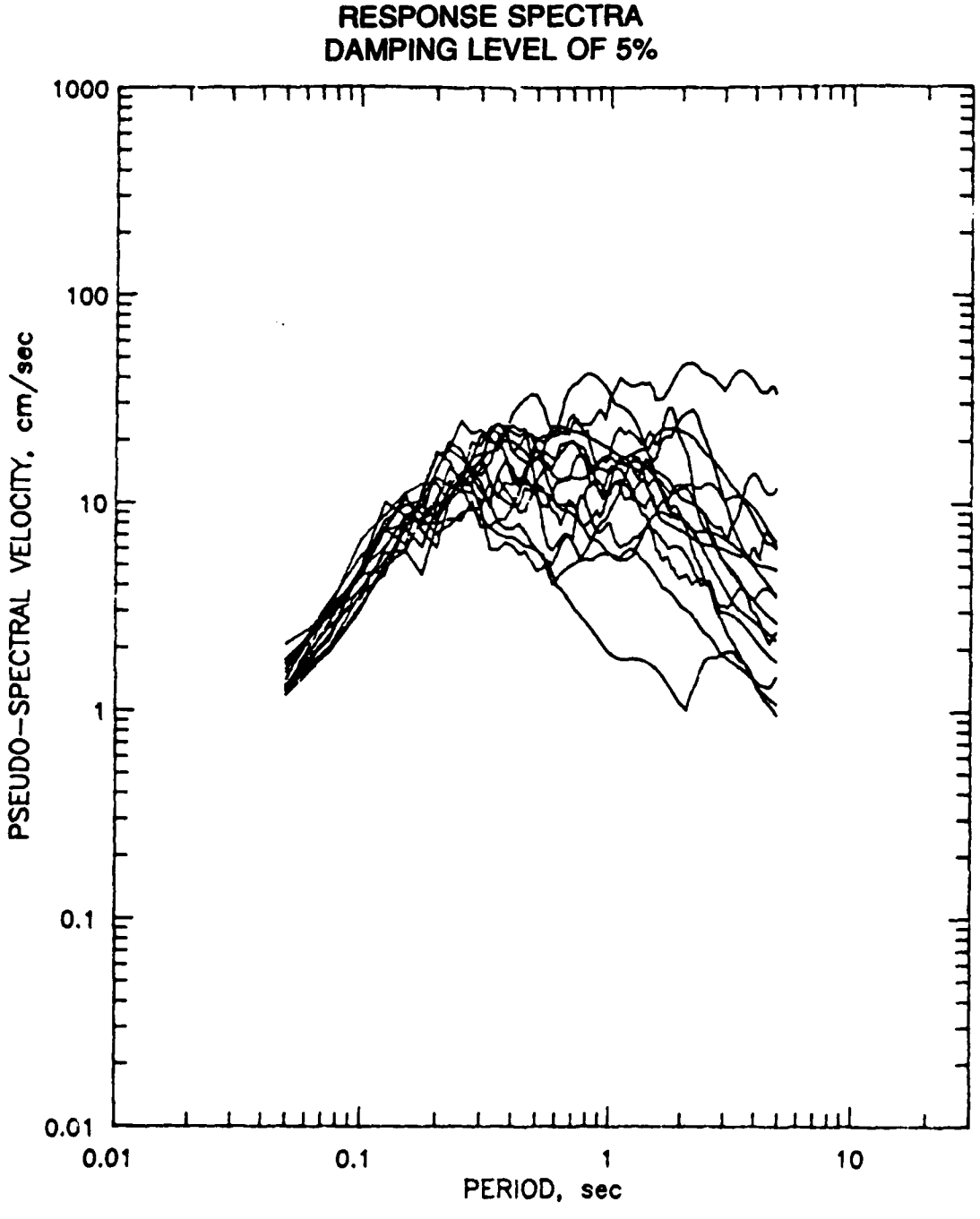

Figure 142. Composite of response spectra for all ground surface accelerograms used in this study at 5-percent damping level

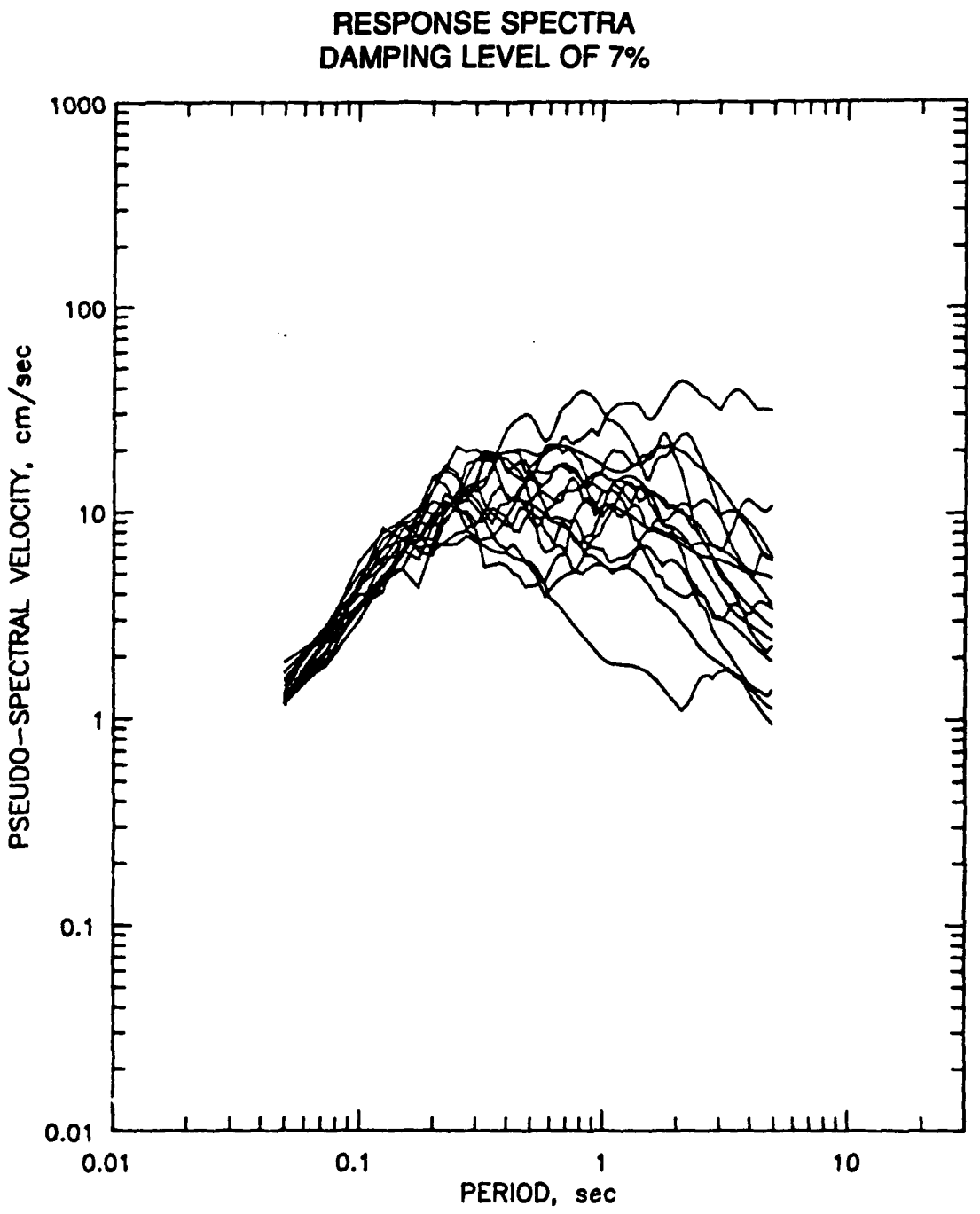

Figure 143. Composite of response spectra for all ground surface accelerograms used in this study at 7-percent damping level

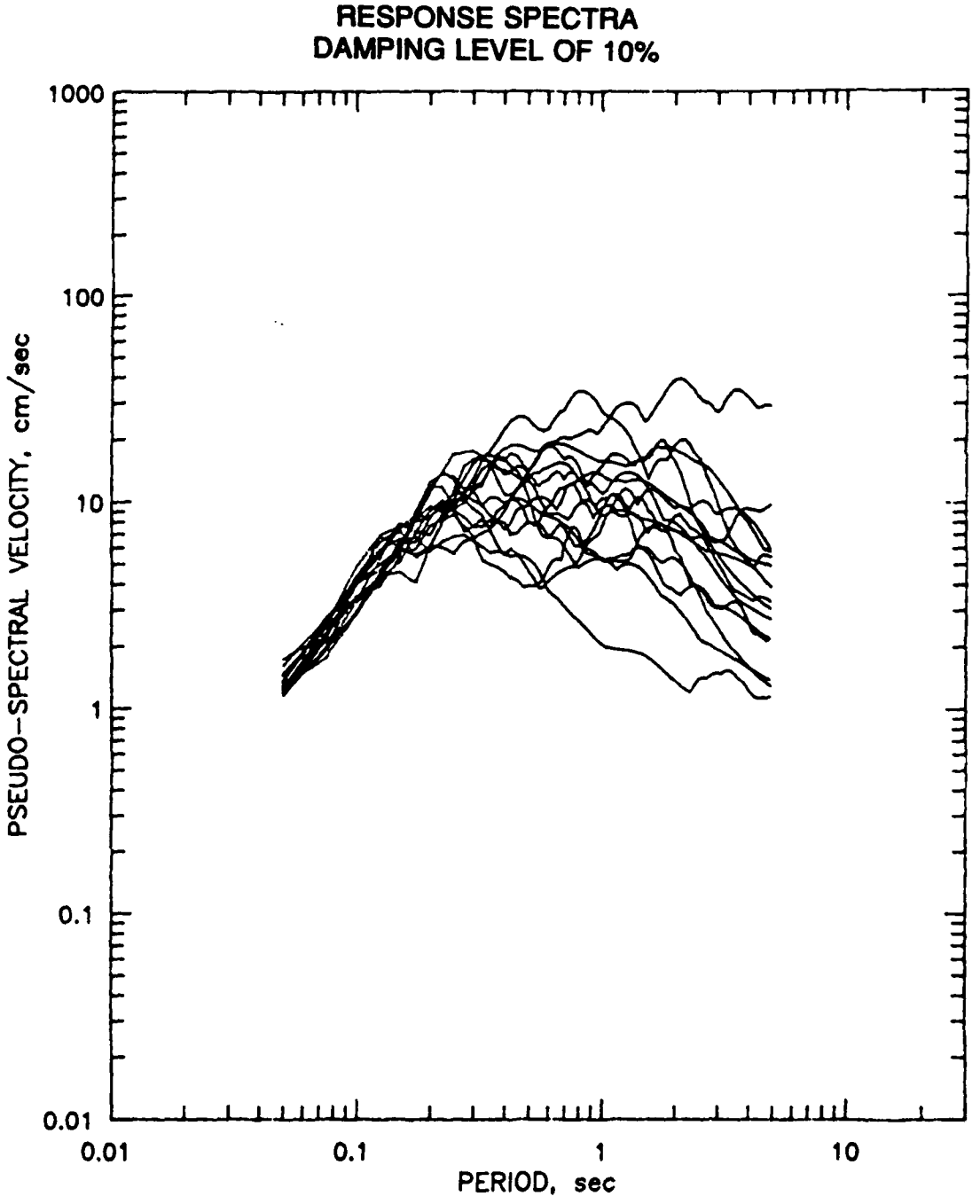

Figure 144. Composite of response spectra for all ground surface accelerograms used in this study at 10-percent damping level

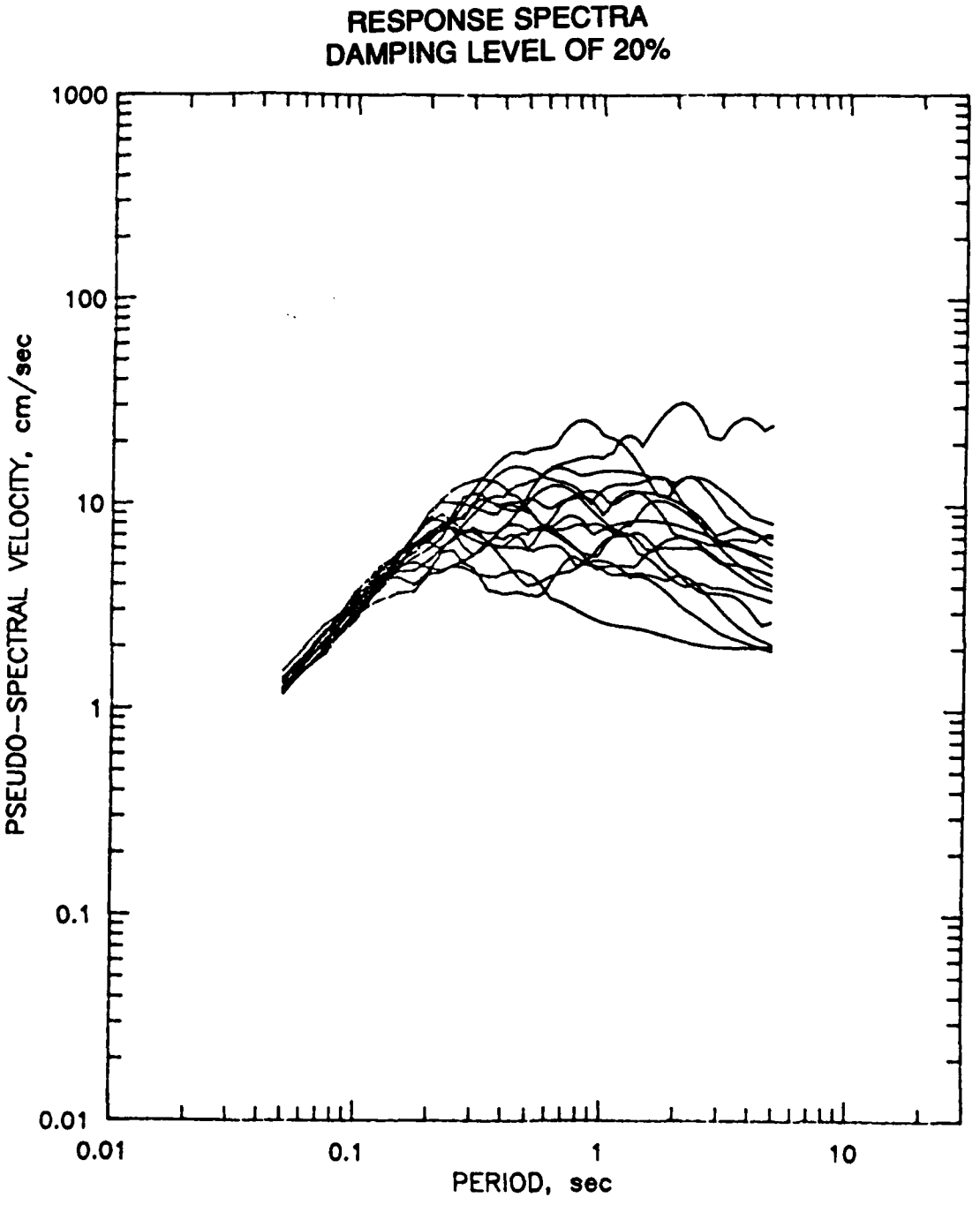

Figure 145. Composite of response spectra for all ground surface accelerograms used in this study at 20-percent damping level

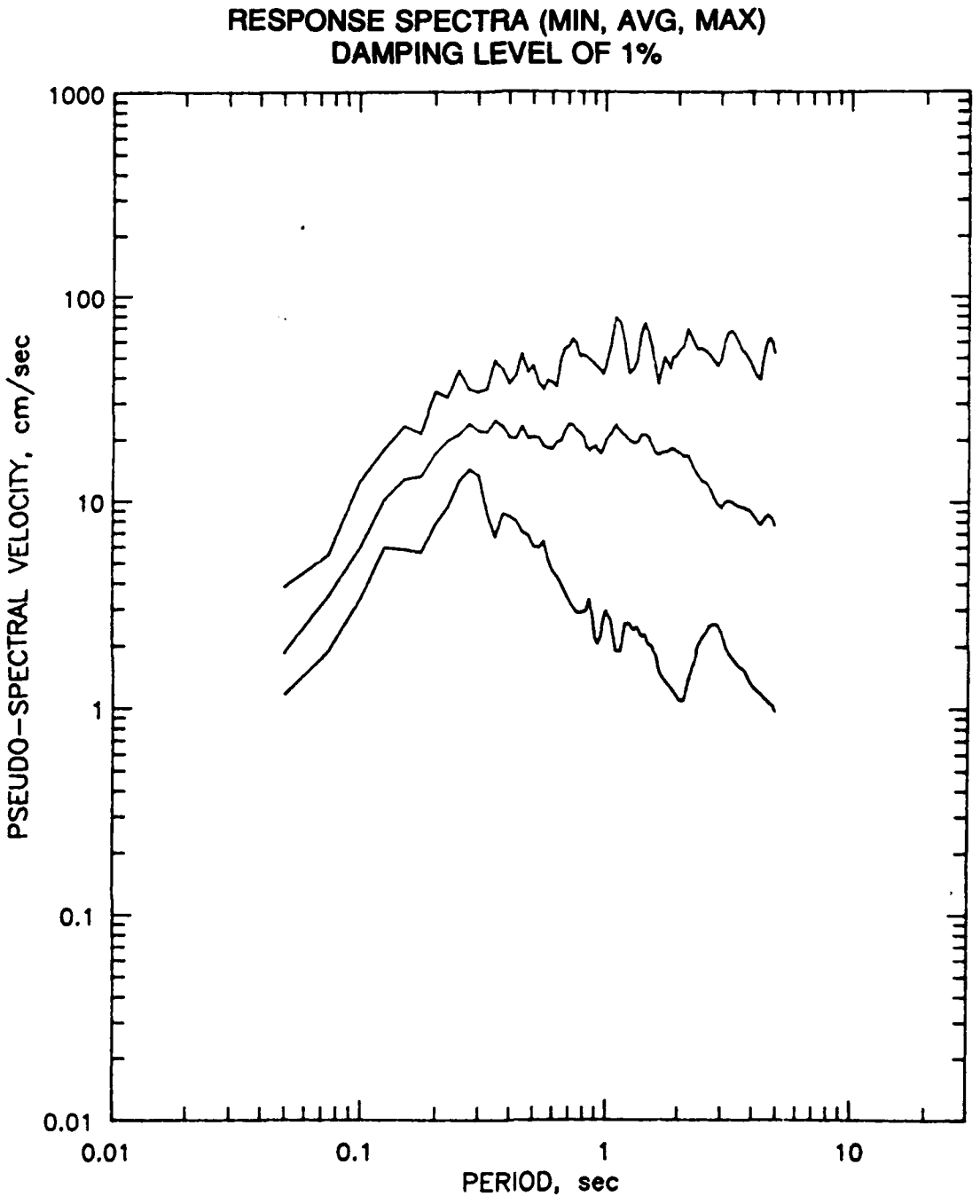

Figure 146. Average and upper and lower bound envelopes of the response spectra of all accelerograms used in this study at the 1-percent damping level

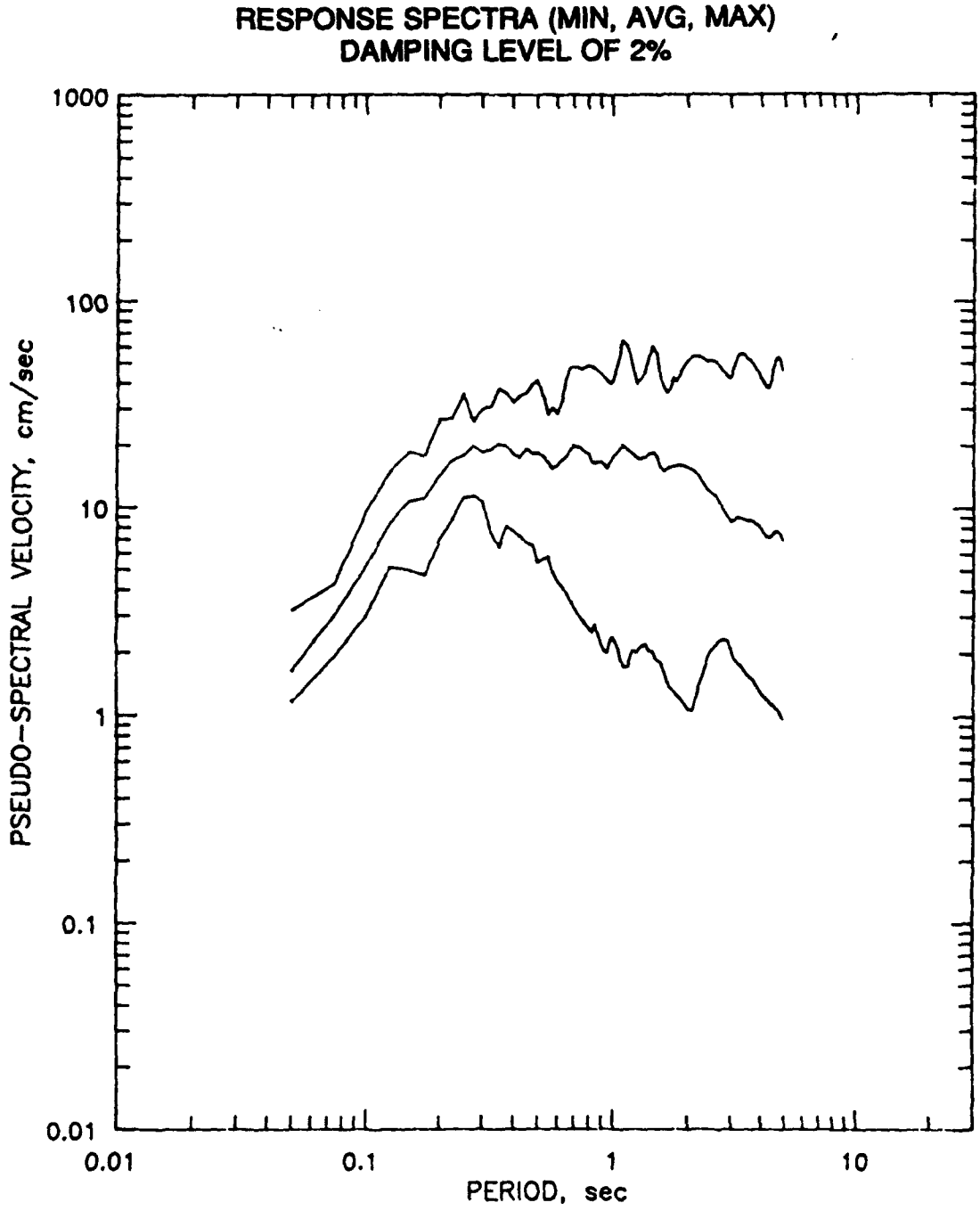

Figure 147. Average and upper and lower bound envelopes of the response spectra of all accelerograms used in this study at the 2-percent damping level

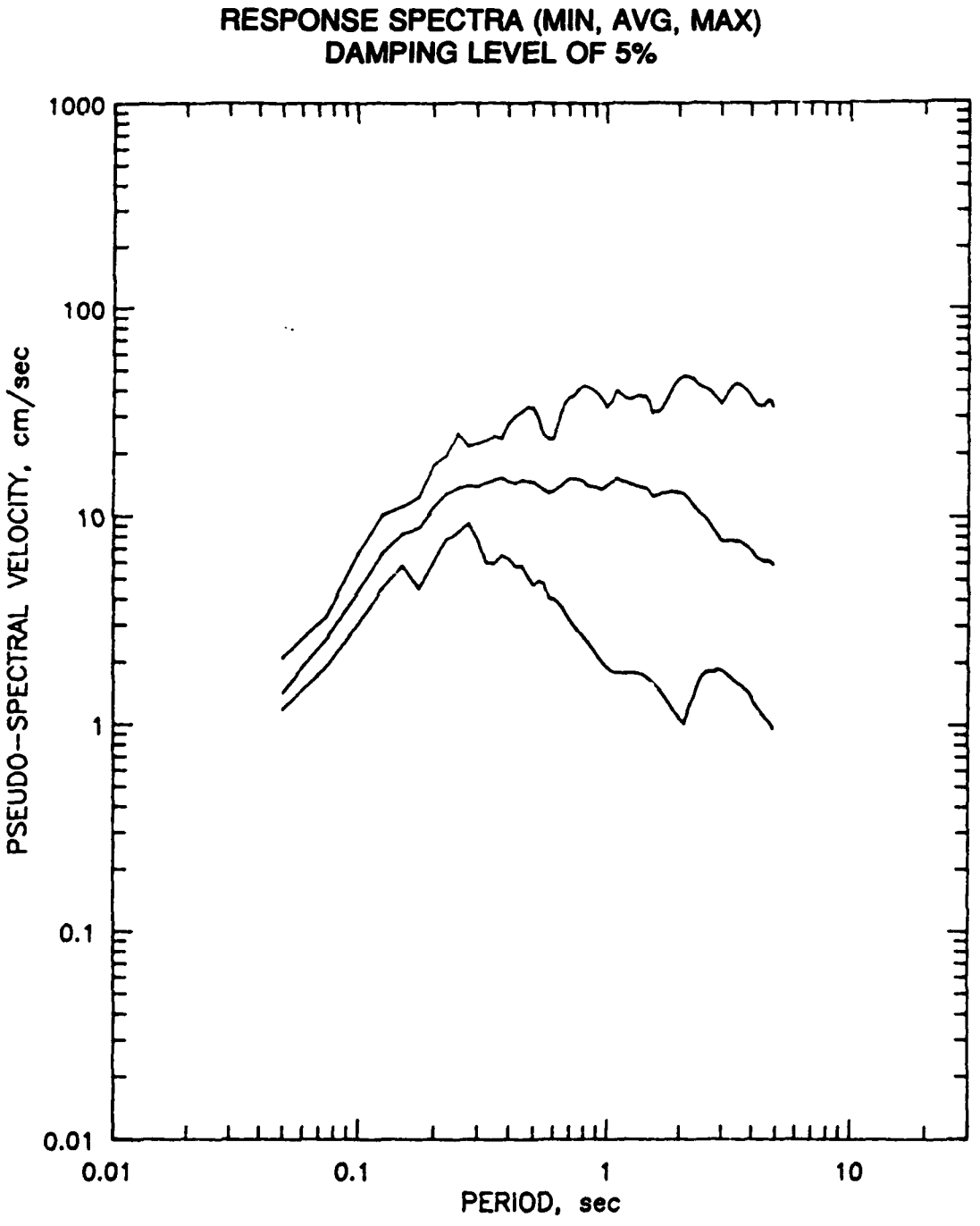

Figure 148. Average and upper and lower bound envelopes of the response spectra cf all accelerograms used in this study at the 5-percent damping level

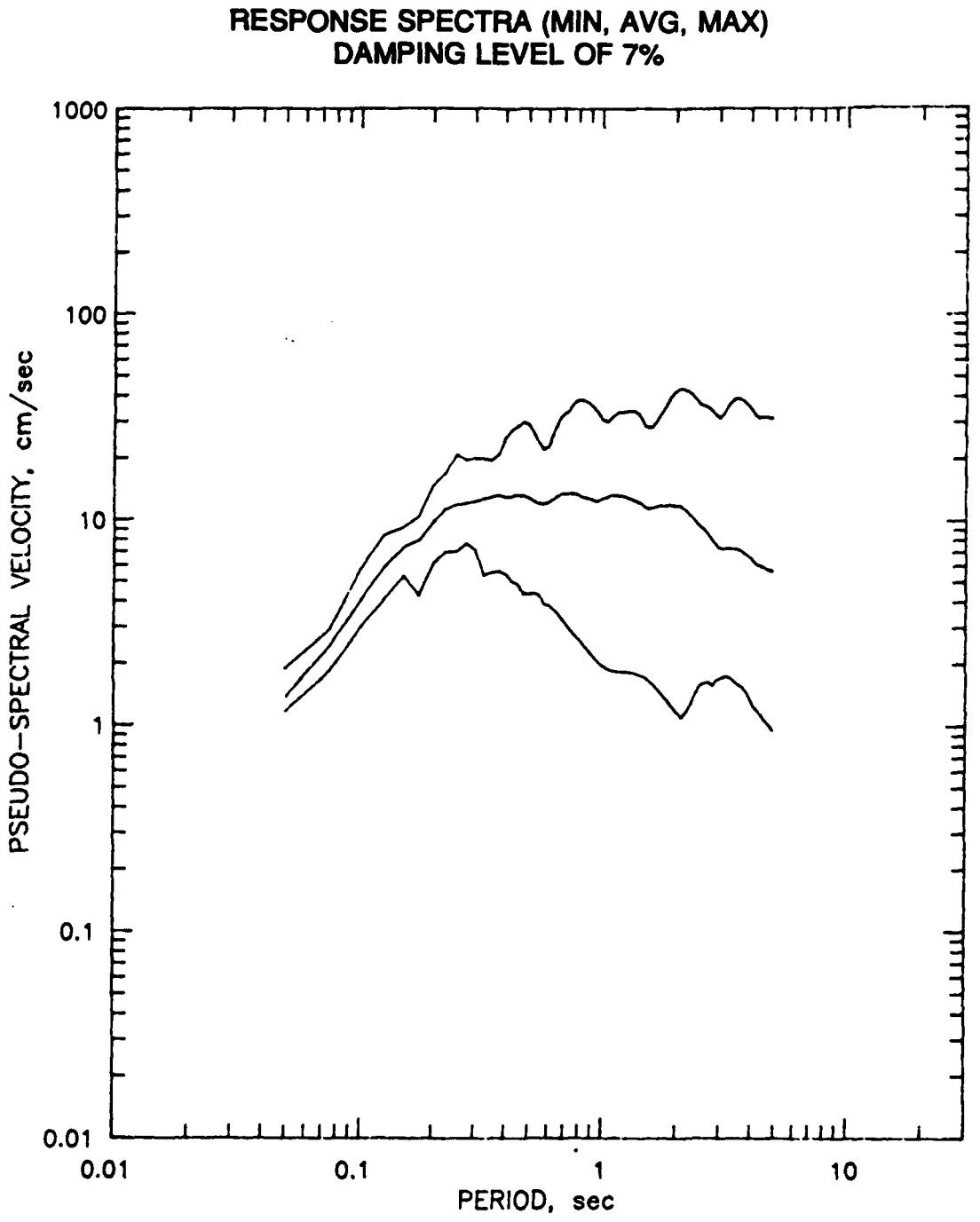

Figure 149. Average and upper and lower bound envelopes of the response spectra of all accelerograms used in this study at the 7-percent damping level

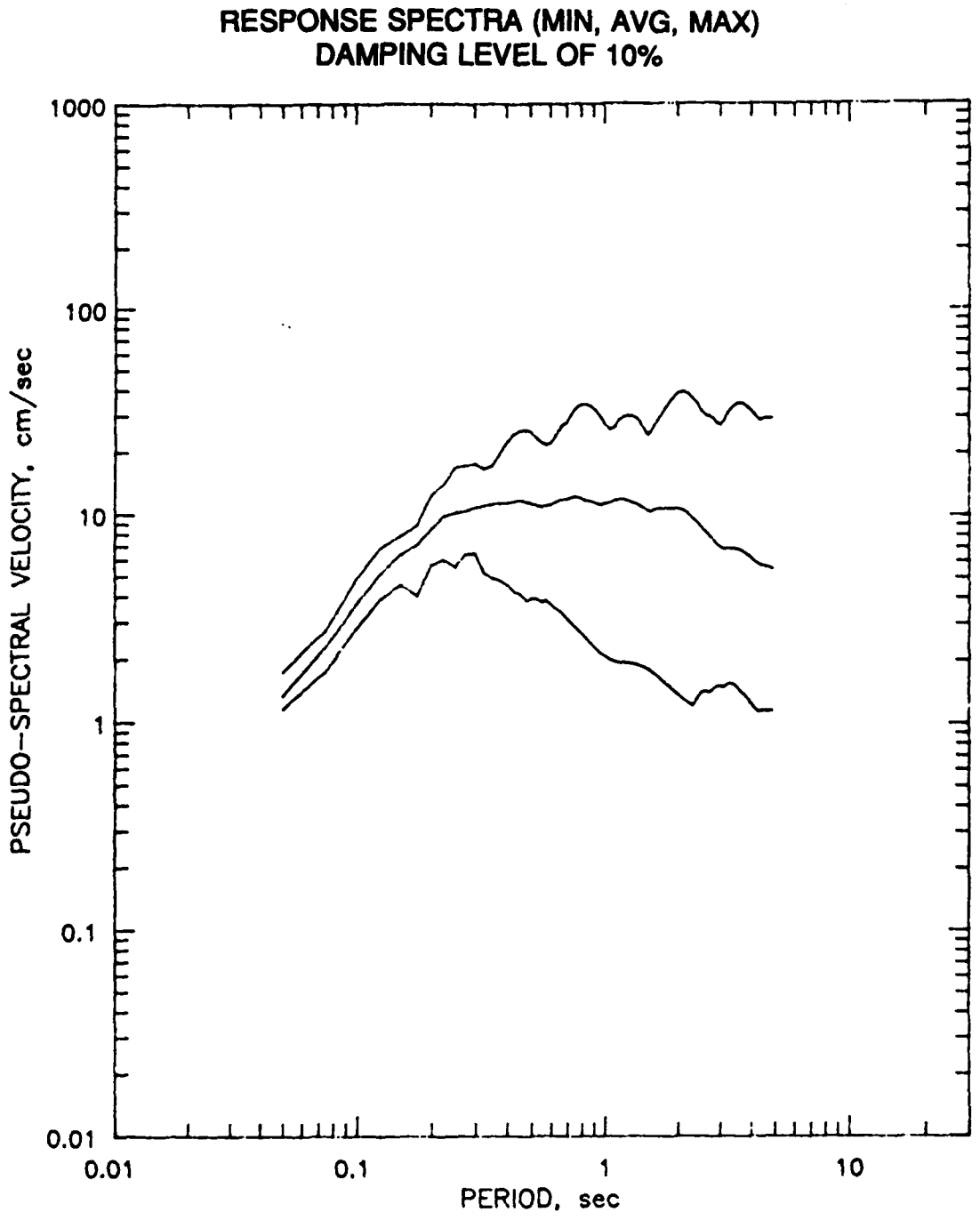

Figure 150. Average and upper and lower bound envelopes of the response spectra of all accelerograms used in this study at the 10-percent damping level

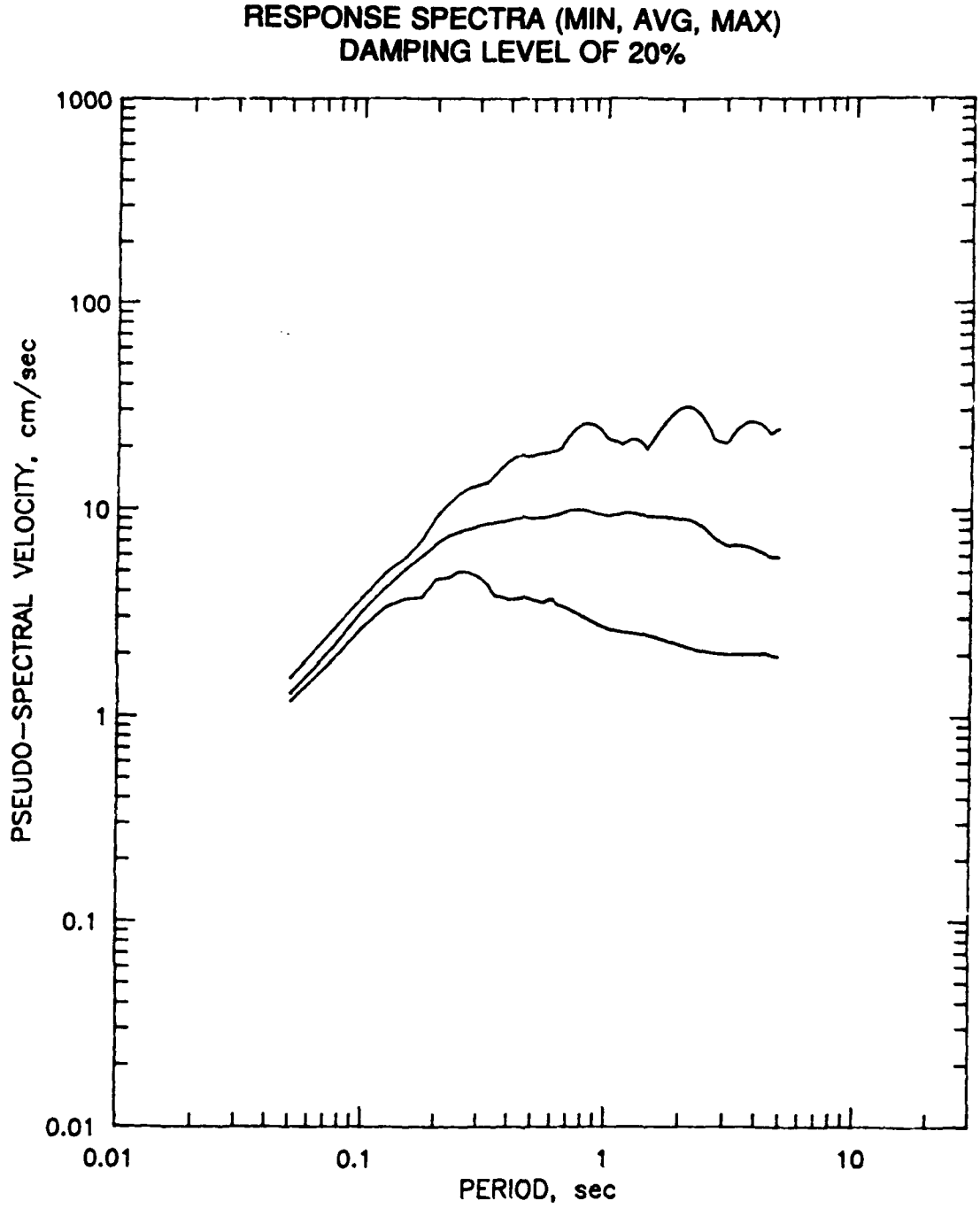

Figure 151. Average and upper and lower bound envelopes of the response spectra of all accelerograms used in this study at the 20-percent damping level

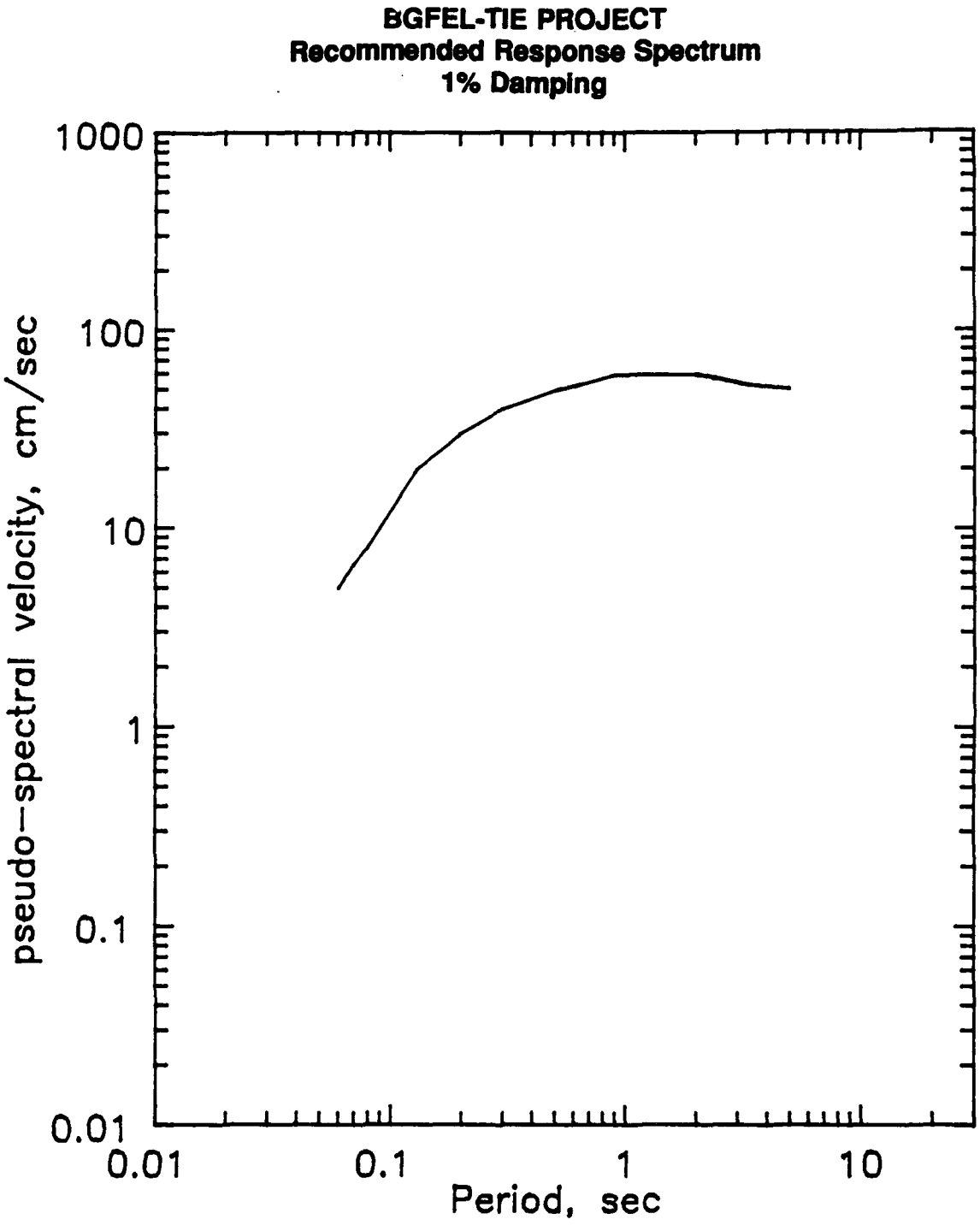

Figure 152. Recommended response spectrum for 1-percent damping

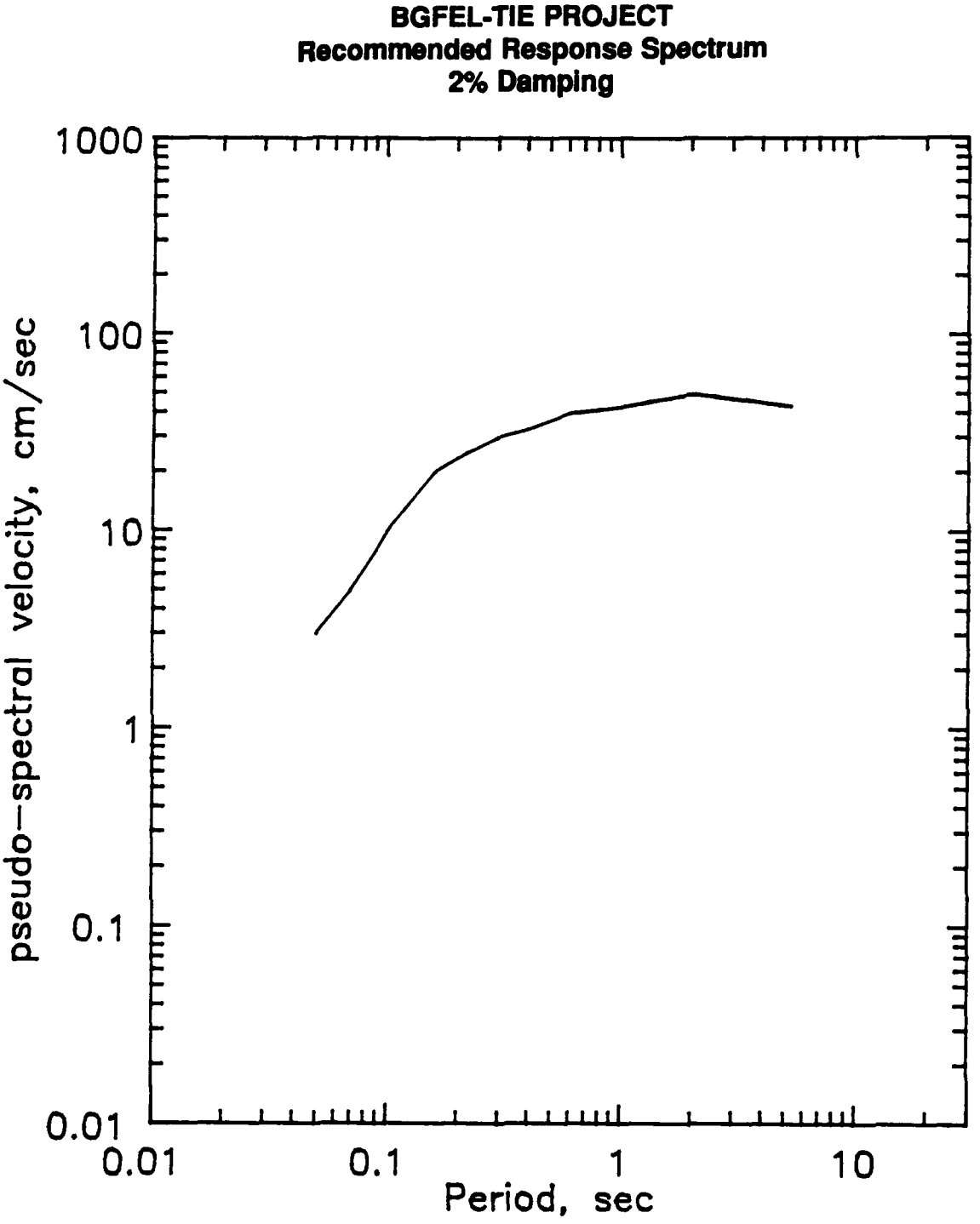

Figure 153. Recommended response spectrum for 2-percent damping

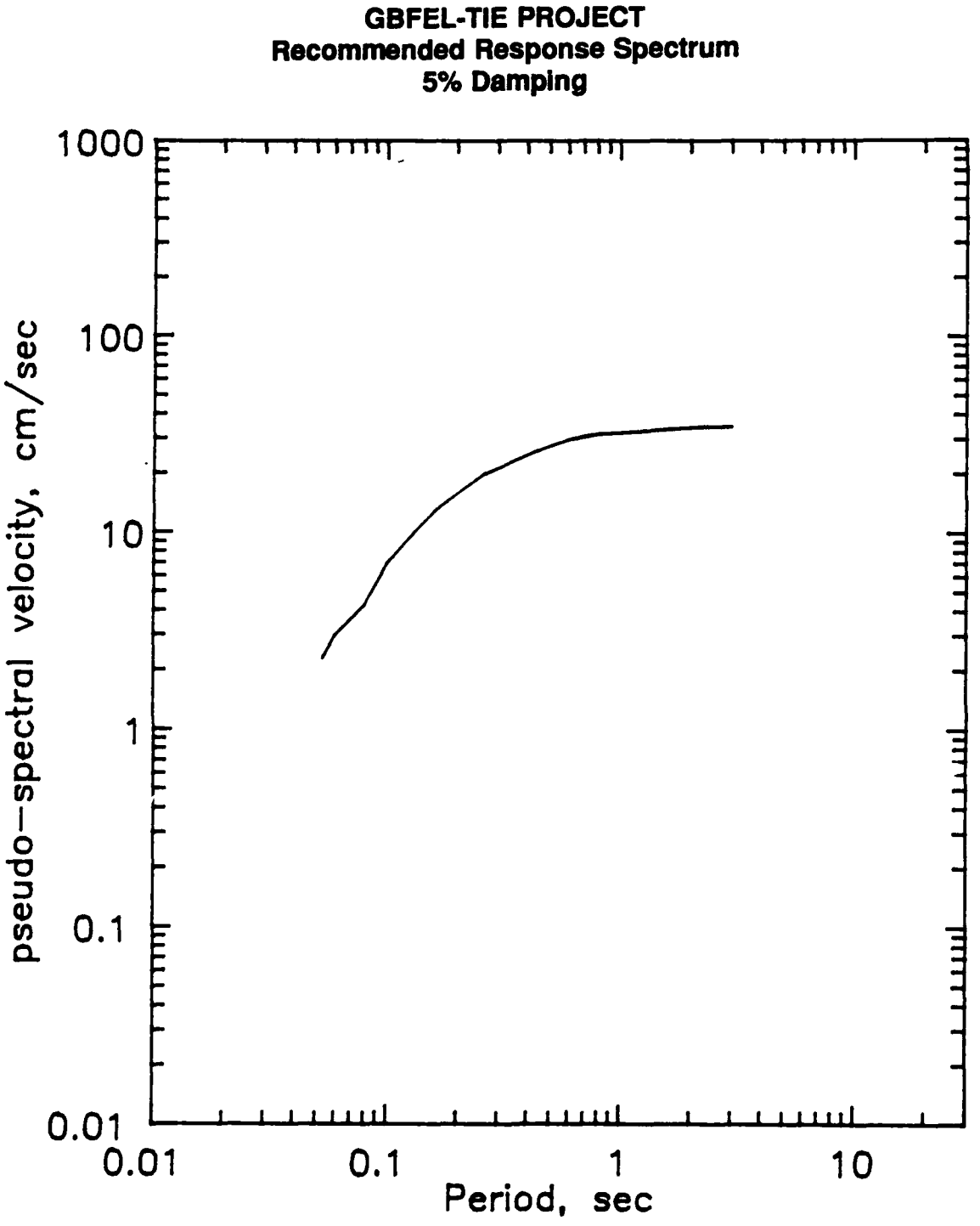

Figure 154. Recommended response spectrum for 5-percent damping

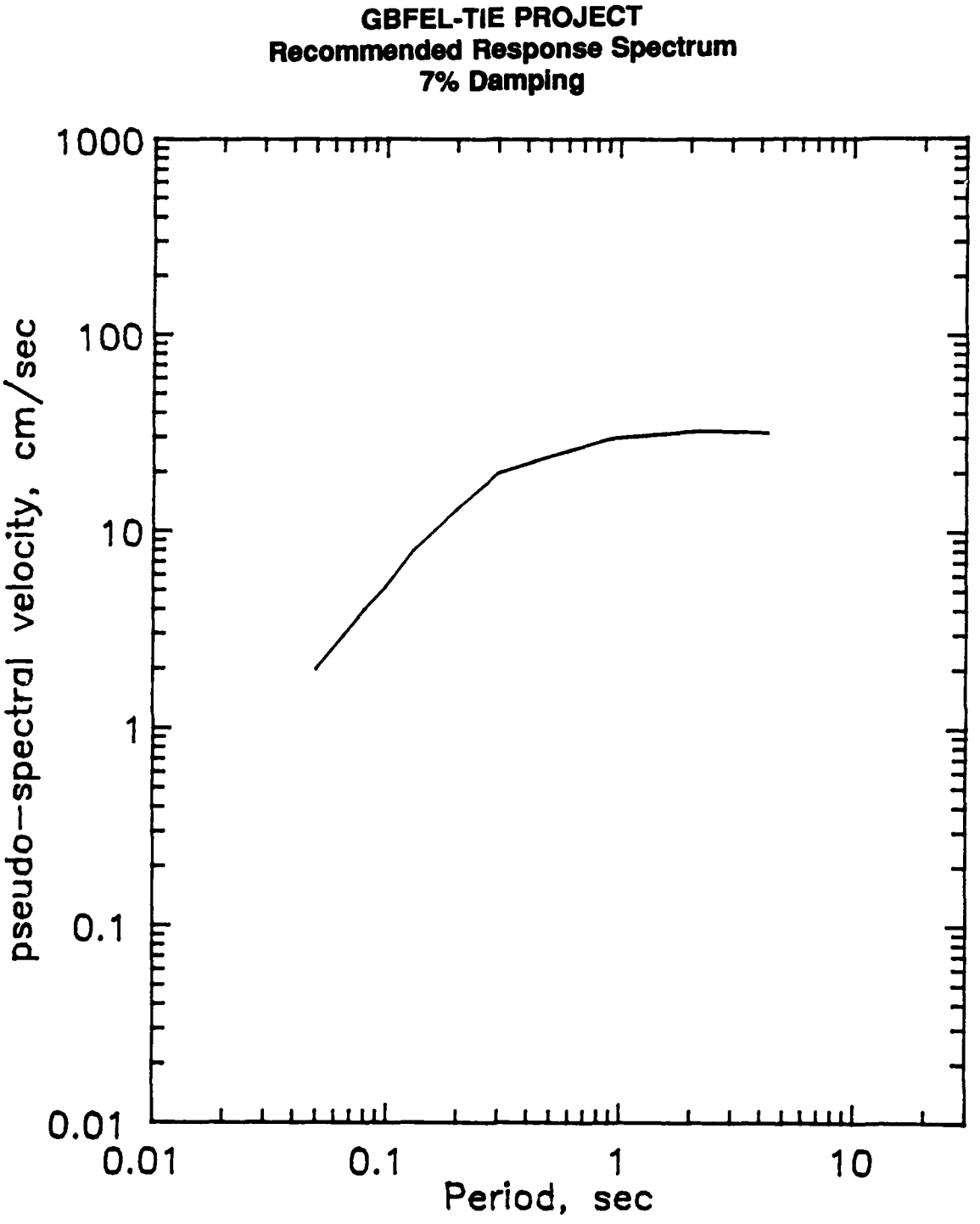

Figure 155. Recommended response spectrum for 7-percent damping

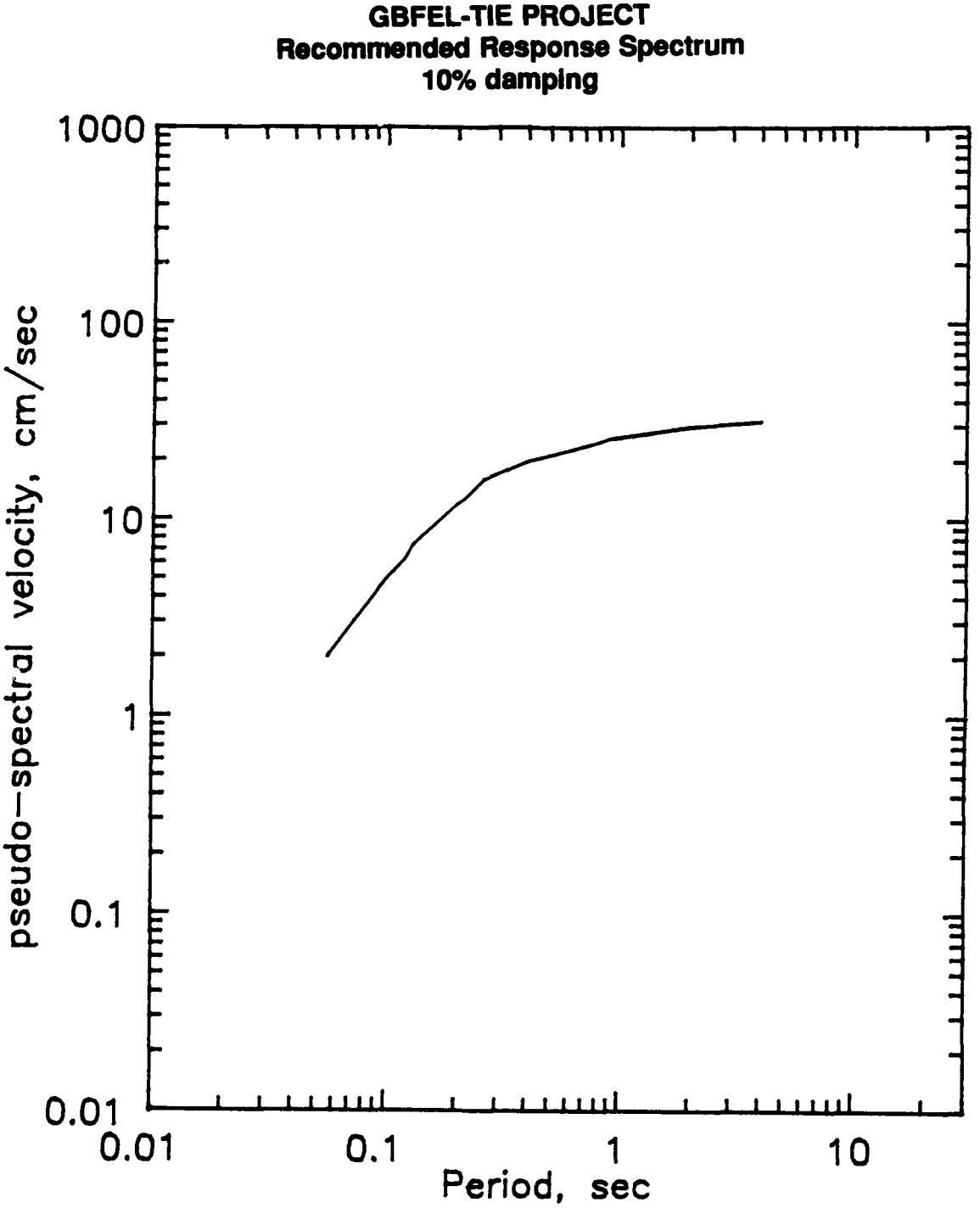

Figure 156. Recommended response spectrum for 10-percent damping

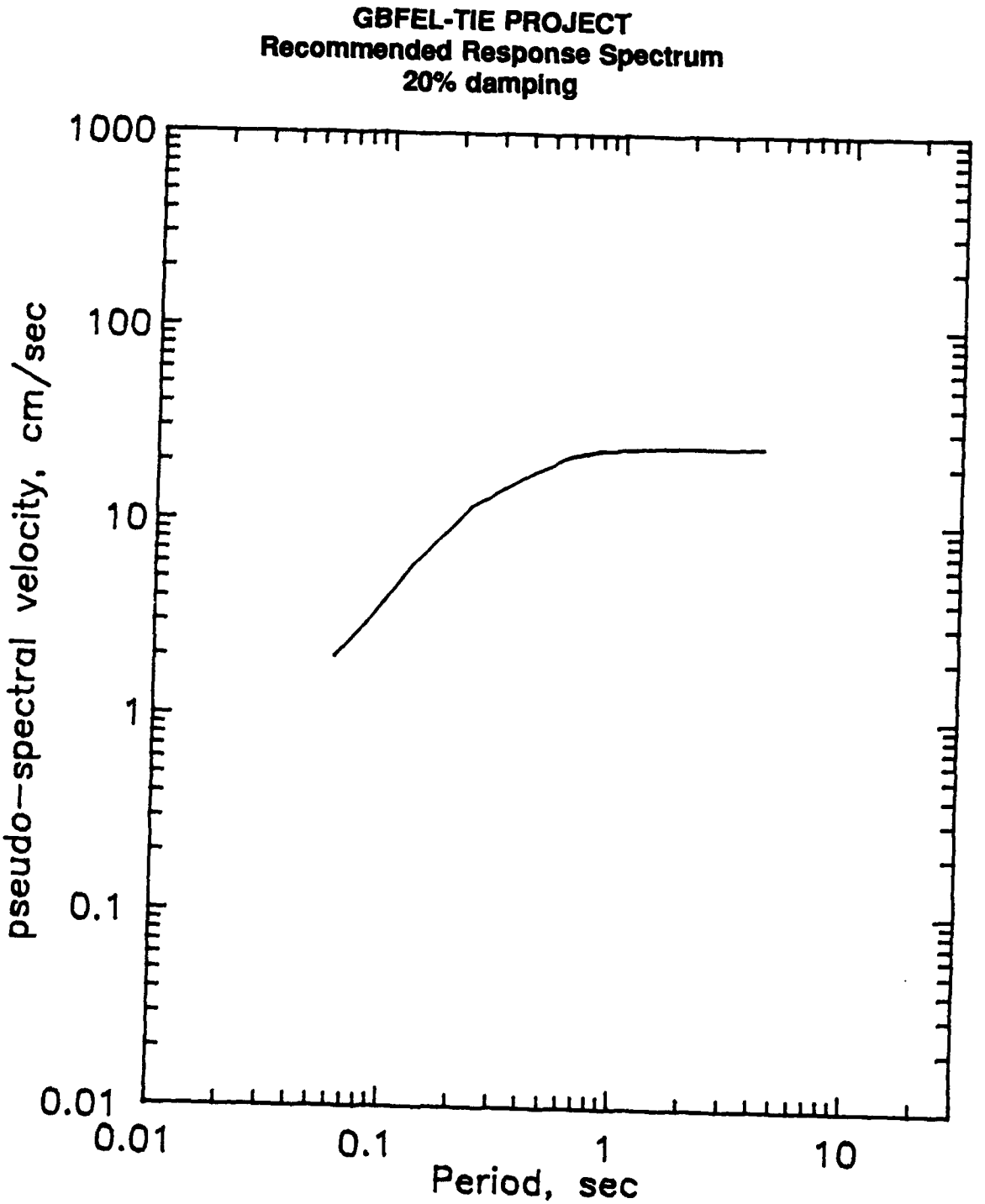

Figure 157. Recommended response spectrum for 20-percent damping

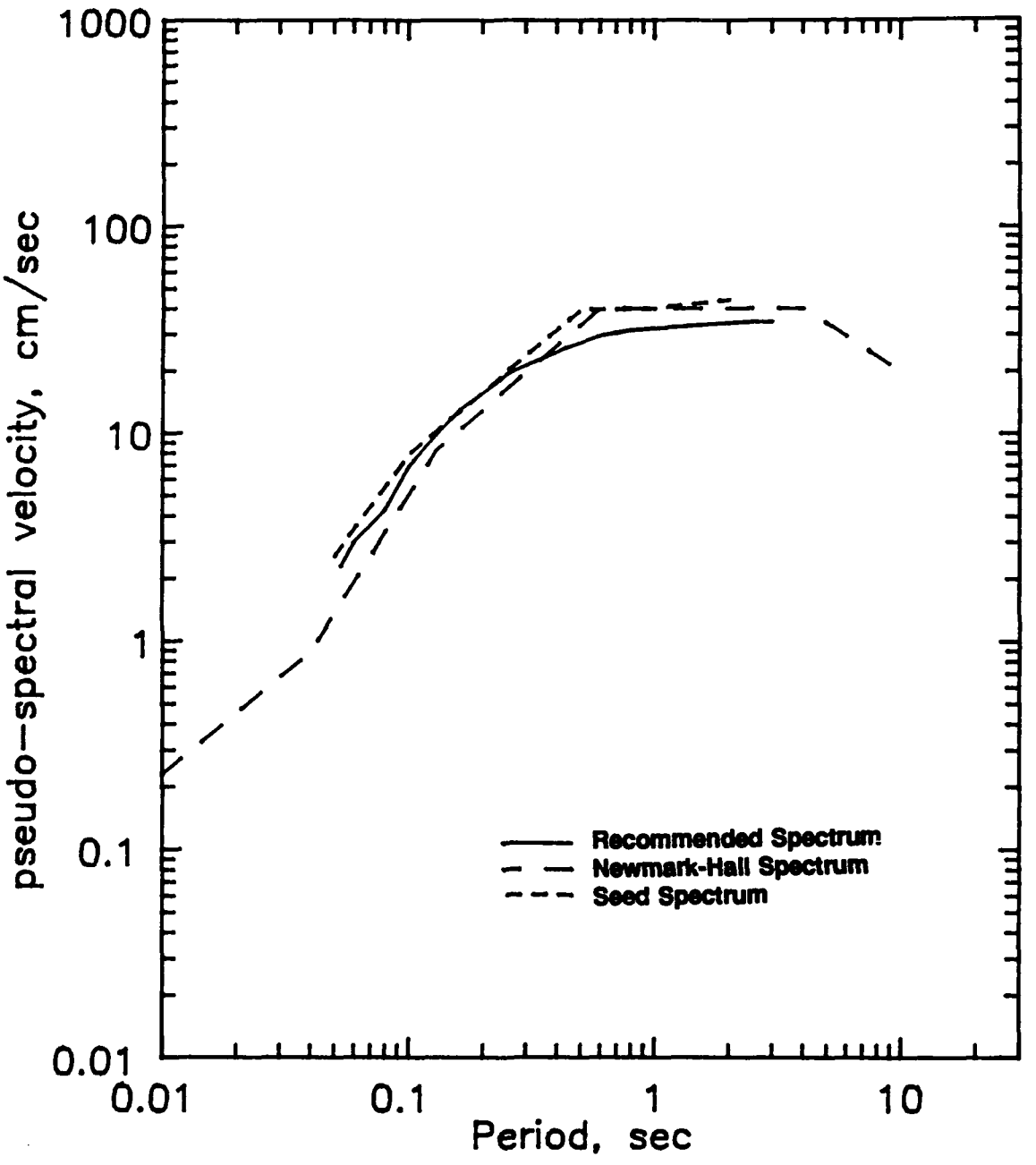

Figure 158. Comparison of recommended design spectrum with spectra of Seed and Newmark-Hall procedures

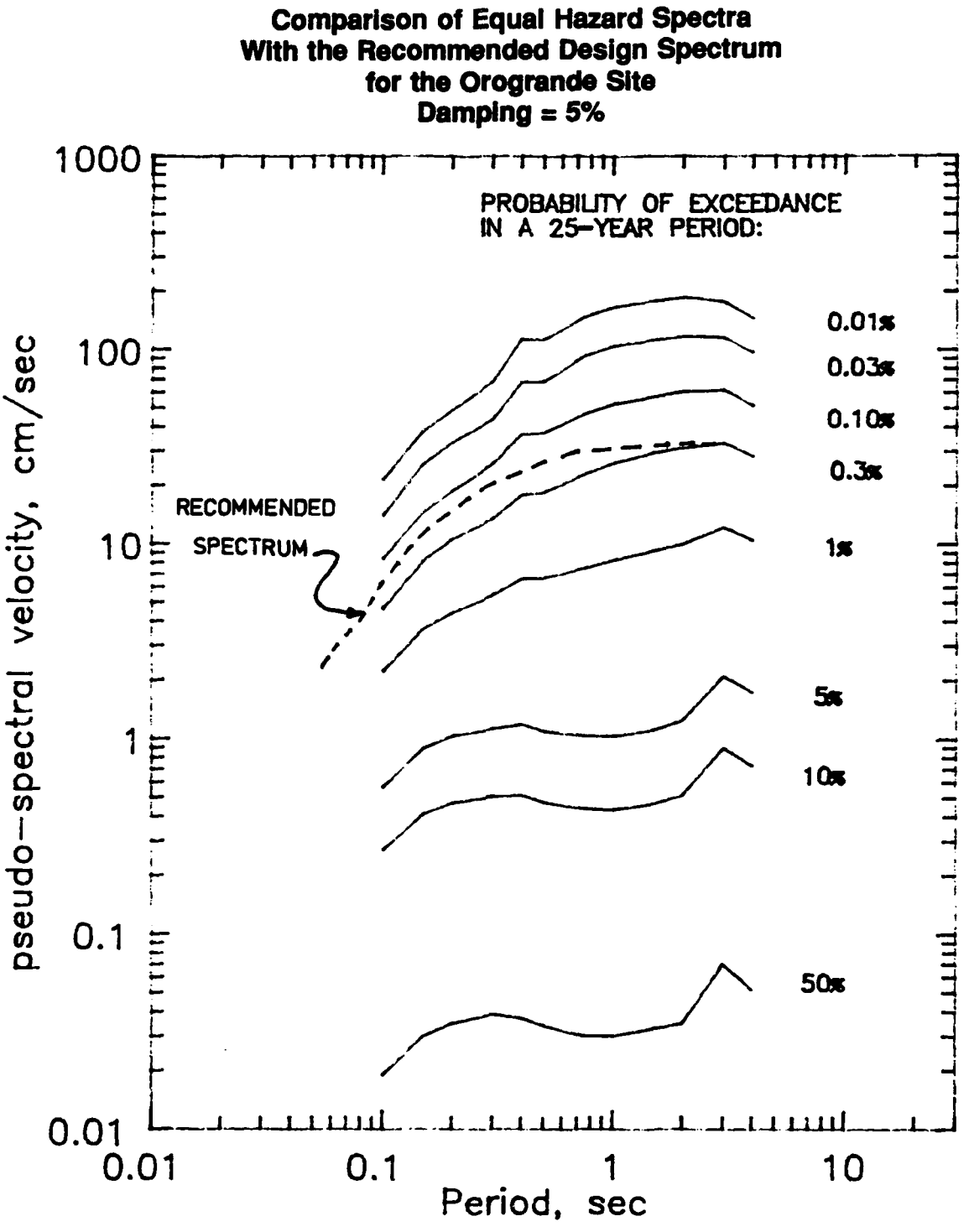

Figure 159. Comparison of equal hazard spectra with the recommended design spectrum for the Orogrande Site at 5-percent damping level

APPENDIX A

DATA BASE OF INSTRUMENTALLY RECORDED EARTHQUAKES IN NEW MEXICO BETWEEN 1962 AND 1977

The following table is list of instrumentally recorded earthquakes in New Mexico during the period spanning the years 1962 through 1977. The list is sorted by year. The list was compiled by Sanford, Olsen, and Jaksha (1981).

Year	Month	Day	Latitude	Longitude	Magnitude	No. of Stations Recording Event
1962	12	15	33.97	106.87	1.87	4
1962	9	1	34.16	106.66	2.97	5
1962	6	25	34.20	108.10	1.56	3
1962	6	27	33.95	107.01	1.63	3
1962	6	14	35.68	106.74	1.87	6
1962	5	2	34.22	107.05	1.56	3
1962	4	9	34.21	106.44	1.76	3
1962	3	22	34.25	106.51	1.74	3
1962	1	24	33.96	106.86	1.50	3
1962	1	24	33.96	106.86	1.84	3
1962	1	3	35.32	103.64	2.60	5
1963	12	30	34.03	106.54	1.66	3
1963	12	19	35.14	104.13	2.88	9
1963	11	25	36.54	105.37	2.41	9
1963	8	19	32.44	107.15	2.11	5
1963	7	3	33.91	106.90	1.92	6
1963	6	2	34.23	106.46	1.96	9
1963	6	6	36.60	104.40	2.74	9
1963	5	27	32.72	107.82	1.61	4
1963	3	8	32.95	107.08	1.56	4
1963	3	6	33.63	107.68	1.68	4
1963	2	22	32.45	106.94	1.51	5
1963	2	22	32.42	106.99	2.47	6
1964	6	19	33.09	105.95	1.71	5
1964	3	3	34.97	103.59	2.22	5
1964	2	11	34.35	103.73	2.49	4
1965	12	22	34.02	106.78	1.91	3
1965	12	22	34.02	106.70	2.15	4
1965	12	29	35.03	105.78	2.65	4
1965	7	28	33.96	106.82	2.26	7
1965	7	28	33.80	106.70	2.59	4
1965	6	4	33.90	106.81	1.73	5
1965	5	27	33.90	107.01	1.82	4
1965	5	27	33.88	106.73	2.01	4
1965	5	27	33.90	106.71	2.03	4
1965	5	29	33.87	106.69	2.03	5
1965	4	10	33.94	107.05	2.00	7
1965	3	9	33.87	106.90	2.54	6
1965	2	3	35.10	103.80	2.92	9
1966	10	6	35.21	104.27	2.30	8
1966	10	6	34.04	106.85	2.35	4
1966	9	17	34.94	103.71	2.23	7
1966	9	24	36.44	105.09	2.44	9

Year	Month	Day	Latitude	Longitude	Magnitude	No. of Stations Recording Event
1966	9	24	36.43	105.08	2.71	9
1966	9	25	36.34	105.08	2.75	8
1966	9	25	36.45	105.14	2.76	8
1966	9	9	36.70	108.30		5
1966	4	21	35.29	103.32	2.28	8
1966	3	24	36.80	108.30		6
1966	1	23	36.96	106.95	4.29	9
1967	9	29	32.27	106.91	2.04	8
1967	7	29	33.25	108.47	2.10	6
1967	1	16	34.43	106.85	1.64	5
1968	8	21	35.10	107.52	1.69	4
1968	8	22	34.33	105.80	2.06	4
1968	7	25	33.99	106.85	1.84	3
1968	5	19	34.50	107.98	2.26	8
1968	5	15	34.27	106.84	2.32	8
1968	5	29	34.39	107.75	2.47	3
1968	5	2	33.02	105.27	2.58	5
1968	3	23	32.70	106.05	2.24	6
1968	3	9	32.70	106.05	2.91	9
1969	9	13	36.86	105.88	2.27	6
1969	8	23	34.70	108.44	2.66	9
1969	7	30	34.39	106.99	1.73	3
1969	7	4	36.15	106.13	2.85	9
1969	6	28	35.26	107.56	1.55	4
1969	6	1	34.23	105.18	1.97	6
1969	6	8	34.23	105.18	2.39	8
1969	5	28	35.45	107.35	2.43	6
1969	3	4	34.72	105.85	2.30	3
1969	1	30	34.22	106.75	3.42	9
1970	11	30	36.25	105.49	2.49	8
1970	11	28	35.10	106.61	3.18	9
1970	8	7	35.40	105.89	1.97	8
1970	7	3	34.90	105.91	1.60	3
1970	7	31	35.28	106.19	2.06	8
1970	5	22	35.64	106.00	1.53	4
1970	1	12	35.89	103.40	3.26	7
1971	12	27	35.79	106.96	1.68	3
1971	12	11	35.72	105.29	1.92	3
1971	12	6	36.09	106.19	2.03	6
1971	12	23	34.42	107.02	2.04	4
1971	12	6	36.10	107.17	2.14	6
1971	12	6	36.08	106.14	2.31	7
1971	12	6	36.15	106.11	2.90	9
1971	6	24	36.70	105.67	1.88	4
1971	6	4	36.19	106.32	2.34	8
1971	5	22	35.43	107.76	2.31	5
1971	4	28	36.13	105.96	2.74	9
1971	3	25	34.58	106.03	1.73	3
1971	2	13	33.18	108.07	1.79	4
1971	2	18	36.30	105.78	2.76	9
1971	1	27	34.06	106.60	2.60	8

Year	Month	Day	Latitude	Longitude	Magnitude	No. of Stations Recording Event
1971	1	6	34.15	106.79	2.75	9
1971	1	4	35.10	106.60	3.55	9
1972	12	18	35.42	107.16	2.68	7
1972	11	24	32.03	108.34	2.72	6
1972	10	11	32.74	107.92	2.34	5
1972	7	26	32.68	103.98	2.90	6
1972	5	16	34.20	106.88	1.68	4
1972	5	6	35.40	107.46	2.16	6
1972	5	20	35.40	107.36	2.70	6
1972	4	15	36.58	108.53	1.74	5
1972	3	28	36.14	106.15	2.26	8
1972	3	31	36.11	106.04	2.37	5
1972	3	28	36.17	106.06	2.67	9
1972	2	20	36.36	104.87	1.50	3
1972	2	27	34.15	106.81	1.64	4
1972	2	20	36.35	104.94	2.21	4
1972	2	27	32.89	106.04	2.24	5
1973	12	24	35.52	106.10	1.80	
1973	12	24	35.26	107.74	3.44	16
1973	11	14	36.95	107.00	2.10	
1973	10	16	35.60	108.25	1.83	3
1973	9	10	34.42	106.85	2.40	7
1973	9	22	34.46	106.95	2.50	8
1973	8	6	32.40	107.30	1.66	3
1973	7	27	36.50	108.60	2.31	3
1973	7	22	33.00	108.10	2.33	3
1973	3	17	36.14	106.19	2.45	8
1973	3	22	31.35	108.50	2.86	4
1973	2	3	36.25	108.17	1.53	3
1973	2	26	35.45	103.50	1.96	4
1973	2	3	36.85	108.25	2.13	4
1973	1	9	32.00	107.40	1.64	3
1974	12	28	35.37	107.37	2.10	
1974	11	22	33.80	105.10	1.60	5
1974	11	1	33.80	106.60	2.00	6
1974	11	21	32.50	106.30	2.70	4
1974	11	28	32.63	104.01	3.80	6
1974	10	15	33.83	106.58	1.80	
1974	10	15	33.83	106.58	1.80	
1974	10	18	35.08	106.82	1.80	
1974	10	15	33.85	106.55	2.00	6
1974	10	15	35.25	107.08	2.10	
1974	10	11	32.80	108.70	2.30	7
1974	9	29	32.80	108.65	2.20	3
1974	9	26	32.80	106.20	3.00	5
1974	9	29	32.80	108.65	3.20	9
1974	8	26	34.40	105.80	2.30	8
1974	8	30	34.87	107.06	2.40	8
1974	7	11	35.32	107.78	2.00	
1974	7	31	33.10	104.20	2.30	4

Year	Month	Day	Latitude	Longitude	Magnitude	No. of Stations Recording Event
1974	6	22	35.08	106.70	1.90	
1974	5	4	35.55	108.98	1.70	
1974	4	8	34.20	106.87	1.60	3
1974	4	12	34.50	107.00	2.30	3
1974	3	28	35.22	107.55	1.50	
1974	3	28	35.22	107.55	1.60	
1974	3	23	36.50	107.08	1.90	
1974	3	13	34.50	106.90	2.20	3
1974	1	17	36.15	106.20	1.80	
1974	1	12	35.20	107.60	1.85	7
1975	12	3	32.83	108.66	3.40	14
1975	10	17	35.38	108.20	1.90	
1975	10	10	33.30	105.00	2.00	3
1975	9	10	36.73	105.67	1.50	
1975	9	29	36.00	106.87	1.50	
1975	9	6	36.18	106.23	1.80	
1975	9	29	36.00	106.87	2.70	9
1975	6	27	34.19	106.93	1.60	6
1975	6	28	34.20	106.90	1.90	10
1975	6	21	36.08	104.03	2.00	
1975	6	26	36.95	105.45	2.90	
1975	5	16	36.92	104.95	1.50	
1975	5	21	36.97	107.22	1.50	
1975	5	16	36.48	104.70	1.90	
1975	3	7	34.50	106.90	1.50	
1975	3	5	34.55	107.12	2.20	7
1975	3	6	34.55	107.14	2.20	6
1975	3	7	34.55	107.16	2.80	10
1975	3	7	34.55	107.16	2.90	10
1975	2	9	36.18	106.23	1.50	
1975	2	2	35.10	103.10	2.90	8
1976	12	31	36.72	106.65	1.80	
1976	12	31	36.57	106.67	1.80	
1976	12	23	34.68	105.77	1.90	
1976	9	17	32.20	103.10	2.10	8
1976	8	30	33.30	105.70	1.50	3
1976	7	6	36.08	106.27	1.50	
1976	7	5	36.13	106.25	1.80	
1976	6	26	36.13	106.27	1.50	
1976	6	9	34.46	106.99	1.70	
1976	6	1	36.30	106.20	1.90	
1976	6	24	35.62	103.28	3.00	19
1976	5	3	32.00	103.20	1.50	4
1976	5	3	32.00	103.10	1.50	4
1976	5	9	34.25	106.86	1.70	
1976	5	6	32.00	103.20	1.80	6
1976	5	2	36.28	106.73	2.20	
1976	5	21	32.30	105.30	2.30	3
1976	5	3	32.40	105.60	2.40	4
1976	5	1	32.40	103.10	2.70	8

Year	Month	Day	Latitude	Longitude	Magnitude	No. of Stations Recording Event
1976	4	1	33.90	105.90	1.50	3
1976	4	30	32.00	103.30	1.50	4
1976	4	1	33.80	105.90	1.60	3
1976	4	18	33.90	106.00	1.60	6
1976	4	30	32.00	103.20	1.60	3
1976	4	1	33.90	106.00	2.10	10
1976	4	6	33.90	106.00	2.70	10
1976	3	7	35.68	107.98	1.70	
1976	3	20	32.20	103.12	1.70	5
1976	3	27	32.20	103.10	2.00	8
1976	1	16	35.57	107.87	1.80	
1976	1	14	34.10	106.80	2.20	8
1976	1	25	32.00	103.10	3.20	12
1976	1	5	35.84	108.34	4.10	95
1977	8	22	35.62	107.23	1.50	
1977	8	19	34.01	107.06	1.90	5
1977	6	2	34.02	107.06	1.50	7
1977	4	22	32.20	103.10	1.70	3
1977	4	3	36.10	106.25	1.90	
1977	4	7	32.20	103.10	2.30	8
1977	4	26	32.00	103.10	2.50	11
1977	3	9	35.80	108.17	1.70	
1977	3	16	36.97	106.98	1.70	
1977	3	20	32.20	103.10	2.10	7
1977	3	5	35.92	108.29	3.70	47
1977	2	18	32.20	103.10	1.50	4
1977	1	5	34.05	106.00	1.70	
1977	1	4	34.03	106.00	2.40	
1977	1	4	32.36	106.92	2.70	10